INTERPRETATION BASICS OF CONE BEAM COMPUTED TOMOGRAPHY

Edited by
Shawneen M. Gonzalez

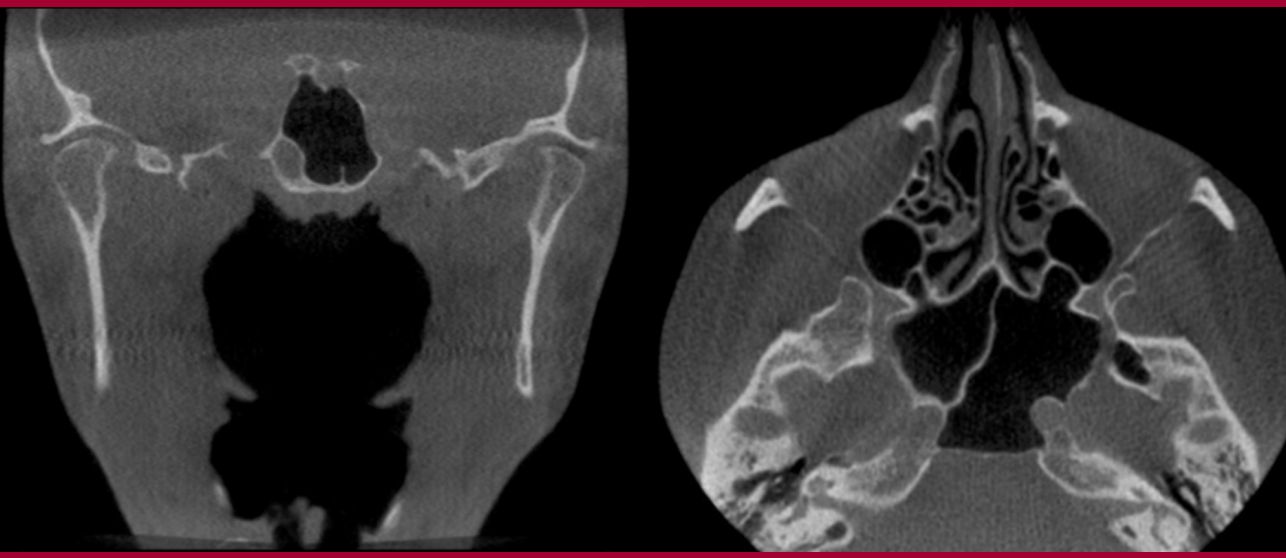

with website

WILEY Blackwell

Interpretation Basics of Cone Beam Computed Tomography

Interpretation Basics of Cone Beam Computed Tomography

Edited by

Shawneen M. Gonzalez

WILEY Blackwell

This edition first published 2014 © 2014 by John Wiley & Sons, Inc

Editorial Offices
1606 Golden Aspen Drive, Suites 103 and 104, Ames, Iowa 50010, USA
The Atrium, Southern Gate, Chichester, West Sussex, PO19 8SQ, UK
9600 Garsington Road, Oxford, OX4 2DQ, UK

For details of our global editorial offices, for customer services and for information about how to apply for permission to reuse the copyright material in this book please see our website at www.wiley.com/wiley-blackwell.

Library of Congress Cataloging-in-Publication Data

Gonzalez, Shawneen, author.
Interpretation basics of cone beam computed tomography / Shawneen Gonzalez.
p. ; cm.
Includes bibliographical references and index.
ISBN 978-1-118-38106-9 (paper : alk. paper) – ISBN 978-1-118-76222-6 (ePub) –
ISBN 978-1-118-76224-0 (ePDF) – ISBN 978-1-118-38106-9
I. Title.
[DNLM: 1. Cone-Beam Computed Tomography. 2. Radiography, Dental–methods.
3. Craniofacial Abnormalities–diagnosis. 4. Skull–radiography. WN 230]
RK309
617.6′07572–dc23
2013024994

A catalogue record for this book is available from the British Library.

Wiley also publishes its books in a variety of electronic formats. Some content that appears in printmay not be available in electronic books.

Cover design by Nicole Teut

Set in 10/12pt Sabon by SPi Publisher Services, Pondicherry, India

1 2014

For Tyson, Max, and Rugan

Contents

Preface

It is the goal of this book to help practitioners and students gain a better understanding of anatomy and common disease processes that frequently present on cone beam computed tomography scans. This book seeks to fill the gap in the current literature where little is presented on common radiographic appearances on cone beam CT. In addition to this book, there are five sample cases with selected images online at www.wiley.com/go/gonzalez/cbct, where you can practice working your way through each region and using the knowledge you will acquire in this book.

The beginning of the book covers general information about different unit parameters and how these can play a role in the outcome of the scan including but not limited to slice thickness and what is recommended based on what is being evaluated (i.e., possible root fracture versus bone quantity for implants). The second chapter is about legal considerations of owning a cone beam CT, referring patients for a cone beam CT scan, and/or interpreting cone beam CT scans. This information is lacking in the current literature and is something many professionals do not consider but should be aware of before purchasing or using a cone beam CT unit.

Each book chapter is an anatomical region covering the topics of normal anatomy, common anatomical variants, and frequently seen disease processes. The first regions presented are the paranasal sinuses and mastoid air cells and nasal cavity and airway, which are intimately involved with each other. The normal anatomy section covers pertinent anatomy to evaluate when interpreting or reviewing a scan. The next section covers common anatomical variants with various images showing how they appear on axial, coronal, and sagittal views. The last section covers commonly seen disease processes, such as sinusitis, that should be noted on a written radiology interpretation.

The following chapters on the cranial skull base and brain and orbits are also intimately involved as they are directly adjacent to each other. There are many anatomical landmarks in the cranial skull base such as canals, foramina, air cells, and more making this a difficult region to interpret. Key anatomy is shown on various views (axial, coronal, and sagittal) to aid the practitioner and the student in orienting themselves on the scan. There is no key anatomy covered for the soft tissue of the

brain due to limitations of soft tissue imaging on cone beam CT scans. Disease processes and anatomical variants of entities such as vascular markings and pineal gland calcifications are covered in their respective chapters.

The region of the cervical spine and soft tissue of the neck cover normal anatomical appearances to disease processes such as degenerative joint disease and arterial calcifications. Degenerative joint disease is progressive with multiple appearances based on the degree of bony damage. This chapter has many example images of degenerative joint disease at various points in the disease process.

The last region covered is the temporomandibular joints, which is very thorough thanks to the contributions of Gayle Reardon who has studied and continues to study this region in depth. The temporomandibular joints have a unique set of disease processes and developmental appearances beyond arthritic changes. This chapter covers entities many practitioners and students should be aware of even if they are not seen in daily practice.

The appendices show example written reports of cone beam CT scans for practitioners and students to view and consider when writing their own radiology interpretation. There is also a short section with recommended websites and books to learn more about cone beam CT with more obscure disease processes such as malignancies, benign neoplasms, and cysts covered in detail in the recommended books.

Acknowledgments

I'd like to thank Gayle Reardon for her contributions to this book and sharing her knowledge of the paranasal sinuses, nasal cavity and airway, and temporomandibular joints. Thanks to the staff at Wiley for guidance and support in the creation of this book. Thank you to my students for their questions and comments as they challenge me to continually improve how I share my radiology knowledge. Last, big thanks to my family (Tyson, Max, and Rugan) for their love and support throughout this entire process. I would not have been able to complete this without them.

About the Companion Website

This book is accompanied by a companion website: www.wiley.com/go/gonzalez/cbct

The website includes:

- Case studies
- Powerpoints of all figures from the book for downloading
- Powerpoints of all tables from the book for downloading

Interpretation Basics of Cone Beam Computed Tomography

1 Introduction to Cone Beam Computed Tomography

Shawneen M. Gonzalez

Introduction

This chapter will cover basics of cone beam computed tomography including comparison to traditional computed tomography, common uses, artifacts frequently seen, and views created with a cone beam computed tomography dataset.

Conventional Computed Tomography (CT)

General Information

Computed tomography (CT) is credited to Godfrey Hounsfield, who in 1967 wrote first about the technology and then created a unit in 1972. He was awarded the Nobel Prize in Physiology/Medicine in 1979. Conventional CT units are both hard-tissue and soft-tissue imaging modalities. The first CT, first generation, had a scan time of 10+ minutes depending on how much of the body was being imaged. The processing time would take 2½ hours or longer. All first-generation CT units were only a single slice. This means that one fan of radiation exposed the patient and would have to circle around the patient several times to cover the area of concern. Current CT units are fifth generation, or helical/spiral. The scan times have gone down to 20–60 seconds with a processing time of 2–20 minutes. The number of slices available is up to 64, 128, and 256. The more slices available makes it possible to scan more of the patient in one circle, hence the lower scan times. Conventional CT units work with the patient lying down on a table while being scanned. The table

Interpretation Basics of Cone Beam Computed Tomography, First Edition.
Edited by Shawneen M. Gonzalez.

moves in and out of the bore to cover the area of concern. Once all the data are received, they are compiled to create a dataset. This dataset can be manipulated to look at the information in many different angles.

Cone Beam Computed Tomography (CBCT)

General Information

Cone beam computed tomography (CBCT) was discovered in Italy in 1997. The first unit created was the NewTom. The NewTom was similar to conventional CT having the patient lying down with an open bore where the radiation exposes the patient. Instead of a fan of radiation (used in conventional CT units), a cone of radiation is used to expose the patient, hence the name cone beam computed tomography. As new CBCT units were created, companies started using seated or standing options. With continued updates to the units, the sizes have become smaller, with many needing only as much space as a pantomograph machine.

Conventional CT Versus Cone Beam CT

Voxels

Voxels are three-dimensional data blocks that representing a specific x-ray absorption. CBCT units capture isotropic voxels. An isotropic voxel is equal in all three dimensions (x, y, and z planes) producing higher resolution images compared to conventional CT units. Conventional CT unit voxels are nonisotropic with two sides equal but the third side (z-plane) different. The voxel sizes currently available in CBCT units range from 0.076 mm to 0.4 mm. The voxel sizes currently available in conventional CT units range from 1.25 mm to 5.0 mm. Resolution of the final image is determined by the unit's voxel size. The smaller the voxel size the higher the resolution. However, the higher the resolution, the higher the radiation dose to the patient as well.

Field of View

Field of view (FOV) is the area of the patient irradiated. CBCT units vary, with some units having a fixed FOV and some having changeable FOVs. The ranges of FOVs are from 5 cm × 3.8 cm, commonly referred to as a small FOV, to 23 cm × 26 cm, commonly referred to as a large FOV (Figures 1.1 to 1.3).

Radiation Doses

Radiation doses with CBCT units are as varied as the field of view options. CBCT units have approximate radiation dose ranges of 12 microSieverts to 1073 microSieverts. Conventional CT units have much higher radiation doses due to their soft tissue capabilities with doses of 1200 microSieverts and higher per each scan, depending on the selected scan field.

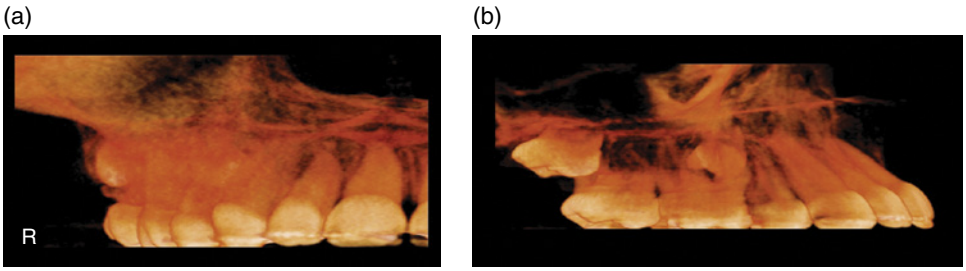

Figure 1.1. (a) 3D rendering of a small FOV of 5 cm×8 cm from an anteroposterior (AP) view; (b) 3D rendering of a small FOV of 5 cm×8 cm from a lateral view.

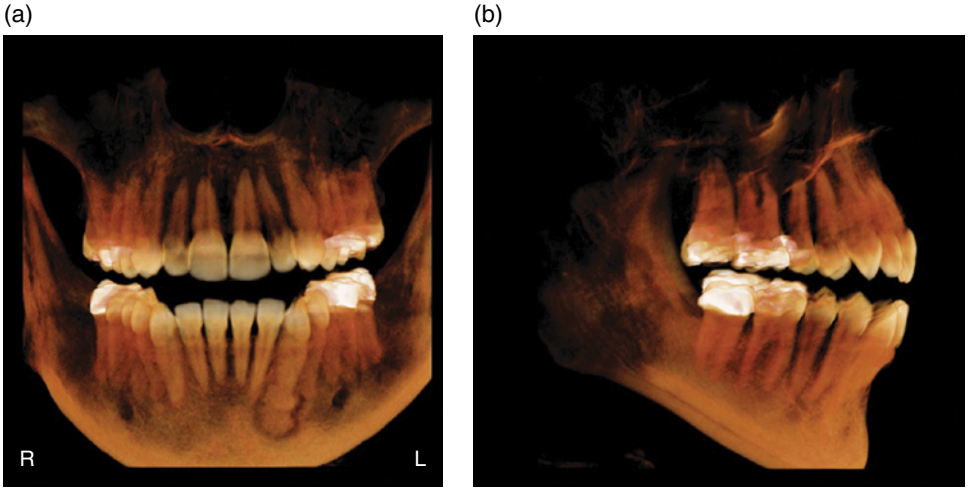

Figure 1.2. (a) 3D rendering of a medium FOV of 8 cm×8 cm from an anteroposterior (AP) view; (b) 3D rendering of a medium FOV of 8 cm×8 cm from a lateral view.

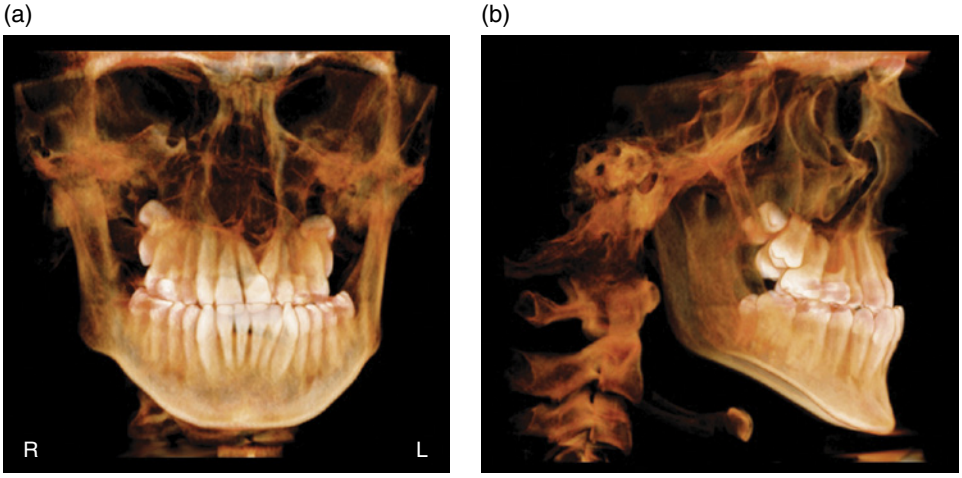

Figure 1.3. (a) 3D rendering of a large FOV of 16 cm×16 cm from an anteroposterior (AP) view; (b) 3D rendering of a large FOV of 16 cm×16 cm from a lateral view.

Viewing CBCT Data

Multiplanar Reformation (MPR)

Multiplanar reformation, or MPR, is a view frequently of three different directional 2D images (axial, coronal, and sagittal planes) (Figure 1.4). Within this view, the images may be manipulated in the thickness of data, and direction of viewing can be altered. Reconstructed pantomographs and lateral cephalometric skulls (Figures 1.5 and 1.6) are possible without distortion from standard 2D radiography. The dataset may also be manipulated to create cross-sectional (orthogonal) views of the jaws and condyles (Figures 1.7 and 1.8).

3D Rendering

The most common form of 3D rendering offered in CBCT software is indirect volume rendering, which determines the grays of the voxels to create a 3D image (Figure 1.9). Another form of 3D rendering is referred to as direct volume rendering, or maximum intensity projection (MIP) (Figure 1.10).

Figure 1.4. Axial (A), sagittal (S), and coronal (C) views.

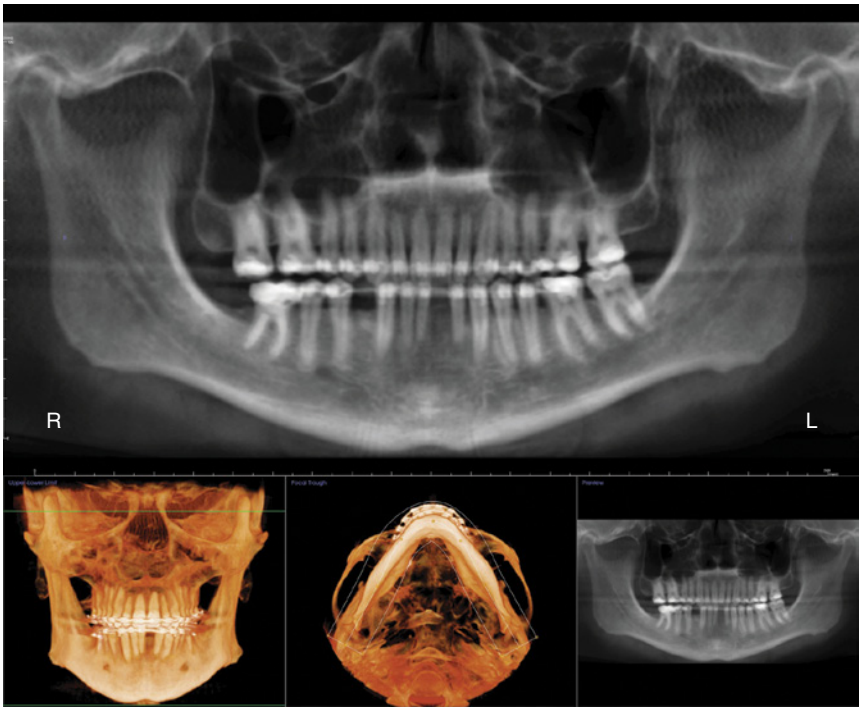

Figure 1.5. Sample reconstructed pantomograph with 3D view on bottom left, focal trough bottom middle, and preview on bottom right.

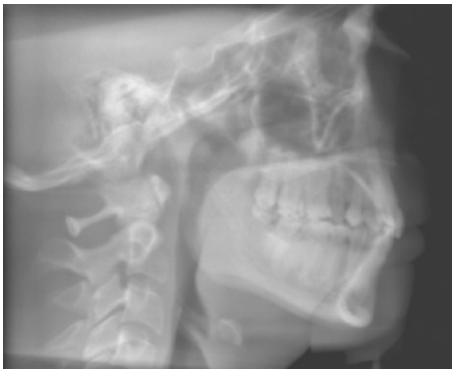

Figure 1.6. Sample reconstructed lateral cephalometric skull.

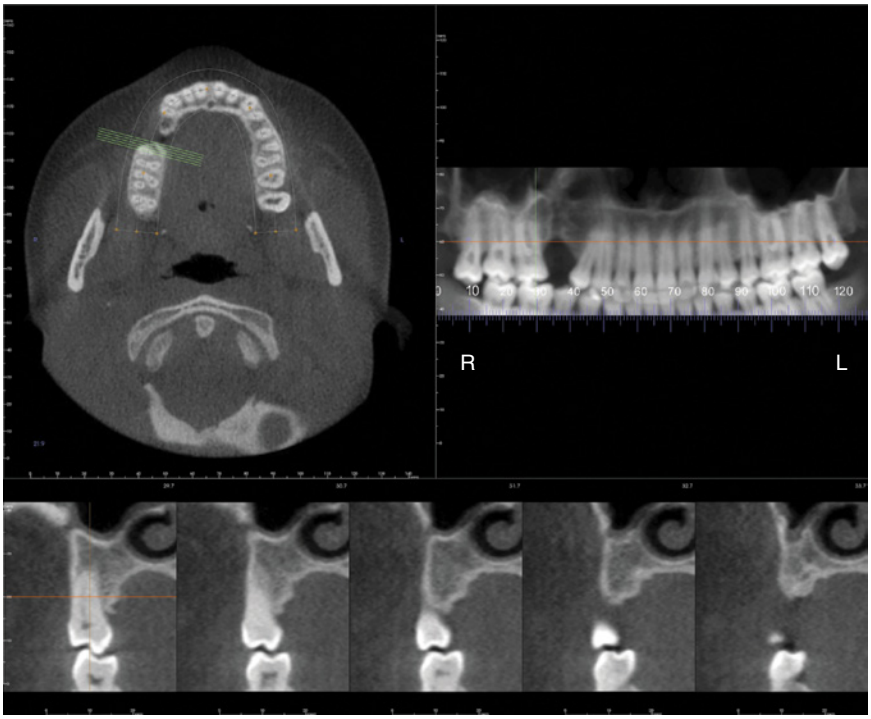

Figure 1.7. Sample cross-sectional slices with axial view and reconstructed pantomograph.

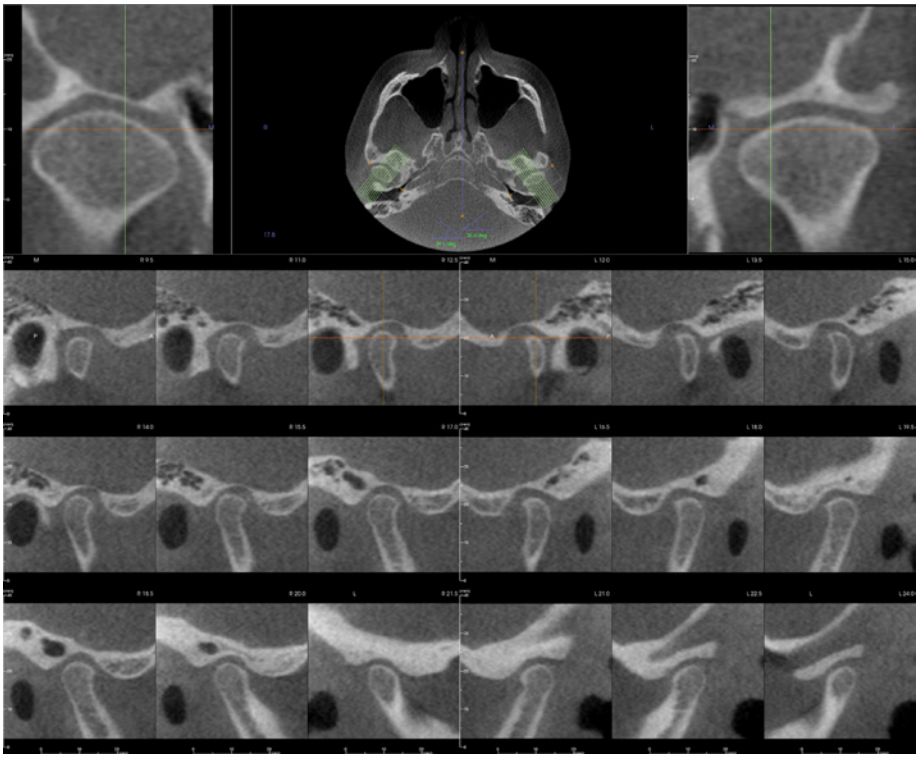

Figure 1.8. Sample temporomandibular joint view with cross-sectional slices.

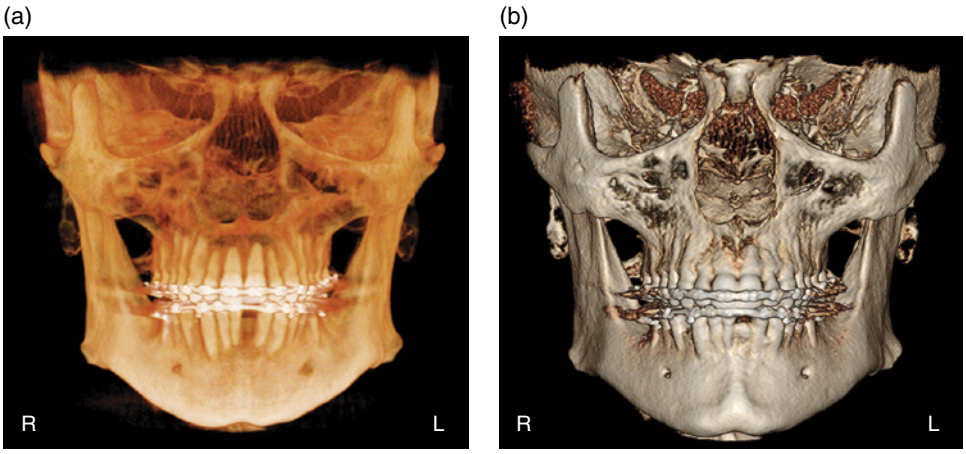

Figure 1.9. (a) 3D rendered view with teeth setting; (b) 3D rendered view with bone setting.

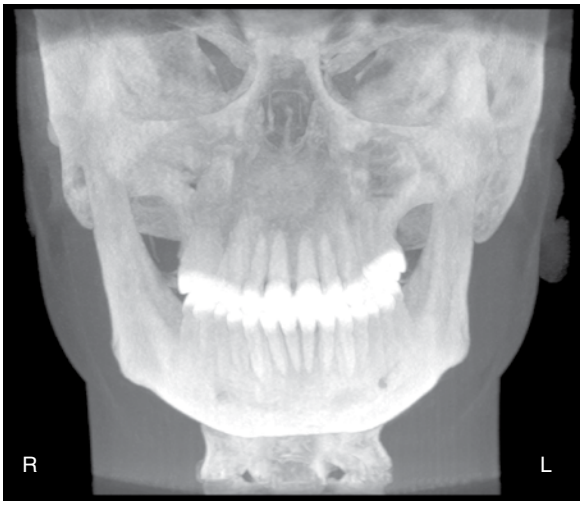

Figure 1.10. MIP view.

Artifacts

Streak Artifacts/Undersampling

Streak artifacts occur when an object with high density (such as metallic restorations) creates areas of undersampling where no viable information is recorded (Figure 1.11). Care should be taken not to interpret anything in the streak. Aliasing is another form of undersampling, when too few images are acquired and appear as small lines throughout a scan (Figure 1.12).

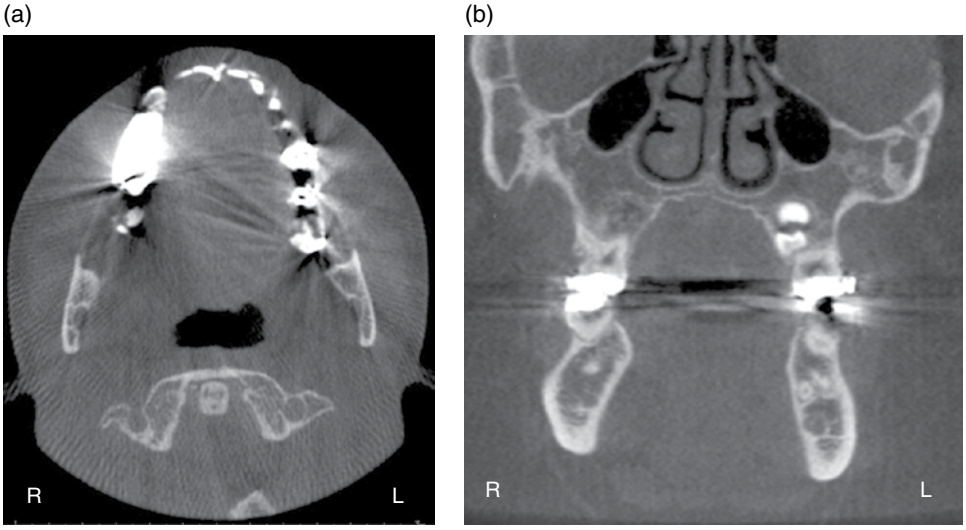

Figure 1.11. (a) Axial view showing streak artifact due to metallic restorations in a linear pattern radiating out from the restorations; (b) Coronal view showing streak artifact due to metallic restorations as multiple horizontal lines obscuring the image at the level of the restorations.

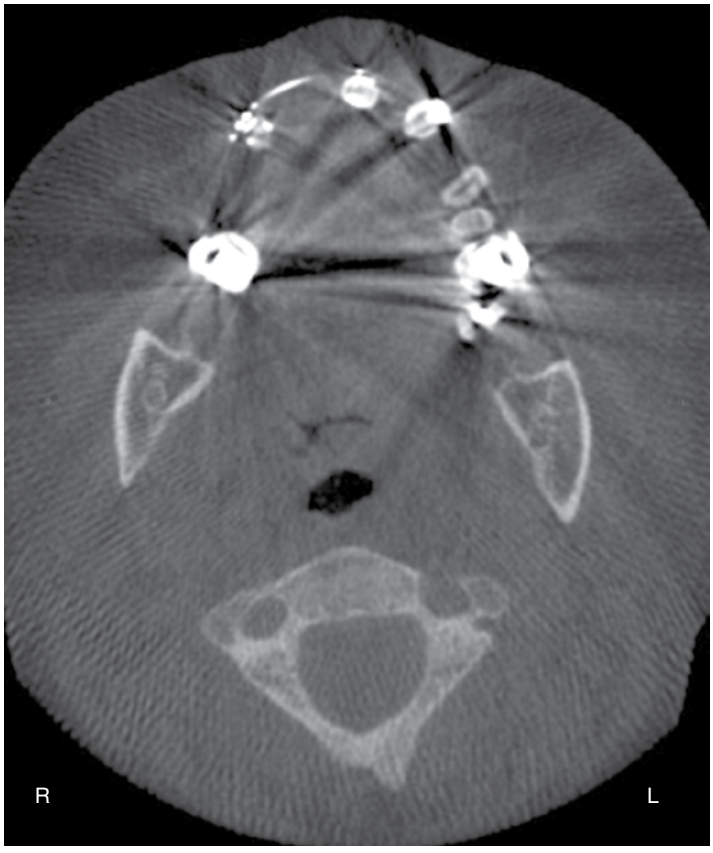

Figure 1.12. Axial view with metallic streak artifact and aliasing of scan as linear radiolucent lines throughout the entire image.

Figure 1.13. (a) Sagittal and (b) axial views showing motion artifact of the cervical vertebrae (black arrow).

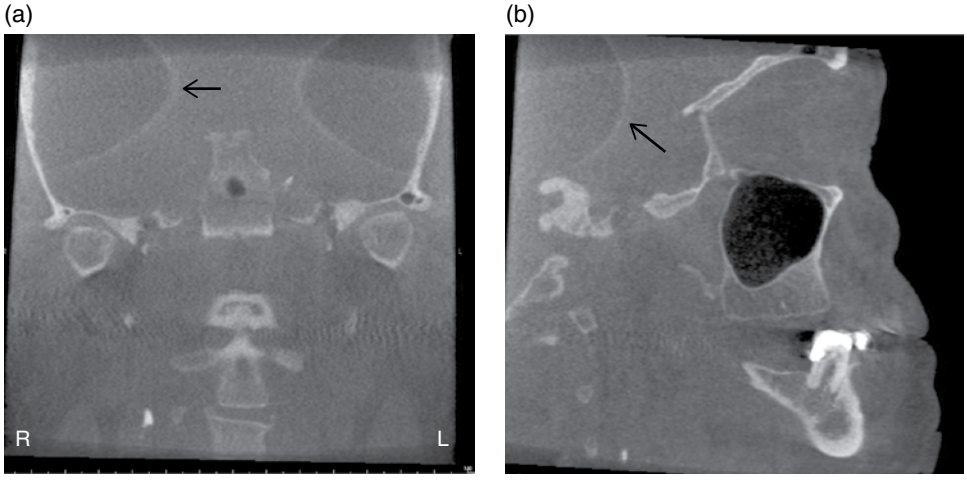

Figure 1.14. (a) Coronal and (b) sagittal views showing white ring artifacts (black arrow).

Motion Artifacts

Motion artifacts occur due to either normal pathophysiological movement or when the patient moves during a scan. This presents as ill-defined edges ranging from a blurring of the edge of an object to multiple visible edges evident (Figure 1.13). This can be minimized by restraining the patient's head and using as short a scan time as possible.

Ring Artifacts

Ring artifacts present as white or black circular artifacts. They typically indicate poor calibrations and imperfections in the scanner detection (Figure 1.14).

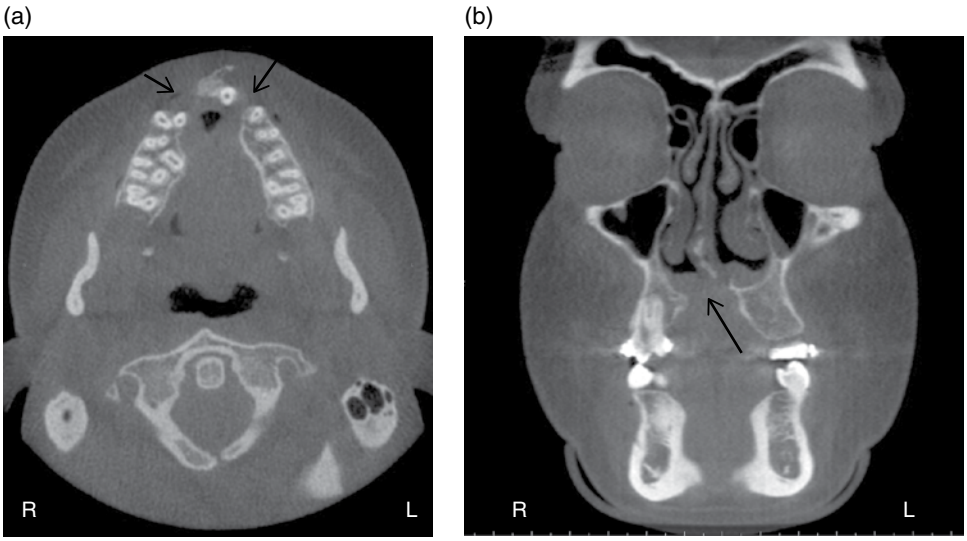

Figure 1.15. (a) Axial view showing a bilateral cleft palate case (black arrows); (b) Coronal view showing discontinuity of nasal cavity associated with cleft palate (black arrow).

Common Uses

Developing Dentition

Cleft Palate and Bone Graft Assessment

CBCT imaging has shown limited research that scans are reliable when determining the bony dimensions of a cleft palate (Figure 1.15). Cleft palate cases are recommended for CBCT imaging, as 2D radiographs cannot show facial-lingual dimensions of a defect. This additional information is helpful to a surgeon especially prior to bone grafting and helpful to an orthodontist prior to movement of teeth near the defect. Axial views are recommended to determine the bone quantity surrounding roots of teeth adjacent to the cleft. The FOV recommended is one large enough to see the entire cleft and portions of the nasal cavity for the surgeon to have all the information necessary. The recommended voxel size is 0.3 mm or larger, so as to reduce the overall radiation exposure since these scans are typically made on growing children.

Localization of Impacted Teeth

The most commonly impacted teeth are third molars and maxillary canines. CBCT imaging provides additional information about third molar location in relation to either the maxillary sinus or mandibular canal (Figures 1.16 and 1.17). CBCT imaging provides exact locations of impacted canines and the presence or absence of external root resorption of adjacent teeth (Figures 1.18 and 1.19). Cross-sectional views are recommended to determine exact facial-lingual width and

(a)

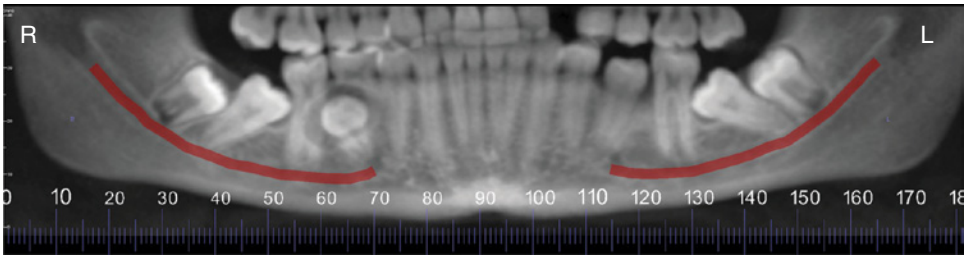

(b)

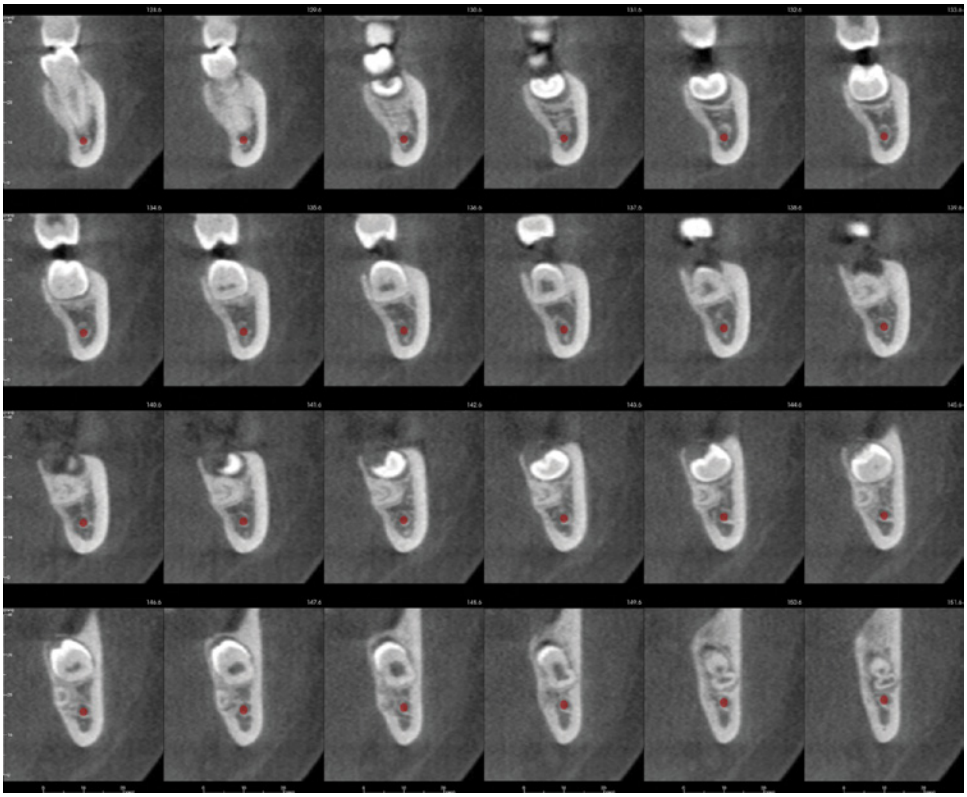

Figure 1.16. (a) Reconstructed pantomograph showing impacted mandibular third molars and mandibular canal noted in red; (b) Cross-sectional slices with 1.0 mm spacing showing location of impacted mandibular left third molar in relation to the mandibular canal (red circle).

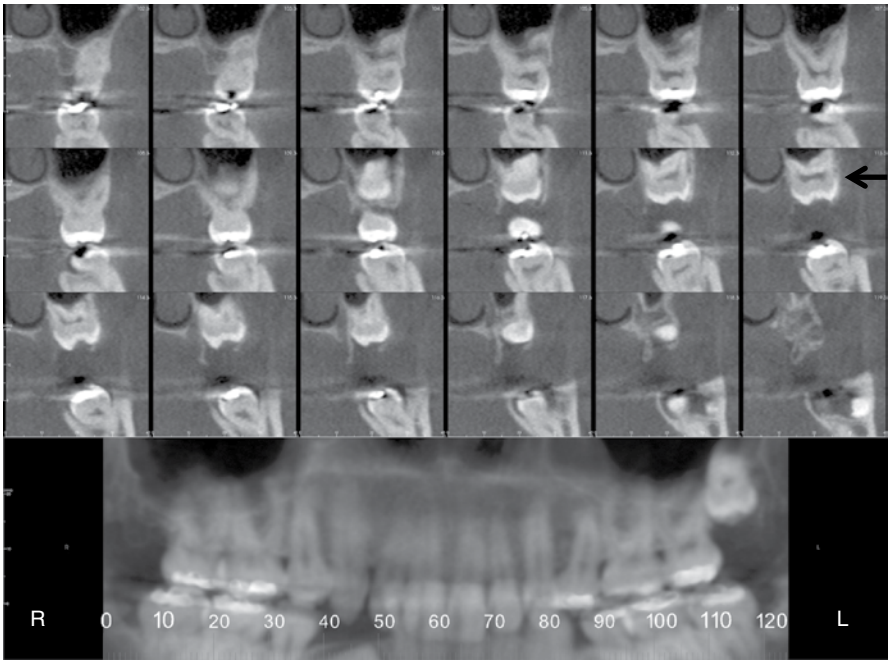

Figure 1.17. Reconstructed pantomograph and cross-sectional slices showing location of impacted maxillary left third molar (black arrow) in relation to the maxillary sinus.

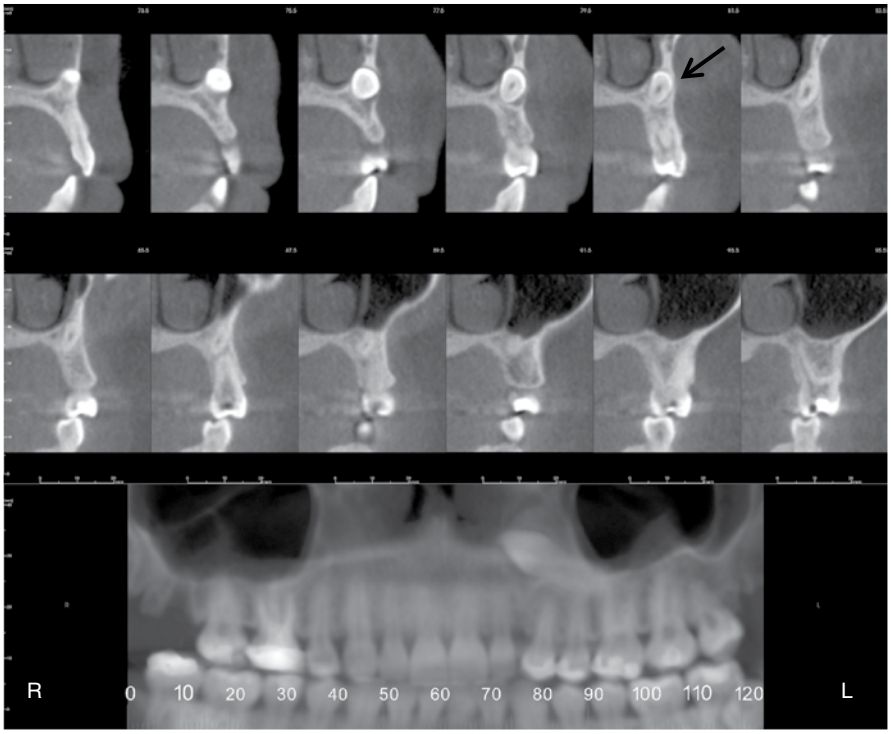

Figure 1.18. Reconstructed pantomograph and cross-sectional slices showing location of an impacted maxillary canine (black arrow).

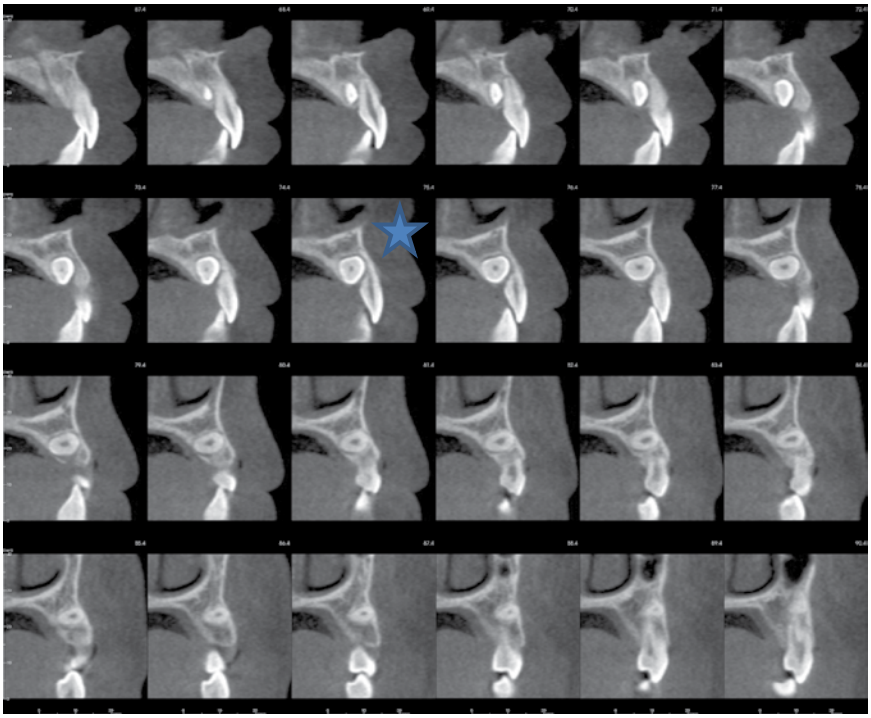

Figure 1.19. Cross-sectional slices of an impacted maxillary canine with external resorption on the lingual aspect of the lateral incisor (blue star).

effect on adjacent teeth. The FOV recommended is one large enough to capture the tooth or teeth in question and surrounding bone and anatomical structures. A voxel size of 0.3 mm is recommended to produce a quality scan with overall low radiation doses to the patient.

Restoring the Dentition

Periapical Pathosis

CBCT imaging has increased sensitivity in the detection of periapical pathosis (Figure 1.20) compared to 2D radiographs. In the presence of clinical signs with the absence of 2D radiographic findings, a CBCT may be recommended to rule out or rule in possible periapical pathosis. It is important to thoroughly check all the teeth on a scan as early periapical pathosis has been noted on CBCT prior to detection on 2D radiographs. Sagittal and cross-sectional views are the recommended views for detecting periapical pathosis. The FOV recommended is dependent on how many teeth you want to evaluate. A single tooth only needs a small FOV; however multiple teeth throughout both jaws will need a medium FOV or larger. A voxel size of 0.2 mm or less is recommended.

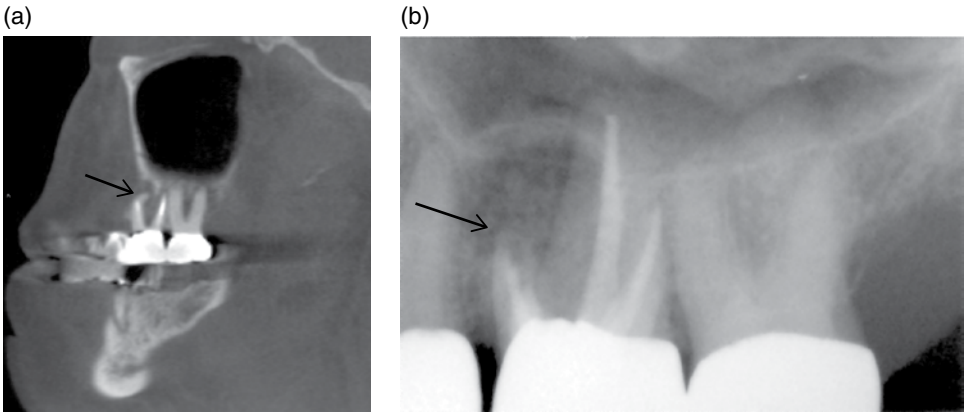

Figure 1.20. (a) Sagittal view showing a distal dilaceration of the mesiobuccal root of the maxillary first molar with a short endodontic filling and rarefying osteitis (black arrow); (b) Periapical radiograph showing a resulting apicoectomy (black arrow) after the findings on the CBCT scan.

Root Fractures

Vertical root fractures are difficult to diagnose on 2D radiographs, typically presenting as a J-shaped lesion around the root with the fracture. CBCT imaging has shown increased sensitivity in detecting vertical and horizontal root fractures (Figures 1.21 and 1.22). One large concern when evaluating for fractures is teeth that have been endodontically treated, as the filling material can cause artifacts leading to small fractures to be obscured. Coronal, sagittal, and cross-sectional views are the recommended views for detecting vertical root fractures. Axial views are the recommended views for detecting horizontal root fractures. The FOV recommended is a small one to include the tooth in question. If more than one tooth is in question and both cannot be visualized on a single small FOV scan, a larger FOV should be used. A voxel size of 0.2 mm or less is recommended.

Surgical Applications

Bony Pathosis

There are various bony lesions that present throughout the jaws (Figures 1.23 and 1.24). CBCT imaging provides additional information about the exact location and possible nature of a bony lesion prior to removal or biopsy. All views (axial, coronal, sagittal, and cross-sectional) are recommended to completely grasp the size, position, and nature of a lesion. The FOV recommended is one large enough to capture the area in question. A voxel size of 0.3 mm is recommended to keep radiation doses to the patient low.

Implants

Quantity of bone, alveolar ridge morphology, maxillary sinus location, and mandibular canal location are important information prior to placing an implant. Standard 2D radiographs can provide the height of bone available but does not show whether there are ridge defects or concavities (Figures 1.25 and 1.26). CBCT imaging provides

(a)

(b)

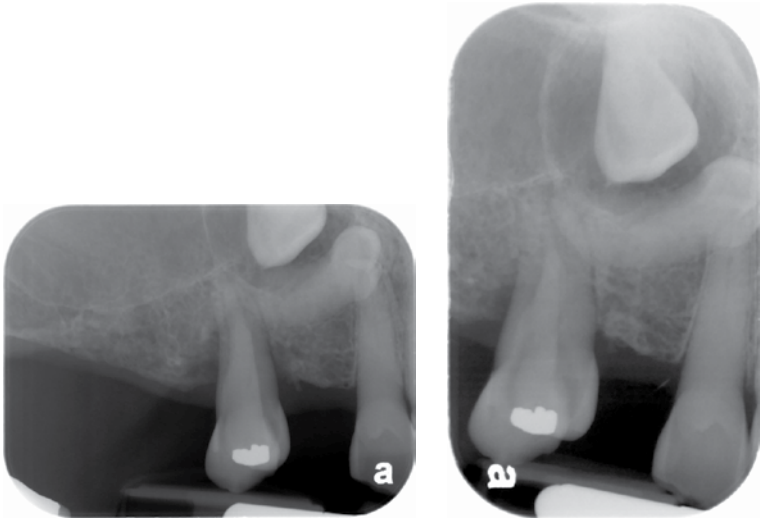

(c)

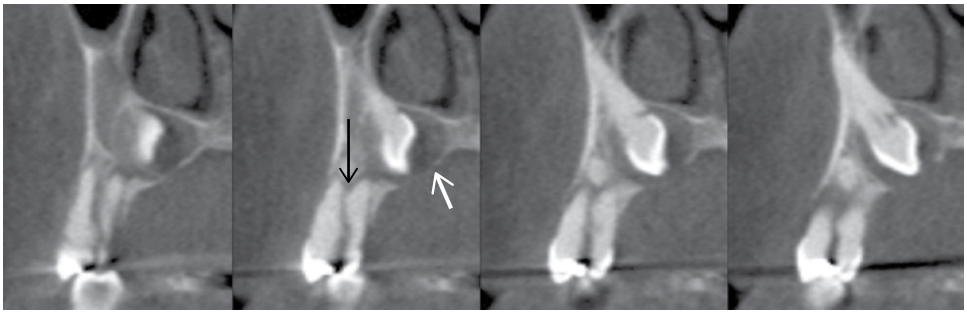

Figure 1.21. (a) Pantomograph and (b) periapical radiographs showing impacted first premolar and canine with a dentigerous cyst; (c) Cross-sectional slices showing a vertical root fracture on the maxillary right second premolar (black arrow) and dentigerous cyst associated with impacted canine (white arrow).

(a)

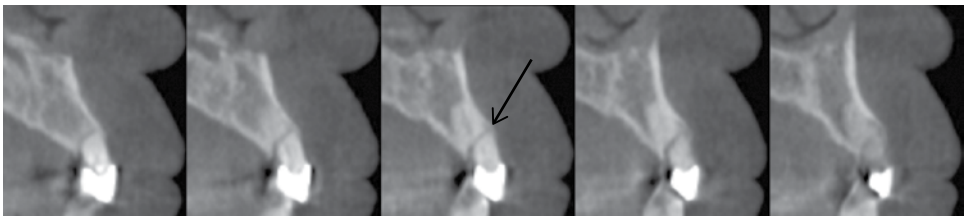

(b)

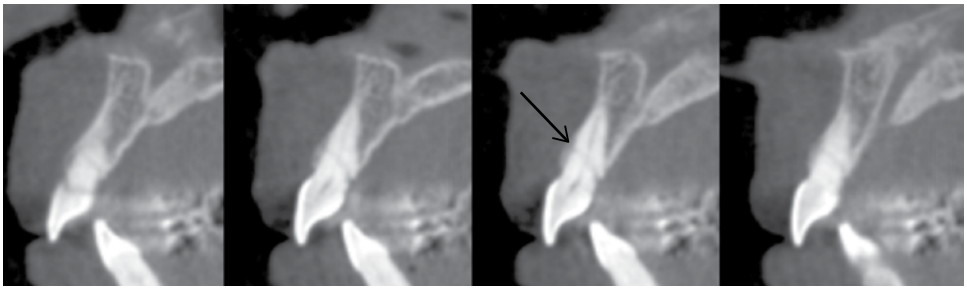

Figure 1.22. Cross-sectional slices (a,b) showing horizontal root fractures (black arrows).

(a)

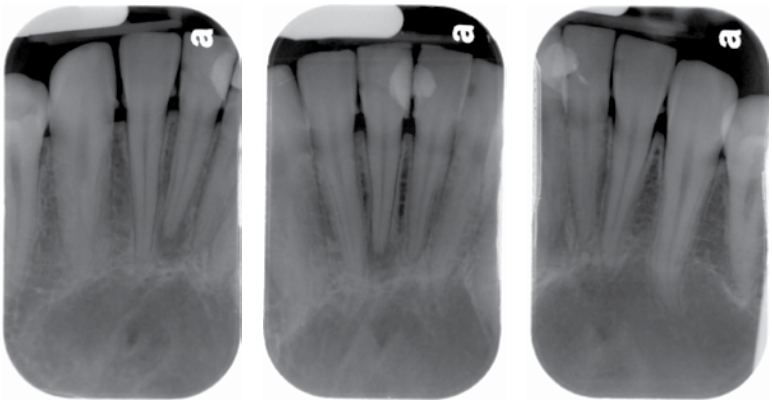

(b)

Figure 1.23. (a) Periapical and (b) pantomograph radiographs showing an odontogenic myxoma in the anterior mandible.

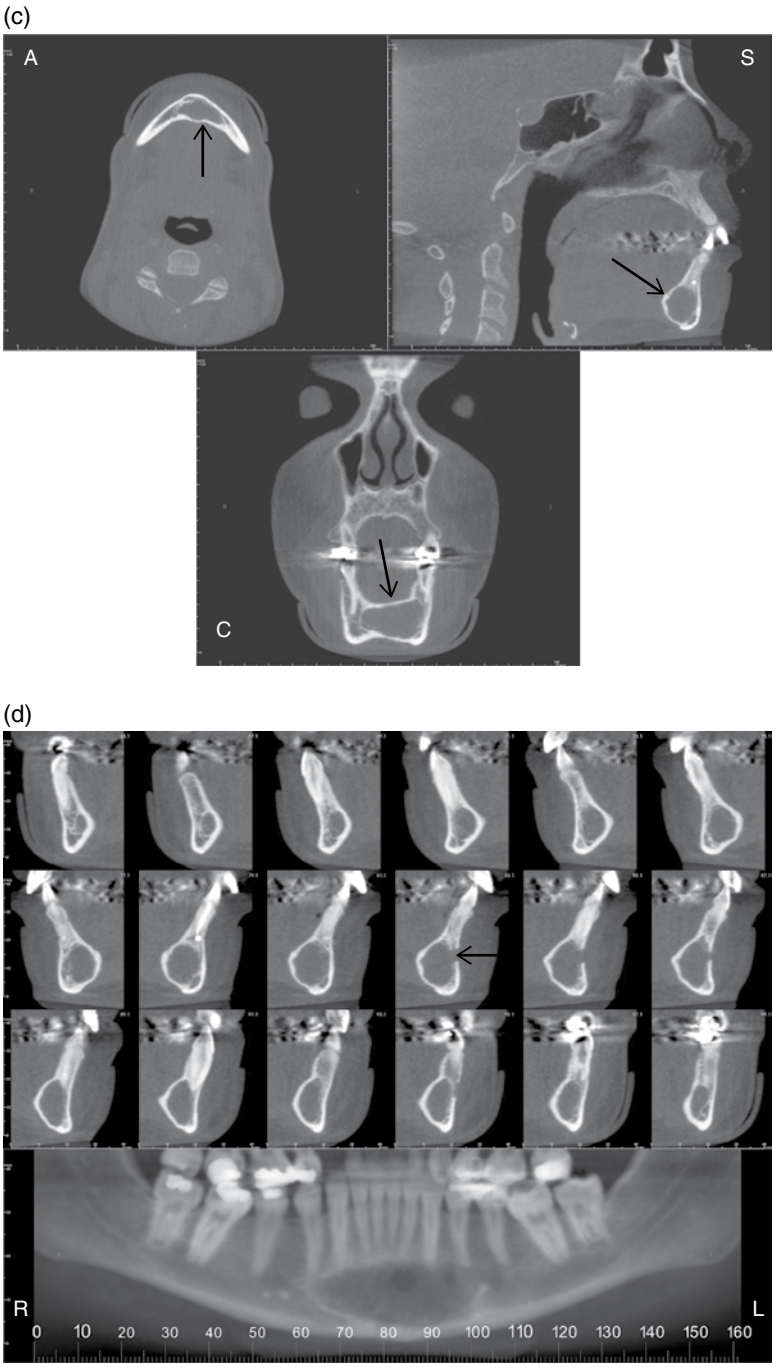

Figure 1.23. (*continued*) (c) Axial (A), sagittal (S), and coronal (C) views showing extent of bone loss (black arrows); (d) Reconstructed pantomograph and cross-sectional slices showing width of odontogenic myxoma. Bone discontinuity on the facial from a prior incisional biopsy (black arrow).

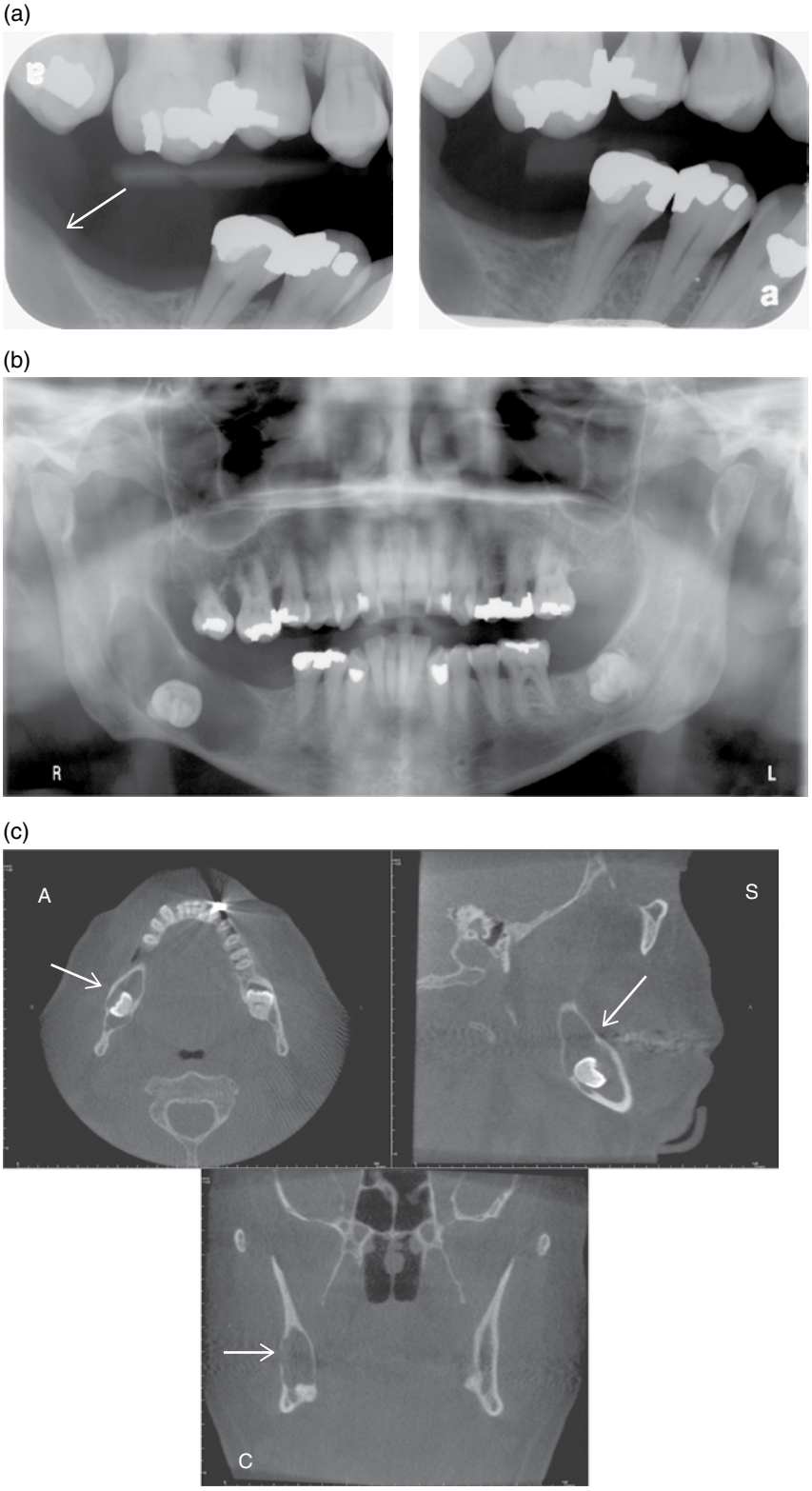

Figure 1.24. (a) Bitewing radiographs and (b) pantomograph showing bone loss with impacted mandibular right third molar consistent with a dentigerous cyst (white arrow); (c) Axial (A), sagittal (S), and coronal (C) views showing extent of bone loss (white arrows).

(d)

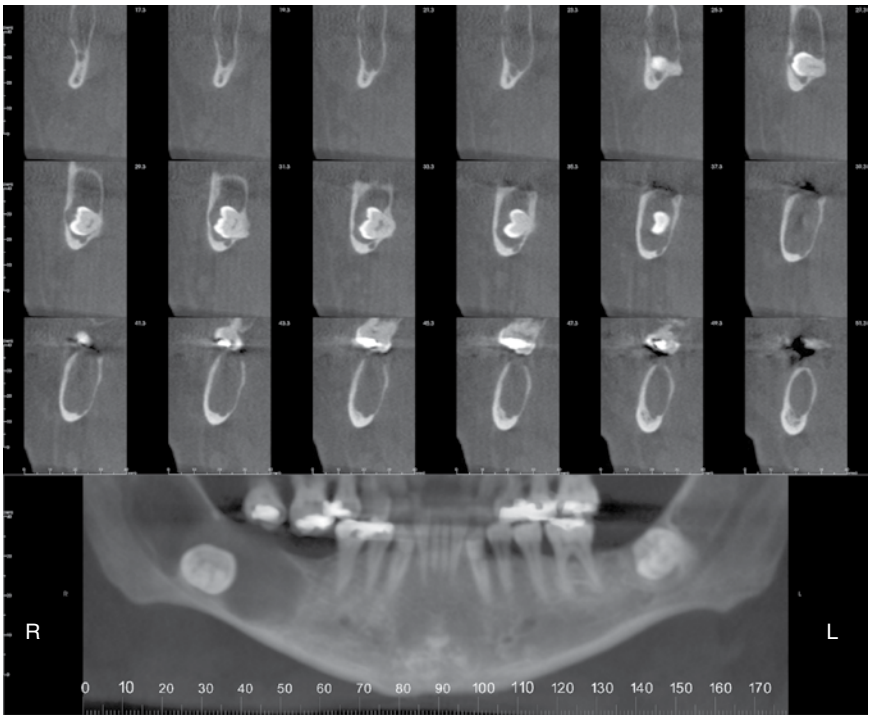

Figure 1.24. (*continued*) (d) Reconstructed pantomograph and cross-sectional slices showing width of dentigerous cyst.

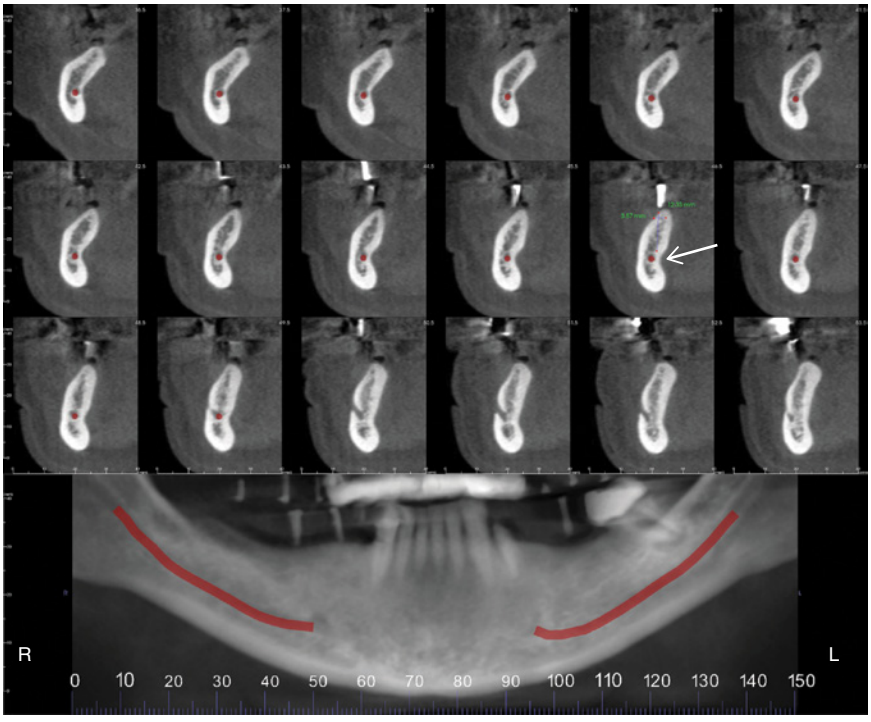

Figure 1.25. Reconstructed pantomograph and cross-sectional slices showing lingual concavity in posterior mandible (white arrow) and mandibular canal noted in red.

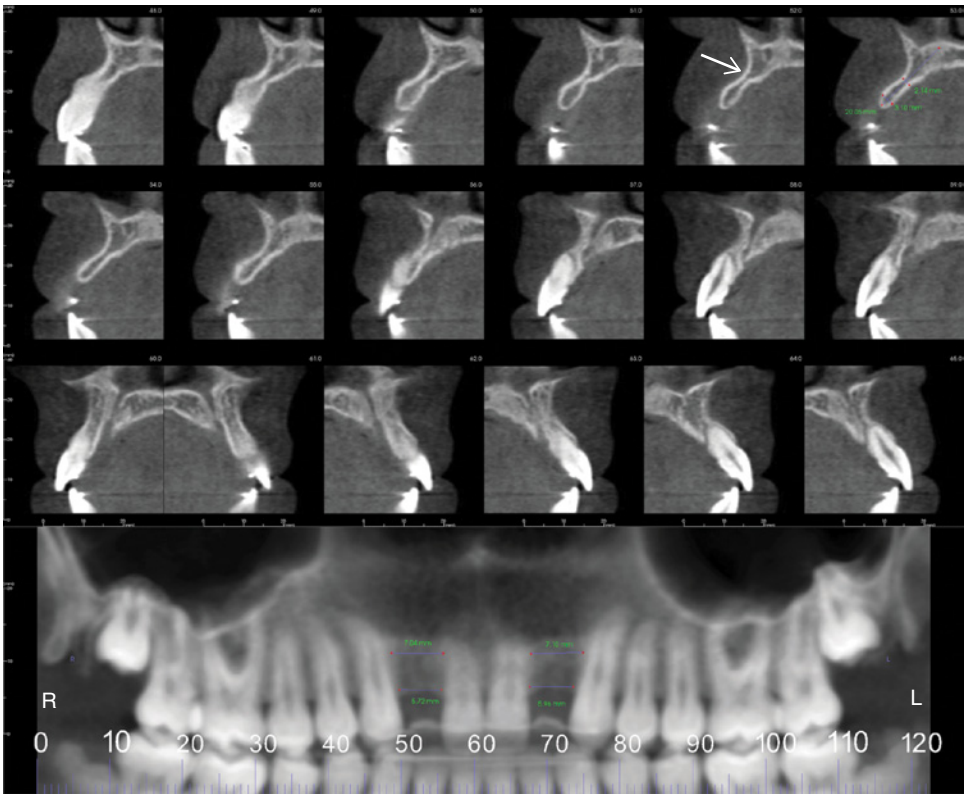

Figure 1.26. Reconstructed pantomograph and cross-sectional slices showing facial concavity in anterior maxilla (white arrow).

information on these things to ensure implant placement within the bone and not surrounding soft tissues. Cross-sectional views are recommended to view the facial-lingual width and morphology of the alveolar ridge. A voxel size of 0.3 mm is recommended to keep the radiation doses to the patient low.

References

Conventional Computed Tomography and Cone Beam Computed Tomography

Dalrymple, N. C., Prasad, S. R., El-Merhi, F. M., et al. (2007). Price of isotropy in multidetector CT. *RadioGraphics*, **27**, 49–62.

Hounsfield, G. (1973). Computerized transverse axial scanning (tomography). 1. Description of the system. *Br J Radiol*, **46**, 1016–22.

Miles, D. E. (2008). *Color Atlas of Cone Beam Volumetric Imaging for Dental Applications*. Quintessence.

Popat, H., Drage, N., Durning, P. (2008). Mid-line clefts of the cervical vertebrae—an incidental finding arising from cone beam computed tomography of the dental patient. *British Dental Journal*, **204**, 303–6.

White, S. C., and Pharoah, M. J. (2008). *Oral Radiology: Principles and Interpretation*. Mosby.

Viewing CBCT Data

White, S. C., and Pharoah, M. J. (2008). *Oral Radiology: Principles and Interpretation*. Mosby.

Artifacts

Popilock, R., Sandrasagaren, K., Harris, L., et al. (2008). CT artifact recognition for the nuclear technologist. *J Nucl Med Technol*, **36**, 79–81.
White, S. C., and Pharoah, M. J. (2008). *Oral Radiology: Principles and Interpretation*. Mosby.
Zoller, J. E., and Nuegebauer, J. (2008). *Cone-beam Volumetric Imaging in Dental, Oral, and Maxillofacial Medicine*. Quintessence, Germany.

Common Uses

Chakravarthy, P. V. K., Telang, L. A., Nerali, J., et al. (2012). Cracked tooth: A report of two cases and role of cone beam computed tomography in diagnosis. *Case Reports in Dentistry*, **2012**, 525364.
Durack, C., and Patel, S. (2012). Cone beam computed tomography in endodontics. *Braz Dent J*, **23** (3), 179–91.
Joint Position Paper AAE and AAOMR (http://c.ymcdn.com/sites/www.aaomr.org/resource/resmgr/Docs/AAOMR-AAE_postition_paper_CB.pdf).
Kapila, S., Conley, R. S., Harrell Jr, W. E. (2011). The current status of cone beam computed tomography imaging in orthodontics. *Dentomaxillofac Radiol*, **40** (1), 24–34.
Nah, K. S. (2012). Condylar bony change in patients with temporomandibular disorders: A CBCT study. *Imaging Sci Dent*, **42** (4), 249–53.
Neves, F. S., Souza, T. C., Almeida, S. M., et al. (2012). Correlation of panoramic radiography and cone beam CT findings in the assessment of the relationship between impacted mandibular third molars and the mandibular canal. *Dentomaxillofac Radiol*, **41** (7), 553–57.
Quereshy, F. A., Barnum, G., Demko, C., et al. (2012). Use of cone beam computed tomography to volumetrically assess alveolar cleft defects—preliminary results. *J Oral Maxillofac Surg*, **70** (1), 188–91.
Rossini, G., Cavallini, C., Cassetta, M., et al. (2012). Localization of impacted maxillary canines using cone beam computed tomography. Review of the literature. *Ann Stomatol (Roma)*, **3** (1), 14–18.
Tsai, P., Torabinejad, M., Rice, D., et al. (2012). Accuracy of cone-beam computed tomography and periapical radiography in detecting small periapical lesions. *J Endod*, **38** (7), 965–70.

2 Legal Issues Concerning Cone Beam Computed Tomography

Shawneen M. Gonzalez

Introduction

This chapter will cover the standard of care and recommendations about cone beam computed tomography use in dentistry. The topics covered include specific recommendations from both American and European oral and maxillofacial radiological societies broken into three separate categories: prescription, use, and interpretation. Legal issues regarding cone beam computed tomography are largely recommendations to date, as there have been no major legal cases involving cone beam computed tomography as of the writing of this book.

Standard of Care

Standard of care is the base level at which a dentist must perform specific duties, including but limited to endodontic procedures, restorative procedures and diagnosis and treatment planning. If a health care professional performs below this level, it is considered malpractice and negligence. Violations of the standard of care can result in a loss of licensure and monetary repercussions for the dental professional.

There are two primary legal cases involving technology and standard of care: *Frye v. United States (1923)* and *Daubert v. Merrell Dow (1993)*. In 1993 the United States Supreme Court dismissed the *Frye* mandate that technology is admissible in court as long as it has "general acceptance" in the scientific community. Even though this ruling rejected the *Frye* mandate on a federal level, there are still several states that continue to follow *Frye*'s test for admission of technology as standard of care.

Interpretation Basics of Cone Beam Computed Tomography, First Edition.
Edited by Shawneen M. Gonzalez.

For those states following *Frye*'s standard, an expert in the field is tapped to determine if the technology has become "general acceptance" for the field in question. The ruling of *Daubert* determined that "scientific knowledge must be derived from the scientific method supported by good grounds in validating the expert's testimony, establishing a standard of evidentiary reliability" (Stevens).

Recommendations

American Academy of Oral and Maxillofacial Radiology and American Dental Association Recommendations

The American Academy of Oral and Maxillofacial Radiology (AAOMR) came out with recommendation in 2008 about the use of cone beam computed tomography (CBCT). Since then, they have come out with more recommendations in specific areas such as implants and endodontics. This chapter will cover only the original basic recommendations, as the others are noted in Chapters 1 (introduction) and 9 (implants). The American Dental Association (ADA) came out with several recommendations about CBCT in 2012. These recommendations apply to those offices that have a CBCT unit as well as those offices that refer out for this procedure. Because there is overlap of the recommendations, I have combined them as recommendations made for the United States of America.

Prescribing a Cone Beam Computed Tomography Scan

There are several things a referring practitioner must perform and consider prior to prescribing a CBCT scan.

1. Review the patient's medical and dental history along with performing a thorough clinical exam. Documentation of these procedures and justification that the excess radiation will result in a benefit outweighing the radiation risk must be included in the patient's chart prior to prescribing a scan.
2. Determine if standard 2D radiographic images show or do not show the area in question to the extent they need.
3. Have basic knowledge and education in CBCT imaging to understand what the scan will or will not show. The ADA recommends using evidence-based articles and continuing education courses to understand cone beam CT basics.

Use of Cone Beam Computed Tomography Scan

These recommendations apply to offices and/or imaging centers that have a CBCT unit or are planning to purchase one.

1. Prior to installing a CBCT in your office, a health physicist should be consulted to determine the desired location of the machine has adequate shielding based on the machine perimeters (kVp, mA, and exposure times). The health physicist will also ensure that the office is in compliance with federal and/or state radiation regulations. The evaluation schedule will be determined by state and/or federal radiation regulations.

2. After a CBCT unit is installed, proper training and education on safe use when performing scans must be achieved by all dental professionals who will be operating the machine. This is typically done by the company of the CBCT unit. After an office is trained on safe use of a CBCT unit, it should create a quality-control program including an evaluation interval to determine the machine is operating at the specified settings.
3. The CBCT unit must be operated by either a licensed practitioner or certified radiologic operator. This will be different for every state/country. In certain states and countries, a CBCT may be either classified as a dental x-ray unit or a medical x-ray unit. For those areas where it is labeled as a dental x-ray unit, any dental professional that is legally allowed to expose a patient to radiation can operate the cone beam CT unit. For those areas where it is labeled as a medical x-ray unit, only a licensed radiologic technician or licensed dentist or physician may operate the machine.
4. The imaging site should always be in compliance with ALARA (as low as reasonably achievable). The office should apply this by using the smallest field of view (FOV) with the shortest exposure time to show the entire area in question. The office should also use thyroid collars and lead aprons as long as they don't interfere with the area being scanned.
5. Offices with a cone beam CT unit should be continually learning about cone beam CT and radiation safety. Technology is consistently changing and the applications of this technology are also changing. An office must stay current to determine the best possible way to manage this new technology so as to aid in its patient care.

Interpretation of a Cone Beam Computed Tomography Scan

There are several recommendations regarding the interpretation of a CBCT scan.

1. The referring practitioner is responsible to interpret the findings of the entire scan and generate a report of the findings. The practitioner is held to the same level as a board certified oral and maxillofacial radiologist. The scan may be interpreted by an oral and maxillofacial radiologist to aid the referring practitioner. Should the scan be interpreted by an oral and maxillofacial radiologist, an issue of licensure and malpractice insurance coverage needs to be determined. In many states, a practitioner must be licensed to practice dentistry in that state. This includes oral and maxillofacial radiologists performing CBCT interpretations for dentists (Friedland 2009).

   For example, we will look at a sample (fictional) case involving the state of Nebraska. Nebraska is a state where the radiologist must be licensed if the patient is being treated by a dentist in the state of Nebraska. If a patient being treated in Nebraska receives a CBCT scan and an oral and maxillofacial radiologist, who is licensed to practice dentistry in the state of Nebraska, performs the interpretation and sends it back to the referring dentist, it complies with the state law and the interpretation (radiology report) would be admissible in a court of law. If the interpretation is performed by an oral and maxillofacial radiologist who is not licensed to practice dentistry in the state of Nebraska,

the court could chose to suppress the interpretation (radiology report), as it could be interpreted as an illegal practice of dentistry in the state of Nebraska. The oral and maxillofacial radiologist malpractice insurance should be determined as to which states they will cover the radiologist providing interpretations to. A dentist who refers out for an interpretation (radiology report) should determine with their malpractice insurance what CBCT scans would or would not be covered in their policy.

2. All CBCT scans should be evaluated by a dentist with training and education in CBCT interpretation. The entire captured CBCT scan must be interpreted and all findings put in the patient's chart. It is the responsibility of the referring dentist to inform the patient of the findings both normal and abnormal.

European Academy of DentoMaxilloFacial Radiology Basic Principles

In 2011, the European Academy of DentoMaxilloFacial Radiology (EADMFR) came out with 20 recommendations about CBCT use in dentistry. The recommendations are very similar to those from the stated previously.

Prescribing a Cone Beam Computed Tomography Scan

1. The referring practitioner must review the patient's history and perform a thorough clinical exam. Documentation of these procedures and justification that the excess radiation will result in a benefit outweighing the radiation risk must be included in the patient's chart prior to prescribing a scan.
2. The referring practitioner should have basic knowledge of CBCT and be aware that a CBCT scan will potentially add new information and aid in the management of the patient.
3. The referring practitioner must use CBCT only when lower-dose traditional 2D radiography does not provide the information necessary to manage a patient.
4. A referring practitioner should not "routinely" prescribe CBCT scans without determining a risk/benefit for each specific scan.
5. If soft tissues are in question, a conventional CT or MRI should be requested instead of a CBCT.

Use of Cone Beam Computed Tomography Scan

1. When a new CBCT unit is being installed in an office, it should be tested to ensure radiation protection is optimal.
2. A quality assurance program must be created for offices with a CBCT unit. The unit must be routinely tested to ensure proper radiation protection for patients and office members.
3. The guidelines in Section 6 of *Radiation Protection 136, European Guidelines on Radiation Protection in Dental Radiology* (European Academy DentoMaxilloFacial Radiology) should be followed.

4. All who will be operating the CBCT unit must have theoretical and practical training in radiation protection. Continued education on CBCT and radiation protection is required. Those offices that have not received adequate training should undergo additional training involving a dentomaxillofacial radiologist.
5. The CBCT unit should have a variety of fields of view and resolution options. The smallest field of view should be used with the lowest amount of radiation necessary to capture the area in question.
6. When positioning a patient, positioning lights must be used.
7. If other dentists refer to your office for a CBCT, they must provide you with adequate clinical information regarding the patient's history and examination.

Interpretation of a Cone Beam Computed Tomography Scan

1. All CBCT scans must have a thorough clinical evaluation (radiological report) made of the entire dataset.
2. When a CBCT scan involves the mandible and maxilla up to the floor of the nose, a radiological report should be made by a trained dentomaxillofacial radiologist or, when this is not possible, an adequately trained general dentist.
3. When a CBCT scan involving large fields of view and/or anatomy beyond the teeth and jaws, a radiological report should be made by a trained dentomaxillofacial radiologist or medical radiologist.

Summary

In summarizing this chapter, it is best to use a quote by Edwin Zinman, DDS, JDS, a California attorney, who stated in a DrBicuspid.com article, "There is no average patient. If a lesion is present on a cone-beam CT scan, then for that individual patient their statistic is 100%. Consequently, 100% of cone-beam CT scans must be diagnosed for pathosis 100% of the time by viewing 100% of cone-beam CT scanned images."

References

American Academy of Oral and Maxillofacial Radiology (2008). Executive opinion statement on performing and interpreting diagnostic cone beam computed tomography. *Oral Surg Oral Med Oral Pathol Oral Radiol Endod*, **106** (4), 561–62.

American Dental Association Council on Scientific Affairs (2012). The use of cone beam computed tomography in dentistry; An advisory statement from the American Dental Association Council on Scientific Affairs. *JADA*, **143** (8), 899–902.

Curley, A. and Hatcher, D. C. (2009). Cone beam CT—anatomic assessment and legal issues: The new standards of care. *CDA Journal*, **37** (9), 653–62.

Daubert v. Merrell Dow Pharmaceuticals, 509 U.S. 579 (1993).

European Academy Dentomaxillofacial Radiology. Guidelines. http://eadmfr.info/sedentexct.

European Academy Dentomaxillofacial Radiology. Radiation Protection Guidelines. Ec.europa.eu/energy/nuclear/radioprotection/publication/doc/136_en.pdf.

Friedland, B. (2009). Medicolegal issues related to cone beam CT. *Semin Orthod*, **15**, 77–84.

Frye v. United States, 293 F. 1013 (D.C. Cir. 1923).

Stevens, Mark. Admissibility of Scientific Evidence under *Daubert*. http://faculty.ncwc.edu/mstevens/425/lecture02.htm.

Zinman, E. J., White, S. C., Tetradis, S. (2010). Legal considerations in the use of cone beam computer tomography imaging. *CDA Journal*, **38** (1), 49–56.

3 Paranasal Sinuses and Mastoid Air Cells

Gayle Reardon

Introduction

The paranasal sinuses of the craniofacial complex are air-filled cavities, including the maxillary sinuses, the frontal sinuses, the sphenoid sinuses, and the ethmoid air cells. The paired maxillary sinuses are of particular significance to dentistry because of the proximity of these sinuses to dental structures, in particular, the roots of the maxillary teeth. The close association of the maxillary sinuses and dental structures produces a quandary for dentists when they consider possible differential diagnoses for disease processes, which could be of either odontogenic or sinus origin. Regardless of the etiology of a specific pathologic process, the disease may spread from the dentition to sinus or from the sinus to the dentition.

With the advent of cone beam multiplanar imaging in dentistry, it is possible to visualize all paranasal sinuses on images made for dental purposes. Therefore, the dentist should be acquainted with the appearance of normal sinuses and their comparative symmetry from side to side. It is through the appreciation and knowledge of normal-appearing structures that the dentist will recognize variants of normal as well as pathology.

Anatomy

Normal Paranasal Development

The paranasal sinuses originate as evaginations from the nasal fossae into their respective bones (the maxillary bone, frontal bone, sphenoid bone, and ethmoid bone). They are lined by a mucosa that is similar to that found in the nasal cavity, which is a pseudostratified columnar ciliated epithelium containing both mucinous

Interpretation Basics of Cone Beam Computed Tomography, First Edition.
Edited by Shawneen M. Gonzalez.

Figure 3.1. Coronal slice at the anterior opening of the nasal cavity showing the frontal sinuses (FS).

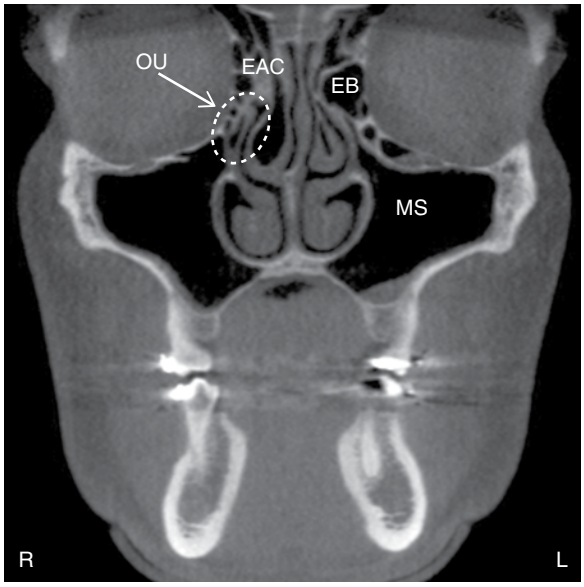

Figure 3.2. Coronal slice at the ostiomeatal unit (OU) showing the maxillary sinuses (MS), ethmoid air cells (EAC), and ethmoid bulla (EB).

(goblet cells) and serous glands. Because the mucosa of the paranasal sinuses is attached directly to the bone, it is frequently referred to as mucoperiosteum. The mucoperiosteum of the sinuses is thinner than the nasal mucosa but is continuous with the nasal mucosa at the various sinus ostia (Figures 3.1–3.14; Table 3.1).

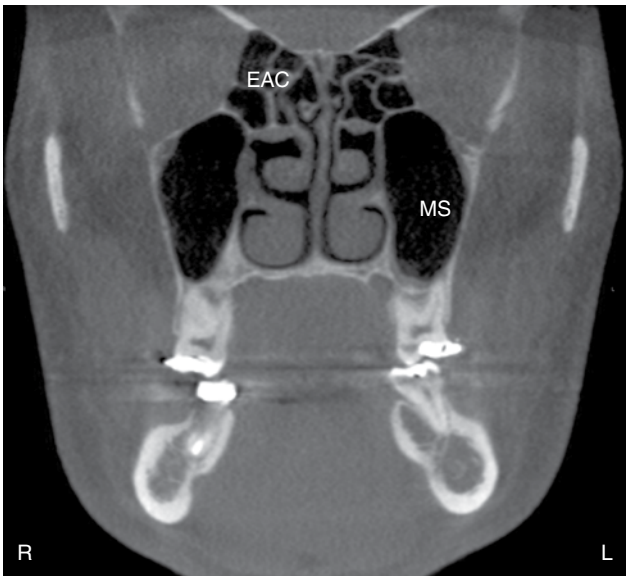

Figure 3.3. Coronal slice at the maxillary second molars showing the maxillary sinuses (MS) and ethmoid air cells (EAC).

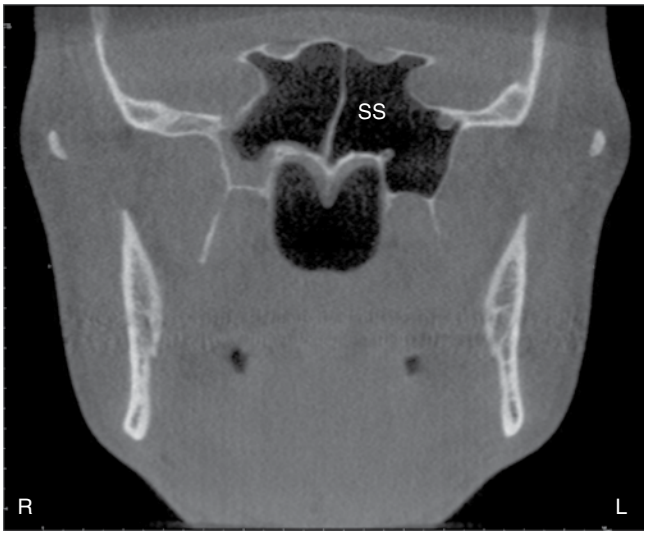

Figure 3.4. Coronal slice at the ramus showing the sphenoid sinuses (SS).

The functional reason for paranasal sinus presence has been discussed since the early descriptions of the sinuses in the 1800s. Proposed functions have included voice resonance, humidification and warmth of inspired air, increase in olfactory membrane area, absorption of shock to the face and head, thermal insulation for the brain, lightening of the skull and facial bones, and a contribution to facial growth. The current thought is that the paranasal sinuses form a collapsible framework, which helps to protect the brain from trauma.

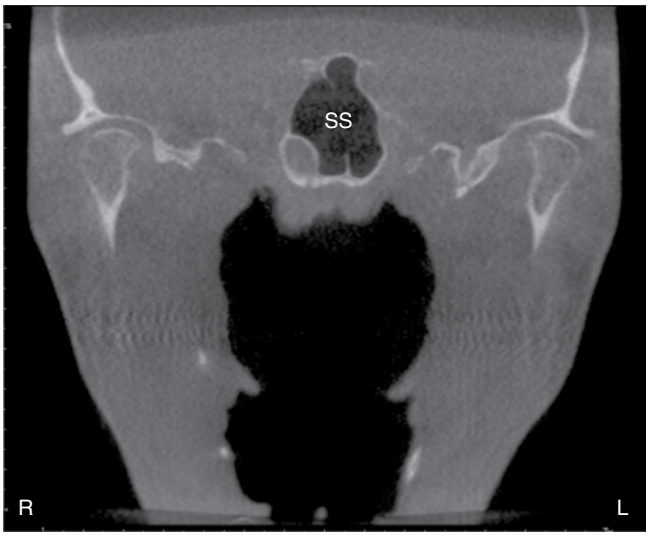

Figure 3.5. Coronal slice at the condyles showing the posterior aspect of the sphenoid sinuses (SS).

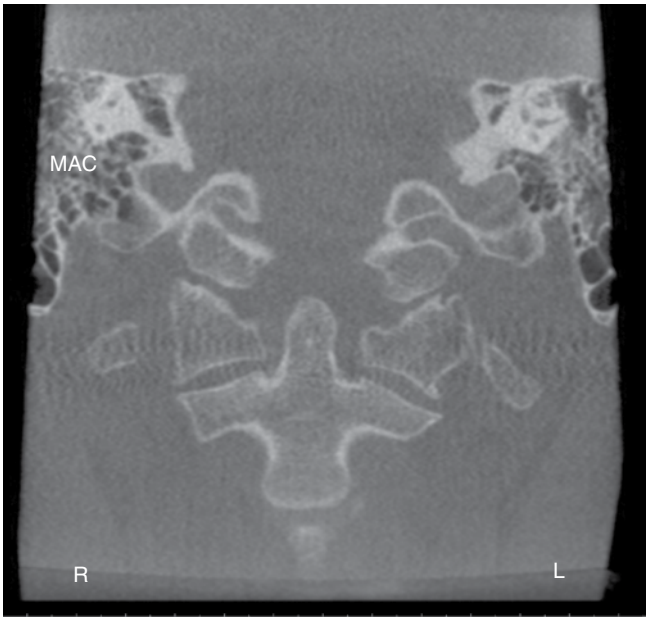

Figure 3.6. Coronal slice at the body of the cervical vertebrae showing the mastoid air cells (MAC).

Maxillary Sinus

The maxillary sinus is the first of the paranasal sinuses to form and is visualized by the 17th day of gestation. After each nasal fossa and its turbinates are established, a small ridge develops just above the inferior turbinate, marking the future uncinate process. Shortly thereafter, an evagination above this ridge, the uncibullous groove, is seen, which then enlarges laterally from the nasal cavity. These early evaginations continue

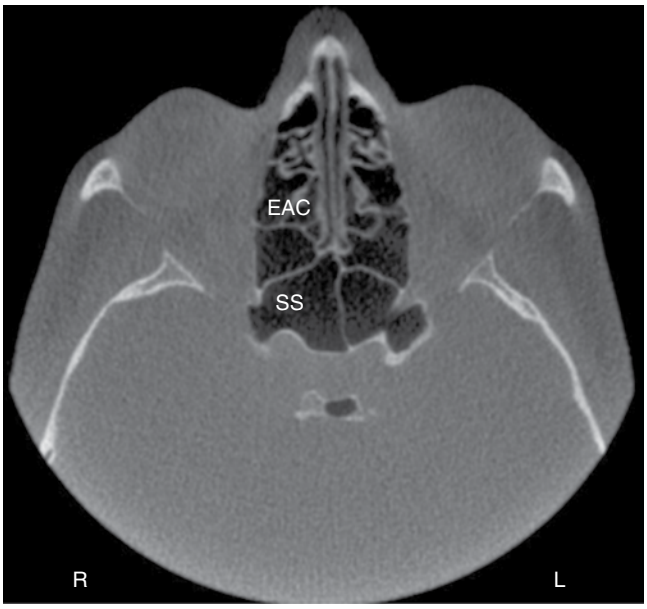

Figure 3.7. Axial slice at the level of the midorbits showing the sphenoid sinuses (SS) and ethmoid air cells (EAC).

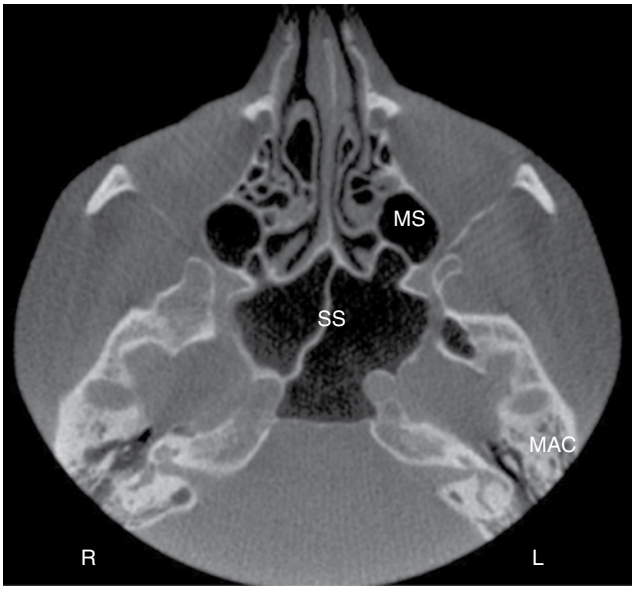

Figure 3.8. Axial slice at the level of the inferior aspect of the orbits and cranial skull base showing the sphenoid sinuses (SS), maxillary sinuses (MS), and mastoid air cells (MAC).

their growth laterally beneath the orbits through a process of pneumatization, which occurs concurrent to the growth of the maxilla and alveolar process. By birth, the rudimentary maxillary sinus appears like a small slit lying just lateral to the maxillary midline. The size of the neonate's maxillary sinus is approximately $7 \times 4 \times 4$ mm, or on average 6 to 8 cm, with the longest dimension being the anteroposterior axis.

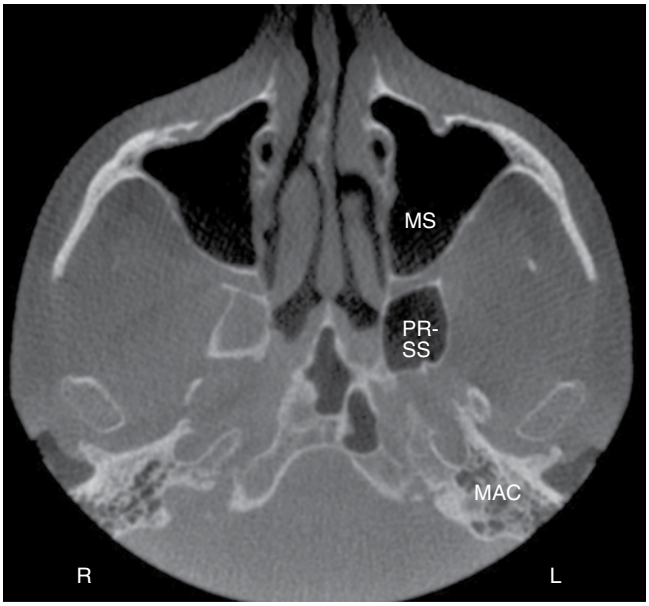

Figure 3.9. Axial slice at the level of the condyles showing the maxillary sinuses (MS), a pterygoid recess of the sphenoid sinus (PR-SS), and the mastoid air cells (MAC).

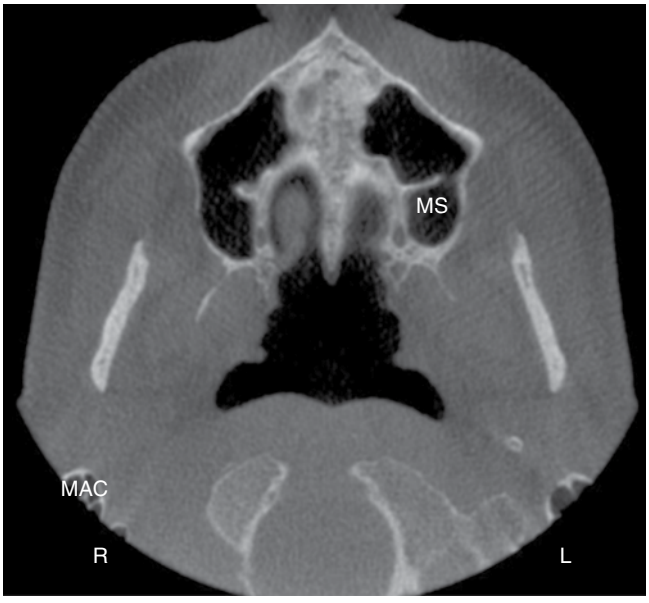

Figure 3.10. Axial slice at the level of the hard palate showing the maxillary sinuses (MS) and a small portion of the mastoid air cells (MAC).

Figure 3.11. Sagittal slice at the condyle showing the mastoid air cells (MAC).

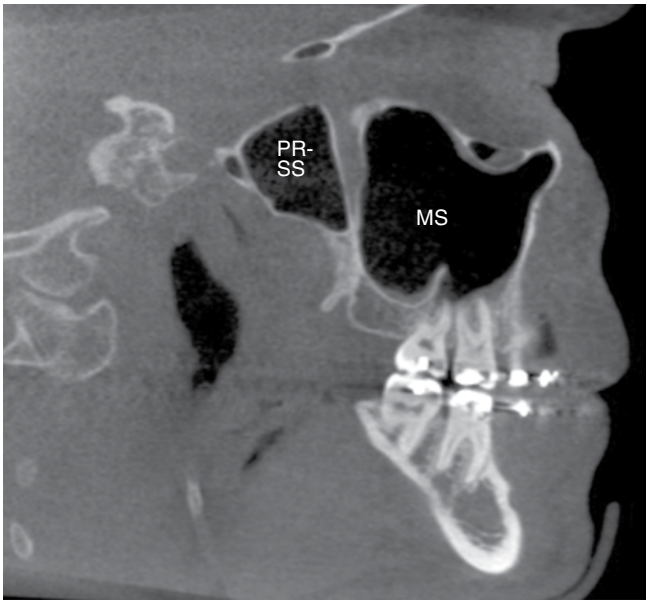

Figure 3.12. Sagittal slice at the maxillary teeth buccal roots showing the maxillary sinus (MS) and a pterygoid recess of the sphenoid sinus (PR-SS).

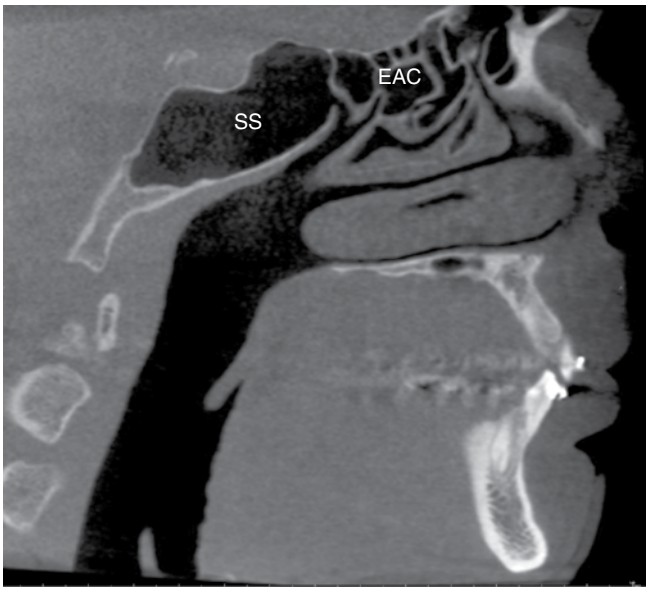

Figure 3.13. Sagittal slice just lateral to the midline showing the ethmoid air cells (EAC) and sphenoid sinus (SS).

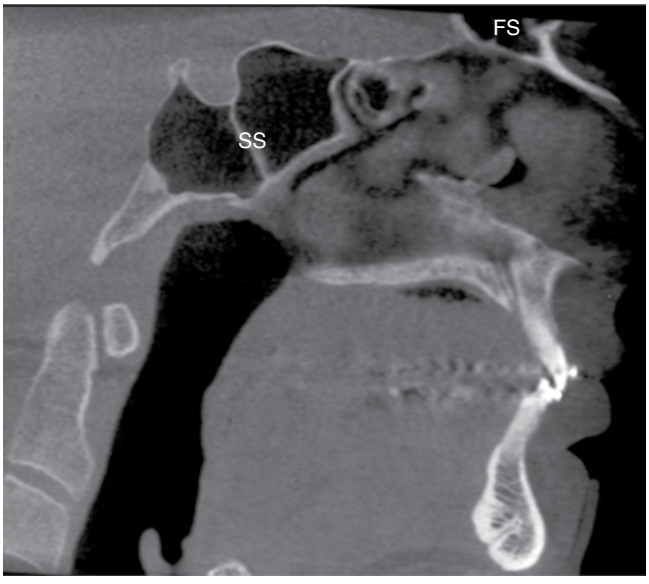

Figure 3.14. Sagittal slice on the midline showing the sphenoid sinuses (SS) and frontal sinuses (FS).

The annual growth rate of the maxillary sinus is approximately 2 mm vertically and 3 mm anteroposteriorly. By the end of year one, the lateral margin extends under the medial portion of the orbit. By 2 years of age, the sinus extends laterally to the intraorbital canal and passes inferolaterally to it during years 3 and 4. At 9 years, the maxillary sinus extends laterally to the zygomatic bone and is level with the floor of the nasal fossa. Lateral growth of the maxillary sinuses continues until midadolescence, approximately

Table 3.1. Anatomical landmarks identifiable in corresponding figures.

Anatomical landmark	Coronal	Axial	Sagittal
Frontal sinus	3.1		3.14
Ethmoid air cells	3.2 3.3	3.7	3.13
Maxillary sinus	3.2 3.3	3.8 3.9 3.10	3.12
Sphenoid sinus	3.4 3.5	3.7 3.8 3.9	3.12 3.13 3.14
Mastoid air cells	3.6	3.8 3.9 3.10	3.11

15 years of age. The final descent of the sinus is not complete until the third molar has erupted. By adulthood, the average volume of the maxillary sinus is approximately 14.75 ml and its mean dimensions are 34 mm deep, 33 mm high, and 25 mm wide.

Generally speaking, the maxillary sinuses develop quite symmetrically and may continue to enlarge or pneumatize throughout life through the formation of air cells or cavities in tissues and adjacent bony structures. However, hypoplasia of the maxilla resulting from trauma, infection, surgical intervention, or irradiation to the developing maxilla can damage maxillary growth centers producing a small maxilla and a hypoplastic sinus. Hypoplastic sinuses are also seen in Treacher Collins syndrome, mandibulofacialdysostosis, and thalassemia major due to brachial arch anomalies when the demand for marrow prohibits sinus pneumatization.

Normal Anatomy of the Ostiomeatal Complex

Given the fact that sinusitis, or sinusoidal inflammatory disease, is a serious health problem affecting between 30 and 50 million people in the United States alone, it is obvious that correct interpretation of sinus imaging studies is of paramount importance. Thus, it is important to understand the anatomy of the ostiomeatal complex. The definition of the ostiomeatal complex is: *The point in the middle meatus where the frontal and maxillary sinuses normally drain into the nasal cavity; obstruction here predisposes inflammation and infection of affected sinus cavities.*

The ostiomeatal complex, known also as the ostiomeatal unit, consists of the lateral nasal wall and its adjacent structures (Figure 3.15). It is the lateral nasal wall that contains the structures known as the concha, which are divided into three levels: superior, middle, and inferior. Occasionally, there is a fourth level of concha called supreme, which is above the superior concha. The superior meatus drains the ethmoid air cells and the sphenoid sinuses via the sphenoethmoidal recess. The middle meatus receives drainage from the frontal sinus, the maxillary sinus, and the anterior

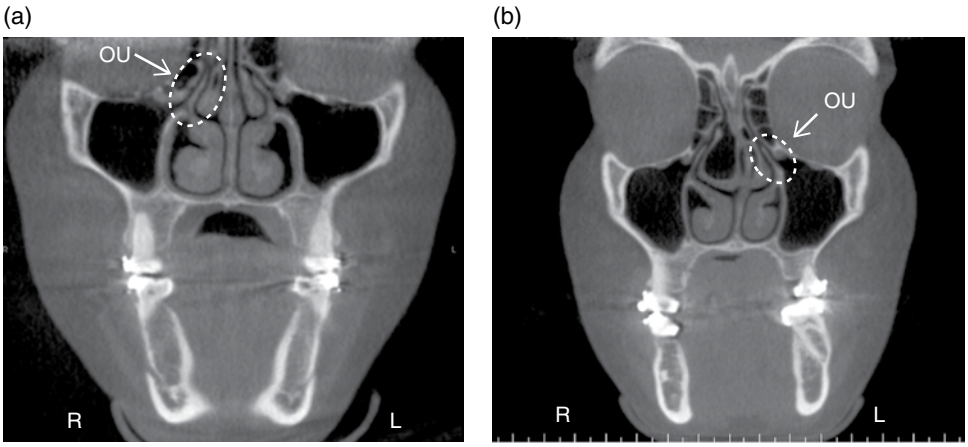

Figure 3.15. Coronal slices (a,b) showing the ostiomeatal unit (OU).

Figure 3.16. Coronal slice showing nasolacrimal duct (white dotted lines) draining into the inferior meatus.

ethmoid air cells. The recesses draining each of these three regions of the paranasal sinuses are as follows:

a) The frontal sinus is drained via the frontal recess.
b) The maxillary sinus is drained via the maxillary ostium and subsequently the ethmoidal infundibulum.
c) The anterior ethmoid air cells are drained via the ethmoid air cell ostia.

The nasolacrimal duct is drained via the inferior meatus (Figure 3.16).

Morphological evaluation in this region must focus upon the anatomy adjacent to these structures that contributes to constrictions in this region. It is the anatomical

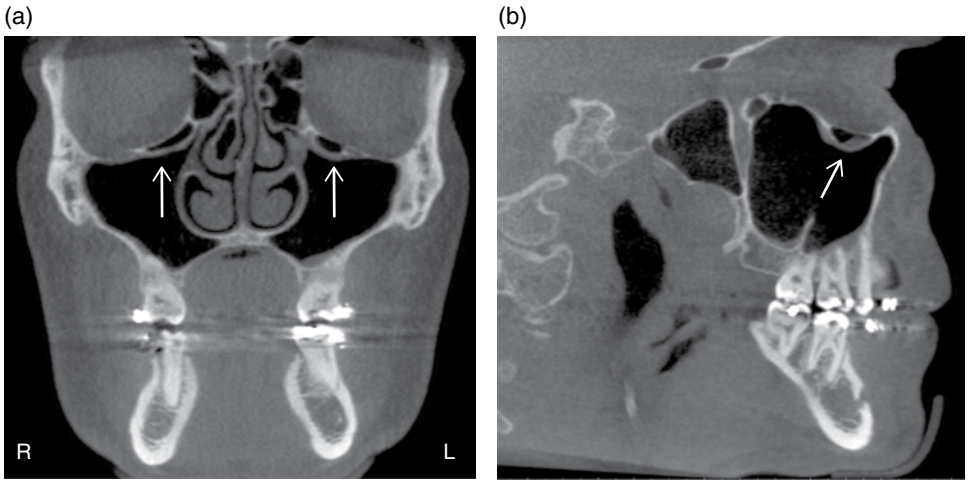

Figure 3.17. (a) Coronal slice showing bilateral Haller cells (white arrows) inferior to the orbit; (b) Sagittal slice showing Haller cell (white arrow) with mucosal thickening at the superior aspect of the maxillary sinus.

"tight spots" or constrictions that create drainage challenges contributing to sinusitis. If potential constrictions are considered by area, the first site encountered is in the anterior region surrounding the frontal recess, followed by the area surrounding the infundibulum and the middle meatus, and, finally, the most posteriorly situated region involving the sphenoethmoid recess.

When observing sinus anatomy on medical CT or CBCT, one will quickly observe there is central septation dividing the right side from the left side. While this left/right division is the most obvious, it should be noted there may be several levels of septation and the floor of the frontal sinus slopes inferiorly toward the midline, an arrangement that is very complimentary to the frontal sinuses' overall funnel shape.

Starting at the superior aspect of the ostiomeatal unit is the frontal recess, which is hourglass-shaped, narrowing between the frontal sinuses and the anterior middle meatus. It is the frontal recess that drains the frontal sinus. The frontal recess is not a tubular or ductlike structure. Rather, it is a recess as the term *nasofrontal recess* (also referred to as the nasofrontal duct) would imply. The nasofrontal recess is the primary ostium located in the depression in the floor of the frontal sinus.

Anterior, lateral, and inferior to the frontal recess and at the superomedial aspect of the orbit is the agger nasi cell, which is a remnant ethmoturbinal cell present in most patients. The agger nasi cell represents the most anterior ethmoid air cell lying deep within the lacrimal bone (see Chapter 4 for more information and figures). It is the size of the agger nasi cell that determines the patency of the frontal recess and the anterior middle meatus. When considering the anterior air channels, it is noteworthy to observe that the frontal recess is the narrowest and thus a common site for inflammation. Obstruction of the agger nasi cell decreases ventilation and mucociliary clearance from the frontal sinus.

There are several anatomical variations that may cause obstruction of the anterior ostiomeatal unit including deviation of the nasal septum, presence of infraorbital ethmoid cells (Haller cells; Figure 3.17), and variations in the size and shape of the ethmoid air bulla, middle turbinate, uncinate process, and frontal cells.

Ethmoid Sinuses

The ethmoid sinuses, also known as the ethmoid air cells, occupy the space between the frontal and sphenoidal sinuses. The paired ethmoidal cell groups bulge into the upper portion of the nasal fossa and have ostia, which drain into the adjacent middle and superior meatus. The ethmoidal sinuses are divided into groups of cells by bony basal lamellae that extend laterally to the laminae papyracea and superiorly to the fovea ethmoidalis. These lamellae serve as attachments for the turbinates. Thus, there are five lamellae, one for each of the primary turbinates (middle, superior, and supreme) and one for each of the secondary turbinates (bullae ethmoidalis and uncinate process).

The ethmoidal sinuses begin their formation in the third to fifth fetal months of life when numerous separate evaginations arise from the nasal cavity. The anterior cells are the first to form as evagination in the lateral nasal wall in the region of the middle meatus. Development of the posterior cells follow as evaginations in the superior meatal area. During the fifth prenatal month of life, the ethmoid air cells have expanded into the ethmoid bones and continue their expansion until puberty, or until the sinus walls reach a layer of compact bone, which halts enlargement. While the lamellae prevent one group of cells from intermingling with another, they do not prevent intramural expansion of one group into another. A concha bullosa results when posterior ethmoid cells extend intramurally to pneumatize the middle turbinate. This can result in a large obstructing turbinate or a focus of infection.

At birth, the anterior ethmoidal complex is about 5 mm high, 2 mm long, and 2 mm wide. The posterior cell group is 5 mm high, 4 mm long, and 2 mm wide. The sinuses reach their adult size by the age of 12 years. The number of ethmoid air cells varies per side with each containing between 8 and 15 chambers. As with the maxillary sinuses, the ethmoid air cells may extend into neighboring bony structures of the maxillary, lacrimal, frontal, sphenoid, and palatine bones.

Frontal Sinus

The frontal sinuses arise from one of several outgrowths originating in the region of the frontal recess of the nose or from anterior ethmoid cells of the infundibulum. While their site of origin can be identified on the mucosa as early as 3 to 4 months *in utero*, as compared to the maxillary and the ethmoid sinuses, the frontal sinuses are absent at birth with their delayed development starting after the second year of life. They reach the frontal bone around the fifth or sixth year of childhood. The frontal sinuses are essentially displaced anterior ethmoid cells, and because they develop from a variable site, their drainage will be either via an ostium into the frontal recess or via a nasofrontal duct into the anterior infundibulum.

Approximately 4% of the population will fail to develop frontal sinuses. On average, the cranial extent of the frontal sinus is half the height of the orbit by the age of 4 years. By 8 years of age, the top of the frontal sinuses is at the level of the orbital roof. At age 10, the sinuses extend into the vertical portion of the frontal bone. Their adult size is reached after puberty.

Each frontal sinus develops separately on the right and left sides of the frontal bone and grows toward the midline. Often the larger sinus extends across the midsagittal plane and appears to be somewhat centered. The frontal sinuses are asymmetric in shape and their size is widely variable. In spite of the wide variability in frontal sinus size, the average frontal sinus has been described as between

28 mm high, 24 mm wide, and 20 mm deep. A direct relationship between the mechanical stresses of mastication and frontal sinus enlargement has been demonstrated, as has a direct relationship with growth hormone, as seen in acromegaly.

Because of its variable origin, about 40% of frontal sinuses drain into the ethmoidal infundibulum. In these cases, the ethmoidal infundibulum acts as a channel carrying secretions from the frontal sinus to the anterior ethmoidal cells and maxillary sinus, or vice versa. The natural frontal sinus ostium is usually located in the posteromedial floor of the sinus.

Sphenoid Sinus

The sphenoid sinuses emerge in the fourth month *in utero* as evaginations from the posterior nasal capsule into the sphenoid bone. This occurs above small crescent-shaped ridges of bone, the sphenoidal conchae, that projects from the under surface of the body of the sphenoid bone. These conchae grow anteriorly, fusing with the posterior ethmoid labyrinth. It is rare for the sphenoid sinuses to be absent. The extent of their pneumatization varies considerably.

Emerging as diminutive spaces in the body of the neonatal sphenoid bone, the sphenoid sinuses remain small; major growth begins in the third to fifth year of life. By the age of 7 years, the sinus has extended posteriorly to the level of the anterior sella turcica wall. By 10 to 12 years of age, the sinus has achieved its adult configuration. Absence of sphenoid sinus pneumatization by age 10 years is suggestive of the possibility of "occult" sphenoid bone pathology.

Like the maxillary and frontal sinuses, the sphenoid sinuses are a paired sinus with asymmetric right and left sides. The two sides are separated by a bony septum. The average adult sphenoid sinus is 20 mm high, 23 mm long, and 17 mm wide. The degree of sphenoid sinus pneumatization is classified as nonpneumatized, presellar or sellar. The sphenoid sinuses communicate with the nasal cavities through ostia that are usually 2 to 3 mm in diameter.

Onodi Cells

The literature presents two alternative definitions for "Onodi cells." The view is the Onodi cells are actually the most posterior ethmoid cells located superolateral to the sphenoid sinus and closely associated with the optic nerve. The other definition describes Onodi cells as posterior ethmoid cells extending into the sphenoid bone, situated either adjacent to or impinging upon the optic nerve (Figure 3.18).

Frontal Cells

The superior extension of the lateral nasal wall, which is also the medial wall of the maxillary sinus, is called the uncinate process. The agger nasi cell, the posteromedial wall of the nasolacrimal duct, and the uncinate process are fused anteriorly leaving the superoposterior edge of the uncinate process '"free." The infundibulum is an air passageway connecting the maxillary sinus ostium with the middle meatus. The ethmoid bulla is posterior to the uncinate process; the ethmoid bullae are generally the largest of the anterior ethmoid cells. The uncinate process courses medially and inferiorly to the ethmoid bulla, which is enclosed laterally by the lamina papyracea medial to the orbit. The lamina papyracea by definition is a thin plate of ethmoidal bone forming part of the medial wall of the orbit and the lateral wall for the ethmoidal labyrinth.

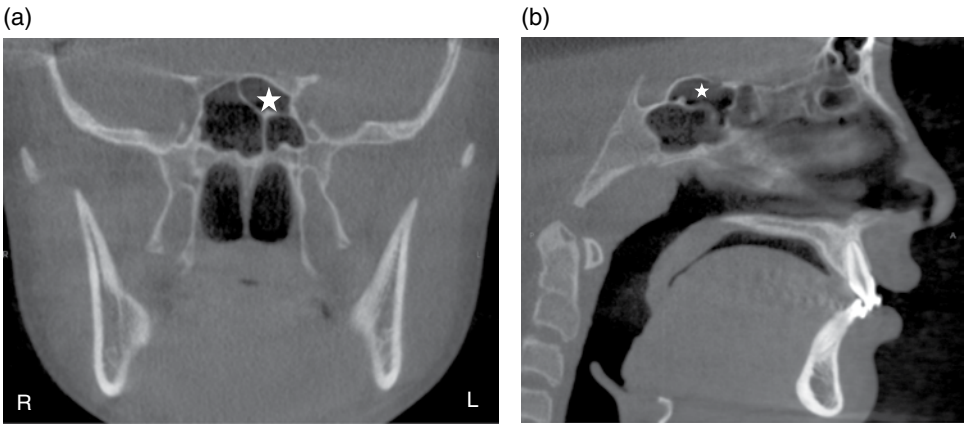

Figure 3.18. (a) Coronal and (b) sagittal slices showing Onodi cell (white star) superior to the left the sphenoid sinus.

There is a space between the ethmoid bulla and the free edge of the uncinate process, which delineates the hiatus semilunaris. The hiatus semilunaris communicates medially with the middle meatus, the air space lateral to the middle concha. The hiatus semilunaris also communicates inferolaterally with the infundibulum, the air passageway between the uncinate process and the inferomedial margin of the orbit. Primary drainage for the maxillary sinus is through the infundibulum.

The middle concha is medial to the ethmoid bulla and uncinate process. It attaches to the medial wall of the agger nasi cell anteriorly as well as the superior edge of the uncinate process. Superiorly, the middle concha adheres to the lateral aspect of the cribriform plate. The middle concha is the source of several posterolaterally coursing bony structures known as "lateral fanning" attachments, which extend to the lamina papyracea. The first of these lateral fanning attachments is the basal lamella situated posterior to the ethmoid bulla. The basal lamella separates the anterior ethmoid air cells from the posterior ethmoid air cells. In most patients, the posterior wall of the ethmoid bulla remains intact with an air passage, the sinus lateralis now known as the retrobullar recess cell, coursing between the basal lamella and the posterior ethmoid bulla and communicating with the frontal recess.

Embedded in the clivus and bordered superoposteriorly by sella turcica, the sphenoid sinus is the most posterior sinus. The ostium for the sphenoid sinus is located mediosuperiorly in the anterior sinus wall and communicates with the sphenoethmoidal recess and posterior aspect of the superior meatus. The nasal septum lies medial to the sphenoethmoidal recess.

All septations in the sphenoid sinuses are vertically oriented. Of particular importance are septations that adhere to the bony canal wall covering the internal carotid artery, which may project into the posterolateral sphenoid sinus. The vidian nerve and the second division of cranial nerve V are other structures projecting into the floor of the sphenoid sinuses. These and all other significant structures of the paranasal sinuses including the anterior cranial fossa, the cribriform plate, the cavernous sinuses, the orbits, and the optic nerves must be observed by surgeons to avoid potential postoperative complications.

Pneumatitic Cells of the Temporal Bone: The Mastoid Air Cells

The air cells of the temporal bone develop as outpouchings of the antrum, epitympanum, tympanic cavity, and Eustachian tube. Tentative epithelial evaginations appear from the antrum as early as 34 weeks but there is no significant pneumatic cellular expansion into the remainder of the temporal bone until after birth. The expansion occurring after birth occurs with stimulation brought about by the presence of air within the middle ear. The pneumatization process ramps up to a high level of activity and proceeds over a period of several years. The petrous apex shows continuing pneumatization into early adulthood. The pneumatizing process occurs as a result of epithelium-lined projections arising from the lining of the middle ear and its extensions. These evaginations probe the spaces between new bone spicules and degenerating bone marrow spaces. The air cells invade the bone after the marrow has been converted into loose mesenchymal tissue. The presence of middle ear infections in infancy causes embryonic subepithelial connective tissue to fibrose, thus impeding the progress of the advancing fingers of evaginating pneumatic cells.

The mastoid process begins its development during the second year of life with downward growth of the squamous portion and partially as a result of extension of the petrous portion of the temporal bone. These two portions of the mastoid process come together at the petrosquamous suture line. Air cells grow down from the antrum vertically toward the mastoid tip and laterally and radially into the squamous portion. Koerner's septum is a dividing bridge of bone that separates these two cell tracks at the junction of the petrous and mastoid ossifications. Koerner's septum is visible radiographically as a pointed bony spicule originating from the antral roof and directed obliquely inferiorly.

The mastoid air cells are a section of the mastoid process of the temporal bone of the cranium that are hollowed out into a number of spaces. These spaces exhibit great variety in size and number. At the anterosuperior portion of the process, the cells are large and irregular and contain air, but toward the lower part of the process, they diminish in size. Those cells at the apex of the process are frequently quite small and contain marrow. Occasionally, the air cells are entirely absent, and the mastoid bone is solid throughout.

Inflammatory Disease of the Paranasal Sinuses

Inflammation may result from a variety of causes, including infection, chemical irritation, allergies, the introduction of a foreign body, or facial trauma. Imaging changes associated with inflammation include thickening of the sinus mucosa, development of an air-fluid level in the sinus(es), polyps, empyema, and retention pseudocysts. Viral infections may not trigger a radiographic change in the involved sinus(s).

Cone beam computed tomography (CBCT) is becoming increasingly more important in the evaluation of sinus disease and is an acceptable substitute for the significantly higher radiation modality, medical computed tomography (medical CT). Because CBCT provides multiple viewing planes and slices through the paranasal sinuses, it may be useful for determining the differential diagnosis of sinus pathology by making it possible to outline the perimeters of the disease process. Axial and

coronal CBCT examinations are the most useful noninvasive techniques for diagnosis of pathology of the paranasal sinuses and adjacent structures. CBCT examination is appropriate to determine the extent of disease in patients who have chronic or recurrent sinusitis. Coronal CBCT provides visualization of the ostiomeatal complexes and nasal cavities, and demonstrates reaction of the surrounding bone to sinus pathology.

Mucositis

Definition/Clinical Characteristics

Mucositis is a thickening of the mucous membrane of the paranasal sinuses. This mucosal lining, normally about 1 mm thick, is made up of respiratory epithelium, which is not normally visualized on radiographic images. However, when the mucosa becomes irritated and inflamed from either an infectious or allergic process, its thickness may increase by 10 to 15 times making visualization of the thickened membrane possible. Mucositis is the change in the thickness of the mucous membrane brought about by inflammation. Mucosal thickening greater than 3 mm is likely pathologic.

Radiographic Description

The appearance of mucositis is that of a minimally thickened noncorticated band. It is more radiopaque than the adjacent air-filled sinus. The somewhat thickened band parallels the bony wall of the affected sinus (Figure 3.19).

Differential Interpretation

There are no differential interpretations based on the location of this finding.

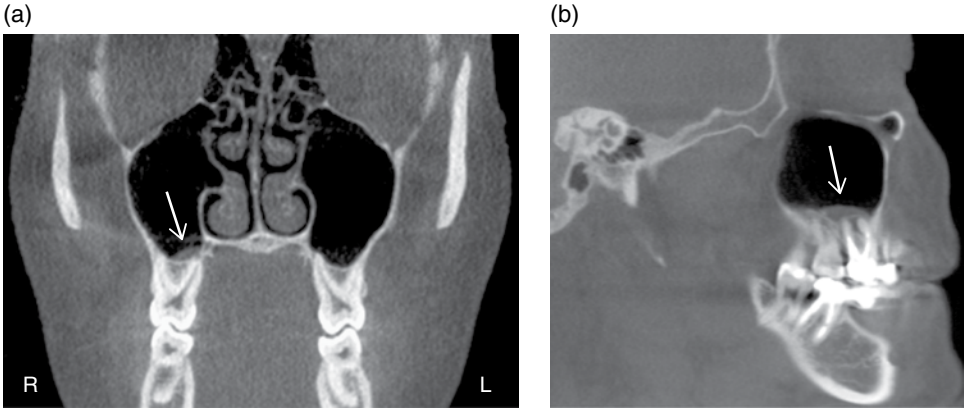

Figure 3.19. (a) Coronal and (b) sagittal slices showing minimal thickening of the mucosal lining in the right maxillary sinus consistent with mucositis (white arrow).

Treatment/Recommendations

No further treatment or imaging is recommended.

Sinusitis

By definition, sinusitis is a condition involving generalized inflammation of the paranasal sinus mucosa. The etiologic agent may be an allergen, bacterial or viral. Sinusitis may impede drainage from the ostiomeatal complex. Inflammatory changes may lead to ciliary dysfunction and retention of sinus secretions. It is estimated that approximately 10% of inflammatory episodes of the maxillary sinuses are secondary extensions of dental infections. Sinusitis may be classified into commonly used subtypes based on length of time the disease has been present.

Acute Sinusitis

Definition/Clinical Characteristics/Radiographic Description

An acute sinusitis usually is due to bacterial infection of an obstructed paranasal sinus. The obstruction is often the result of apposition of edematous mucosal surfaces from an antecedent viral upper respiratory tract infection. The edematous mucosa disrupts the normal mucociliary drainage pattern of the sinus resulting in obstruction of the sinus ostium. This obstruction of the ostium alters the oxygen tension within the obstructed sinus and predisposes the sinus to a bacterial superinfection.

Acute sinusitis refers to a condition present for a short time, generally less than two weeks. It usually involves only a single sinus with the ethmoid sinus being the most common location. Acute maxillary sinusitis, often a complication of the common cold, is accompanied by a clear nasal discharge or pharyngeal drainage (Figure 3.20). After a few days, the stuffiness and nasal discharge increase, and the patient may complain of pain and tenderness to pressure over the involved sinus.

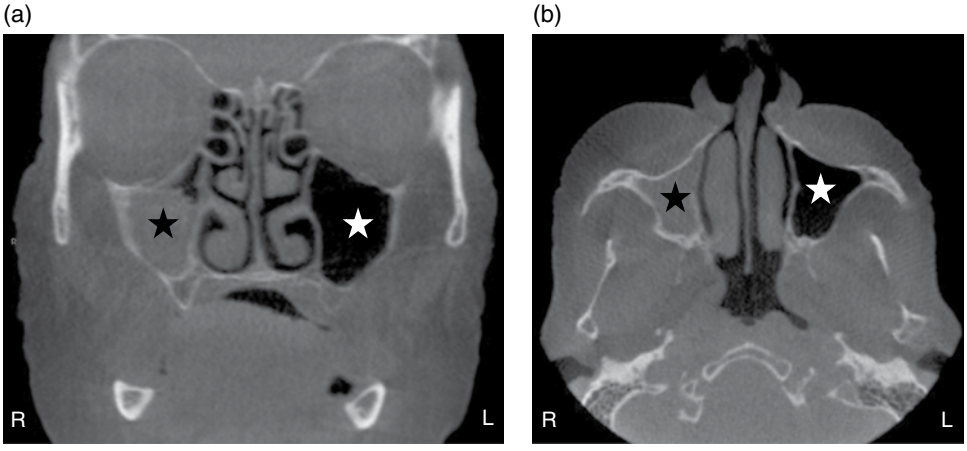

Figure 3.20. (a) Coronal and (b) axial slices showing radiopacification of the right maxillary sinus (black star) compared to the air-filled left maxillary sinus (white star).

Differential Interpretation/Treatment/Recommendations

The pain may also be referred to the premolar and/or molar teeth on the affected side, and may produce tooth sensitivity to percussion. When there is tooth tenderness to percussion, the dentist must rule out teeth as the possible source of pain and/or infection.

Chronic Sinusitis

Definition/Clinical Characteristics/Radiographic Description

"Chronic sinusitis" is diagnosed when the patient has repeated bouts of acute infection or persistent inflammation commonly due to staphylococcus, streptococcus, corynebacteria, bacteroides, fusobacteria, and other anaerobes. Anaerobes are more frequently involved in chronic sinusitis than in acute sinusitis. The sinuses most commonly involved with chronic sinusitis are the anterior ethmoid air cells.

Opacification of the ostiomeatal unit has been found to predispose patients to sinusitis. In chronic sinusitis, the inflammation may stimulate the periosteum of the sinus to produce bone, resulting in thickened sclerotic borders of the maxillary sinus (Figure 3.21). Chronic sinusitis is often associated with anatomic derangements that inhibit mucous outflow, such as deviated nasal septum and the presence of a concha bullosa (pneumatization of the middle concha).

Differential Interpretation/Treatment/Recommendations

Chronic sinusitis may also be associated with allergic rhinitis, asthma, cystic fibrosis, and dental infections. Referral to an ear, nose, and throat physician or a primary physician is recommended.

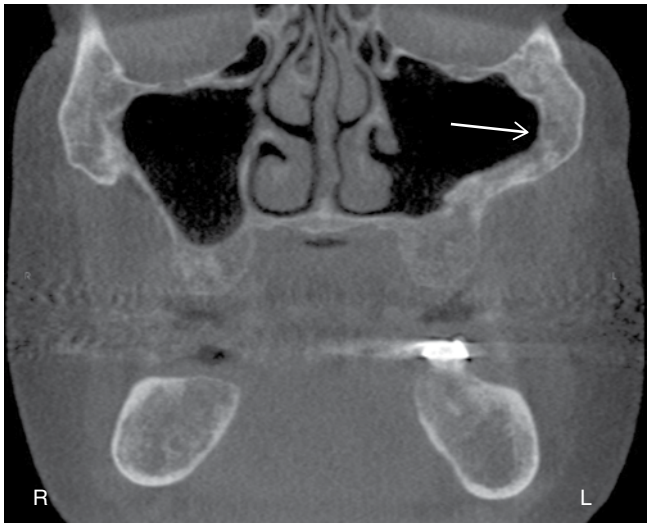

Figure 3.21. Coronal slice showing thickened bone border (white arrow) of the left maxillary sinus.

Fungal Sinusitis

Definition/Clinical Characteristics/Radiographic Description

Fungal sinusitis may be suspected when the patient fails to respond to standard antibiotic therapy. According to Som and Curtin (2003), the presence of fungal infection is suggested when soft tissue changes present with thickened reactive bone with localized areas of osteomyelitis and the association of inflammatory sinus disease with involvement of the adjacent nasal fossa and soft tissues of the neck. These signs of aggressive infection are atypical of bacterial pathogens of the sinus.

Allergic Sinusitis

Definition/Clinical Characteristics/Radiographic Description

Allergic sinusitis occurs in 10% of the population and typically produces a pansinusitis with symmetric involvement. CT often shows a nodular mucosal thickening with thickened turbinates; air-fluid levels are rare unless bacterial superinfection occurs.

Many of the descriptions contained within the following section are credited to Dr. Axel Ruprecht, my teacher and mentor, while at the University of Iowa in the Oral and Maxillofacial Radiology Residency program. The flavor may also resemble the same section in White and Pharoah's *Oral Radiology* (2004), which was written by Dr. Ruprecht.

Intrinsic Diseases of the Paranasal Sinuses

The most common radiopaque patterns that occur in the coronal CT view are localized mucosal thickenings along the floor of the sinus, generalized thickening of the mucosal lining around the entire wall of the sinus, and near complete or complete opacification (or radiopacification) of the sinus as seen in "silent sinus." Such changes are best seen in the maxillary sinuses, but the frontal and sphenoid sinuses may produce a similar appearance.

Scrutinizing the area around the maxillary ostium on the coronal views of CT and CBCT images may reveal the presence of thickened mucosal tissue, which may cause blockage of the ostium. Mucosal thickening in just the base of the sinus may not represent sinusitis. Rather, it may represent the more localized thickening that can occur in association with rarefying osteitis from a tooth with a nonvital pulp. However, this may, over time, progress to involve the entire sinus.

The inability to perceive the delicate walls of the ethmoid air cells is a sign of ethmoid sinusitis. The image of thickened sinus mucosa on CT may be uniform or polypoid. In the case of an allergic reaction, the mucosa tends to be more lobulated. In cases of sinus infection, the thickened mucosa tends to be smoother, with contours following the sinus wall.

The goal of sinusitis is to control the infection by promoting drainage, which will then relieve pain. Acute sinusitis is usually treated over the counter or prescribed decongestants to reduce mucosal swelling and, in cases of bacterial sinusitis, with

antibiotics. As stated above, chronic sinusitis is generally a disease of ostia obstruction. Therefore, the goal is to drain and ventilate through means such as endoscopic surgery to enlarge obstructed ostia or establish an alternate path for drainage.

Retention Pseudocyst

Definition/Clinical Characteristics

Retention pseudocysts are known by many names, including the following: antral pseudocyst, benign mucous cyst, mucous retention cyst, mucous retention pseudocyst, mesothelial cyst, pseudocyst, interstitial cyst, lymphangiectatic cyst, false cyst, retention cyst of the maxillary sinus, benign cyst of the antrum, benign mucosal cyst of the sinus, serous nonsecretory retention pseudocyst, and mucosal antral cyst.

Retention pseudocyst is a term used to describe several related conditions with controversial etiologies but clinical and radiographic similarities. One explanation suggests that seromucous gland secretory duct blockage results in a pathologic submucosal secretion accumulation, producing swelling of the tissue. A second possibility for serous nonsecretory retention cyst formation suggests there is cystic degeneration within the inflamed, thickened sinus lining. Regardless of the explanation, both lesions are termed *pseudocysts* because they have no epithelial lining.

Retention pseudocysts may be found in any of the paranasal sinuses at any time during the year, occurring most frequently around April and November. This timing suggests that the pseudocyst may be related to seasonal environmental changes.

Studies indicate that retention pseudocysts are more common in males and rarely cause symptoms. Because of an absence of signs and symptoms, the affected patient usually has no awareness of the lesion and, thus, the lesion is often noticed as an "incidental finding" on images made for other purposes. When a pseudocyst completely fills the maxillary sinus cavity, it may extrude through the ostium causing nasal obstruction and postnasal discharge. Enlarged retention pseudocysts may rupture as a result of changes in pressure due to sneezing or nose blowing. Also, an expanded pseudocyst may herniate through the ostium into the nasal cavity where it can rupture. The pseudocyst may be present on CT examination of the maxillary sinus one day, absent only a few days later, and then may reappear on a subsequent examination.

The maxillary sinus is the most common site of mucous retention pseudocysts, although they are occasionally found in the frontal or sphenoid sinuses. Mucous retention pseudocysts are not associated with extractions or periapical disease.

Radiographic Description

Retention pseudocysts appear as smooth, dome-shaped radiopaque masses with no osseous border. The base of the lesion may be narrow, although most have broad bases. Partial images of retention pseudocysts of the maxillary sinus may appear on the axial, coronal, and sagittal images of cone beam CT (Figure 3.22). Although pseudocysts may occur bilaterally, pseudocysts usually develop unilaterally. Occasionally, multiple pseudocysts may form within one sinus. These pseudocysts usually project from the floor of the sinus; some may form on the lateral or medial walls of the antrum. The size of the mucous retention pseudocysts may vary

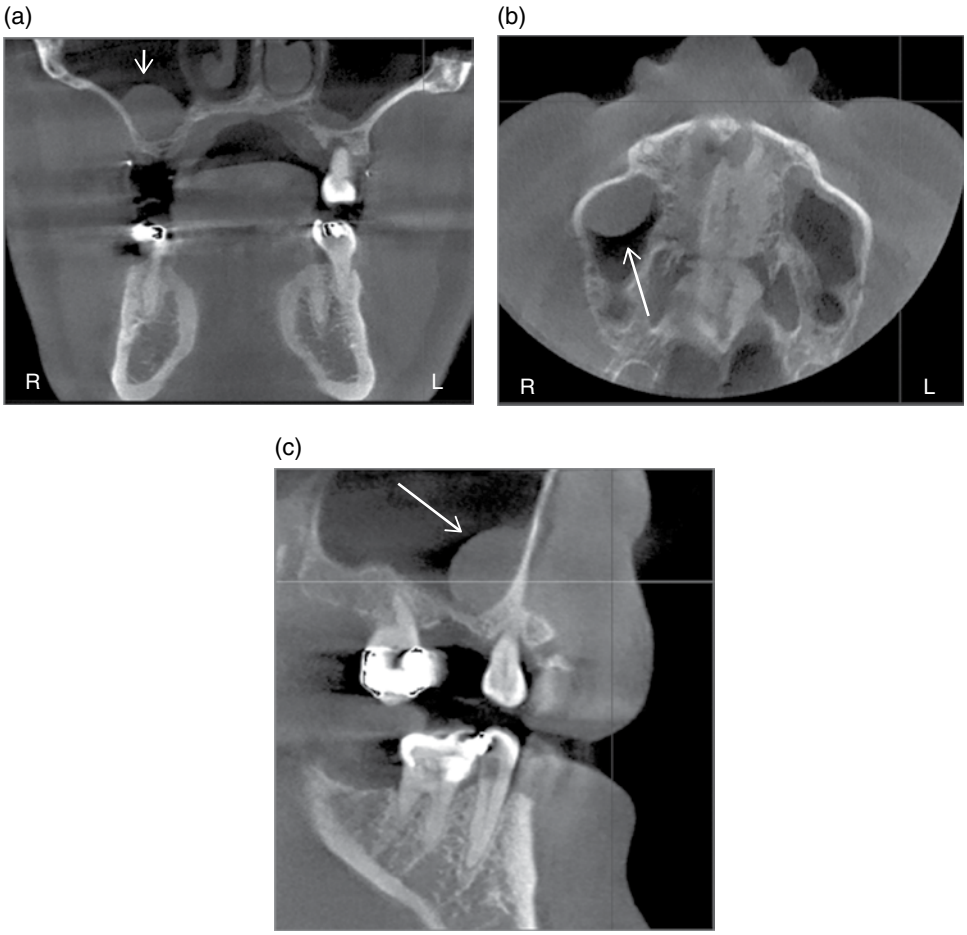

Figure 3.22. (a) Coronal, (b) axial, and (c) sagittal slices showing radiopaque dome-shaped entity on the floor of the maxillary sinus consistent with a retention pseudocyst (white arrow).

from that of a fingertip to a size large enough to completely fill the sinus causing the sinus to appear completely opacified. The roots of healthy teeth projecting over an area of an antral cavity occupied by a retention pseudocyst usually have intact lamina dura.

Imaging allows for differentiation between antral polyps of an infectious or allergic nature and antral retention pseudocysts in that they are more often seen in multiples. They are commonly associated with a thickened mucous membrane, a characteristic less frequently observed with retention pseudocysts.

Differential Interpretation

Neoplasms may also mimic retention pseudocysts. If the neoplasms are benign and originate from outside the sinus, they are separated from the antrum of the sinus by a radiopaque border similar to that of odontogenic cysts. Malignant neoplasms may destroy the osseous border of the affected sinus, regardless of whether it arises from

within the sinus or from the alveolar process. It is less likely that a neoplasm will appear as dome shaped as is characteristic of the mucous retention pseudocyst.

Treatment/Recommendations

Retention pseudocysts in the maxillary sinus usually require no treatment because they customarily resolve spontaneously without any residual effect on the antral mucosa.

Polyps

Definition/Clinical Characteristics

Polyp is the term used to describe irregular folds occurring in the thickened mucous membrane of a chronically inflamed sinus. Polyposis of the sinus mucosa may occur in an isolated area or in multiple sites throughout the sinus.

Radiographic Description

The internal structure of the polyp is homogeneous and more radiopaque than the surrounding sinus antrum's air-filled cavity. The radiopacity of the lesion is caused by the accumulation of fluid, thus leaving normal osseous landmarks visible through its image. Polyps may cause bony displacement and/or destruction. Polyps found in the ethmoid air cells may cause destruction of the medial wall of the orbit, the lamina papyracea of the ethmoid bone, causing a unilateral proptosis to develop. Polyps have no effect on the floor of the affected sinus which remains intact (Figure 3.23).

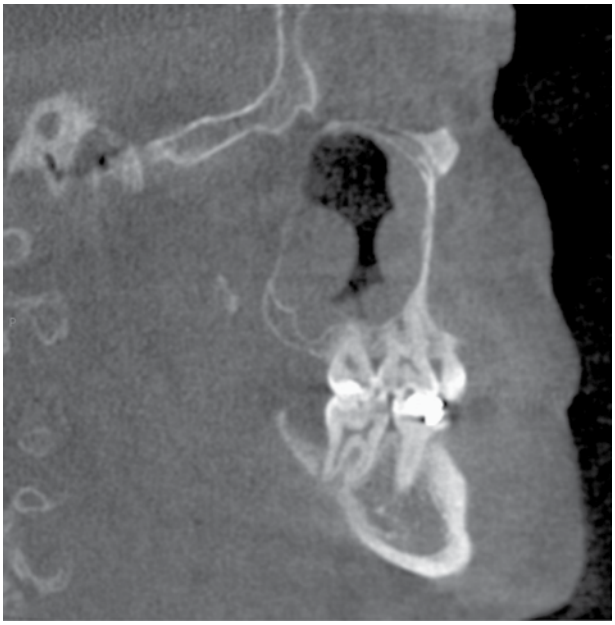

Figure 3.23. Sagittal slice showing multiple mucous retention cysts versus sinus polyposis.

Differential Interpretation

A polyp may be differentiated from a retention pseudocyst on a CT image by noting that a polyp usually occurs with a thickened mucous membrane lining because the polypoid mass is essentially an accentuation of the mucosal thickening. In the case of a mucous retention pseudocyst, an adjacent mucous membrane lining is not seen. If multiple mucous retention pseudocysts are seen within a sinus, sinus polyposis should be part of the differential diagnosis. The radiographic image of the bone displacement or destruction associated with polyps may mimic a benign or malignant neoplasm.

Treatment/Recommendations

Because many sinus neoplasms are asymptomatic, examination of a paranasal sinus evidencing bony destruction associated with radiopacification should lead to biopsy.

Empyema

Definition/Clinical Characteristics/Radiographic Description

An empyema is a pus-filled space that may be the result of blockage of the sinus ostium by a thickened, inflamed mucous membrane or another pathologic process, especially in cases where the maxillary sinus is involved. Empyema is most likely a variant of the mucocele or pyocele.

Antrolith

Definition/Clinical Characteristics

Antroliths occur within the maxillary sinuses and are the result of the deposition of mineral salts such as calcium phosphate, calcium carbonate, and magnesium around a nidus, which has been introduced into the sinus through either an extrinsic or intrinsic mechanism. Smaller antroliths are asymptomatic and are discovered as "incidental findings" on radiographic examination. If a small antrolith continues its growth, the patient may experience an associated sinusitis with bloody nasal discharge, a nasal obstruction, or facial pain.

Radiographic Description

Antroliths occur within the maxillary sinus superior to the floor of the maxillary antrum in axial, coronal, and sagittal CT. Antroliths are well defined and may have a smooth or irregular shape. The internal structure may vary in density from a slight radiopacity to extreme radiopacity. The internal density may be homogenous or heterogeneous. In some instances, layers of radiolucency and radiopacity are seen appearing as laminations (Figures 3.24 and 3.25).

Differential Interpretation

Antroliths may be distinguished from root fragments in the sinus by inspection of the mass for the normal root anatomy, specifically the presence of a pulp canal. Rhinoliths are similar calcifications but are found within the nasal fossae.

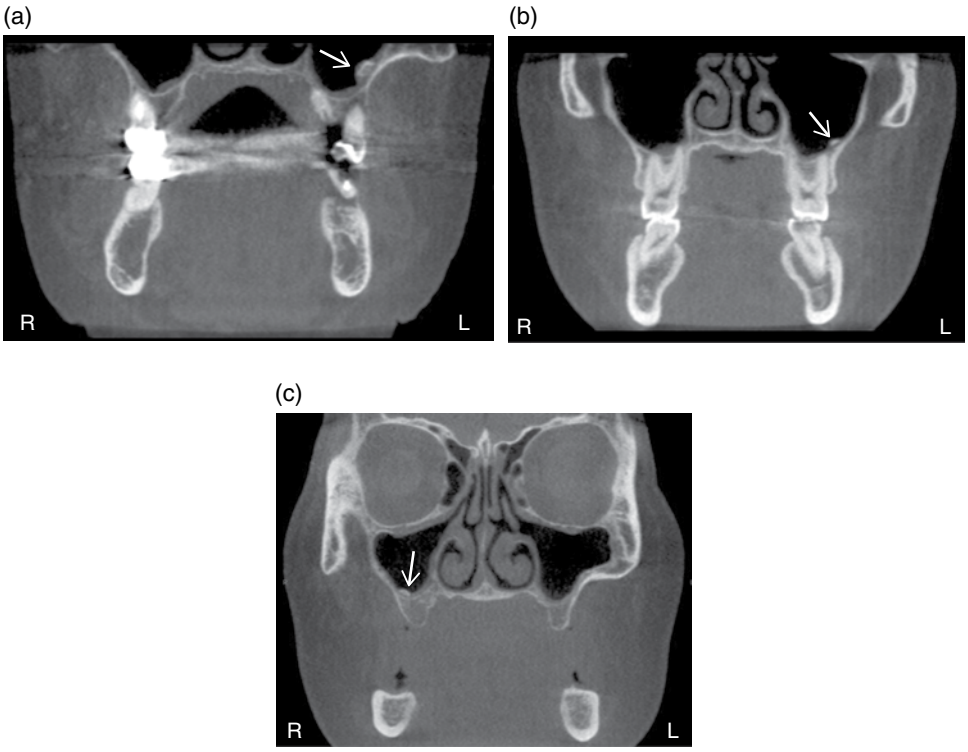

Figure 3.24. Coronal slices (a,b,c) showing antroliths (white arrows).

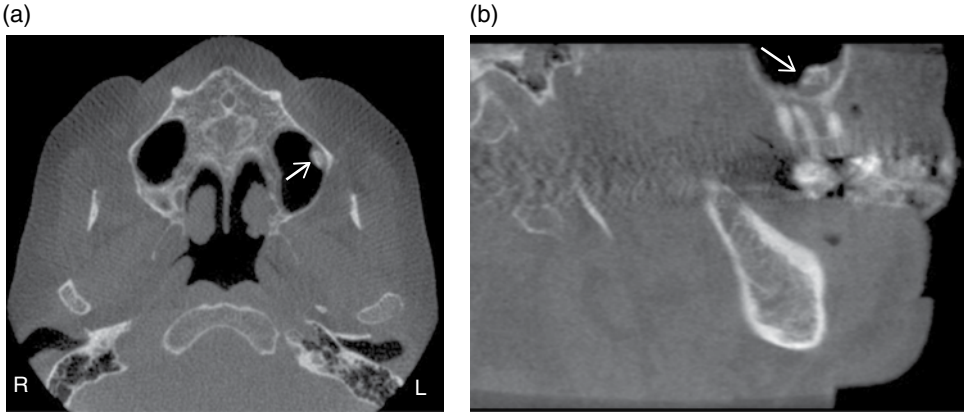

Figure 3.25. (a) Axial slice showing antrolith (white arrow) in the left maxillary sinus; (b) Sagittal slice showing antrolith (white arrow).

Treatment/Recommendations

Referral to an ear, nose, and throat physician or primary care physician is recommended to determine if further treatment such as surgical removal is necessary.

Mucocele

Definition/Clinical Characteristics

A mucocele is an expanding, destructive lesion resulting from blockage of a sinus ostium. The blockage may be the result of intra-antral or intranasal inflammation, a polyp, or a neoplasm. Thus, the entire sinus becomes a cystlike lesion. Accumulated mucus fills the sinus cavity, increases the intra-antral pressure, which then results in a thinning, displacement, and, often, destruction of the sinus walls. If the mucocele becomes infected, it is called a pyocele or amucopyocele.

The effect of pressure from a mucocele in the maxillary sinus may be radiating pain produced in the region of the superior alveolar nerves. First, the patient may complain of a sensation of cheek fullness and swelling. This swelling may become apparent over the anteroinferior aspect of the antrum where the wall of the sinus is thin or destroyed. Inferior expansion of the lesion may cause loosening of posterior teeth. If the medial wall of the sinus is expanded, the lateral wall of the nasal cavity will, which may contribute to obstruction of the nasal airway. When expansion includes the orbit, diplopia or proptosis may occur.

Radiographic Description

With bony expansion comes a change in the shape of the sinus. Septa and the bony walls may be thinned and/or destroyed. When the mucocele is associated with the maxillary sinus antrum, teeth may be displaced or roots may be resorbed. In the frontal sinus, expansion causes smoothing of the usually scalloped border and, potentially, displacement of the intersinus septum. The orbit's supramedial border may be displaced or destroyed. In the ethmoid air cells, displacement of the lamina papyracea may occur contributing to displacement of the orbital contents. In the sphenoid sinus, expansion occurs superiorly and may be suggestive of a pituitary neoplasm. About 90% of mucoceles occur in the ethmoidal and frontal sinuses and are rare in the maxillary and sphenoid sinuses (Figure 3.26).

Differential Interpretation

While it may not be possible to distinguish between a mucocele located in the maxillary antrum from a cyst or neoplasm, a suggestion that the lesion is associated with an occluded ostium increases the likelihood that the lesion is indeed a mucocele. Blockage of the ostium is usually the result of a prior surgical procedure, although a deviated nasal septum or polyp may be a factor. A large odontogenic cyst displacing the maxillary antral floor may mimic a mucocele. CT is the imaging method of choice for differentiating these entities.

Figure 3.26. (a) Sagittal slice showing a mucocele (white star) of the ethmoid air cells altering the shape the air cells; (b) Coronal and (c) axial slices showing a mucocele (white star) of the right ethmoid air cells.

Treatment

Treatment of a mucocele is usually surgical, using a Caldwell-Luc procedure to allow excision of the lesion. The prognosis is excellent.

Postsurgical Changes of Paranasal Sinuses

Uncinectomy

Definition

One of the most accepted means of functionally enlarging the maxillary ostium is to perform an uncinectomy via the "swing door" technique. This initially removes the vertical process of the uncinate via backbiter inferiorly and sickle knife superiorly.

The uncinate is swung medially and then severed at its lateral attachment. This is followed by a submucosal removal of the horizontal process of the uncinate and subsequent trimming of the mucosa to fully visualize the maxillary ostium.

Controversy exists as to whether or not the maxillary ostium should be enlarged or not depending on the disease status of the maxillary sinus. However, the medical literature would support a wide antrostomy and complete clearance down to healthy mucosa if fungal mucin is present within the sinus.

Radiographic Description

In this circumstance, the ostium is enlarged superiorly to orbital floor and posteriorly to posterior fontanelle to allow wide access for clearance.

Caldwell-Luc Procedure

Definition/Radiographic Description

For persistent symptoms and disease in patients who have failed medical and the functional endoscopic approaches, older techniques can be used to address the inflammation of the maxillary sinus, such as the Caldwell-Luc radical antrostomy. This surgery involves an incision in the upper gum, opening in the anterior wall of the antrum, and removal of the entire diseased maxillary sinus mucosa. Drainage is allowed into inferior or middle meatus by creating a large window in the lateral nasal wall.

References

Bent, J. P., Cuilty-Siller, C., Kuhn, F. A. (1994). The frontal cell as a cause of frontal sinus obstruction. *American Journal of Rhinology*, **7**, 185–91.

Dolan, K. D. (1982). Paranasal sinus radiology, part 2A: Ethmoidal sinuses. *Head and Neck*, July/August, p. 486.

Gotwald, T. F., Zinreich, S. J., Fishman, E. K. (2001). Three-dimensional volumetric display of the nasal ostiomeatal channels and paranasal sinuses. *American Journal of Rhinology*, January, **176**, 241–45.

Huang, B. Y., Lloyd, K. M., DelGaudio, J. M., et al. (2009). Failed endoscopic sinus surgery: Spectrum of CT findings in the frontal recess. *Radiographics*. Jan–Feb, **29**(1), 177–95.

Som, P. M., and Curtin, H. D. (2003). *Head and Neck Imaging, Volume One*. Mosby, St. Louis, MO, pp. 97–101.

Som, P. M., and Curtin, H. D. (2003). *Head and Neck Imaging, Volume Two*. Mosby, St. Louis, MO, pp. 1061–62.

White, S., and Pharoah, M. (2004). *Oral Radiology, Principles and Interpretation*. Mosby, St. Louis, MO, pp. 581–85.

4 The Sinonasal Cavity and Airway

Gayle Reardon

Introduction

This chapter will cover the sinonasal cavity and airway. It is common for allergies and infectious diseases to affect not only the paranasal sinuses but also the nasal cavities. Therefore, the nasal cavity is a partner with the paranasal sinuses in terms of frequency for imaging indications. In addition to allergies and infectious disease, facial fractures are common and may range from a broken nose to more complex fractures secondary to traumas. Also, there are disfiguring tumors of the sinonasal cavities that have poor prognoses and wreak facial carnage, thus contributing to their fearsome reputations.

Anatomy

Nose is the term generally used to describe the pyramid-shaped external soft tissue projecting ventral to the surface of the face. Nasal fossa, or nasal cavities, refer to the internal nasal airways.

Topographically, the nose is divided into subunits that have practical importance for reconstructive surgeons. The subunits consist of the nasal dorsum, the nasal sidewalls, the nasal tip and columella, the alar lobule, and the supraalar facets. The nasion is the junction of the root of the nose with the forehead. The lower or caudal free margin of the nose is formed by the alar rim, columella, and tip. Bilaterally, the lateral lower margin of the nose has a rounded expansile region referred to as the alar lobule and consists of skin and soft tissue posterior and inferior to the lateral crus of

Interpretation Basics of Cone Beam Computed Tomography, First Edition.
Edited by Shawneen M. Gonzalez.

the lower lateral cartilage. The dorsum of the nose consists of the nasal bones' dorsal surfaces superiorly and the dorsal border of the quadrangular cartilage attaching to the upper lateral cartilages inferomedially. The junction of the alae with the face is known as the alar-facial junction.

Som and Curtin (2003) describe the journey of inspired air as it enters the nasal cavity in the following manner:

> Inspired air traverses the nasal valve. This is a circular area encompassed by the nasal septum, upper lateral cartilage, tip of the inferior turbinate, and floor of the nose. The total area encompassed by this valve provides the most important resistance to air flow in the nasal cavity. Of slightly lesser importance is the angle formed by the meeting of the quadrangular cartilage of the nasal septum and the inferior border of the upper lateral cartilages which is known as the nasal valve angle. Due to its mobile nature, it is a dynamic structure that narrows and widens with the phases of respiration. It is thus a critical factor in determining airflow through the nasal cavity.

The two sides of the nasal cavity are separated by the nasal septum. The septum supports the bony and cartilaginous vault and the tip of the nose. The main components of the nasal septum are the vomer, the perpendicular plate of the ethmoid, the quadrangular cartilage, the membranous septum, and the columella. The vomer may be bilaminar due to its embryologic origin; the vomer and the perpendicular plate of the ethmoid bone may become pneumatized.

The perpendicular plate of the ethmoid bone fuses with the cribriform plate superiorly. The vomer articulates superiorly with the perpendicular plate of the ethmoid and the crest of the sphenoid, anteriorly with the quadrangular cartilage, and inferiorly with the palatine bone and nasal crest of the maxilla. The thin groove of the quadrangular cartilage has as "tongue-in-groove" relationship with the vomer. The posterior border of the vomer is free and divides the posterior choanae.

The inferior concha is a separate bone of the skull. The inferior turbinate is larger than the other turbinates. The nasolacrimal duct drains tears into the inferior meatus. The superior and middle conchae are parts of the ethmoid bone. The middle meatus receives drainage from the frontal sinus (via the frontal recess) drains through the middle meatus, or infundibulum to middle meatus, to the nasal cavity to the nasopharynx. The maxillary sinus (via the maxillary ostium) drains through the infundibulum, the middle meatus, the nasal cavity, and, finally, the nasopharynx. The anterior ethmoid air cells drain via the anterior ethmoid ostia into the nasal cavity. In the ethmoid bone, the uncinate process is a curved lamina that projects downward and backward from this part of the labyrinth. It forms a small part of the medial wall of the maxillary sinus and articulates with the ethmoid process of the inferior nasal concha (Figures 4.1–4.10; Tables 4.1 and 4.2).

Normal Anatomy of the Ostiomeatal Complex

See Chapter 3 for additional information.

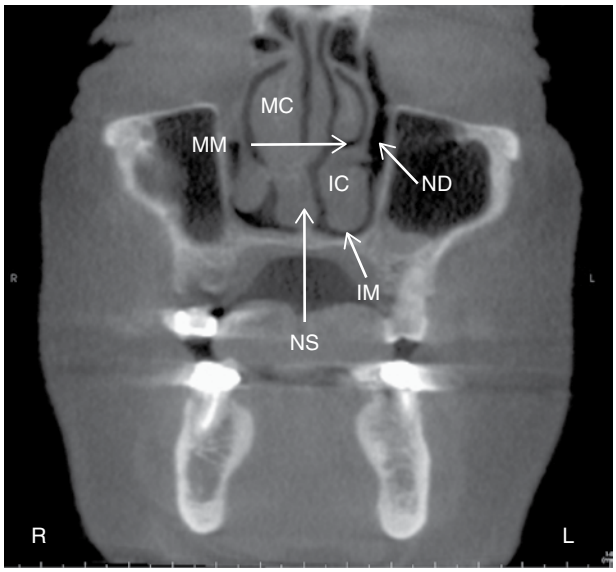

Figure 4.1. Coronal slice at the maxillary first premolar showing the middle concha (MC), middle meatus (MM), nasolacrimal duct (ND), inferior concha (IC), inferior meatus (IM), and nasal septum (NS).

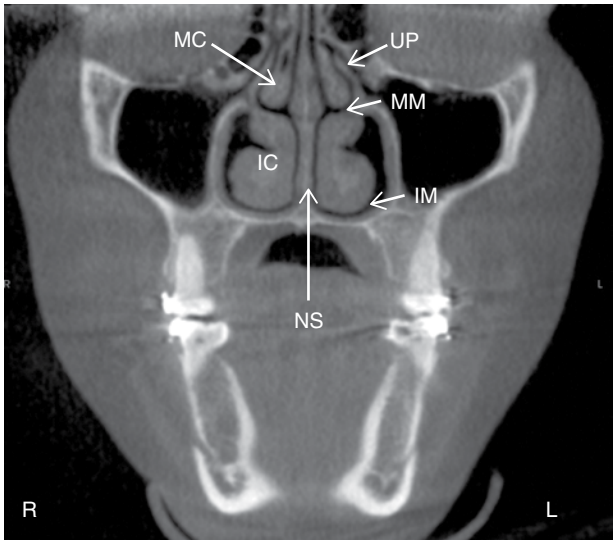

Figure 4.2. Coronal slice at the ostiomeatal unit showing the uncinate process (UP), middle concha (MC), middle meatus (MM), inferior concha (IC), inferior meatus (IM), and nasal septum (NS).

Anatomical Variations of the Nasal Septum

The nasal septum is fundamental to the development of the nose and paranasal sinuses. Deviations of the nasal septum are usually congenital but are due to previous experiences of trauma in some patients. Developmentally, there may be malalignment of the components of the nasal septum (the septal cartilage,

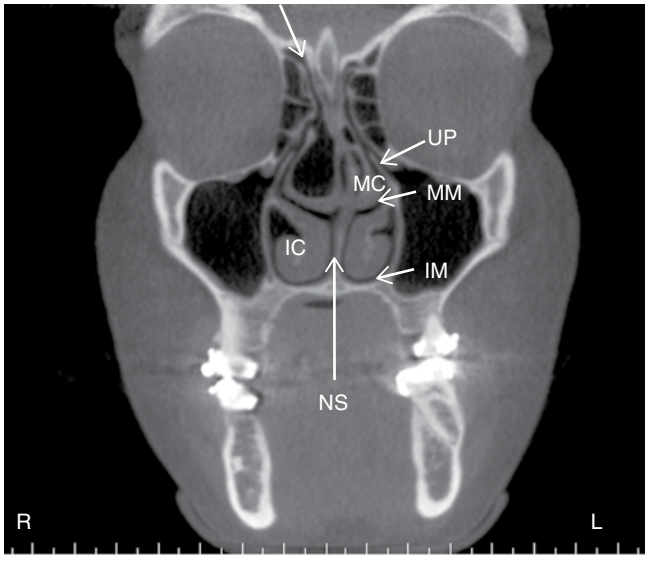

Figure 4.3. Coronal slice at the ostiomeatal unit showing the frontal recess (white arrow), uncinate process (UP), middle concha (MC), middle meatus (MM), inferior concha (IC), inferior meatus (IM), and nasal septum.

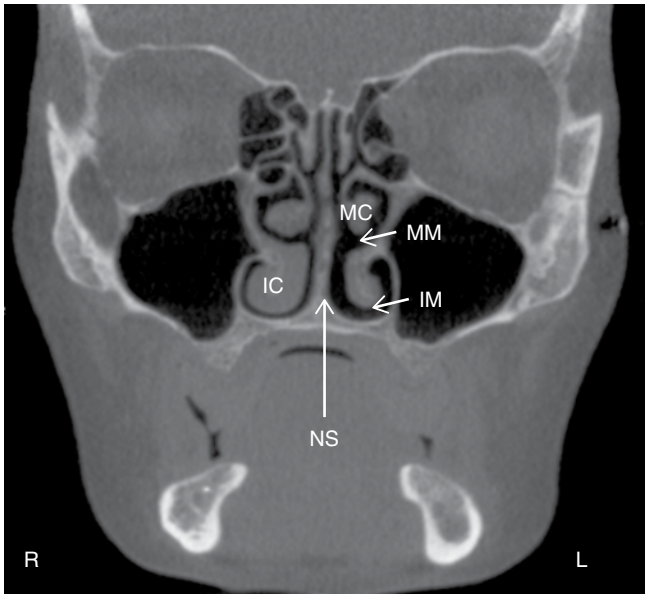

Figure 4.4. Coronal slice at the zygomatic process of the maxilla showing the middle concha (MC), middle meatus (MM), inferior concha (IC), inferior meatus (IM), and nasal septum (NS).

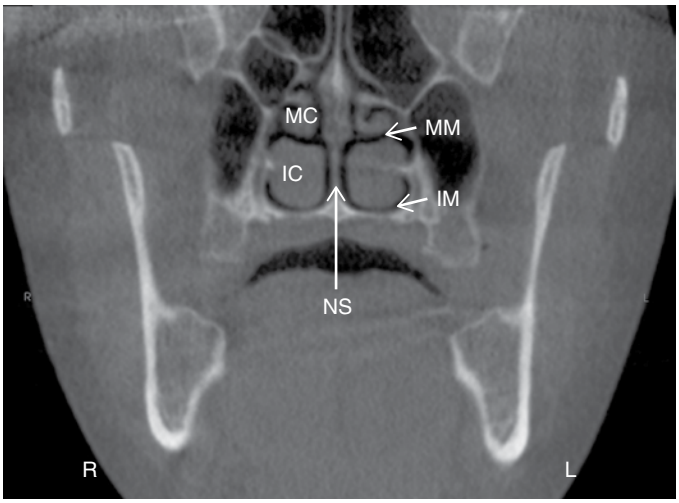

Figure 4.5. Coronal slice at the posterior aspect of the maxillary sinuses showing the middle concha (MC), middle meatus (MM), inferior concha (IC), inferior meatus (IM), and nasal septum (NS).

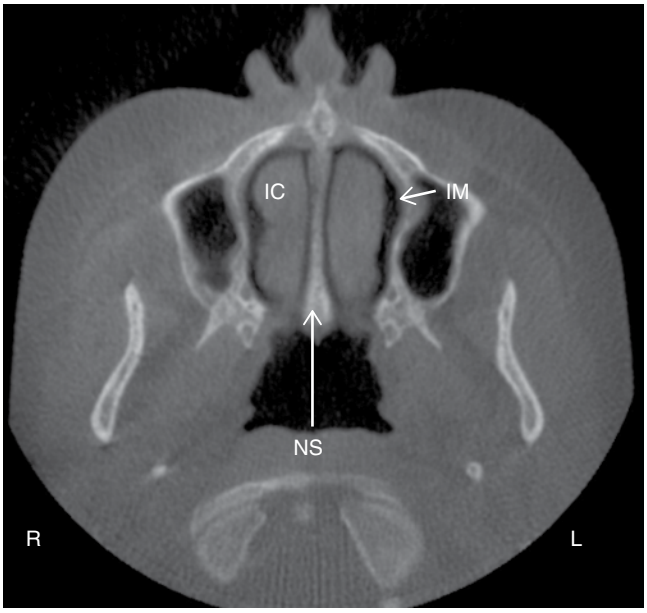

Figure 4.6. Axial slice at the level of the inferior aspect of the maxillary sinuses showing the inferior meatus (IM), inferior concha (IC), and nasal septum (NS).

perpendicular ethmoid bone, and vomer), which may cause deviation of the nasal septum, deformities of the tongue-in-groove relationship of the cartilage and vomer, or a septal bony spur. About one-third of septal deviations are asymptomatic, however more severe chondrovomer articulation problems may contribute to sinusitis symptoms. Obstruction, secondary inflammation, and infection of the middle meatus have been observed secondary to severe nasal septal deviations (Figures 4.11–4.12).

Figure 4.7. Axial slice at the midlevel of the maxillary sinuses showing the nasolacrimal duct (ND) and nasal septum (NS).

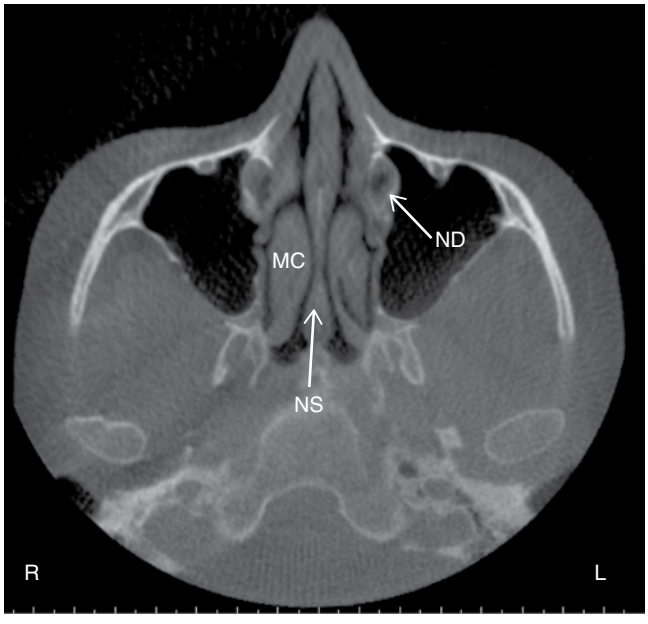

Figure 4.8. Axial slice at the level of the condyles showing the nasolacrimal duct (ND), middle concha (MC), and nasal septum (NS).

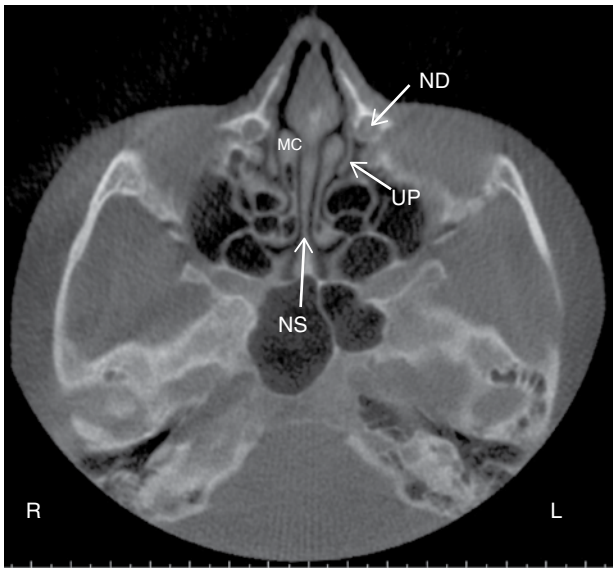

Figure 4.9. Axial slice at the level of the inferior orbits showing the nasolacrimal duct (ND), uncinate process (UP), middle concha (MC), and nasal septum (NS).

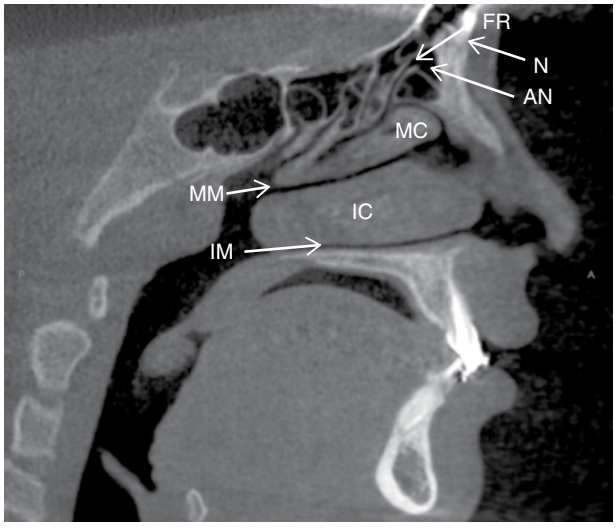

Figure 4.10. Sagittal slice slightly lateral to the midline showing the frontal recess (FR), nasion (N), agger nasi cell (AN), middle concha (MC), middle meatus (MM), inferior concha (IC), and inferior meatus (IM).

Anatomical Variations of the Middle Turbinate

There are several variations of the middle turbinate including paradoxic curvature, concha bullosa, lamellar concha, medial/lateral displacement, L-shaped lateral branding, and sagittal transverse clefts. The first three, which are more common, are described in detail below.

Table 4.1. Anatomical landmarks identifiable on coronal views with corresponding figures.

Anatomical landmark	Figures visible on
Nasolacrimal duct	4.1
Nasal septum	4.1 4.2 4.3 4.4 4.5
Inferior meatus	4.1 4.2 4.3 4.4 4.5
Inferior concha	4.1 4.2 4.3 4.4 4.5
Middle meatus	4.1 4.2 4.3 4.4 4.5
Middle concha	4.1 4.2 4.3 4.4 4.5
Uncinate process	4.2
Frontal recess	4.3

Table 4.2. Anatomical landmarks identifiable on axial views with corresponding figures.

Anatomical landmark	Figures visible on
Nasolacrimal duct	4.7 4.8 4.9
Nasal septum	4.6 4.7 4.8 4.9
Inferior meatus	4.6
Inferior concha	4.6
Middle concha	4.8 4.9
Uncinate process	4.9

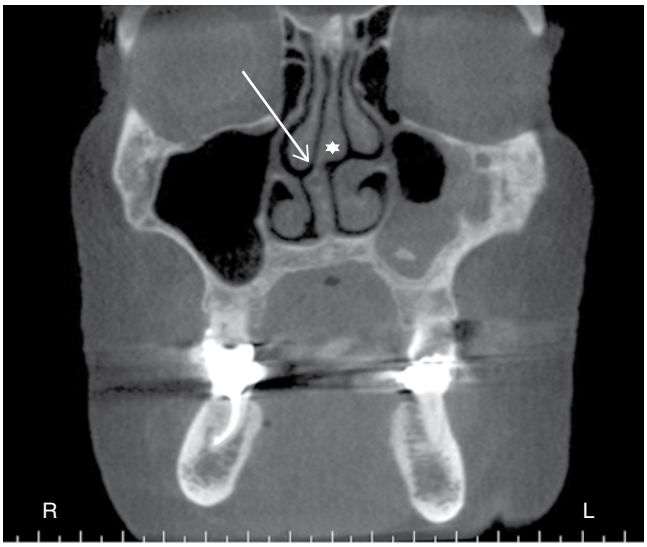

Figure 4.11. Coronal slice showing nasal septum deviated to the right (white arrow) with enlargement of the septal cartilage (septal tubercle) (white star).

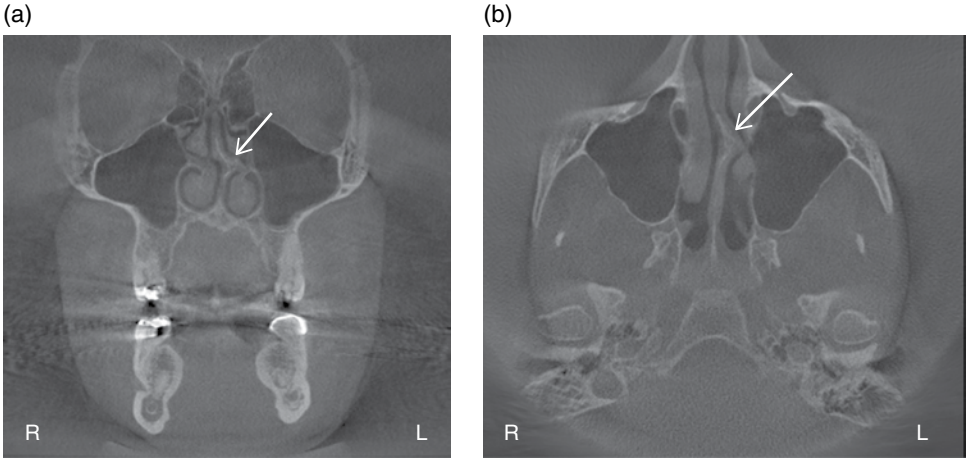

Figure 4.12. (a) Coronal slice showing left-sided bony spur formation at the level of the middle meatus (white arrow); (b) Axial slice showing left-sided bony spur formation (white arrow).

Paradoxic Curvature

Normally the convexity of the middle turbinate is directed laterally, toward the lateral sinus wall. When paradoxically curved, the convexity is directed medially toward the nasal septum. The inferior edge of the middle turbinate may take on excessive curvature, which may then narrow or obstruct the nasal cavity, infundibulum, or middle meatus. Because of the potential narrowing and/or obstruction associated with paradoxic curvature, it is considered a contributing factor to sinusitis by authors Som and Curtin (2003) (Figure 4.13).

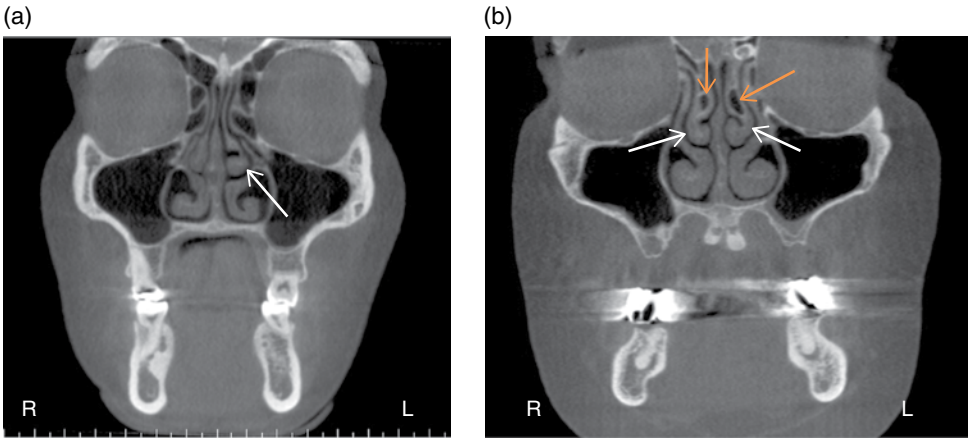

Figure 4.13. (a) Coronal slice showing paradoxical curvature of the left middle concha (white arrow); (b) Coronal slice showing paradoxical curvature of the right and left middle conchae (white arrows) with lamellar concha at the attachment of right and left middle conchae (orange arrows).

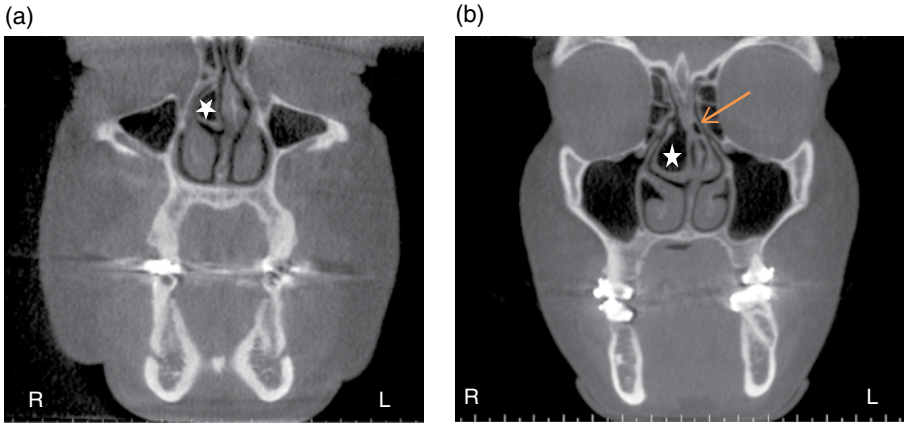

Figure 4.14. (a) Coronal slice showing concha bullosa (aerated concha) of the right middle concha (white star); (b) Coronal slice showing concha bullosa (white star) and lamellar concha (orange arrow).

Concha Bullosa

A concha bullosa is an aerated turbinate; the turbinate most often associated with concha bullosa is the middle turbinate (Figures 4.14–4.16). Concha bullosa may be either unilateral or bilateral; however it is more frequently bilateral in its presentation. Less frequently, aeration of the superior turbinate may occur; an aerated inferior turbinate is uncommon. Classifications of concha bullosae are divided according to degree of turbinate pneumatization. When the pneumatization involves the bulbous segment of the middle turbinate, the term *concha bullosa* applies. If the pneumatization is limited to the attachment portion of the middle turbinate and does not extend into the bulbous segment, it is called lamellar concha. A concha bullosa of the middle turbinate may cause enlargement of the turbinate such that the middle meatus or

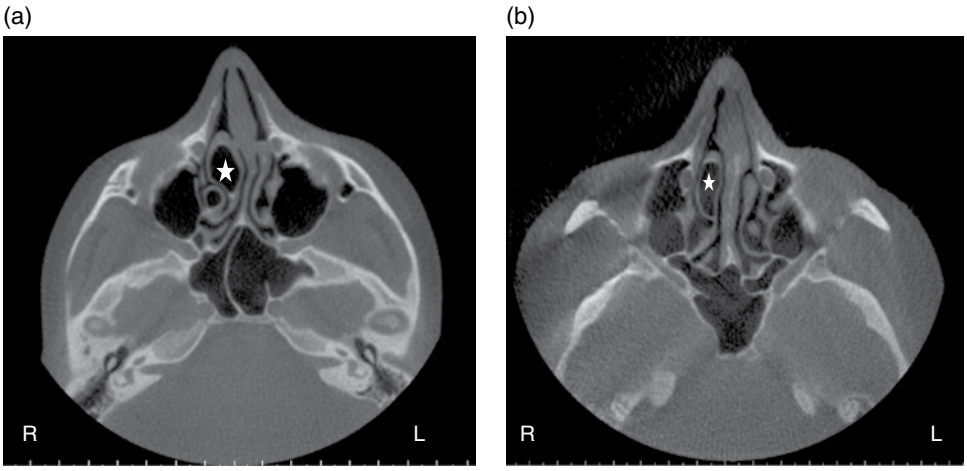

Figure 4.15. Axial slices (a,b) showing concha bullosa (aerated concha) of the right middle concha (white stars).

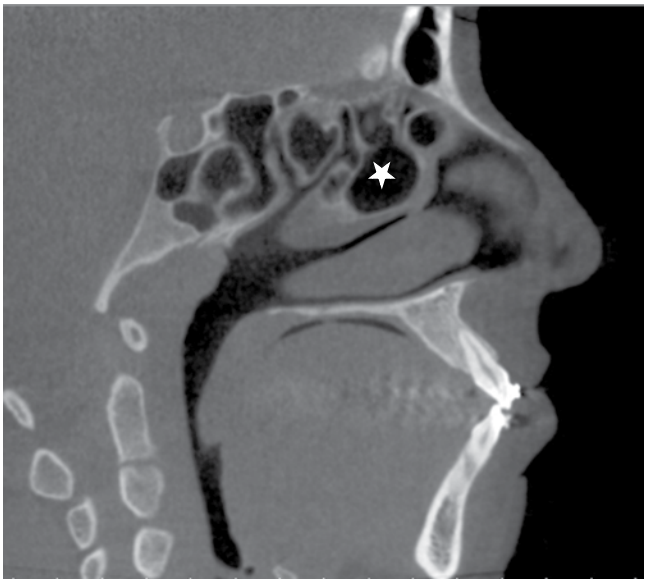

Figure 4.16. Sagittal slice showing concha bullosa (white star).

infundibulum are obstructed, thus associating concha bullosa with a higher prevalence of ipsilateral sinus disease.

Lamellar Concha

Only the attachment portion of the middle turbinate is pneumatized, and the pneumatization does not extend into the bulbous segment (see Figures 4.13b, 4.14b, and 4.17).

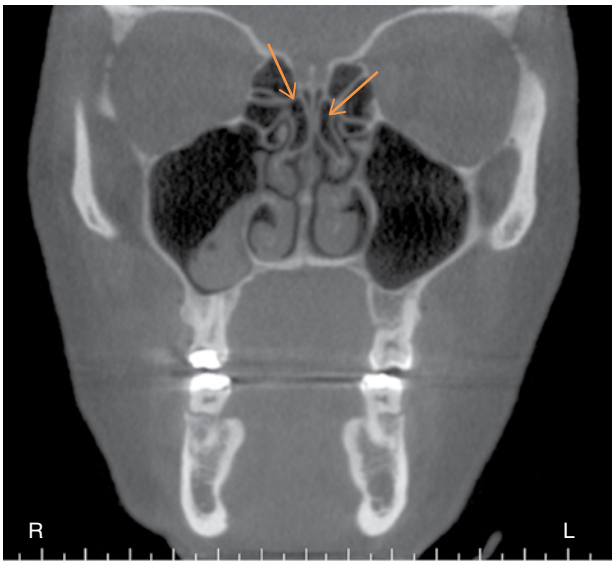

Figure 4.17. Coronal slice showing bilateral lamellar concha (orange arrows).

Anatomy of the Uncinate Process

Attachment

Normally, the upper tip of the uncinate process attaches to the lateral nasal wall where the agger nasi cells are commonly located. Anatomic variations of the uncinate attachment include attachment to the lamina papyracea, the lateral surface of the middle turbinate, or the fovea ethmoidalis in the floor of the anterior cranial fossa. Sometimes the free edge of the uncinate process may adhere to the orbital floor or the inferior aspect of the lamina papyracea, a condition known as an atelectatic uncinate process , and is associated with a hypoplastic, and often opacified, ipsilateral maxillary sinus secondary to closure of the infundibulum. Yet another variant of the uncinate process configuration is its extension superiorly to the roof of the anterior ethmoid sinus causing the superior infundibulum to end as a "blind pouch." This continuation of the uncinate is referred to as lamina terminalis. In these causes, the infundibulum drains via the posterior aspect of the middle meatus.

The uncinate process may also become pneumatized, a condition referred to as uncinate bulla (Figures 4.18 and 4.19). Uncinate bulla is considered a predisposing factor for impaired sinus ventilation in the anterior ethmoid, frontal recess, and infundibular regions. Functionally, the pneumatized uncinate process resembles concha bullosa and is believed to be an extension of the agger nasi cell within the anterosuperior portion of the uncinate process.

Deviation

The uncinate process is one of the crucial bony structures of the wall of the lateral nasal cavity. The uncinate process together with the ethmoid bulla form the boundaries of the hiatus semilunaris and ethmoid infundibulum, the structures through which the frontal and maxillary sinuses drain. It is the free edge of the

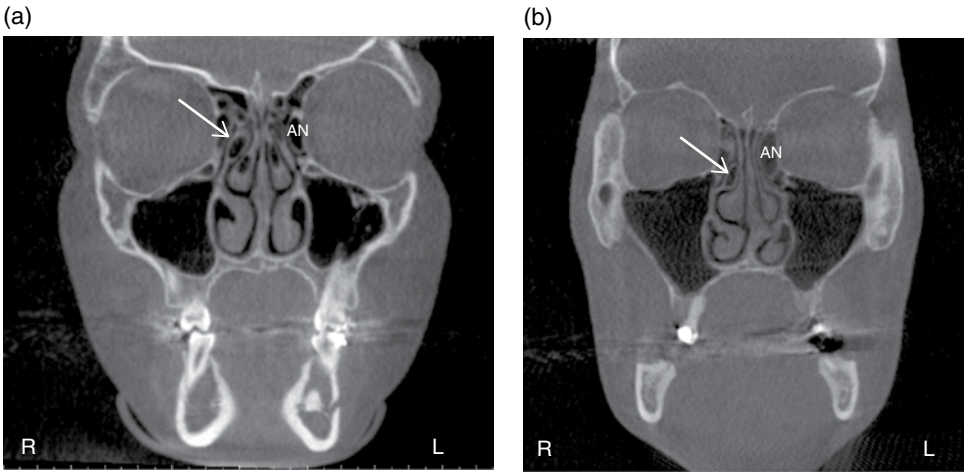

Figure 4.18. Coronal slices (a,b) showing uncinate bulla of the right uncinate process (white arrow) and left agger nasi cells (AN).

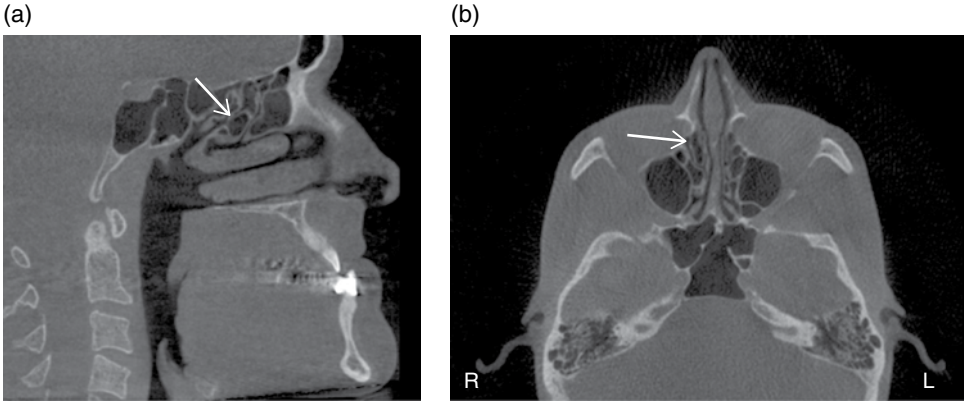

Figure 4.19. (a) Sagittal slice showing uncinate bulla (white arrow); (b) Axial slice showing uncinate bulla of the right uncinate process (white arrow).

uncinate process that may vary in configuration. Medial and lateral deviation of uncinate process may cause narrowing or obstruction of the middle meatus, the hiatus semilunaris, and infundibulum.

Anatomy of the Frontal Recess

The frontal recess is an hourglass-like narrowing between the frontal sinus and the anterior middle meatus through which the frontal sinus drains. It is not a tubular structure as "nasofrontal duct" might imply, thus the use of the term *frontal recess*. The frontal recesses are the narrowest anterior air channel and common site of inflammation resulting in loss of ventilation and mucociliary clearance of the frontal sinus (see Figures 4.3 and 4.10).

The boundaries of the frontal recess are agger nasi cells anteriorly and the ethmoid bulla, its associated bulla lamella, and the suprabullar cell (if present) posteriorly. The lateral border is the lamina papyracea. The medial border is the most anterior and superior portion of the middle turbinate.

In approximately 40% of cases, secretions from the frontal recess drain into the ethmoid infundibulum and subsequently into the middle meatus through the hiatus semilunaris. In the remaining cases, the frontal recess drains directly into the middle meatus.

The frontal recess may be pneumatized by various anterior ethmoid cells, which are collectively known as frontal recess cells. These cells are normal anatomic variations that are present in some combination in most individuals. The clinical relevance of frontal recess cells lies in their potential for causing frontal sinusitis by obstructing frontal sinus outflow at the level of the frontal recess. Any endoscopic surgical procedure aimed at clearing frontal recess obstruction must address these variant cells; failure to do so may result in surgical failure. For this reason, the radiologist's report must accurately characterize any frontal recess cells present by using standard accepted nomenclature.

The frontal recess cells include agger nasi cells, frontal cells (Type 1, 2, 3, and 4), supraorbital ethmoid cells, frontal bullar cells, suprabullar cells, and interfrontal sinus septal cells. The frontal cells along with the agger nasi cells constitute the anterior group of frontal recess cells

The supraorbital ethmoid cells, frontal bullar cells, and suprabullar cells make up the posterior group of frontal recess cells. All of the cells in this group are located along the posterior wall of the frontal recess and are bordered posteriorly or superiorly by the anterior skull base.

Agger Nasi Cell

Agger nasi is a Latin term meaning "nasal mound." The agger nasi appears as an eminence located on the lateral nasal wall at the leading edge of the middle turbinate; it represents the intranasal portion of the frontal process of the maxilla. The agger nasi serves as the anterior limit of the frontal recess. Pneumatization of the agger nasi (resulting in the agger nasi cell) occurs in 78%–98.5% of individuals. When present, agger nasi cells are considered the most anterior of all ethmoid cells and can pneumatize posteriorly to narrow the frontal recess (see Figures 4.10, 4.18, 4.20, and 4.21).

Frontal Cells

Frontal cells, along with the agger nasi cell, constitute the anterior group of frontal recess cells. Frontal cells are present at CT in 20%–33% of patients. The anterior boundaries of these cells are made up of the anterior wall of the frontal recess or the frontal sinus; these cells do not extend posteriorly to abut the skull base. There are four types of frontal cells described under the system known as the Kuhn classification.

Type 1 Frontal Cells Seen in up to 37% of frontal recesses, they are defined as single anterior ethmoid cells within the frontal recess sitting above the agger nasi cell. These cells do not extend into the frontal sinus (Figure 4.21).

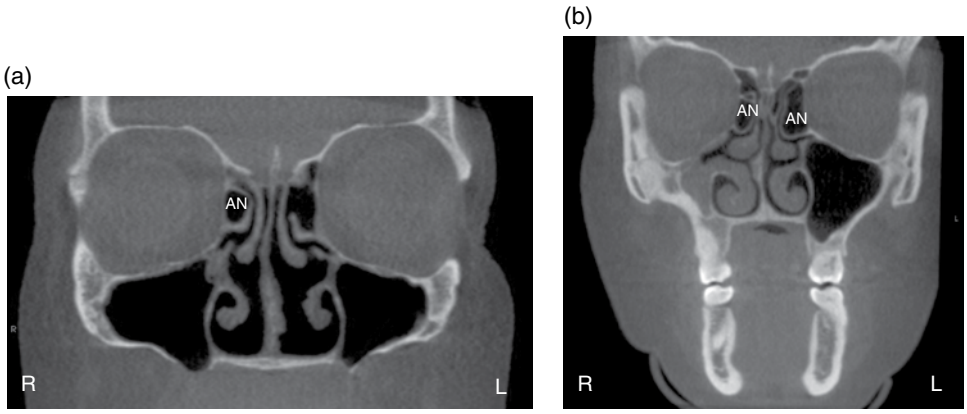

Figure 4.20. Coronal slices (a,b) showing agger nasi cells (AN) directly medial to the orbits.

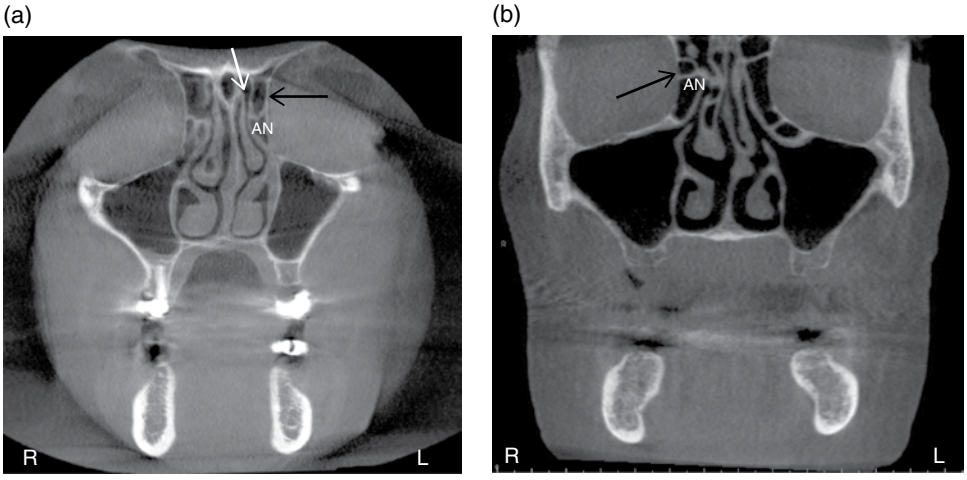

Figure 4.21. (a) Coronal slice showing type 1 frontal cell (black arrow) directly superior to agger nasi cell (AN) and lateral to the frontal recess (white arrow); (b) Coronal slice showing type 1 frontal cell (black arrow) directly medial to the right orbit and superior to an agger nasi cell (AN).

Type 2 Frontal Cells Seen in up to 19% of frontal recesses, they are defined as a tier of two or more anterior ethmoid cells sitting above the agger nasi cell (Figure 4.22).

Type 4 Frontal Cells Type 4 frontal cells account for 2.4% of all frontal recesses. Type 4 frontal cells are unique among the frontal cells in that they do not directly touch the agger nasi cell. They are defined as an isolated air cell located within the frontal sinus. It is bordered anteriorly by the anterior frontal sinus table, with their posterior walls representing free partitions in the frontal sinus. Recognition of type 4 cells often requires both coronal and sagittal CT reformation. On sagittal images, these cells have been described as having the appearance of a "balloon on a string," with the cell itself representing the balloon and the narrow outflow tract of the cell representing the string. Most often, type 4 cells have no identifiable connection to

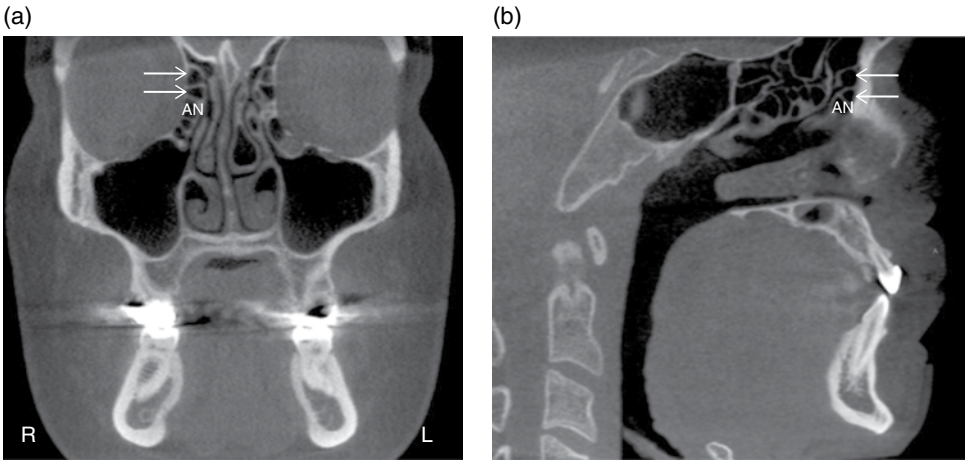

Figure 4.22. (a) Coronal and (b) sagittal slices showing type 2 frontal cells (white arrows) superior to an agger nasi cell (AN).

the frontal recess on imaging. In patients with frontal sinus disease, an isolated aerated cell abutting the anterior sinus wall in an otherwise opacified frontal sinus (the "cell within a cell") usually represents a type 4 frontal cell. It has been observed that frontal mucosal thickening is more prevalent in patients with type 3 and type 4 frontal cells than in those without frontal cells.

Supraorbital Ethmoid Cells

The supraorbital ethmoid cells are anterior ethmoid air cells that extend superiorly and laterally over the orbit from the frontal recess. These cells represent pneumatization of the orbital plate of the frontal bone posterior to the frontal recess and the frontal sinus. Identification of these cells at CT requires review of both axial and coronal images (Figure 4.23). They typically drain into the lateral aspect of the frontal recess. Up to 15% of adults may have one or more supraorbital ethmoid cells, with approximately 5% of frontal sinuses having multiple supraorbital cells. Supraorbital ethmoid cells can obstruct frontal sinus drainage. Preoperative identification is essential because these cells can be readily mistaken for the frontal ostium during endoscopic dissection.

Frontal Bullar Cell

This presents as a pneumatization of the anterior skull base in the posterior frontal recess with extension into the true frontal sinus. These cells lie above the ethmoid bulla and, when present, define a portion of the posterior boundary of the frontal recess and frontal sinus.

Suprabullar Cells

Suprabullar cells are nearly identical to frontal bullar cells, with the only distinguishing feature being that suprabullar cells lie entirely below the level of the frontal sinus ostium and do not extend into the frontal sinus. They sit above the ethmoid bulla and form a portion of the posterior wall of the frontal recess. They are best demonstrated

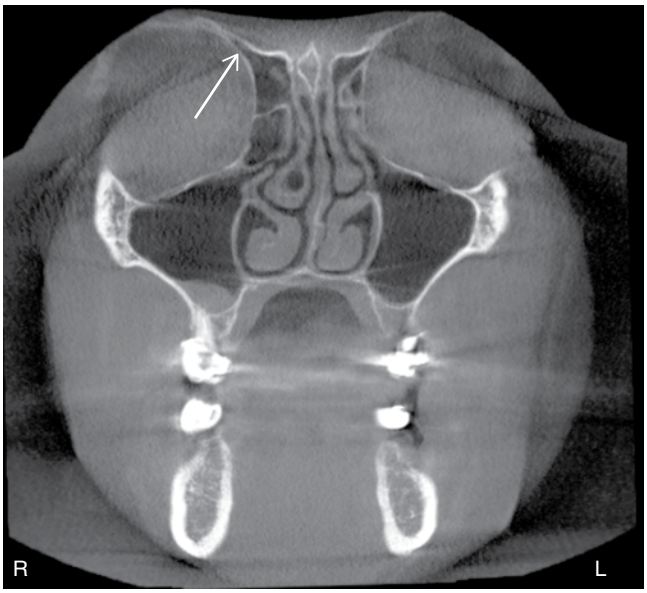

Figure 4.23. Coronal slice showing supraorbital ethmoid cell extending partially superior to the right orbit (white arrow).

on sagittal CT images. The suprabullar cell is bordered superiorly by the skull base, however, unlike a frontal bullar cell, the suprabullar cell does not extend above the level of the frontal ostium into the frontal sinus. During endoscopic frontal sinusotomy, both suprabullar and frontal bullar cells can be mistaken for the skull base; failure to recognize their presence preoperatively can result in incomplete surgical dissection.

Interfrontal Sinus Septal Cell

The interfrontal sinus septal cell represents pneumatization of the interfrontal sinus septum. When extensive, such pneumatization can extend into the crista galli. These cells drain into the medial frontal recess and can impinge on the frontal sinus. Axial and coronal are the best planes for demonstrating these cells.

Surgical Variations

Frontal Sinuses

Endoscopic Frontal Recess Approach (Draf Type I Procedure)

This surgery consists of removal of obstructing structures, including anterosuperior ethmoid cells (agger nasi cell and any obstructing frontal recess cells) and the uncinate process. The dissection does not extend above the frontal ostium, hence the nasofrontal beak remains (best seen on the sagittal image).

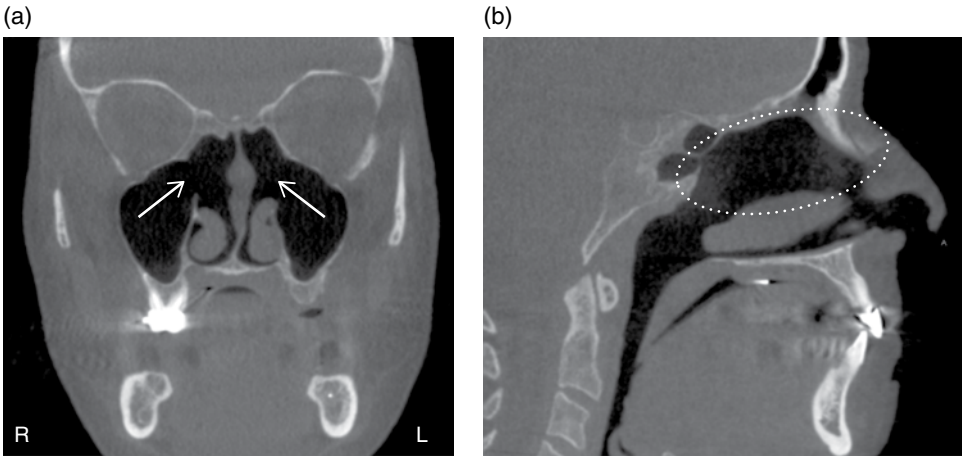

Figure 4.24. (a) Coronal slice showing draf type III surgery (white arrows); (b) Sagittal slice showing draf type III surgery (white dotted circle).

Extended Frontal Sinusotomy (Draf Type II Procedure)

This procedure can be difficult to distinguish from the less-invasive endoscopic frontal recess approach (Draf type I surgery) at postoperative CT. Unlike the Draf type I procedure, Draf type II surgery includes resection of the frontal sinus floor and may extend into the frontal sinus, resulting in a less-pronounced or absent nasofrontal beak on sagittal images.

Modified Lothrop Procedure (Draf Type III Procedure)

This procedure consists of contiguous bilateral enlargement of the frontal outflow tract, a result achieved by removal of the frontal sinus floors and adjacent parts of the inferior interfrontal sinus septum, superior nasal septum, and anterior middle turbinates (Figure 4.24).

FESS Failure in Frontal Recess

Most cases of recurrent frontal sinusitis after functional endoscopic sinus surgery (FESS) can be attributed to stenosis of the frontal recess caused by:

a) Inadequate removal of the agger nasi and frontal recess cells
b) A retained superior portion of the uncinate process
c) Lateralization of the middle turbinate
d) Osteoneogenesis secondary to chronic inflammation or mucosal stripping
e) Scarring or inflammatory mucosal thickening
f) Recurrent polyposis

Residual Frontal Recess Cells

Postoperative coronal and sagittal CT images obtained through the left frontal recess show complete opacification of the frontal sinus and frontal recess. There are

remnant opacified frontal recess cells, including an agger nasi cell and a tier of type 2 frontal cells, which narrow the frontal ostium and frontal recess.

Effect of the Superior Attachment of the Uncinate Process on Frontal Recess Drainage

The uncinate process has attached to the lamina papyracea. As a result, the ethmoid infundibulum terminates in a "blind recess" known as the recessus terminalis. In this case, frontal recess drainage passes directly into the middle meatus.

Coronal CT image shows the uncinate process attached to the skull base at the junction of the cribriform plate and lateral lamella. Therefore, frontal recess drainage is directed into the ethmoid infundibulum. In patients who have not undergone surgery, one of the most common causes of obstruction at the level of the frontal recess is a medially displaced uncinate process. This occurs when disease in the recessus terminalis displaces the uncinate process medially so that it lies close to or even against the middle turbinate. Occasionally, the uncinate process and middle turbinate may become fused. It is not uncommon for surgeons to ignore the superior attachment of the uncinate process. Not surprisingly, if a medialized uncinate process is left behind during FESS, then the frontal recess will have a tendency to restenose postoperatively.

Retained Uncinate Process

The uncinate process is attached to the lamina papyracea and forms a recessus terminalis, which is opacified. The frontal recess is opacified at the level of the recessus terminalis. The medialized left middle turbinate may adhere to the nasal septum; this appearance is a normal and often expected postsurgical finding.

Lateralized Middle Turbinate Remnant

In patients who have undergone middle turbinate manipulations, including partial middle turbinate resection, the amputated anterior stump may lateralize and obstruct the frontal recess. It has been suggested that recurrent frontal sinusitis occurs significantly more often in patients who have undergone partial middle turbinate resection than in surgically treated patients with intact middle turbinates; recent studies have disputed this claim.

Inflammatory Diseases

CT of the paranasal sinuses should not be performed until 4–6 weeks after initiation of medical therapy, and scanning should be delayed in patients with acute upper respiratory infections. Review of both sagittal and coronal reformatted images together significantly improves the practitioner's ability to identify and measure the frontal recess and is critical in assessment of obstructing anterior ethmoid cells. Helical scanning with a maximum section thickness of no greater than 1 mm is recommended.

Sinusitis

Sinusitis accounts for approximately 11.6 million office-based outpatient visits annually. In a significant proportion of patients with sinusitis, medical management alone is insufficient, necessitating surgical management. Functional endoscopic sinus surgery (FESS) has become the treatment of choice for patients with medically refractory rhinosinusitis. FESS is performed more than 200,000 times per year in the United States. FESS has a published success rate of 76%–98%. Up to 23% of patients require revision surgery. In patients presenting with sinusitis after FESS, the frontal sinus outflow tract is the region where disease recurrence is most likely to occur. In addition, most medically refractory disease of the frontal sinuses can be attributed to obstruction at the level of the frontal recess. The frontal recess is a notoriously difficult area to treat with endoscopy owing to its anterior location and its tight confines between the orbit and anterior skull base. Furthermore, the frontal recess has a significant predilection for stenosis after FESS. Evaluation of patients in whom FESS has failed typically includes CT of the paranasal sinuses to identify the potential causes of sinus outflow tract stenosis. Practitioners need to be familiar with the complex anatomy of the frontal recess and the processes that may contribute to surgical failure in order to generate accurate and meaningful reports for the referring rhinologists (see Chapter 3 for more information on sinusitis).

Osteoneogenesis

Among the primary objectives of FESS is preservation of normal mucociliary function. Failure to preserve the normal mucosa will tend to result in scarring and osteoneogenesis. Osteoneogenesis, also referred to as osteitis or hyperostosis, refers to bone remodeling and new bone formation caused by chronic inflammation. Sinus CT demonstrates osteoneogenesis in 36%–64% of patients with chronic rhinosinusitis, and the presence of hyperostosis at preoperative CT has been shown to be a predictor of poorer surgical outcome after FESS. The relatively high prevalence of osteoneogenesis in postoperative patients is believed to be related to a combination of surgical mucosal trauma, persistent inflammation, and chronic refractory infection. As for the reason why the presence of osteoneogenesis may contribute to surgical failure, it has been suggested that osteitic bone remnants serve as an inflammatory nidus, inducing overlying mucosal edema and hypertrophy, which in turn may contribute to frontal recess stenosis. In normal individuals, the bony septa of the ethmoid sinuses have an average thickness of approximately 0.5 mm, with the upper limit of normal being about 1 mm. In addition, on axial images the middle turbinate measures, on average, 1.5 mm at its midpoint in thickness. The normal upper limit of the middle turbinate measures 2.5 mm. When seen on CT, osteoneogenesis appears as thickening of the ethmoid septa or sinus walls and is often accompanied by scarring or mucosal edema. There is associated mucosal thickening, which may represent inflamed edematous mucosa, scar tissue, or secretions, causing sinus opacification.

Scarring and Inflammatory Mucosal Thickening

Scarring and inflammatory mucosal thickening in the frontal recess are extremely common after FESS, even in asymptomatic patients not requiring revision surgery. Although mucosal disease probably plays a role in most cases of recurrent frontal

sinusitis after FESS, its presence at CT or endoscopy does not necessarily correlate with the presence of symptoms after surgery. Chronic sinus disease may be underdiagnosed with CT, as mucosal disease may be endoscopically visible even when it is not seen at CT. It is impossible to differentiate scarring from inflamed edematous mucosa at CT because both appear as mucosal thickening, and they should be reported as such. Within the paranasal sinuses, mucosal thickness up to 3 mm may be normal. In evaluation of the frontal recess, it is generally sufficient to report the presence or absence of mucosal thickening and, when mucosal thickening is present, a representative measurement of the degree of mucosal thickness.

Recurrent Polyposis

Sinonasal polyps are among the most frequent complications of sinusitis and among the most common findings in patients undergoing sinus surgery. They are formed by expansion of fluid in the deep lamina propria of the sinonasal Schneiderian mucosa and are the most common expansile lesions in the nasal cavity. Polyps have been associated with multiple causes including infectious rhinosinusitis, cystic fibrosis, aspirin intolerance, and allergic fungal sinusitis. Sinonasal polyposis is considered a predictor of poorer surgical outcome (surgical failure rates of 75% have been reported in patients with extensive sinonasal polyposis before surgery). Recurrent polyposis is seen in 29.9%–40% of patients undergoing revision FESS. On CT images, polyps are usually homogeneous soft-tissue masses with smooth convex borders and may be single or multiple. As they enlarge, they may fill a sinus and go on to remodel or even destroy adjacent bony structures. Postoperative coronal and sagittal CT images show opacification of the frontal sinuses and polypoid soft tissue completely opacifying the frontal recess, findings consistent with recurrent polyposis.

Other Causes of Frontal Recess Obstruction

- Previously undetected mucoceles
- Polyps
- Mucous retention cyst
- Neoplasms
- Fibro-osseous lesions

Conclusions

CT is an invaluable adjunct to diagnostic nasal endoscopy in identifying various causes of frontal recess obstruction after FESS. Proper interpretation of CT scans obtained in patients being considered for frontal recess revision surgery requires a clear understanding of frontal recess anatomy, which in turn requires reviewing images in axial, coronal, and sagittal planes. In addition, a working knowledge of the most common causes of surgical failure in the frontal recess will ensure that these entities are not overlooked during revision surgery. Recognition and effective communication of the presence of these findings should lead to better patient care and may reduce the likelihood of additional surgical failures.

The Pharynx

The pharynx extends behind the oral cavity from the skull base to the level of the caudal cricoid cartilage. The pharynx is a mucosa-lined musculomembranous tube, which has historically been subdivided into three sections, the nasopharynx extending from the skull base to the level of the hard palate, the oropharynx extending from the level of the hard palate to the level of the hyoid bone, and the hypopharynx extending from the level of the hyoid bone to the caudal cricoid cartilage.

The Nasopharynx

The nasopharynx is a stratified squamous and columnar epithelium-lined cavity situated at the superior-most aspect of the aerodigestive tract. It measures about 2 cm in diameter anteroposteriorly and 4 cm in length. The nasopharynx communicates anteriorly with the nasal cavity and inferiorly with the oropharyngeal cavity. It is limited superiorly by the base of the skull, posteriorly by the prevertebral musculature of C1 and C2, and laterally by the pharyngeal constrictors and deep soft-tissue planes of the parapharyngeal space and infratemporal fossa. The inferior margin of the nasopharynx is the level of the hard palate and Passavant's muscle, which opposes the soft palate when elevated. It is Passavant's ridge that meets the elevated soft palate to close off the nasopharynx during swallowing. Overlying the nasopharyngeal structures is the pharyngobasilar fascia, which attaches to the base of the skull superiorly and the medial pterygoid plate anteriorly but has a free inferior margin. Patency of the nasopharynx is retained by the pharyngobasilar fascia. The visceral fascia and pharyngeal constrictor muscles form the lateral soft tissue borders supported by a bony framework composed of the maxilla anteriorly, the mandible laterally, and the base of the skull and vertebral bodies posteriorly. The visceral fascia surrounds the nasopharyngeal mucosa and constrictor muscles separating the nasopharynx from the deep fascial spaces and is thought to be a barrier to the spread of infection and malignancy.

The superior border of the nasopharynx consists of part of the vomer and the body of the sphenoid bone. If not surgically removed or atrophied, adenoidal tissues are located in the midline of the roof of the nasopharynx. The lateral bony border of the nasopharynx is the medial plate of the pterygoid process of the sphenoid bone with the medial pterygoid muscle attaching on the medial surface of the lateral plate and the pterygoid fossa. The anterior part of the nasopharynx is in direct communication with the nasal cavity by way of the posterior nasal choanae. It communicates with the middle ear cavity via the Eustachian tubes, which gain access to the nasopharynx through the sinus of Morgagni, a defect in the anterior portion of the pharyngobasilar fascia, which is superior to the pharyngeal constrictor muscle and along the superior posterior border of the medial pterygoid plate. The sinus of Morgagni is also a route of entry into the pharynx for the levatorvelli palatine muscle; it is this pathway that may provide access to the parapharyngeal region and central skull base for advanced nasopharyngeal cancer spread. The openings of the Eustachian tubes are located about 1 cm posteroinferiorly to the inferior turbinate, which predisposes the Eustachian tubes to obstruction by nasopharyngeal masses. Such obstructions may result in serous otitis in 50% of patients with history of nasopharyngeal masses.

Just posterosuperiorly to the torus tubarius is the fossa of Rosenmuller, a mucosa-lined recess at the most laterosuperior aspect of the nasopharynx. The fossa of Rosenmuller is lateral to flexor muscles of the neck, longus capitis, and colli, and is a common origination site for nasopharyngeal cancers.

It is not uncommon for children to present with prominent adenoids, which reach their maximal size around 5 years of age. Involution of the adenoids begins around the time of puberty with the majority of adenoidal tissue being absent by 30 years of age. Normal adenoidal tissue is seen in adults in their thirties, forties, and fifties; however, it is unusual for the adenoidal mass to extend up to the posterior margin of the medial pterygoid plate. The presence of such a mass in an older patient should be evaluated by a physician.

Anatomy

The size of the nasopharynx is approximately 2 cm (anterior to posterior) and 4 cm (superior to inferior). The boundaries are the nasal cavity communication via posterior nasal choanae and nasal septum anteriorly and the opening of the Eustachian tube (torus tubarius and fossa of Rosenmuller) posteriorly. The superior boundary is the base of the skull (C1 and C2). The inferior boundary is the soft palate and Passavant's ridge. The lateral boundaries are the superior constrictor muscles/visceral fascia.

The Eustachian tube is the most anterior of nasopharynx landmarks along posterolateral wall of nasopharynx, anterior to torus tubarius. It crosses superior constrictor muscle to reach the nasopharynx from the middle ear cavity. The torus tubarius is a prominent cartilaginous structure. The anterior forms the posterior lip of the Eustachian tube orifice. The lateral wall is formed by the fossa of Rosenmuller and the Eustachian tube opening. The inferior aspect is formed by the soft palate. The fossa of Rosenmuller is the nasopharynx extension posterosuperior to the middle end of the Eustachian tube just posterior and superior to torus tubarius. It may be up to 1.5 cm deep in an adult. Cranial nerve V_3 lies anteriolateral to apex of fossa within parapharyngeal space. The most common site of origin of nasopharyngeal cancers are Type I—keratinizing squamous cell carcinoma; Type II—nonkeratinizing epidermoid carcinoma; and Type III—undifferentiated carcinoma. In ancient Greece, ancient Rome, and during the Middle Ages, the posterior opening of the nasal passage (Greek *choane*=funnel) was known as an anatomical structure.

Incidental Findings

Adenoidal Hyperplasia

Definition/Clinical Characteristics/Radiographic Description Adenoidal hyperplasia is a common incidental finding in younger individuals. It is categorized by the amount of hyperplasia encroaching into the airway in thirds. Mild adenoidal hyperplasia is 1/3 encroachment of the airway (Figures 4.25). Moderate adenoidal hyperplasia is 2/3 encroachment of the airway (Figure 4.26). Marked adenoidal hyperplasia is greater than 2/3 encroachment of the airway.

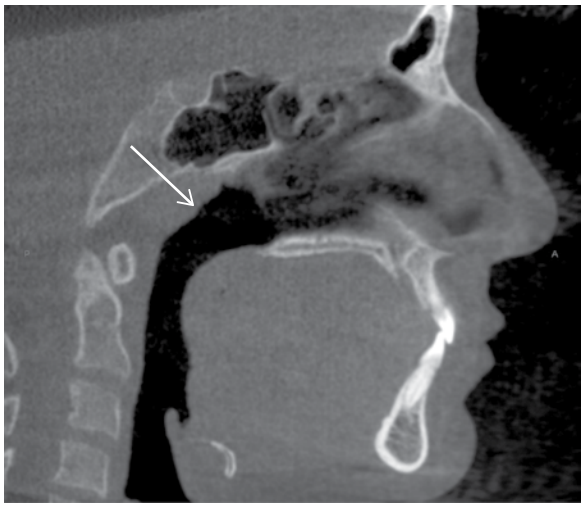

Figure 4.25. Sagittal slice showing mild adenoidal hyperplasia (white arrow).

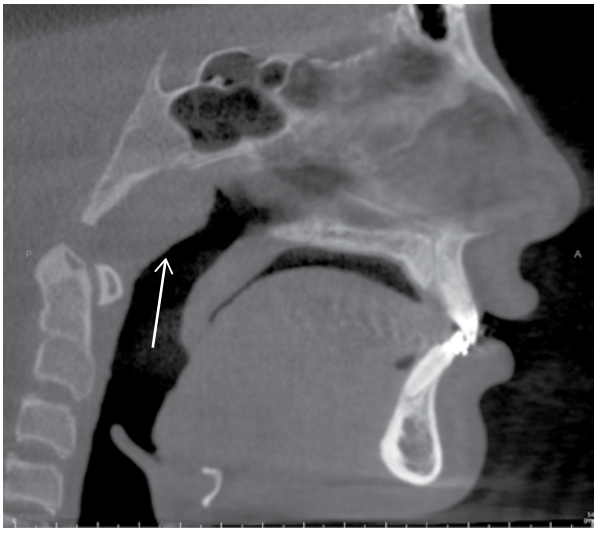

Figure 4.26. Sagittal slice showing moderate adenoidal hyperplasia (white arrow).

Differential Interpretation/Treatment In an older patient, adenoidal hyperplasia may indicate a possible tumor. No treatment is necessary as this is an incidental finding.

The Oropharynx

The region inferior to the nasopharynx is divided into two major components: the oropharynx and the oral cavity. The oral cavity is inferior to the nasal fossa and the bilateral maxillary sinuses. The oropharynx is the area directly inferior to the nasopharynx and posterior to the oral cavity with its superior border formed by

the soft palate. The anterior aspect of the oropharynx begins at the circumvallate papillae and includes the posterior one-third of the tongue. Its lateral parameters are the palatine tonsils. The oropharyngeal mucosa and the constrictor muscles extend from the soft palate to the superior aspect of the epiglottis. The posterior oropharyngeal wall is related to C2 and C3, the second and third cervical vertebrae.

The pharynx is surrounded by visceral fascia surrounding its mucosa and musculature, which acts as a barrier to contain tumor. If the fascia is violated, tumor may invade posteriorly into the longus capitis and colli muscles and the lower parapharyngeal space.

Simply stated, the skeletal support for the airway superiorly is the cranial base and associated pterygoid processes, posteriorly the cervical spine, anterosuperiorly the nasal cavity, and anteriorly the mandible and hyoid bone. Structures encroaching upon the airway include the nasal conchae, adenoids, soft palate, tongue, and the pharyngeal and lingual tonsils. Polyps and tumors may also contribute to obstruction in an otherwise "open" system.

The Hypopharynx (Also Called Laryngopharynx)

The hypopharynx extends from the level of the hyoid bone to the cricopharyngeus, the lower level of the cricoids cartilage. According to Som and Curtin (2003), most authors divide the hypopharynx into the following three regions: the pyriform sinuses, the posterior wall, and the postcricoid region.

The pear-shaped pyriform sinus is situated on either side of the pharynx above by the inner surface of the thyrohyoid membrane and below by the thyroid cartilage and the lateral surface of the aryepiglottic fold. These two are referred to as the membranous and cartilaginous portions of the lateral pyriform sinus wall. The medial and posteriors walls of the pyriform sinus are formed by the lateral surface of the aryepiglottic fold and the inferior continuation of the posterior wall of the oropharynx, respectively. The hypopharynx superior boundary is considered to be at the level of the hyoid bone. The posterior and lateral walls of the hypopharynx merge with the cricopharyngeus, which in turn merges with the cervical esophagus.

The postcricoid region is the anterior wall of the lower hypopharynx and is the interface between the hypopharynx and larynx. It extends from the level of the cricoarytenoid joints down to the inferior aspect of the cricoids cartilage.

The Parapharyngeal Space

The parapharyngeal space is a dominant fat plane on either side of the pharynx that is best defined on T1-weighted images. Infiltration of the parapharyngeal space fat indicates deep invasion of a neoplasm.

On either side of the oropharyngeal airway are bilaterally symmetric soft-tissue masses, the tonsils and faucial pillars. Asymmetry in the size or configuration of these tonsils is an indication of possible tumor or infection presence on the enlarged side. A cystic enlargement of the palatine tonsil may indicate lymphoma, a tumor, or

an abscess. Infection is generally associated with pain and malaise while a tumor causes little pain. It is not unusual to visualize dystrophic calcifications within the tonsillar crypts and benign minor salivary gland retention cysts may occur.

References

The Sinonasal Cavity

Bent, J. P., Cuilty-Siller, C., Kuhn, F. A. (1994). The frontal cell as a cause of frontal sinus obstruction. *American Journal of Rhinology.* 185–91(7).

Gotwald, T. F., Zinreich, S. J., Corl, F., Fishman, E. K. (2001). Three dimensional volumetric display of the nasal ostiomeatal channels and paranasal sinuses. *American Journal of Rhinology*, **176**, 241–45.

Huang, B. Y., Lloyd, K. M., DelGaudio J. M., et al. (2009). Failed endoscopic sinus surgery: Spectrum of CT findings in the frontal recess. *Radiographics*, **29**(1), 177–95.

Som, P. M., and Curtin, H. D. (2003). *Head and Neck Imaging*, *Vols. 1 and 2*. Mosby, St. Louis, MO, Chapters 2, 3, 28.

The Pharynx

Harnsberger, H. (2006). *Diagnostic and Surgical Imaging Anatomy: Brain, Head and Neck, Spine (Diagnostic and Surgical Imaging Anatomy)*. Lippincott Williams & Wilkins, Altona, Manitoba.

Ikushima, I., Korogi, Y., Makita, O., Komohara, Y., Kawano, H., Yamura, M., Arikawa, K., Takahashi, M. (1999). MR imaging of Tornwaldt's cysts. *American Journal of Roentgenology*, **172**, 1663–65.

Netter, F. N. (2006). *Netter Atlas of Human Anatomy*, **63**, 66.

Ruprecht, A., and Dolan, K. D. (1991). The nasopharynx in oral and maxillofacial radiology. *Oral Surgery, Oral Medicine, and Oral Pathology*, **72**(4), 484–91.

Scarpace, S. L., et al. (2009). Treatment of head and neck cancers: Issues for clinical pharmacists. *Pharmacotherapy*, **29**(5): 578–92.

Singal, R., et al. (1996).CT and MR imaging of squamous cell carcinoma of the tongue and floor of the mouth. *RadioGraphics*, **16**, 787–810.

Stambuk, H. E., et al. (2007). Oral cavity and oropharynx tumors. *Radiologic Clinics of North America*, **47**, 1–20.

5 Cranial Skull Base

Shawneen M. Gonzalez

Introduction

This chapter will cover basic anatomy of the cranial skull base along with common radiographic findings. The topics covered include developmental appearances and anatomical variants. Calcifications within the soft tissue of the brain are included in Chapter 6. Different portions of the cranial skull base will be seen on CBCT scans depending on the FOV used. Some of the radiographic findings covered in this chapter may not be visible on all scans and therefore should not be commented on by someone reviewing a scan.

Anatomy

This section will highlight anatomical landmarks of the cranial skull base and the bones they are a part of. Many of these landmarks are only identifiable when using a scan with a large field of view.

Axial

The axial figures (Figures 5.1–5.5) start from the superior aspect of the cranium moving inferiorly. The following anatomy is readily identifiable on axial views (Table 5.1).

Interpretation Basics of Cone Beam Computed Tomography, First Edition.
Edited by Shawneen M. Gonzalez.

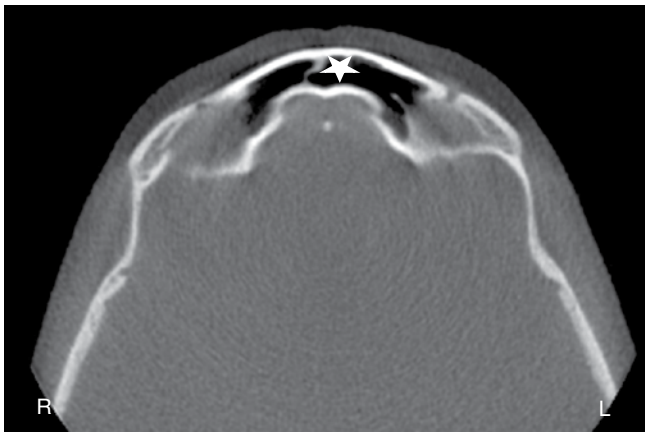

Figure 5.1. Axial slice at the level superior to the orbits showing the frontal sinus (star).

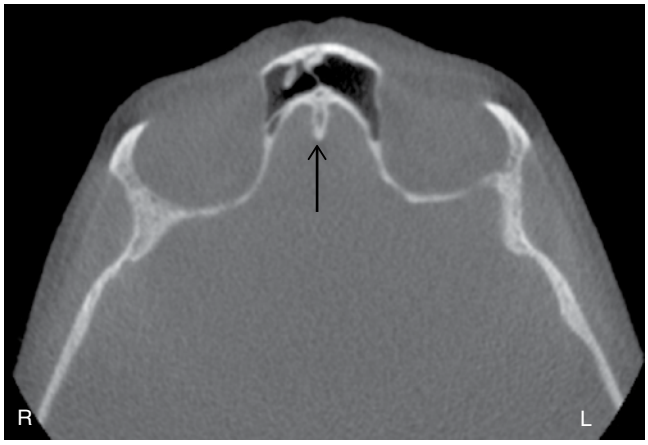

Figure 5.2. Axial slice at the level of the superior aspect of the orbits showing the crista galli (black arrow).

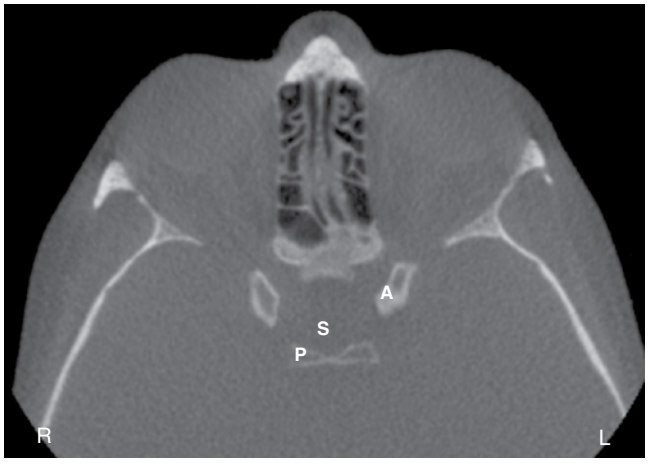

Figure 5.3. Axial slice at the level of the midorbits showing the following sphenoid bone anatomy: the anterior clinoid process (A), sella turcica (S), and posterior clinoid process (P).

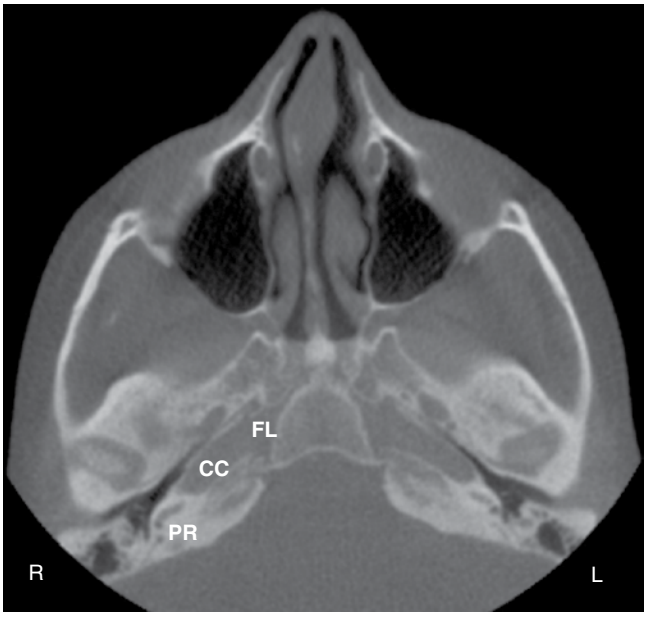

Figure 5.4. Axial slice at the level of the inferior orbit/superior maxillary sinus showing the foramen lacerum (FL), carotid canal (CC), and petrous ridge (PR).

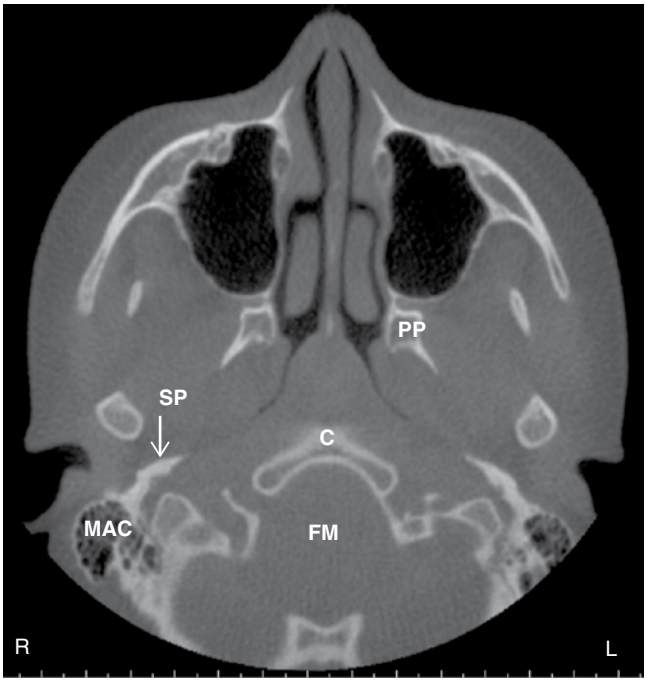

Figure 5.5. Axial slice at the level of the midmaxilla showing the mastoid process with mastoid air cells (MAC), styloid process (SP), clivus/occipital bone (C), foramen magnum (FM), and pterygoid process (PP).

Table 5.1. Anatomical landmarks identifiable on axial views with corresponding figures.

Bone	Anatomical landmark	Figures visible on
Frontal	Frontal sinus	5.1
Ethmoid	Crista galli	5.2
Sphenoid	Anterior clinoid process	5.3
	Sella turcica	5.3
	Posterior clinoid process	5.3
	Foramen lacerum	5.4
	Pterygoid process	5.5
Temporal	Carotid canal	5.4
	Petrous ridge	5.4
	Mastoid process	5.5
	Styloid process	5.5
Occipital	Clivus / occipital bone	5.5
	Foramen magnum	5.5

Figure 5.6. Coronal slice at the anterior aspect of the nasal cavity showing the frontal sinus (star).

Coronal

The coronal figures (Figures 5.6–5.11) start from the anterior aspect of the face moving posteriorly. The following anatomy is readily identifiable on coronal views (Table 5.2).

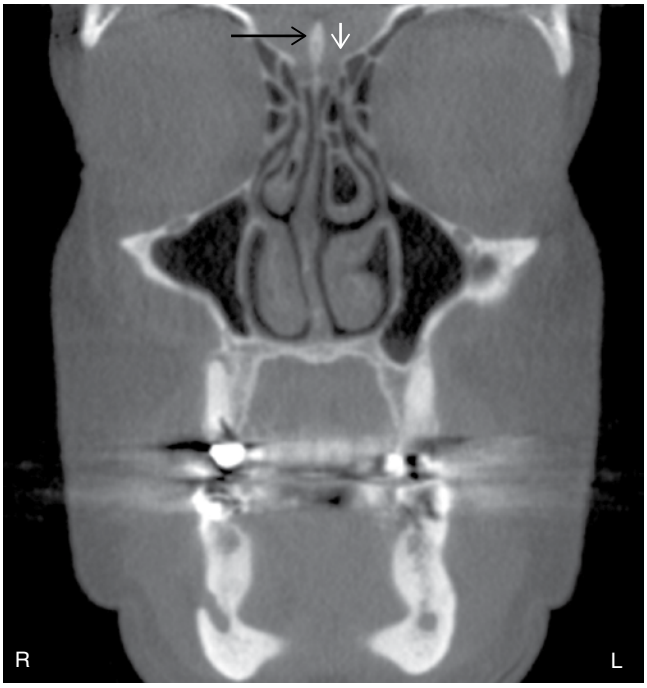

Figure 5.7. Coronal slice at the lateral aspect of the orbits showing the cribriform plate (white arrow) and crista galli (black arrow).

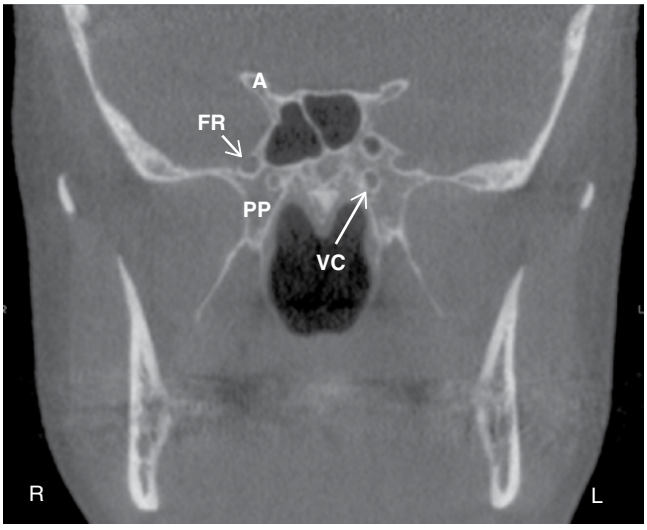

Figure 5.8. Coronal slice at the aspect of the coronoid process showing the pterygoid process (PP), vidian canal (VC), foramen rotundum (FR), and anterior clinoid process (A).

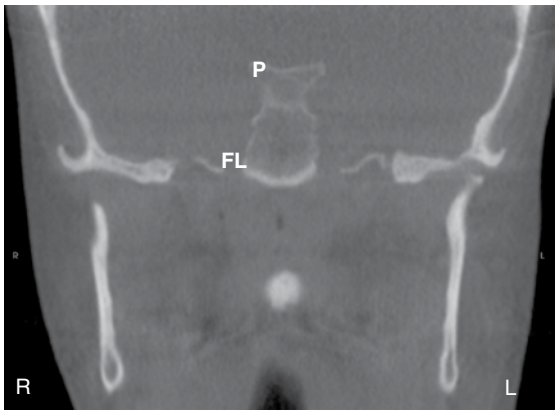

Figure 5.9. Coronal slice at the posterior aspect of the ramus showing the posterior clinoid process (P) and foramen lacerum (FL).

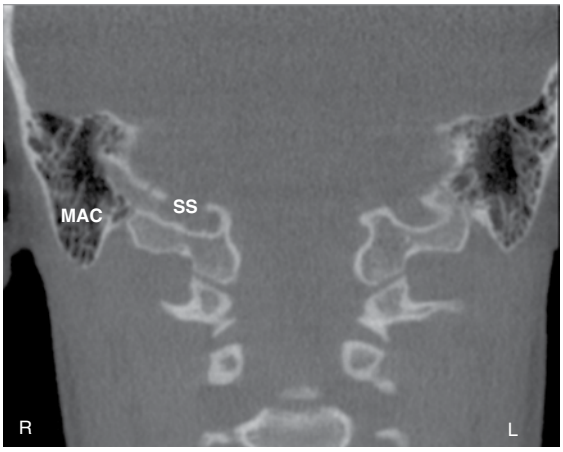

Figure 5.10. Coronal slice at the aspect of the mastoid process showing the mastoid process with mastoid air cells (MAC) and depression of the sigmoid sinus (SS).

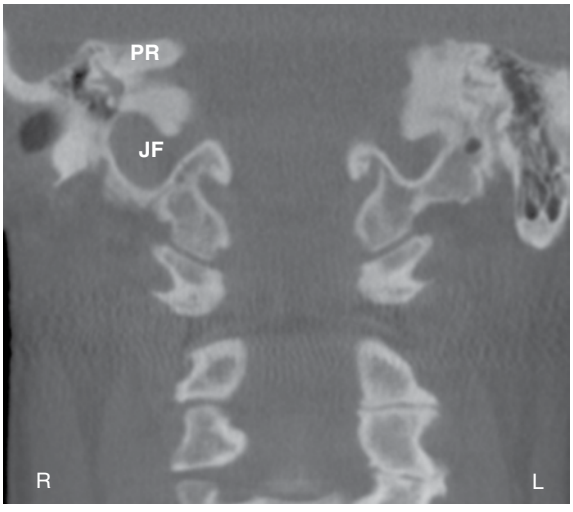

Figure 5.11. Coronal slice at the posteriormost aspect showing the jugular foramen (JF) and petrous ridge (PR).

Table 5.2. Anatomical landmarks identifiable on coronal views with corresponding figures.

Bone	Anatomical landmark	Figures visible on
Frontal	Frontal sinus	5.6
Ethmoid	Cribriform plate	5.7
	Crista galli	5.7
Sphenoid	Anterior clinoid process	5.8
	Posterior clinoid process	5.9
	Foramen lacerum	5.9
	Foramen rotundum	5.8
	Pterygoid process	5.8
	Vidian canal	5.8
Temporal	Petrous ridge	5.11
	Mastoid process	5.10
	Sigmoid sinus depression	5.10
Occipital	Jugular foramen	5.11

Figure 5.12. Sagittal slice at the lateral aspect of the mastoid process showing the mastoid process with mastoid air cells (MAC) of the temporal bone is evident along with the external auditory meatus (EAM).

Sagittal

The sagittal figures (Figures 5.12–5.15) start from the lateral aspect of the cranium moving medially. The following anatomy is readily identifiable on sagittal views (Table 5.3).

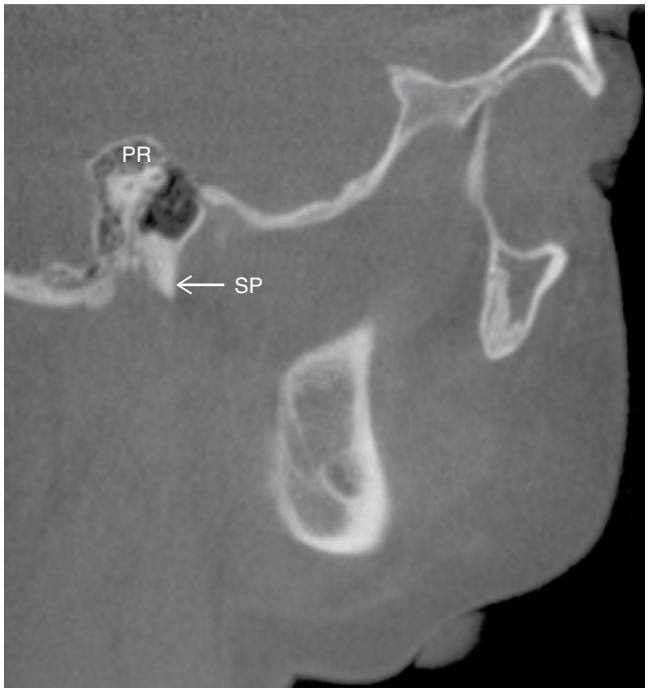

Figure 5.13. Sagittal slice at the lateral aspect of the angle of the mandible showing the styloid process (SP) and petrous ridge (PR).

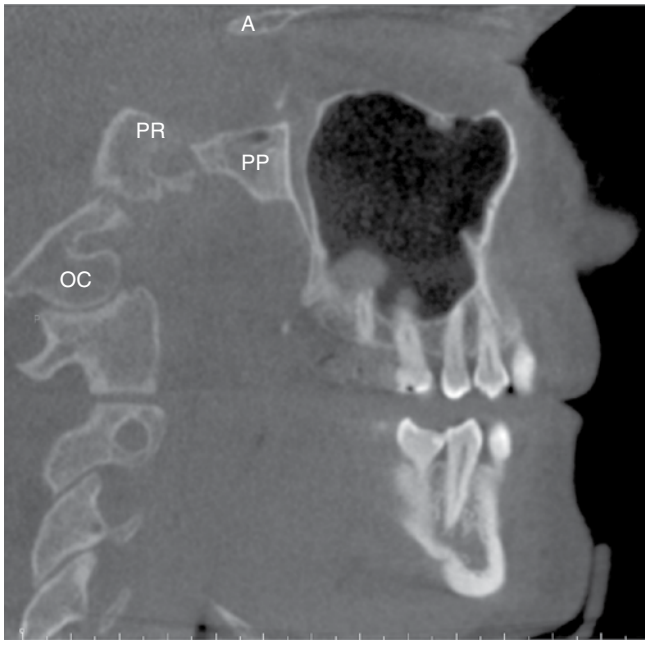

Figure 5.14. Sagittal slice at the lateral aspect of the posterior teeth showing the occipital condyle (OC), petrous ridge (PR), pterygoid process (PP), and anterior clinoid process (A).

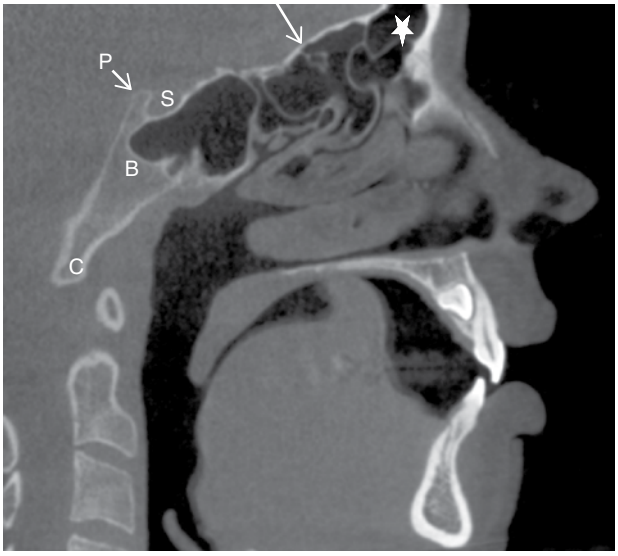

Figure 5.15. Sagittal slice on the midline showing the frontal sinus (star), cribriform plate (white arrow), sella turcica (S), posterior clinoid process (P), clivus/basisphenoid (B), and clivus/occipital bone (C).

Table 5.3. Anatomical landmarks identifiable on sagittal views with corresponding figures.

Bone	Anatomical landmark	Figures visible on
Frontal	Frontal sinus	5.15
Ethmoid	Cribriform plate	5.15
Sphenoid	Anterior clinoid process	5.14
	Sella turcica	5.15
	Posterior clinoid process	5.15
	Clivus / basisphenoid	5.15
	Pterygoid process	5.14
Temporal	Petrous ridge	5.13, 5.14
	Mastoid process	5.12
	Styloid process	5.13
	External auditory meatus	5.12
Occipital	Clivus / occipital bone	5.15
	Occipital condyle	5.14

Incidental Findings

Developmental Appearances

Spheno-Occipital Synchondrosis (Basisphenoid-Basiocciput Synchondrosis)

Definition/Clinical Characteristics A suture between the clivus and basisphenoid portions of the sphenoid bone: the suture typically closes near puberty (approximately

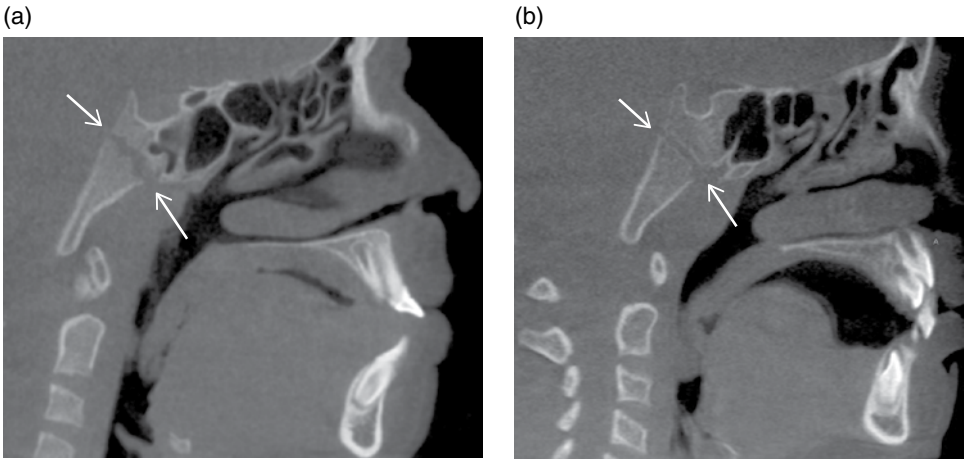

Figure 5.16. (a, b) Sagittal slice on the midline showing the spheno-occipital synchondrosis (arrows) as a discontinuity of the clivus.

between the ages of 11 to 16 for females and 12 to 18 for males) but may remain open until the age of 20.

Radiographic Description This is seen on the sphenoid bone most often on sagittal views (Figure 5.16). It appears as a well-defined, radiolucent band traversing obliquely or horizontally through the bone. There may be incomplete fusion or no fusion of the suture based on the age of the patient when scanned. It may be seen on coronal (Figure 5.17) and axial views as well.

Differential Interpretation There is no differential interpretation due to the appearance and age of patients.

Treatment/Recommendations There is no recommended treatment or further imaging necessary for this finding.

Anatomical Variants

Cranial Thickness

Definition/Clinical Characteristics The thickness of the cranium has a wide range of appearances. The thickness of the cranium does not correlate with the sex, age, or weight of an individual.

Radiographic Description This presents as an equal thickness of entire cranium (all bones visualized). The thickness can range from approximately 2 mm to 11 mm

Figure 5.17. (a) Coronal slice at the aspect of the condyles showing the spheno-occipital synchondrosis (arrows) as a discontinuity of the clivus; (b) Axial slice at the level of the petrous ridge showing the spheno-occipital synchondrosis (arrows) as a discontinuity of the clivus.

(Figure 5.18). The cranium will have intact cortical border throughout all bones evident. This is seen on all views (axial, coronal, and sagittal) equally.

Differential Interpretation With uneven thickness variations of the frontal bone, one would need to consider the possibility of hyperostosis frontalis interna. Hyperostosis frontalis interna results with increased thickness of the frontal bone but no other aspects of the cranium. This is typically superior to the orbits and not captured on most CBCT scans. The natural cranium thickness for a patient will be equal in size throughout all bones of the cranium visualized on a scan.

Treatment/Recommendations There is no recommended treatment or further imaging necessary for this finding.

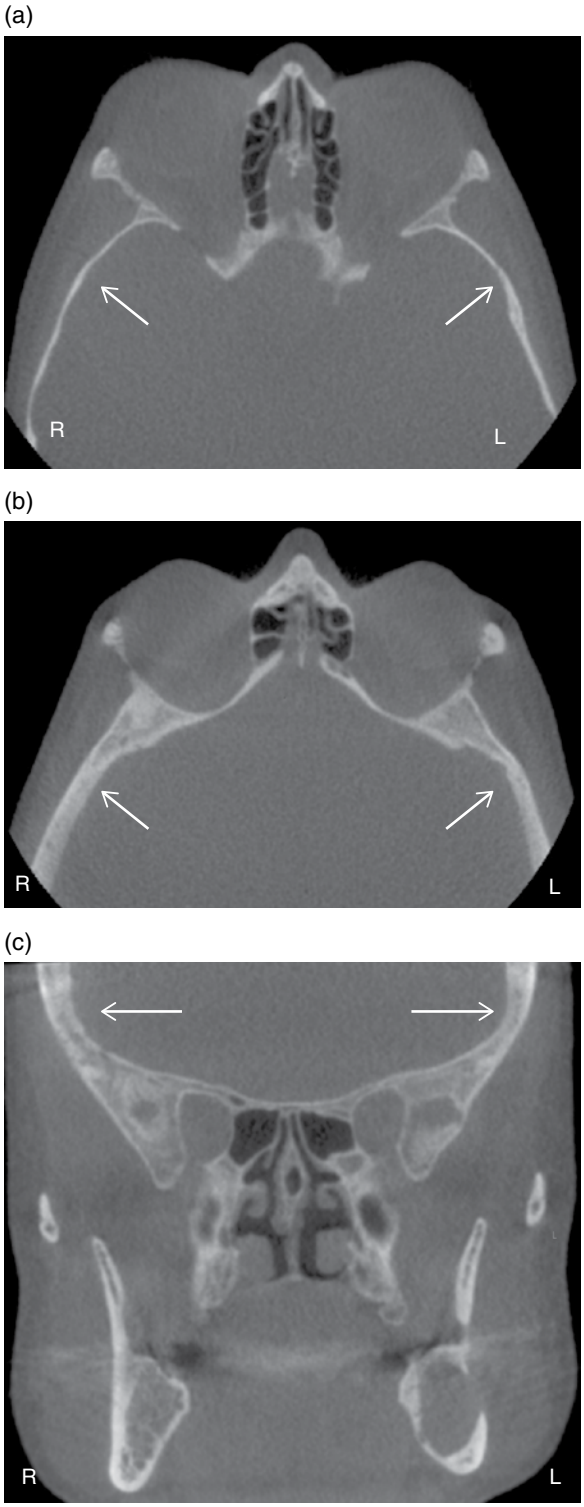

Figure 5.18. (a) Axial slice at the level of the midorbits showing a thin cranium (arrows) within the range of normal; (b) Axial slice at the level of the midorbits showing a thick cranium (arrows) within the range of normal; (c) Coronal slice at the level of the angle of the mandible showing a thick cranium (arrows) within the range of normal.

Vascular Markings

Definition/Clinical Characteristics The definition is indentations on the internal aspect of the cranium created by blood vessels. The presence of vascular markings is an anatomical variant.

Radiographic Description These may be evident on any internal aspect of the cranium. It appears as a well-defined, radiolucent area. There is no universal shape for the markings. There is an intact corticated border of the cranium adjacent to the area of the marking (Figures 5.19 and 5.20). It may be unilateral or bilateral. These are seen on all views (axial, coronal, and sagittal) equally.

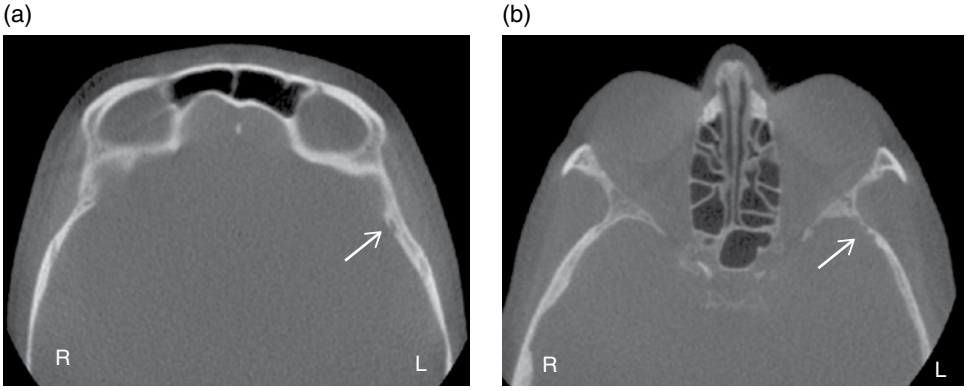

Figure 5.19. (a) Axial slice at the level of the superior aspect of the orbits showing a radiolucent indent on the internal aspect of the cranium caused by vessel markings (arrow); (b) Axial slice at the level of the midorbits showing multiple radiolucent indentations on the internal aspect of the left cranium posterior to the orbits caused by vessel markings (arrow).

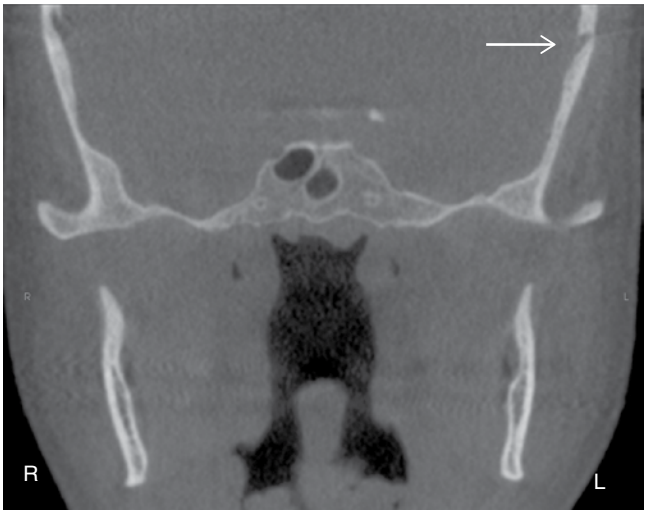

Figure 5.20. Coronal slice at the aspect of the midramus showing a radiolucent indent on the internal aspect of the cranium caused by vessel markings (arrow).

Differential Interpretation There is no differential interpretation due to the location and appearance of this finding.

Treatment/Recommendations There is no recommended treatment or further imaging necessary for this finding.

Interclinoid Ligament Calcification

Definition/Clinical Characteristics It is defined as calcification of the ligament attached to the anterior and posterior clinoid processes of the sella turcica. There is no clinical significance of this finding; however, it has been noted as an incidental finding in basal cell nevus syndrome. The incidence of complete calcification of the ligament ranges from 4% to 19% of the population; however, these studies were performed on lateral cephalometric skull radiographs and not CT images.

Radiographic Description This is located between the anterior and posterior processes of the sella turcica. It appears as a well-defined, radiopaque line. There may be partial calcification to complete calcification (Figure 5.21) connecting the two processes (anterior to posterior). It may be either unilateral or bilateral. This is most evident on sagittal and axial views (Figure 5.22).

Differential Interpretation There is no differential interpretation due to the location of this finding.

Treatment/Recommendations There is no recommended treatment or further imaging necessary for this finding.

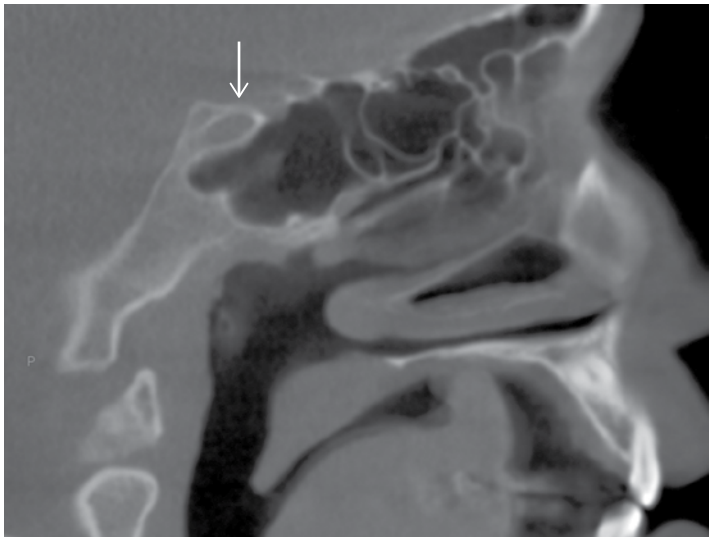

Figure 5.21. Sagittal slice just lateral to the midline showing a thin radiopaque line covering superior aspect of the sella turcica consistent with complete calcification of the interclinoid ligament (arrow).

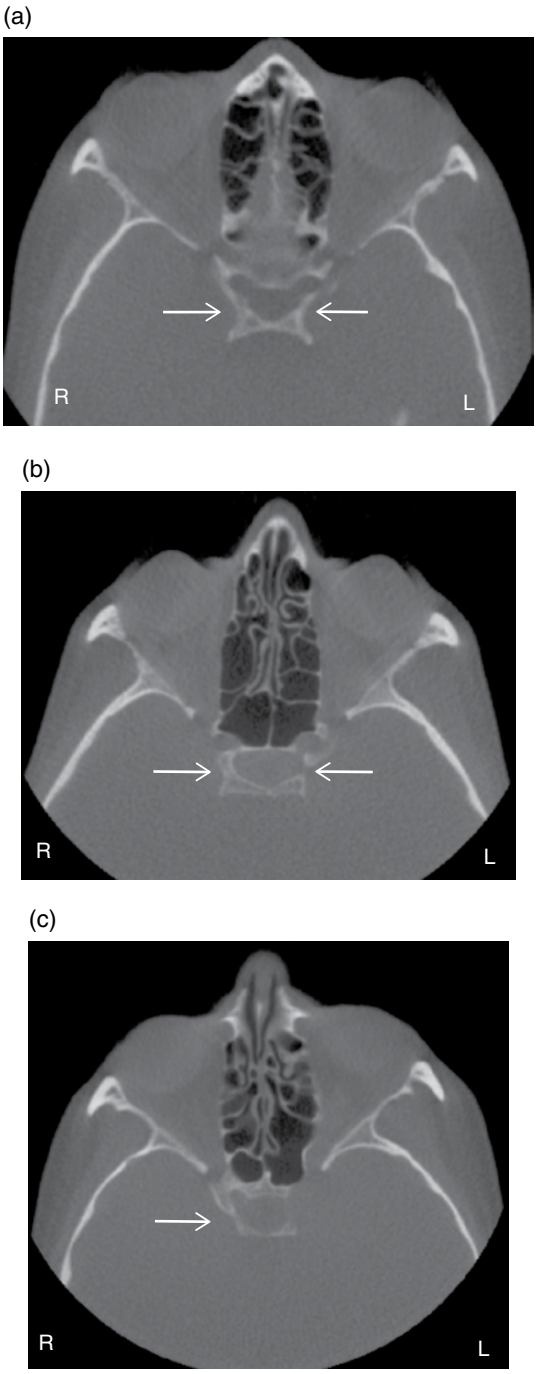

Figure 5.22. (a, b) Axial slice at the level of the midorbits showing bilateral radiopaque bands of the sella turcica consistent with interclinoid ligament calcification (arrows). There is complete calcification on the right and near complete calcification on the left; (c) Axial slice at the level of the midorbits showing right radiopaque band of the sella turcica consistent with complete interclinoid ligament calcification (arrows).

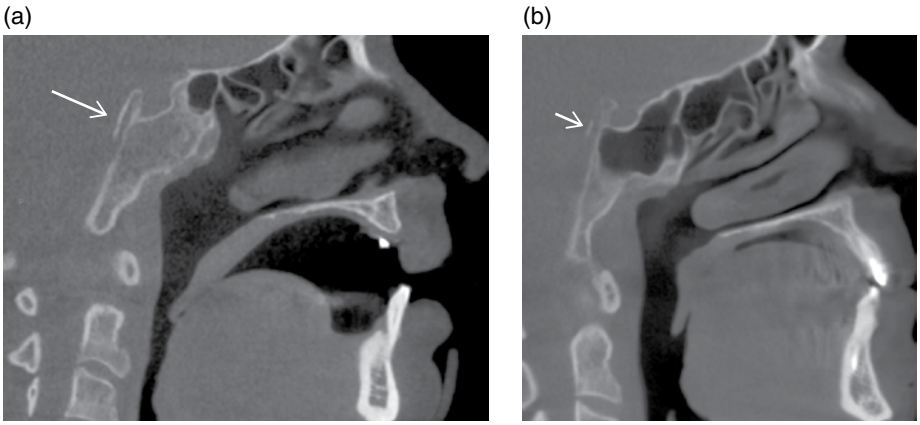

Figure 5.23. (a, b) Sagittal slice just lateral to the midline showing a thin radiopaque line posterior to sphenoid bone consistent with partial petroclinoid ligament calcification (arrow).

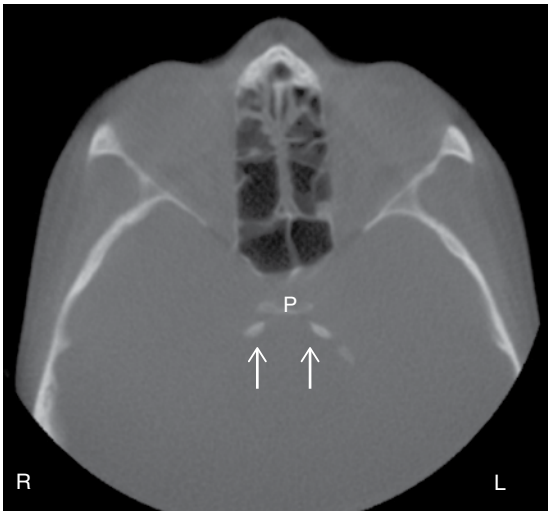

Figure 5.24. Axial slice at the level of the midorbits showing bilateral radiopaque bands posterior to posterior clinoid process (P) consistent with petroclinoid ligament calcification (arrows).

Petroclinoid Ligament Calcification

Definition/Clinical Characteristics It is defined as calcification of the ligament attached to the posterior clinoid process to the petrous ridge of the temporal bone. There is no clinical significance of this finding; however, it has been noted as an incidental finding in basal cell nevus syndrome. The incidence of complete calcification of the petroclinoid ligament is approximately 10% of the population; however, these studies were performed on lateral cephalometric skull radiographs and not CT images.

Radiographic Description This is located between the posterior process of the sella turcica and the petrous ridge of the temporal bone. It appears as a well-defined, radiopaque line. There may be partial calcification (Figures 5.23 and 5.24) to complete

calcification. It may be either unilateral or bilateral. This is most evident on sagittal and axial views.

Differential Interpretation There is no differential interpretation due to the location of this finding.

Treatment/Recommendations There is no recommended treatment or further imaging necessary for this finding.

References

Anatomy

Netter, F. (2004). *Atlas of Human Anatomy*, 3d ed. Icon Learning Systems, Teterboro, NJ.

Spheno-occipital Synchondrosis

Keats, T., and Anderson, M. (2007). *Atlas of Normal Roentgen Variants That May Simulate Disease*, 8th ed. Mosby, Philadelphia, PA.

Shirley, N. R., and Jantz, R. L. (2011). Spheno-occipital synchondrosis fusion in modern Americans. *Journal of Forensic Sciences*, **56** (3), 580–85.

Cranial Thickness

Lynnerup, N. (2001). Cranial thickness in relation to age, sex and general body build in a Danish forensic sample. *Forensic Science International*, **117**, 45–51.

Ross, A. H., Jantz, R. L., McCormick, W. F. (1998). Cranial thickness in American females and males. *Journal of Forensic Sciences*, **43** (2), 267–72.

Vascular Markings

Keats, T., and Anderson, M. (2007). *Atlas of Normal Roentgen Variants That May Simulate Disease*, 8th ed. Mosby, Philadelphia, PA.

Interclinoid Ligament Ossification/Petroclinoid Ligament Ossification

Cederberg, R. A., Benson, B. W., Nunn, M., et al. (2003). Calcification of the interclinoid and petroclinoid ligaments of sella turcica: A radiographic study of the prevalence. *Orthodontic Craniofacial Research*, **6**, 227–32.

6 Soft Tissue of the Brain and Orbits

Shawneen M. Gonzalez

Introduction

This chapter will cover basic anatomy of the soft tissue of the brain and orbits along with common radiographic findings. The topics covered include pathosis and variants of normal anatomy. Different portions of the soft tissue of the brain and orbits are seen on CBCT scans depending on the FOV used. Some of the radiographic findings covered in this chapter may not be visible on all scans and therefore should not be commented on by someone reviewing a scan.

Anatomy—Soft Tissue of the Brain and Orbits

As cone beam CT scans are not made to differentiate soft tissue, this chapter will not identify specific soft tissue anatomy but more general areas. This anatomy is identifiable when using a scan with a large field of view.

Axial

The axial figures start from the superior aspect of the cranium moving inferiorly (Figures 6.1–6.5).

Interpretation Basics of Cone Beam Computed Tomography, First Edition.
Edited by Shawneen M. Gonzalez.

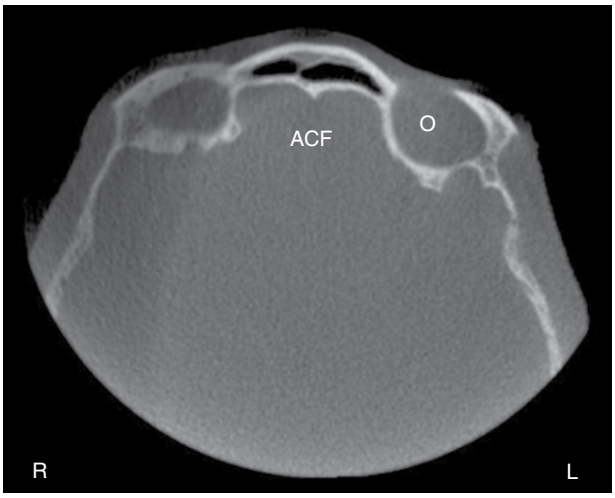

Figure 6.1. Axial slice at the level of the superior aspect of the orbits (O) showing the anterior cranial fossa (ACF).

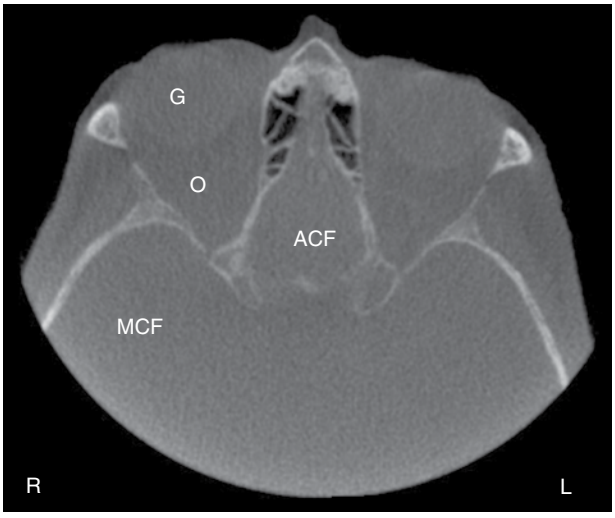

Figure 6.2. Axial slice at the level of the midorbits (O) showing the anterior cranial fossa (ACF), middle cranial fossa (MCF), and globe of the eye (G).

Coronal

The coronal figures start from the anterior aspect of the face moving posteriorly (Figures 6.6–6.11).

Sagittal

The sagittal figures start from the lateral aspect of the cranium moving medially (Figures 6.12–6.15).

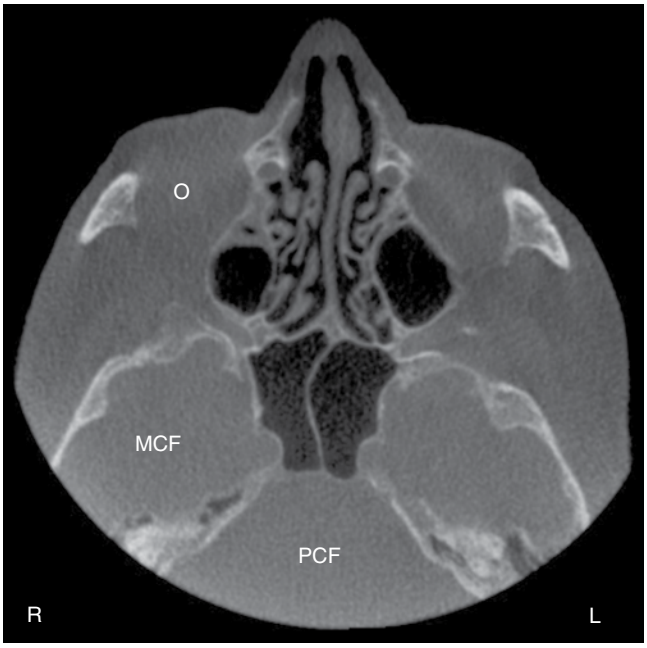

Figure 6.3. Axial slice at the level of the inferior orbit (O) and superior maxillary sinus showing the middle cranial fossa (MCF) and posterior cranial fossa (PCF).

Figure 6.4. Axial slice at the level of the midmaxillary sinus showing the posterior cranial fossa (PCF).

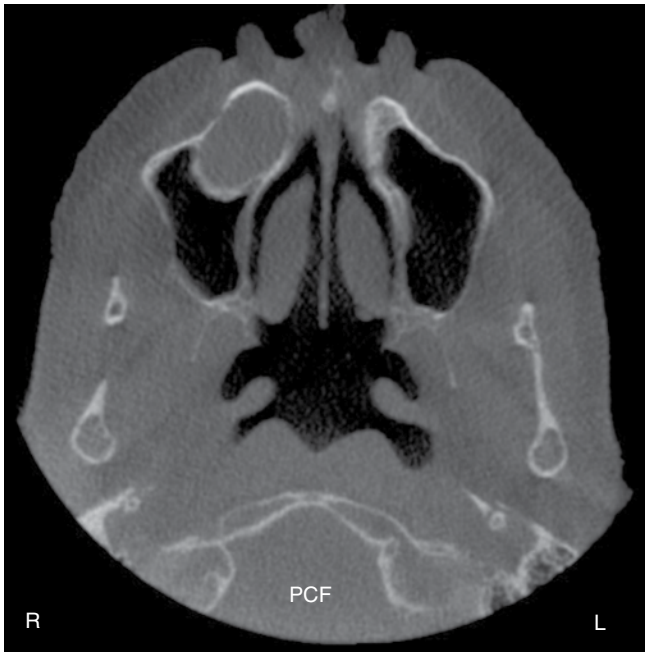

Figure 6.5. Axial slice at the level of the inferior maxillary sinus showing the posterior cranial fossa (PCF).

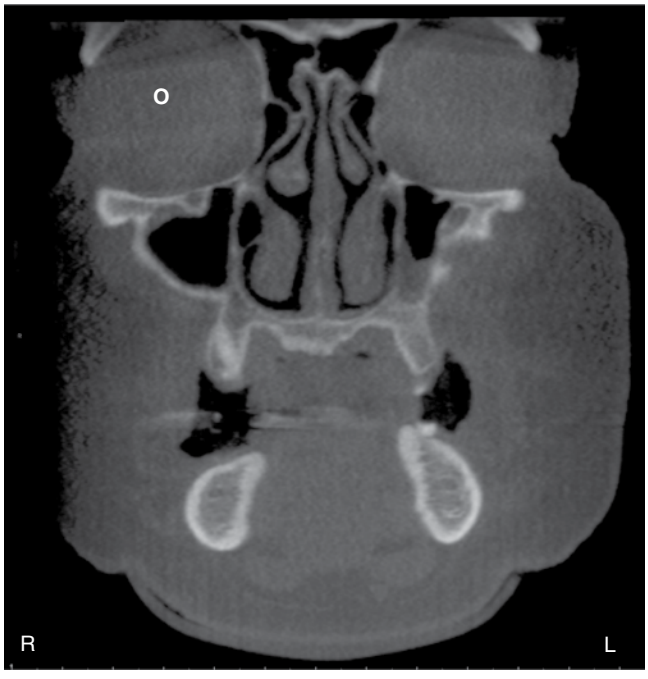

Figure 6.6. Coronal slice at the anterior aspect of the maxillary sinuses showing the orbits (O).

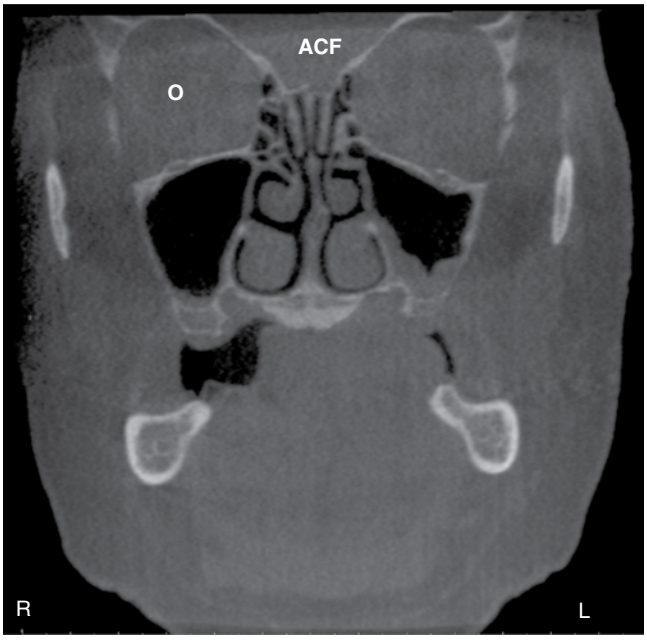

Figure 6.7. Coronal slice at the midmaxillary sinus and midorbits (O) showing the anterior cranial fossa (ACF).

Figure 6.8. Coronal slice at the posterior aspect of the orbits (O) showing the anterior cranial fossa (ACF).

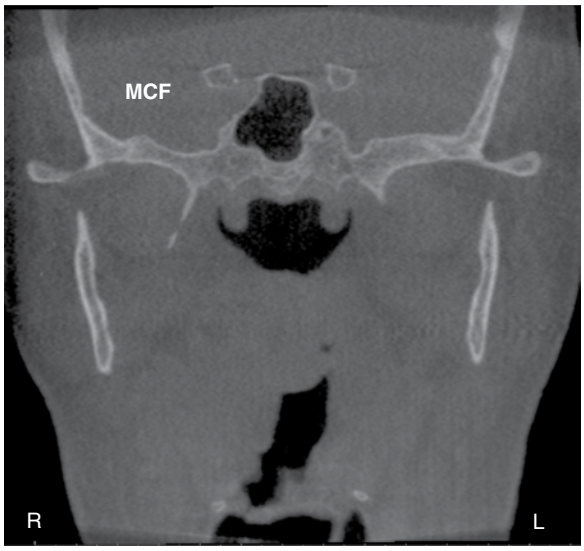

Figure 6.9. Coronal slice at the posterior aspect of the ramus showing the middle cranial fossa (MCF).

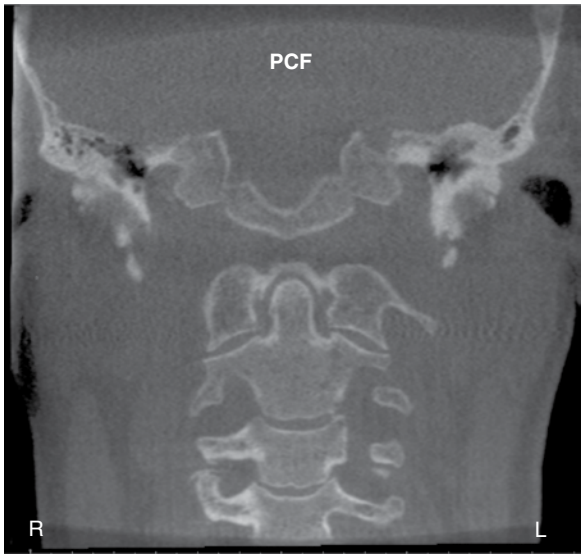

Figure 6.10. Coronal slice at the midcervical vertebrae showing the posterior cranial fossa (PCF).

Incidental Findings—Soft Tissue of the Brain

Incidental Calcifications

Choroid Plexus Calcification

Definition/Clinical Characteristics Choroid plexus calcifications are common physiologic calcifications that increase with age. They occur in approximately 12% to 43.3% of the population.

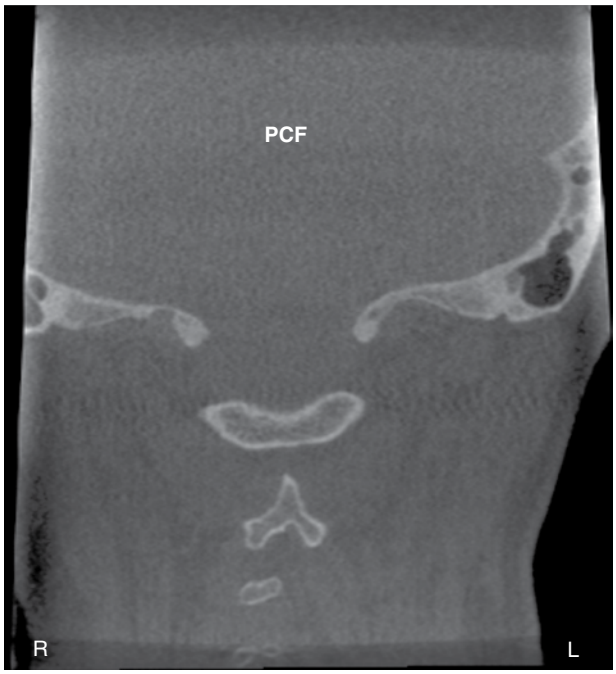

Figure 6.11. Coronal slice at the posterior aspect of the cervical vertebrae showing the posterior cranial fossa (PCF).

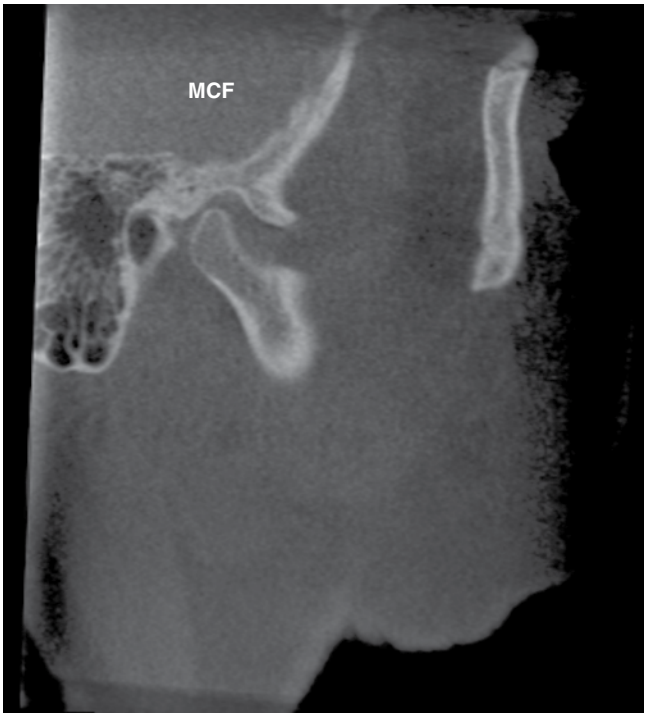

Figure 6.12. Sagittal slice at the lateral aspect of the mastoid process showing the middle cranial fossa (MCF).

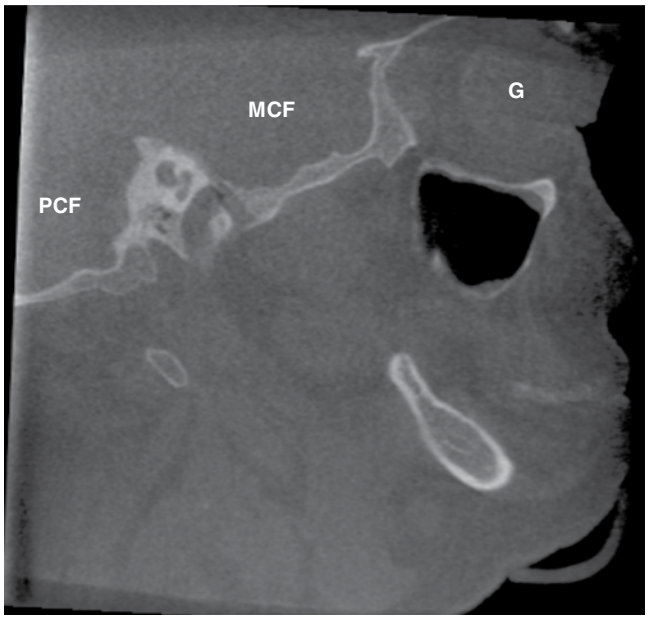

Figure 6.13. Sagittal slice at the lateral aspect of the angle of the mandible showing the middle cranial fossa (MCF), posterior cranial fossa (PCF), and globe of the eye (G).

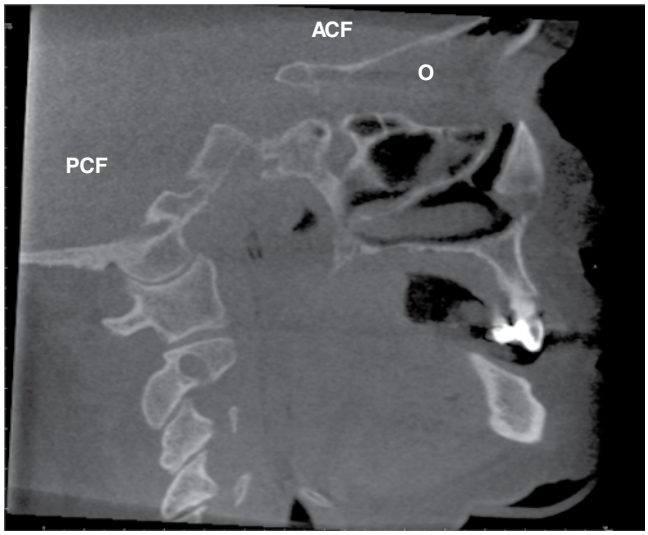

Figure 6.14. Sagittal slice at the lateral aspect of the nasal cavity showing the anterior cranial fossa (ACF), posterior cranial fossa (PCF), and orbits (O).

Radiographic Description Choroid plexus calcification is noted in the posterior aspect of the soft tissue of the brain. It is either unilateral or bilateral. It appears as diffuse radiopaque entities lateral to the midline (Figure 6.16). They are commonly visualized on axial and coronal views (Figure 6.17).

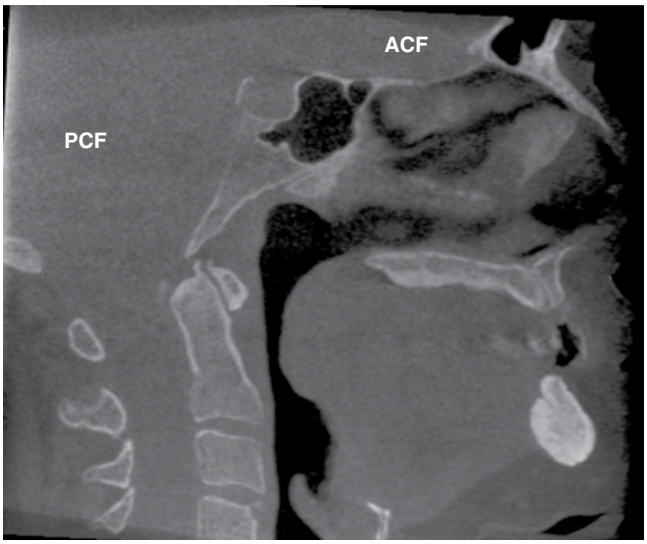

Figure 6.15. Sagittal slice on the midline showing the anterior cranial fossa (ACF) and posterior cranial fossa (PCF).

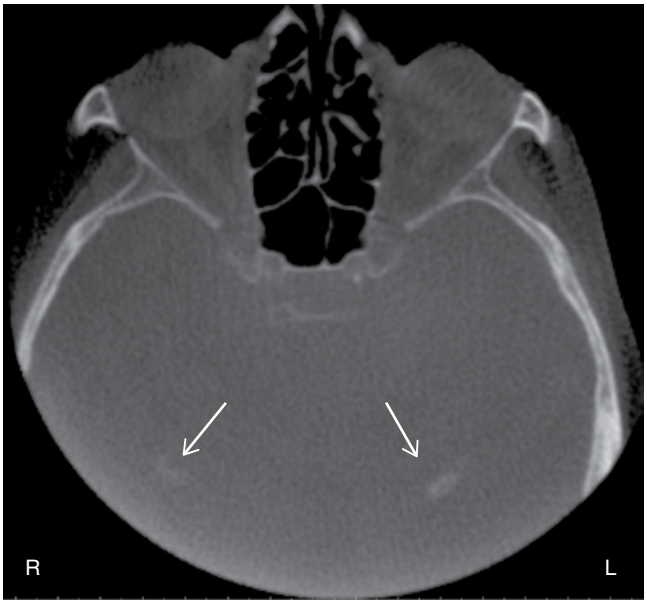

Figure 6.16. Axial slice at level of midorbits showing bilateral choroid plexus calcifications (arrows) lateral to the midline.

Differential Interpretation There are no differential interpretations based on the location of this finding.

Treatment/Recommendations No further treatment or imaging is recommended.

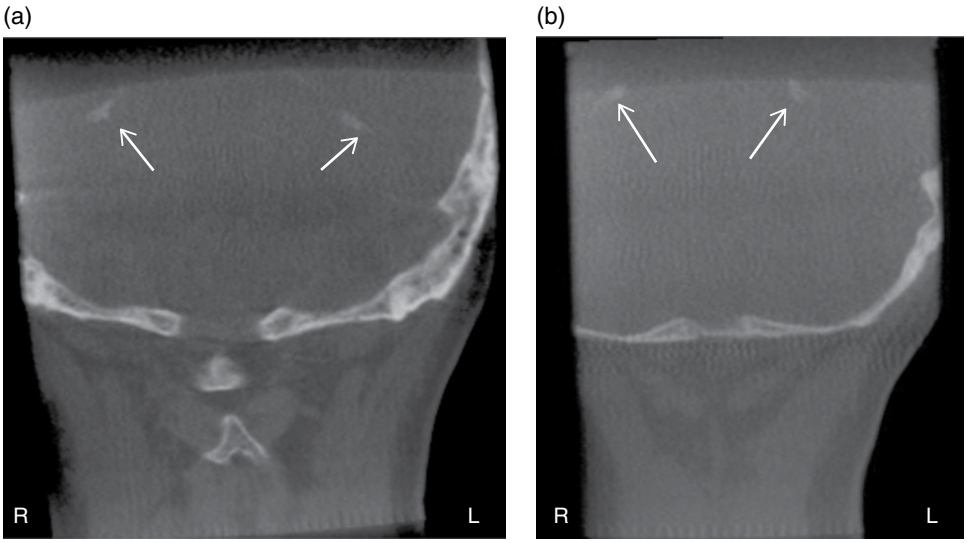

Figure 6.17. (a) Coronal slice at aspect of posterior cervical vertebrae showing bilateral choroid plexus calcifications (arrows) lateral to the midline; (b) Coronal slice at posterior to cervical vertebrae showing bilateral choroid plexus calcifications (arrows) lateral to the midline near the superior aspect of the field of view.

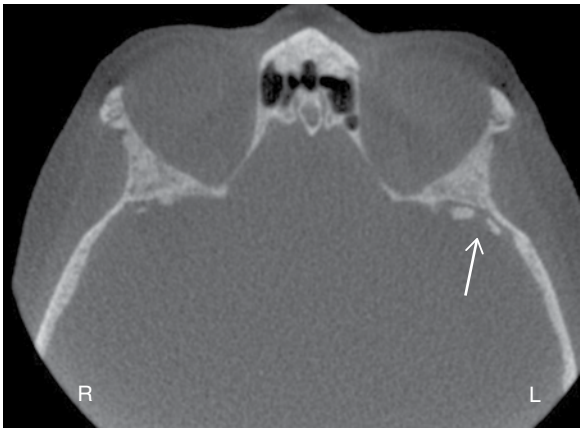

Figure 6.18. Axial slice at the level of the superior midorbital region showing dural calcifications (arrow).

Dural Calcifications

Definition/Clinical Characteristics Dural calcifications are age-related calcifications found in the dura of the brain. They occur in approximately 10% of the elderly population.

Radiographic Description Dural calcifications may occur near the cranium or in the midline. They appear as either linear radiopaque entities in the midline to radiopaque masses near the cranium (Figure 6.18). They are visualized on all views (axial, coronal, and sagittal; Figure 6.19).

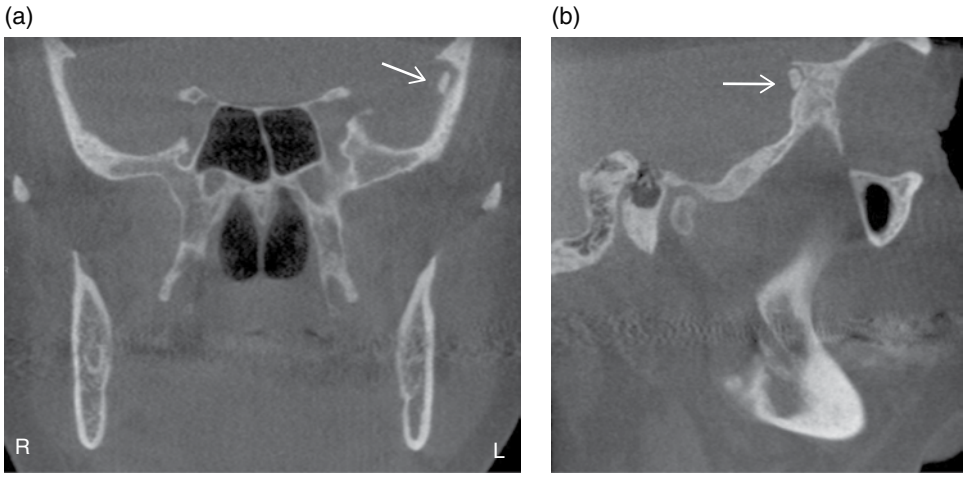

Figure 6.19. (a) Coronal and (b) sagittal slices at the level of the ramus showing a single dural calcification (arrow).

Differential Interpretation There are no differential interpretations based on the location and appearance of this finding.

Treatment/Recommendations No treatment or further investigation is recommended.

Pineal Gland Calcification

Definition/Clinical Characteristics Pineal gland calcifications are incidental calcifications that increase with age. There is a wide range of incidence from 2% to 69%. There is a slight increased incidence in males. Populations exposed to increased sunlight and living at higher altitudes have shown decreased incidence of pineal gland calcification. Pineal gland calcification is frequently associated with choroid plexus calcification.

Radiographic Description Pineal gland calcification appears in the midline of a patient superior to the spinal cord. It is a small well-defined radiopaque mass (Figure 6.20). It is equally seen on all three views (axial, coronal, and sagittal; Figures 6.21 and 6.22).

Differential Interpretation Based on the location and small size, there is no other differential interpretation of patients over the age of 9. When noted in patients under the age of 9 or larger than 1 cm in diameter, a neoplastic process of the pineal gland cannot be ruled out. There has been reported up to 10% incidence in children under the age of 10.

Treatment/Recommendations If found in a patient under the age of 9, referral to a primary care physician is recommended for further investigation of a possible neoplastic origin.

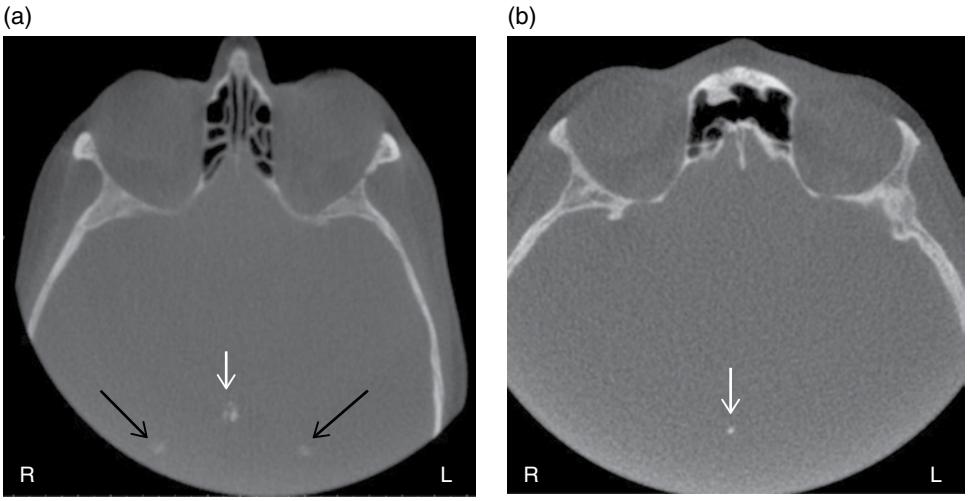

Figure 6.20. (a) Axial slice at the level of the superior midorbital region showing pineal gland calcification (white arrow) in the midline and choroid plexus calcification (black arrows); (b) Axial slice near superior aspect of orbits showing pineal gland calcification (arrow) in the midline.

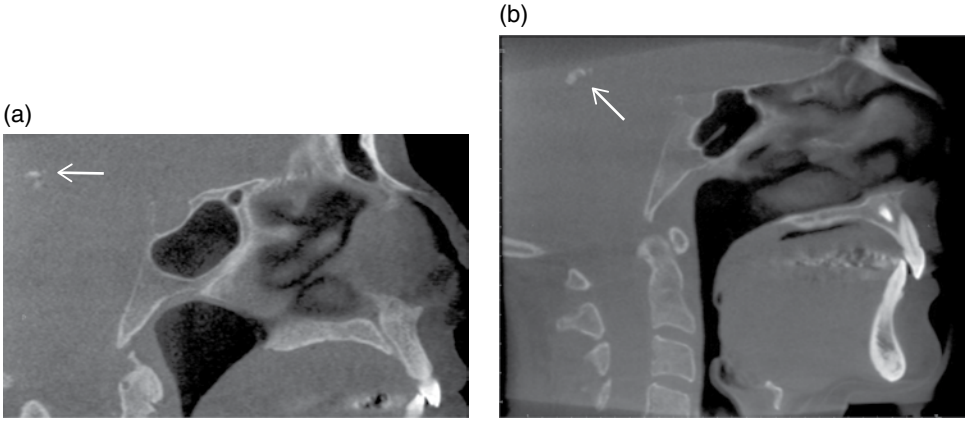

Figure 6.21. (a,b) Sagittal slice in the midline showing pineal gland calcification (arrow).

Pathosis

Cavernous Carotid Artery Calcification

Definition/Clinical Characteristics Atherosclerotic plaques of the internal carotid artery near the cavernous sinus. These calcifications are strongly associated with existing systemic disease such as hypertension, hypercholesterolemia, and diabetes mellitus. There is a slight male predilection. There is no evidence that the presence of these calcifications are predictors of future strokes, but should be used as a sign of the state of the overall atherosclerosis of an individual. The incidence increases with age.

Radiographic Description The calcifications are evident lateral to sella turcica. It appears as a well-defined radiopaque entity. The shape may present as either linear

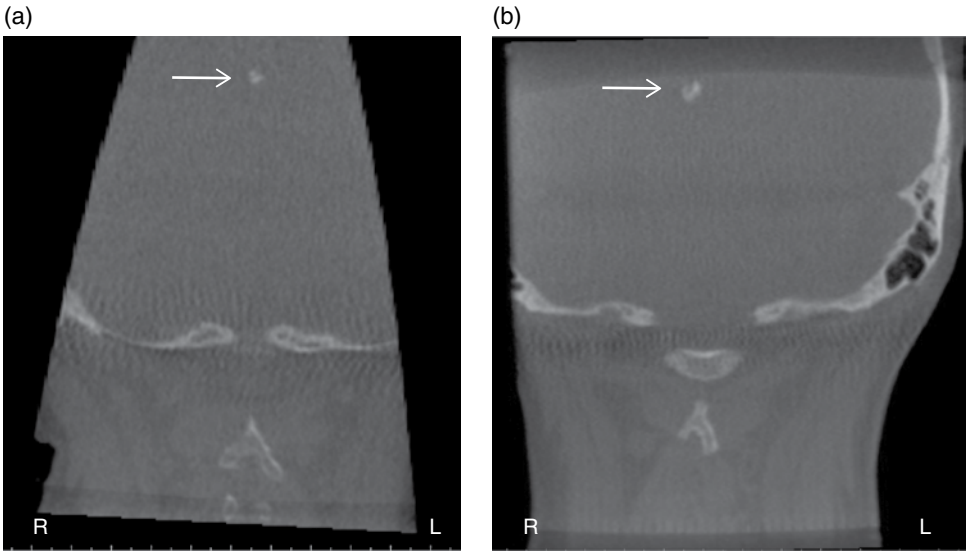

Figure 6.22. (a,b) Coronal slice at the aspect of the posterior cervical vertebrae showing pineal gland calcification (arrow) in the midline.

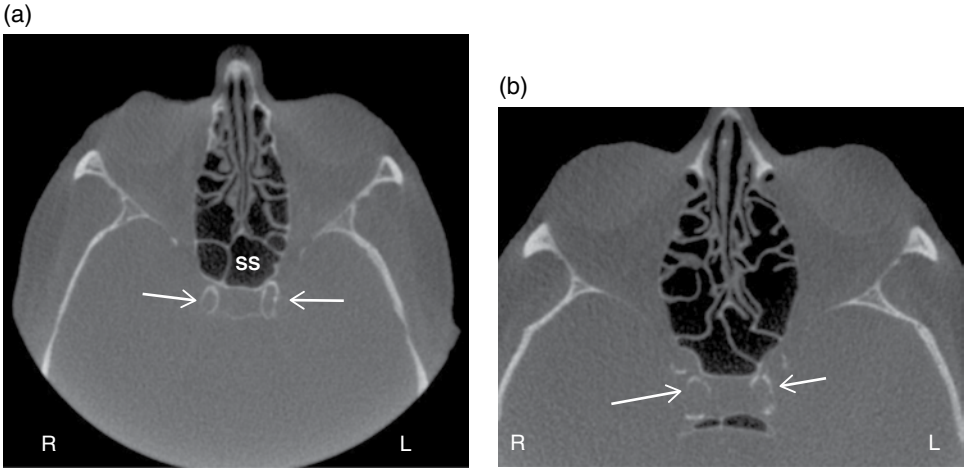

Figure 6.23. (a) Axial slice showing bilateral cavernous carotid artery calcifications (arrows) as ovoid radiopaque entities directly posterolateral of the sphenoid sinuses (SS); (b) Axial slice showing bilateral cavernous carotid artery calcifications (arrows) as curved radiopaque entities.

or a curved line on axial (Figure 6.23) and sagittal views (Figure 6.24) to circular on coronal views (Figure 6.25). It may be unilateral or bilateral. Small plaques are more evident on coronal views, but calcifications may be seen on all views.

Differential Interpretation There is no differential interpretation due to the location of this finding.

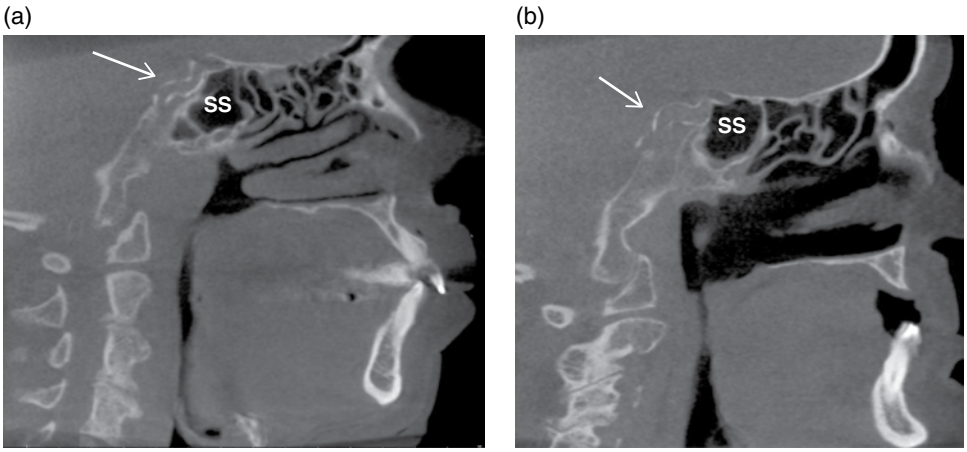

Figure 6.24. (a,b) Sagittal slice lateral to midline showing carotid artery calcification (arrow) as two curved radiopaque lines directly posterior to the sphenoid sinuses (SS).

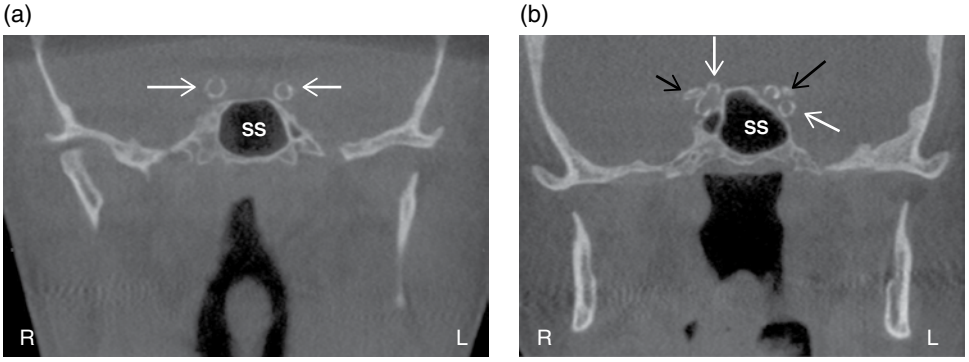

Figure 6.25. (a) Coronal slice at the posterior aspect of the ramus showing bilateral cavernous carotid artery calcifications (arrows) as round radiopaque entities directly superolateral to the sphenoid sinus (SS); (b) Coronal slice at the posterior aspect of the ramus showing bilateral cavernous carotid artery calcifications (white arrows) as curved radiopaque entities lateral to the sphenoid sinus (SS) and medial to the posterior clinoid process (black arrows).

Treatment/Recommendations The patient should be referred to his or her primary care physician. This ensures that the patient and primary care physician are aware of the full extent of any underlying atherosclerotic disease and/or other systemic disease contributing to the calcifications.

Vertebral (Basilar) Artery Calcification

Definition/Clinical Characteristics It is defined as atherosclerotic plaques of the vertebral (basilar) artery near the cranial skull base at the superior aspect of the spinal canal. These calcifications are strongly associated with existing systemic disease such as hypertension, hypercholesterolemia, and diabetes mellitus. There is a slight male predilection. There is no evidence that the presence of these calcifications are predictors of future strokes, but should be used as a sign of the state of the overall atherosclerosis of an individual. The incidence increases with age.

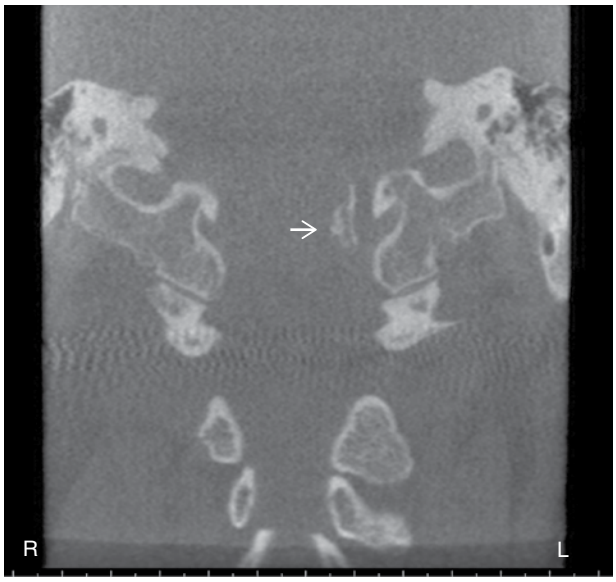

Figure 6.26. Coronal slice at the posterior aspect of the cervical vertebrae showing left unilateral vertebral artery calcification (arrow) as two linear radiopaque lines.

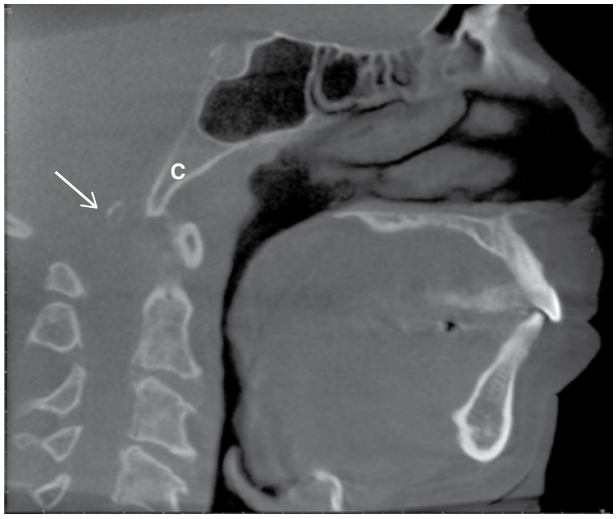

Figure 6.27. Sagittal slice lateral to the midline showing vertebral artery calcification (arrow) as an ovoid radiopaque entity posterior to the clivus (C).

Radiographic Description The calcifications are evident medial and posterior to the clivus and C1. It appears as a well-defined radiopaque entity. The shape may present as either linear or a curved line on coronal views (Figure 6.26) and sagittal views (Figure 6.27) to circular on axial views (Figure 6.28). It may be unilateral or bilateral. Small plaques are more evident on axial views, but calcifications may be seen on all views.

Differential Interpretation There is no differential interpretation due to the location of this finding.

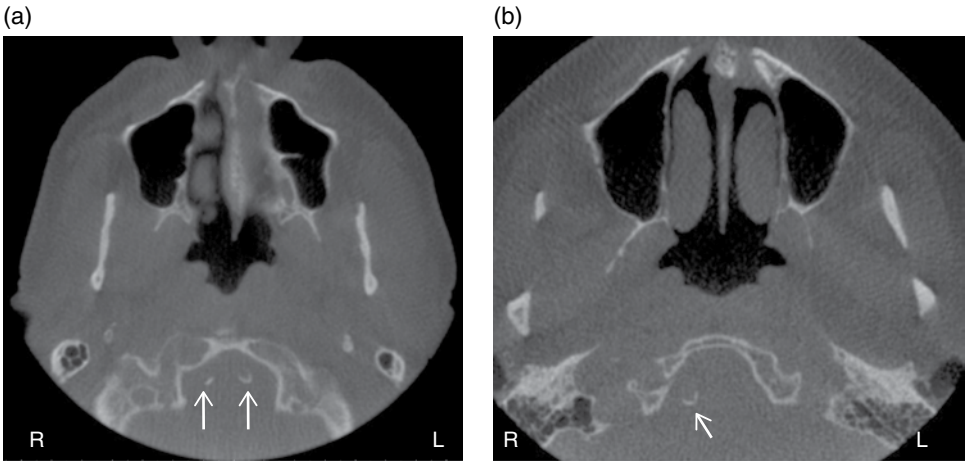

Figure 6.28. (a) Axial slice at the level of inferior portion of the maxillary sinus showing bilateral vertebral artery calcifications (arrows); (b) Axial slice at the level of inferior portion of the maxillary sinus showing unilateral vertebral artery calcification (arrow).

Treatment/Recommendations The patient should be referred to his or her primary care physician. This ensures that the patient and primary care physician are aware of the full extent of any underlying atherosclerotic disease and/or other systemic disease contributing to the calcifications.

Incidental Findings—Orbits

Bony Variations

Displacement of the Lamina Papyracea

Definition/Clinical Characteristics It is defined as the protrusion of the lamina papyracea either medially from the orbit into the ethmoid air cells or laterally into the orbit. Causes include trauma and iatrogenic and congenital reasons.

Radiographic Description This occurs on the medial aspect of the orbit approximately in the middle of the orbital cavity (anterior-posterior). There is a discontinuity of the medial bony border with displacement of the bony border medially. Due to the nature of CBCT, it is not possible to determine if there is fat or muscle entrapment in this area. This is visualized on axial and coronal views (Figures 6.29 and 6.30).

Differential Interpretation There is no differential interpretation based on the location and appearance of this finding.

Treatment/Recommendations Referral to primary care physician is recommended for further investigation as this area is prone to increased risk during surgery.

Figure 6.29. Axial slice at the level of the midorbits showing right-sided medial displacement of the lamina papyracea (arrow).

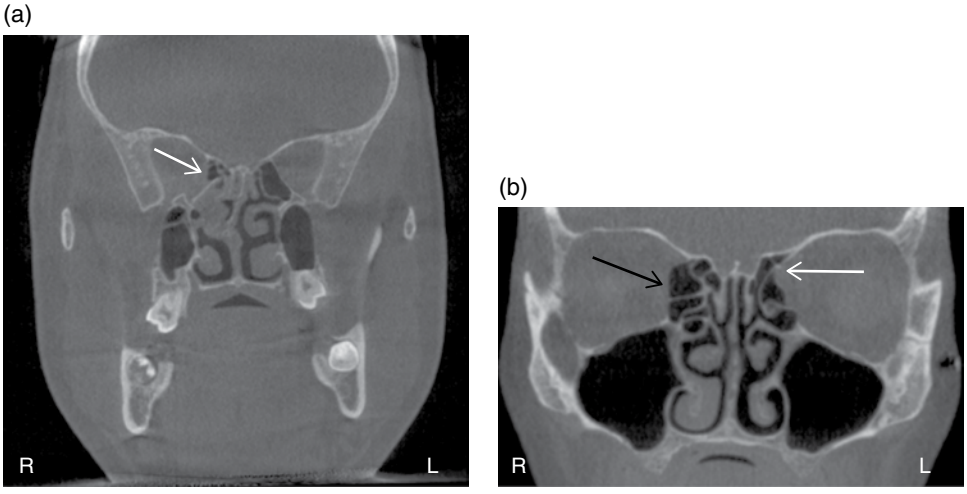

Figure 6.30. (a) Coronal slice at the posterior aspect of the orbits showing right-sided medial displacement of the lamina papyracea (arrow); (b) Coronal slice at midorbits showing right-sided lateral displacement of the lamina papyracea (black arrow) toward the orbit and left-sided medial lamina papyracea displacement (white arrow) toward the ethmoid air cells.

Incidental Calcifications

Scleral plaques

Definition/Clinical Characteristics Incidental calcifications of the sclera. This is commonly seen in elderly patients.

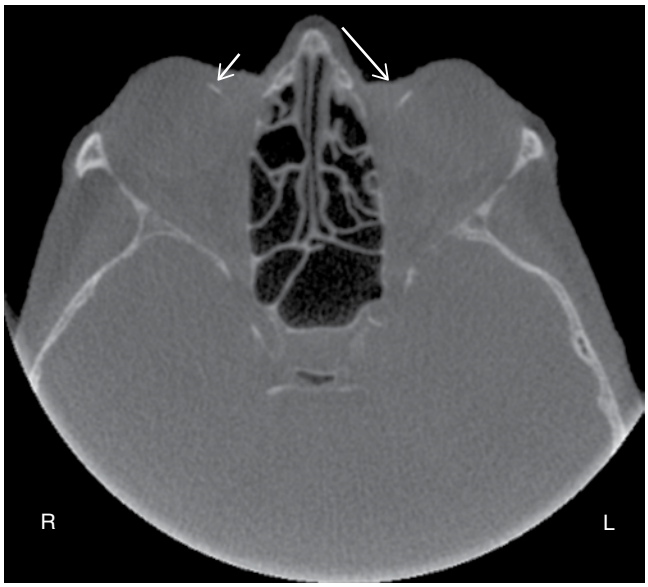

Figure 6.31. Axial slice at the midorbits showing bilateral medial scleral plaques (arrows) as linear radiopaque entities.

Figure 6.32. (a) Coronal slice at the anterior orbits showing left-sided medial scleral plaque (arrow) as a curved linear radiopaque entity; (b) Sagittal slice showing scleral plaque (arrow) as a linear radiopaque entity.

Radiographic Description They are located at the insertion sites of the medial and lateral rectus muscles. They are radiopaque entities that are linear (Figure 6.31) to small masses in shape. They may be single or multiple per globe. They may be unilateral or bilateral effecting both globes. They are visualized on all views (axial, coronal, and sagittal; Figure 6.32).

Differential Interpretation Calcifications noted on the globe not at the insertion point of the muscles may indicate macular degeneration, infection, inflammation, or trauma.

Treatment/Recommendations There is no treatment or further investigation necessary for this finding.

References

Anatomy

Netter, F. (2004). *Atlas of Human Anatomy*, 3d ed. Icon Learning Systems, Teterboro, NJ.

Choroid Plexus Calcification

Admassie, D., and Mekonnen, A. (2009). Incidence of normal pineal and chroids plexus calcification on brain CT (computed tomography) at TikurAnbessa Teaching Hospital Addis Ababa, Ethiopia. *Ethiop Med J*, **47** (1), 55–60.

Kiroglu, Y., Calli, C., Karabulut, N., et al. (2010a). Intracranial calcifications on CT. *Diagn Interv Radiol*, **16**, 263–69.

Sedghizadeh, P. P., Nguyen, M., Enciso, R. (2012). Intracranial physiological calcifications evaluated with cone beam CT. *Dentomaxillofac Radiol*, **41** (8), 675–78.

Dural Calcifications

Kiroglu, Y., Calli, C., Karabulut, N., et al. (2010). Intracranial calcifications on CT. *Diagn Interv Radiol*, **16**, 263–69.

Pineal Gland Calcifications

Doyle, A. J., and Anderson, G. D. (2006). Physiologic calcification of the pineal gland in children on computed tomography: Prevalence, observer reliability and association with choroid plexus calcification. *Acad Radiol*, **13** (7), 822–26.

Kiroglu, Y., Calli, C., Karabulut, N., et al. (2010). Intracranial calcifications on CT. *Diagn Interv Radiol*, **16**, 263–69.

Turgut, A. T., Karakas, H. M., Ozsunar, Y., et al. (2008). Age-related changes in incidence of pineal gland calcification in Turkey: A prospective multicenter CT study. *Pathophysiology*, **15**, 41–48.

Cavernous Carotid Artery Calcifications

Babiarz, L. S., Yousem, D. M., Bilker, W., et al. (2005). Middle cerebral artery infarction: Relationship of cavernous carotid artery calcification. *Am J Neuroradiol*, **26**, 1505–11.

Babiarz, L. S., Yousem, D. M., Wasserman, B. A., et al. (2003). Cavernous carotid artery calcification and white matter ischemia. *Am J Neuroradiol*, **24**, 872–77.
Ptak, T., Hunter, G. H., Avakian, R., et al. (2003). Clinical significance of cavernous carotid calcifications encountered on head computed tomography scans performed on patients seen in the emergency department. *Journal of Computer Assisted Tomography*, **27** (4), 505–9.

Vertebral (Basilar) Artery Calcifications

Kiroglu, Y., Calli, C., Karabulut, N., et al. (2010d). Intracranial calcifications on CT. *Diagn Interv Radiol*, **16**, 263–69.

Medial Displacement of the Lamina Papyracea

Kendi, T. K., Rodrigez, C., Kemal, G., et al. (2004). Medial orbital wall protusion: Computed tomography findings. *European Journal of Radiology Extra*, **51**, 69–71.

Scleral Plaques

LeBedis, C. A., and Sakai, O. (2008). Nontraumatic orbital conditions: Diagnosis with CT and MR imaging in the emergent setting. *RadioGraphics*, **28**, 1741–53.
Murray, J. L., Haymany, L. A., Tang, R. A., et al. (1995). Incidental asymptomatic orbital calcifications. *J Neuroophthalmol* **15** (4), 203–8.

7 Cervical Spine and Soft Tissues of the Neck

Shawneen M. Gonzalez

Introduction

This chapter will cover common findings associated with the cervical spine and soft tissue of the neck surrounding the spine. The topics covered include pathosis and variants of normal anatomy. Different portions of the soft tissue of the neck are seen on CBCT scans depending of the FOV used. Some of the radiographic findings covered in this chapter may not be visible on all scans and therefore should not be commented on by someone reviewing a scan.

Anatomy—Cervical Spine and Soft Tissues of the Neck

This section will highlight anatomical landmarks of the cervical spine, specifically the cervical vertebrae.

As cone beam CT scans are not made to differentiate soft tissue, this chapter will not identify specific soft tissue anatomy. It will look at more general areas, many of which are only identifiable when using a scan with a large field of view.

Axial

The axial figures start from the superior aspect of the cranium moving inferiorly (Figures 7.1–7.4).

Interpretation Basics of Cone Beam Computed Tomography, First Edition.
Edited by Shawneen M. Gonzalez.

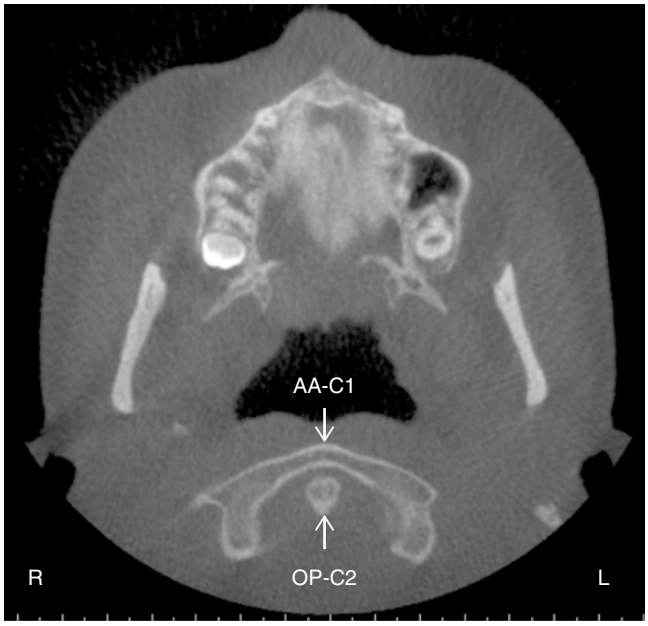

Figure 7.1. Axial view at the level of the inferior aspect of the maxillary sinuses showing the anterior arch of C1 (AA-C1) and the odontoid process of C2 (OP-C2).

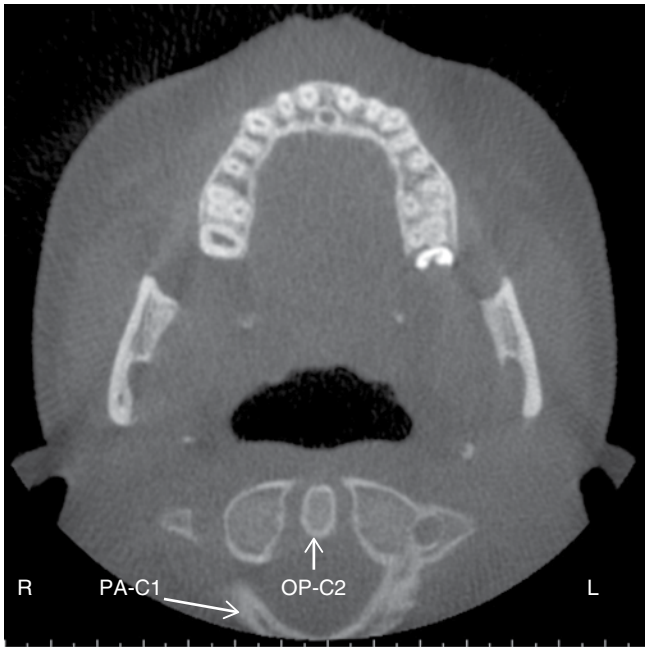

Figure 7.2. Axial view at the level of the mandibular foramina showing the odontoid process of C2 (OP-C2) and posterior arch of C1 (PA-C1).

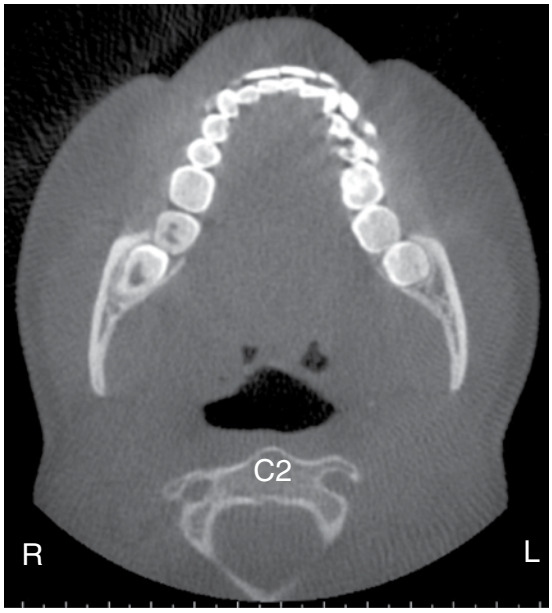

Figure 7.3. Axial view at the level of mandibular teeth at the cemento-enamel junction showing the entire arch of C2.

Figure 7.4. Axial view at the level of the hyoid bone showing the entire arch of C3.

Coronal

The coronal figures start from the anterior aspect of the face moving posteriorly (Figures 7.5–7.8).

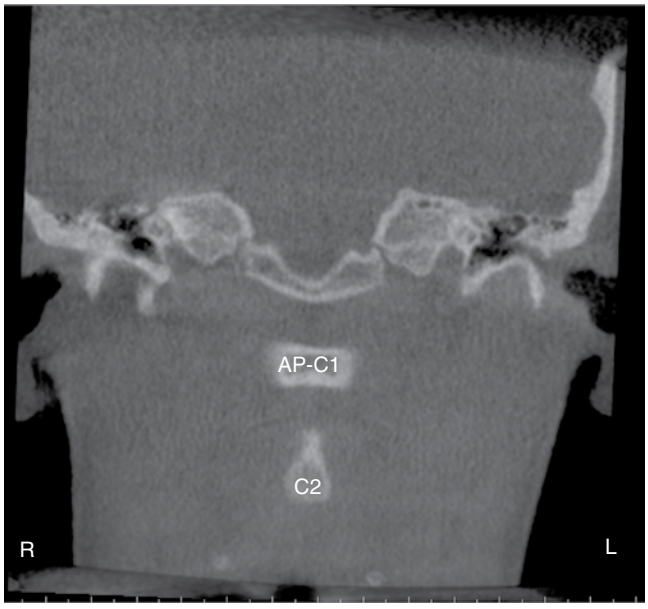

Figure 7.5. Coronal view at the aspect of the auditory canal showing the anterior arch of C1 (AP-C1) and portions of the body of C2.

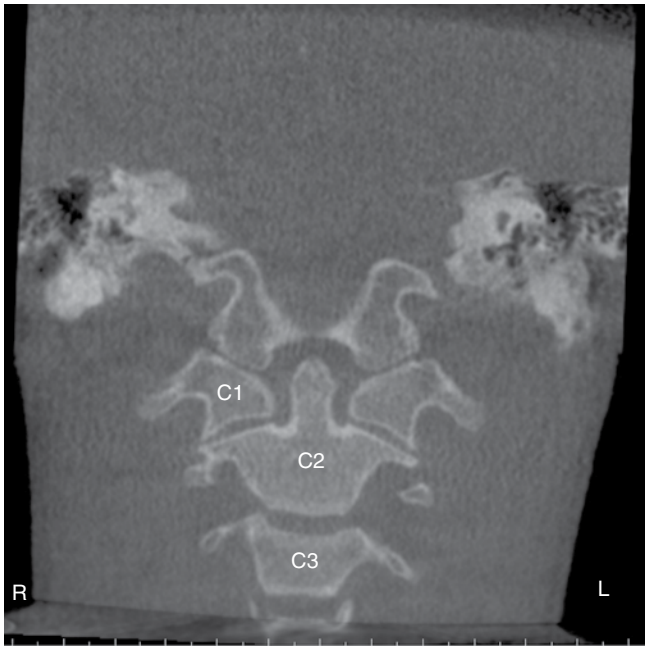

Figure 7.6. Coronal view at the aspect of the mastoid air cells showing cervical vertebrae C1, C2, and C3.

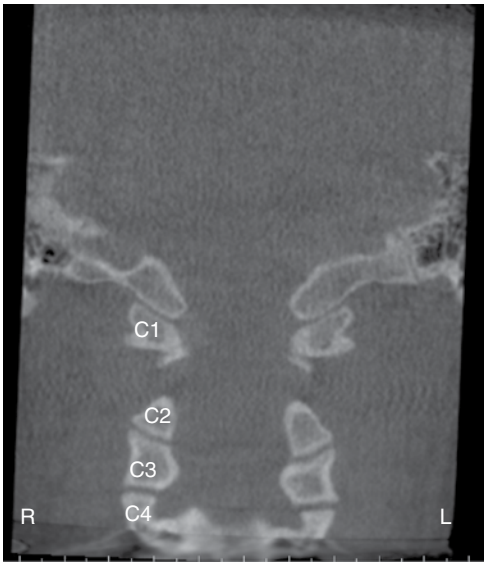

Figure 7.7. Coronal view at aspect of the posterior cranial base showing C1, C2, C3, and portions of C4.

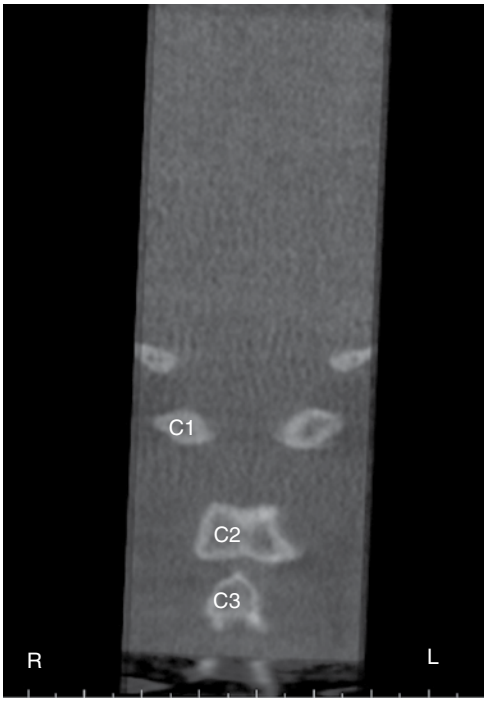

Figure 7.8. Coronal view showing C1, C2, and C3.

Sagittal

The sagittal figures start from the lateral aspect of the cranium moving medially (Figures 7.9–7.10).

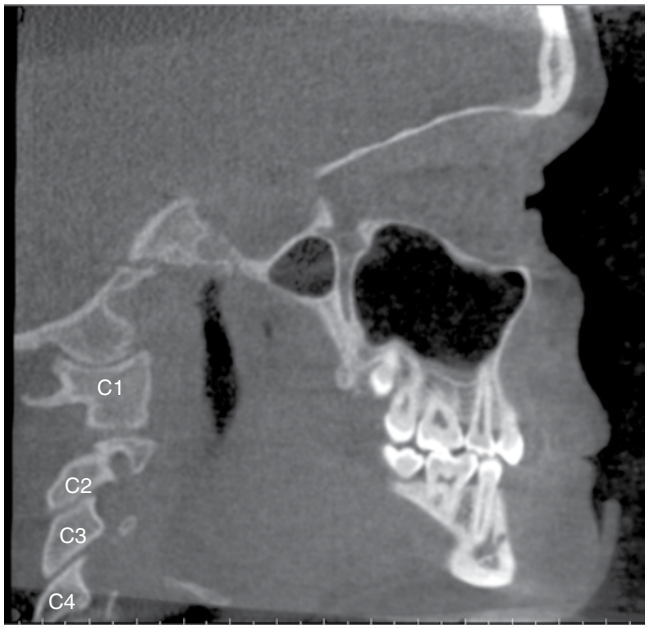

Figure 7.9. Sagittal view at the lateral aspect of the maxillary posterior teeth showing cervical vertebrae C1, C2, C3, and portions of C4.

Figure 7.10. Sagittal view on the midline showing cervical vertebrae C1, C2, and C3.

Incidental Findings

Developmental

There are many variations of developmental anomalies that may present in the cervical vertebrae. This book cannot encompass them all and will list some of the most commonly occurring ones. The developmental anomalies are listed in order of most superior cervical vertebrae moving inferiorly.

Clefts (C1)

Definition/Clinical Characteristics They are incomplete fusions of the ossification centers of either the anterior or posterior arch of C1 (atlas) or a combination of both. The fusion of the anterior arch occurs by the age of 10 and the posterior arch completes fusion between the ages of 3 or 4. Posterior arch clefts have an incidence of 4% of all adults with 97% of these clefts occurring in the midline. Anterior arch clefts are less common, occurring in only 0.1% of all adults. Cervical vertebral clefts occur more commonly in patients with cleft lip, cleft palate, or both.

Radiographic Description It appears as a well-defined radiolucent line or band of the anterior or posterior arch of C1. There may be multiple radiolucent lines (thee or more) visible in the anterior arch (Figure 7.11). The posterior arch rarely presents with more than one radiolucent line. The bony borders of the arch and ossification centers are corticated. When both anterior and posterior clefts are noted, the appropriate descriptive term is *split* atlas. This is best visualized on axial and coronal views (Figures 7.12 and 7.13).

Differential Interpretation Radiolucent line(s) in the anterior or posterior arch of C1 that are not corticated means one would need to consider the possibility of a fracture. A fracture typically presents with swelling combined with a history of trauma to the area.

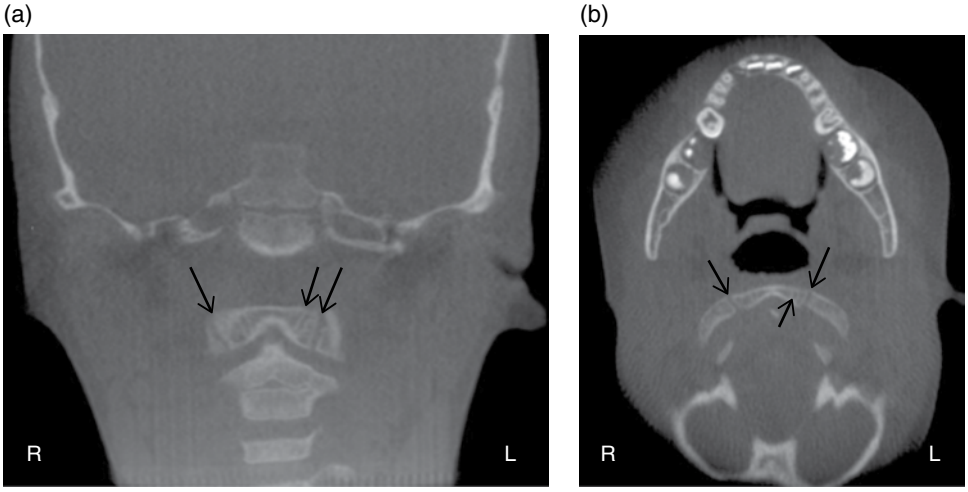

Figure 7.11. (a) Coronal view showing three anterior arch clefts (black arrows) in a 5 year 11 month old; (b) Axial view showing three anterior arch clefts (black arrows) in a 5 year 11 month old.

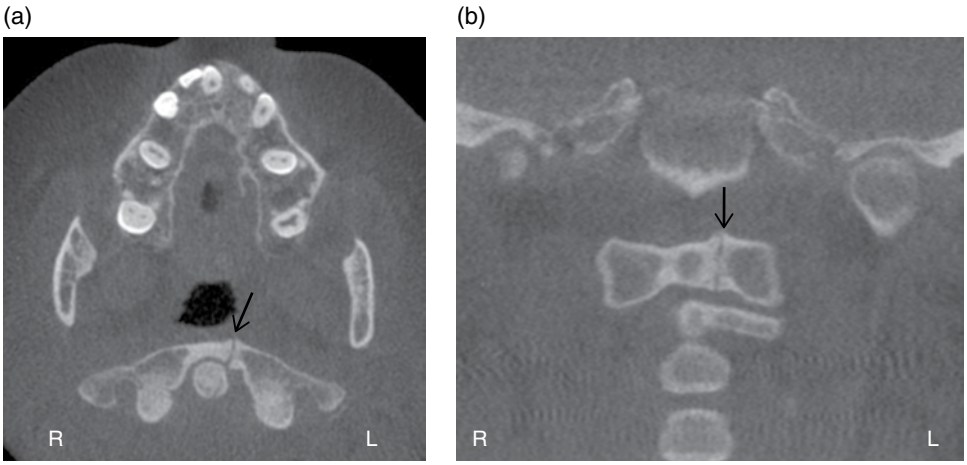

Figure 7.12. (a) Axial and (b) coronal views showing a single anterior arch cleft (black arrow) in a 20 year old.

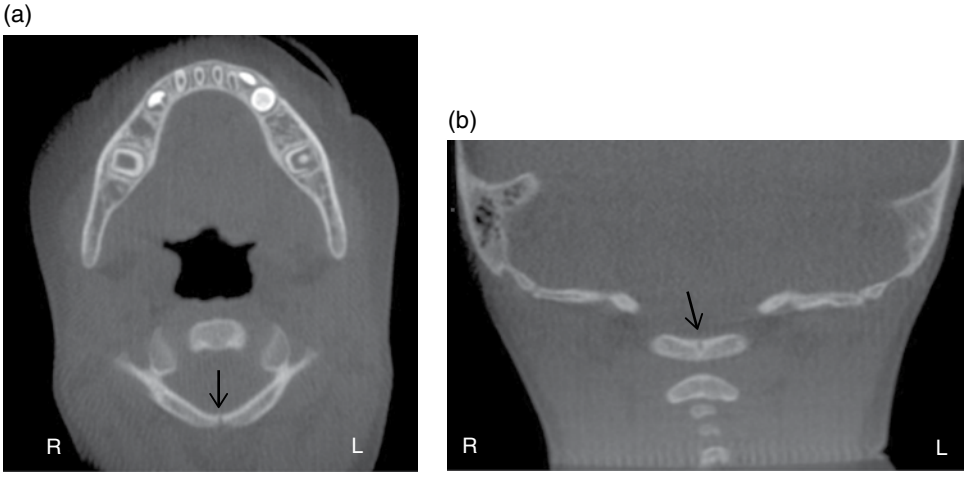

Figure 7.13. (a) Axial and (b) coronal views showing a single posterior arch cleft (black arrow).

Treatment/Recommendations There is no recommended treatment or further imaging necessary for this finding.

Os Terminale (C2)

Definition/Clinical Characteristics There are three ossification centers that develop to form the body of C2 (axis). Two form the body and one forms the tip of the odontoid process. The ossification center that forms the tip of the odontoid process is referred to as os terminale. It is typically evident by the age of 3 and fuses with the body of C2 by the age of 12. It has been reported in 1.3%–9.9% of children.

Radiographic Description Os terminale presents as a well-defined radiopaque entity at the tip of the body of C2. The body of C2 has a V-shaped notch on

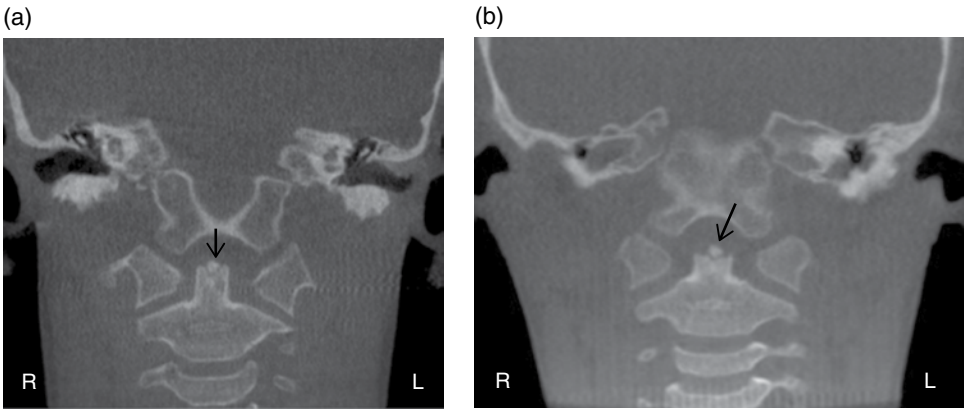

Figure 7.14. Coronal views (a,b) showing os terminale at the superior aspect of the odontoid process of C2 (black arrow).

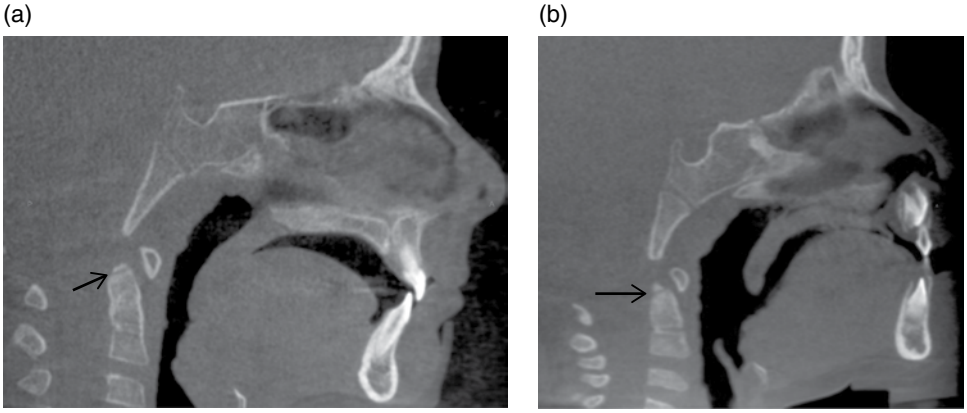

Figure 7.15. Sagittal views (a,b) showing os terminale (black arrow) at the superior aspect of the odontoid process of C2.

the superior aspect where the ossification center is located on coronal views (Figure 7.14). There is a complete to incomplete radiolucent line separating the ossification center from the remainder of the body of C2. This is best visualized on coronal and sagittal views (Figure 7.15).

Differential Interpretation If the ossification center for the tip of the odontoid process is evident beyond the age of 12, it is referred to as ossiculum terminale persistens. A fracture of the tip of the odontoid process will also present as a radiopaque entity separated from the body of C2. The bony fragment and body will not have corticated borders at the area of separation and a history of trauma indicates a fracture more likely than a persistent ossification center.

Treatment/Recommendations There is no recommended treatment or further imaging necessary for this finding.

Subdental Synchondrosis (C2)

Definition/Clinical Characteristics An incomplete or partial fusion of the superior and inferior ossification centers of the body of C2. Fusion occurs in 80% of the population by the age of 9.

Radiographic Description This will appear as a horizontal radiolucent line or band in the middle of the C2 body. It may extend completely from one side to the other (anterior–posterior or laterally; Figure 7.16) or only partially (Figure 7.17) depending on the stage of fusion. Complete separation of the two ossification centers is typically not seen beyond the age of 4. This is best visualized on sagittal and coronal views (Figure 7.18).

Figure 7.16. Sagittal view showing complete subdental synchondrosis of C2 (black arrow).

Figure 7.17. Sagittal view showing partial subdental synchondrosis of C2 (black arrow).

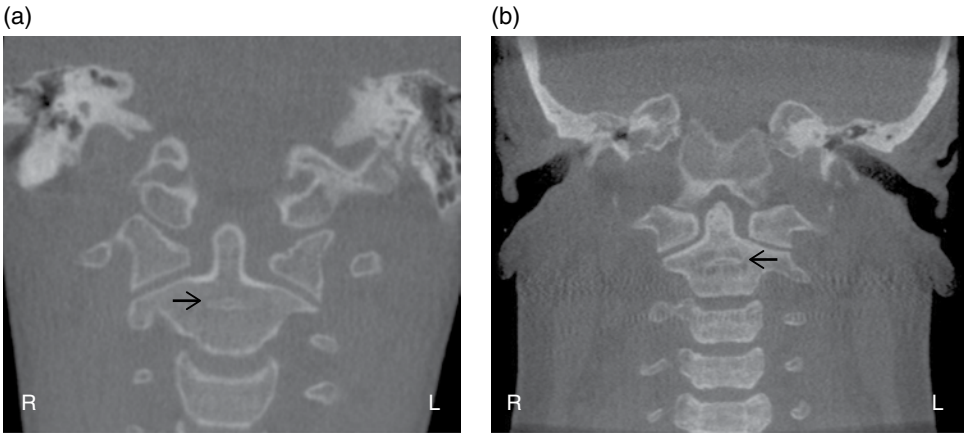

Figure 7.18. Coronal views (a,b) showing partial subdental synchondrosis of C2 (black arrow).

Differential Interpretation Persistence of the synchondrosis is referred to as a "dentocentral ghost." A fracture of the C2 body in this location can occur; however, the presence of swelling along with a history of trauma to this area would rule out persistent synchondrosis.

Treatment/Recommendations There is no recommended treatment or further imaging necessary for this finding.

Congenital Block Vertebrae (C2-C3), Nonsegmentation

Definition/Clinical Characteristics Congenital block vertebrae is the failure of separation of two or more adjacent vertebral bodies or lateral processes. This occurs in 5.5% of the population.

Radiographic Description This most commonly occurs at the C2-C3 junction. It may be either the bodies of right or left lateral processes or both lateral processes. An enlarged body and/or lateral process with the absence of a radiolucent disc space is evident (Figure 7.19). This is best visualized on sagittal and coronal views (Figure 7.20).

Differential Interpretation Fusion of C2 and C3 vertebra is associated with type 2 Klippel-Feil syndrome (KFS). These patients may present with scoliosis (60%) or have limited range of motion, specifically lateral bending of the spine (more commonly seen in patients with 4+ vertebrae fused). Many patients are asymptomatic throughout their entire life. KFS occurs in approximately 1 in 40,000 to 42,000 births.

Treatment/Recommendations Referral to the patient's primary care physician is recommended to rule out or rule in the presence of Klippel-Feil syndrome.

Figure 7.19. Coronal view showing congenital block vertebrae of the bodies of C2 and C3.

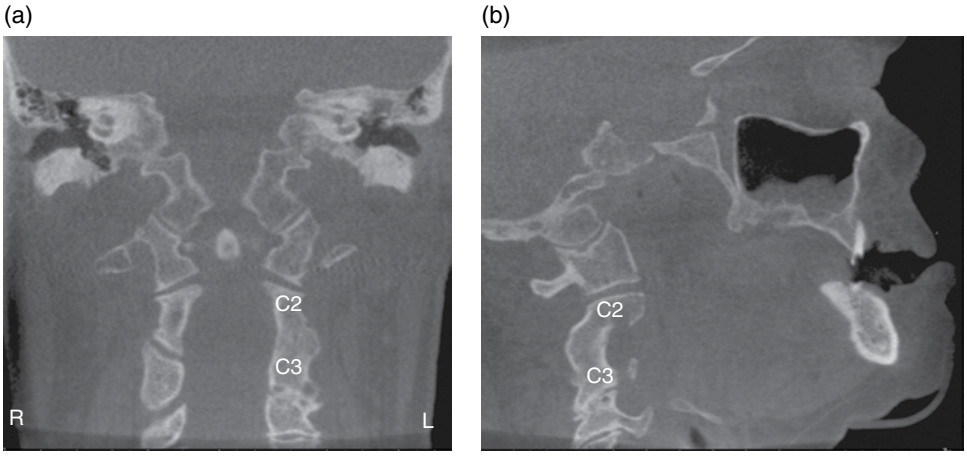

Figure 7.20. (a) Coronal and (b) sagittal views showing congenital block vertebrae of the left lateral processes of C2 and C3.

Pathosis

Degenerative Joint Disease (Osteoarthritis, Spondylosis)

Definition/Clinical Characteristics Degenerative joint disease (DJD) is a common age-related disease process resulting in degenerative changes of the intervertebral joints. Degenerative joint disease affects 50% of the population over the age of 40 increasing to 85% of the population over the age of 60. Activities or occupations that involve increased loads on the cervical spine increase the risk of developing DJD. Patients with DJD of the cervical spine may be asymptomatic or have a range

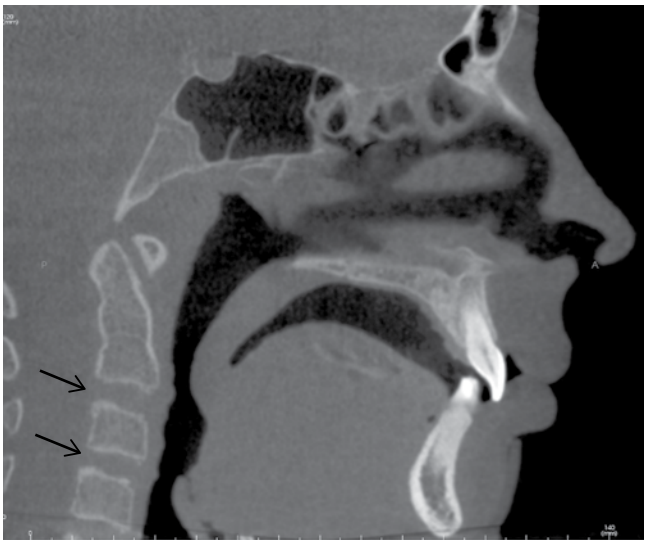

Figure 7.21. Sagittal view on midline showing normal joint spacing between the bodies of C2-C3-C4 (black arrows).

of symptoms including neck pain, cervical radiculopathy, and cervical myelopathy. There is a wide range of classifications of DJD; however, we will only cover the radiographic classifications in this book.

Radiographic Description There are five basic radiographic findings associated with DJD: intervertebral joint spacing, osteophytes, bone erosions, subchondral cysts, and facet hypertrophy.

Intervertebral Joint Space Narrowing. The radiolucent intervertebral joint spaces should appear uniform in size when viewed on sagittal views (Figure 7.21). Asymmetrical joint space narrowing is one of the first signs of DJD (Figure 7.22). Evaluating the joint spaces is best visualized on sagittal views.

Osteophytes. Osteophytes form in an attempt to increase stability of the cervical vertebrae. They may increase in size such that they impinge on the spinal cord producing myeloradiculopathy. Osteophytes appear as radiopaque bone spurs at the lateral aspects of the joints (Figure 7.22). They enlarge toward the adjacent vertebra. They are best visualized on sagittal views.

Bone Erosions. Bone erosions appear on the surfaces of the vertebra in direct contact with the joint space. They appear as a discontinuity of the cortical border of the bone with saucering and loss of the bone. They are best visualized on sagittal and coronal views (Figure 7.23).

Subchondral Cysts. Subchondral cysts are degenerative cysts that form at the junctions of the bone with the intervertebral joints. They appear as well-defined radiolucent areas within the vertebra (see Figures 7.22, 7.24). They are visualized on all three views equally (axial, coronal, and sagittal).

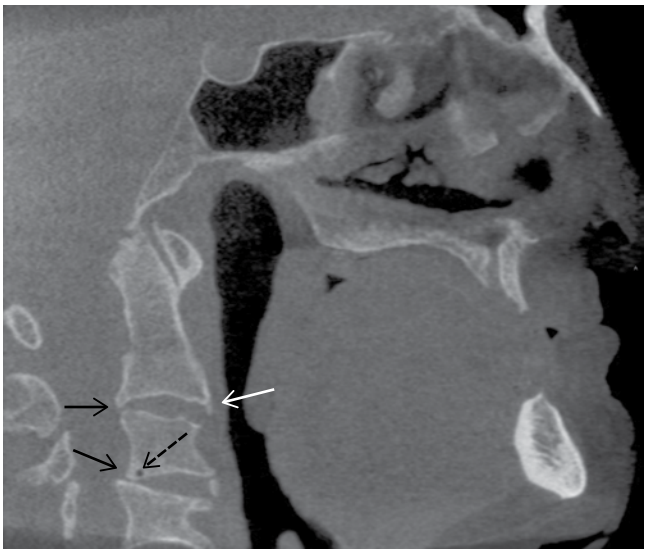

Figure 7.22. Sagittal view on midline showing asymmetrical joint space narrowing (black arrows), osteophyte formation (white arrow), and subchondral cyst formation (black dotted arrow).

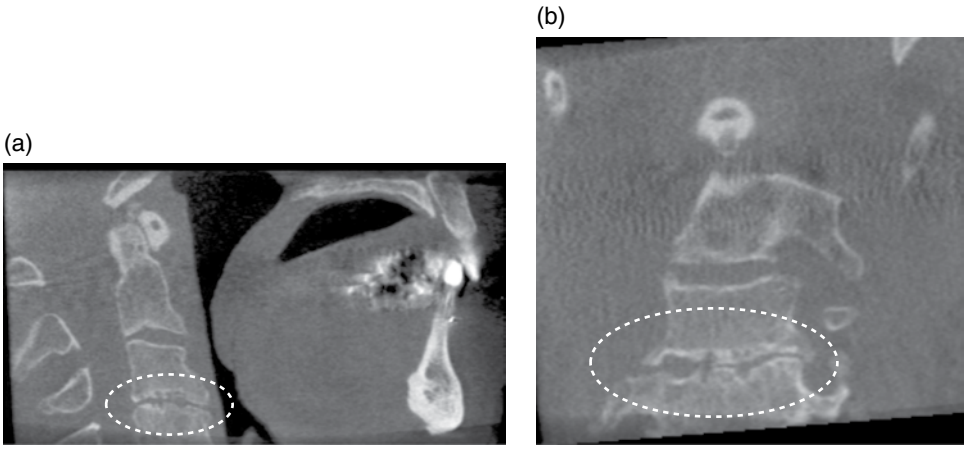

Figure 7.23. (a) Sagittal and (b) coronal views showing bone erosions between the bodies of C3 and C4 (white dotted circle).

Facet Hypertrophy. Facet hypertrophy is an increase in bone formation at the facet between two adjacent vertebrae. It will appear as a radiopaque enlargement of the junction of lateral processes. It is best visualized on axial views (Figure 7.25).

Luoma et al. (2009) classified spinal DJD in four groups ranging from Grade 0 to Grade 4. The classification is based on the presence or absence of the five previous radiographic findings (Table 7.1).

Differential Interpretation There is no differential interpretation due to the presence of multiple pathognomic radiographic findings of this process.

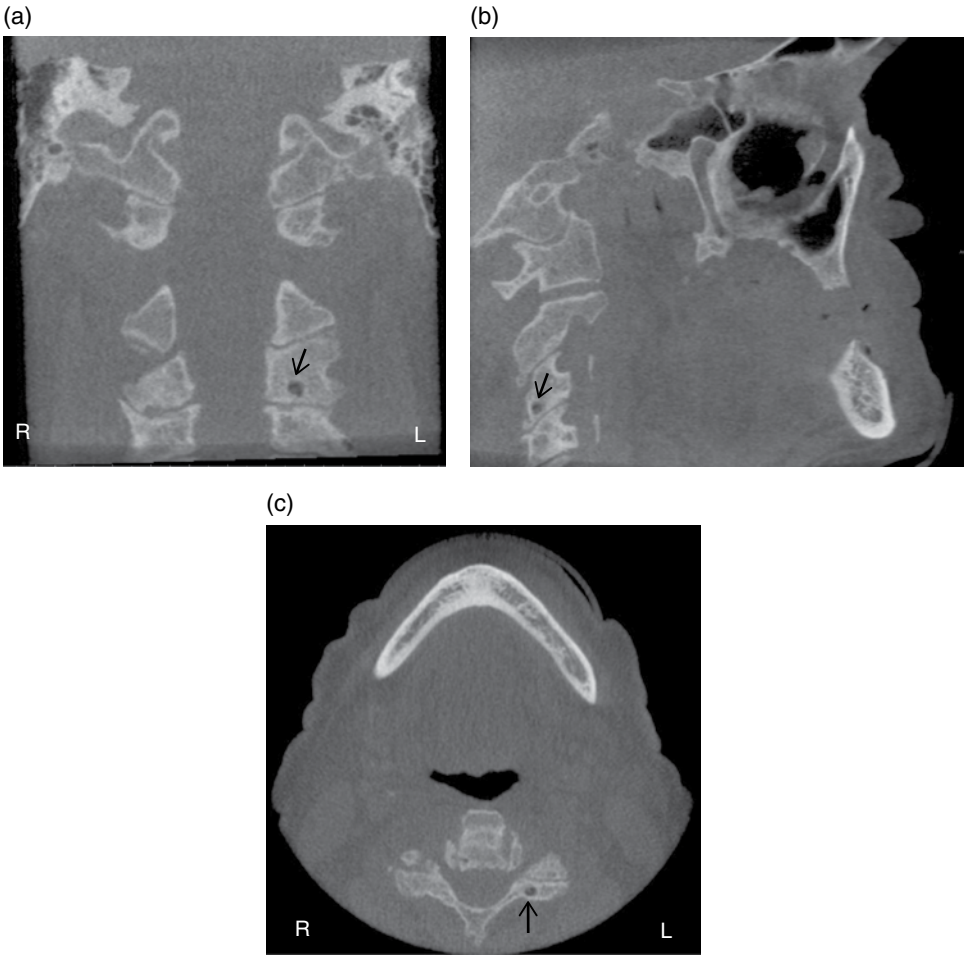

Figure 7.24. (a) Coronal, (b) sagittal, and (c) axial views showing subchondral cysts in the left lateral process of C3 (black arrow).

Treatment/Recommendations The patient should be referred to his or her primary care physician. The primary care physician will determine whether treatment is necessary. Treatment ranges from no treatment to pharmaceutical treatment or surgical fusion of the vertebrae.

Carotid Artery Calcification

Definition/Clinical Characteristics The definition is atherosclerotic plaques of the carotid artery near the bifurcation of the internal and external carotid arteries. These calcifications are strongly associated with existing systemic disease such as hypertension, hypercholesterolemia, and diabetes mellitus. There is a slight male predilection. They are evident in approximately 5.5%–10% of the population on CBCT scans covering this area. There is no evidence that the presence of these calcifications are a predictor of future strokes, but it should be used as a sign of the state of the overall atherosclerosis of an individual. The incidence increases with age.

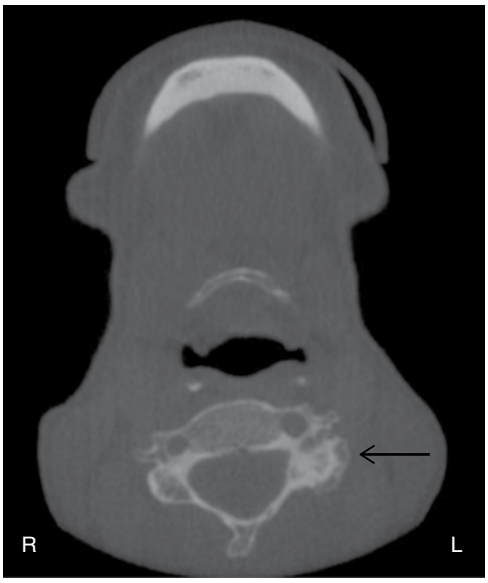

Figure 7.25. Axial view showing left facet hypertrophy (black arrow).

Table 7.1 Radiographic degenerative joint disease (DJD) classification.

Radiographic finding	Grade 0 (no radiographic DJD)	Grade 1 (mild radiographic DJD)	Grade 2 (moderate radiographic DJD)	Grade 3 (severe radiographic DJD)
Asymmetrical joint space narrowing	None present	Present	Present	Present
Osteophytes	None present	Small	Small	Large
Bone erosions	None present	None present	Mild	Severe
Subchondral cysts	None present	None present	Small	Large
Facet hypertrophy	None present	None present	Moderate	Severe

Source: Based on Luoma et al. (2009), Relationship of Modic type 1 change with disc degeneration: A prospective MRI study, *Skeletal Radiol*, **38**, 237–44.

Radiographic Description The calcification presents near the junction of C3 and C4. It appears as a well-defined radiopaque entity. The shape may present as either linear or masslike entities on coronal views (Figure 7.26) and sagittal views (Figure 7.27) to circular on axial views (Figure 7.28). It may be unilateral or bilateral. Small plaques are more evident on axial views, but calcifications may be seen on all views.

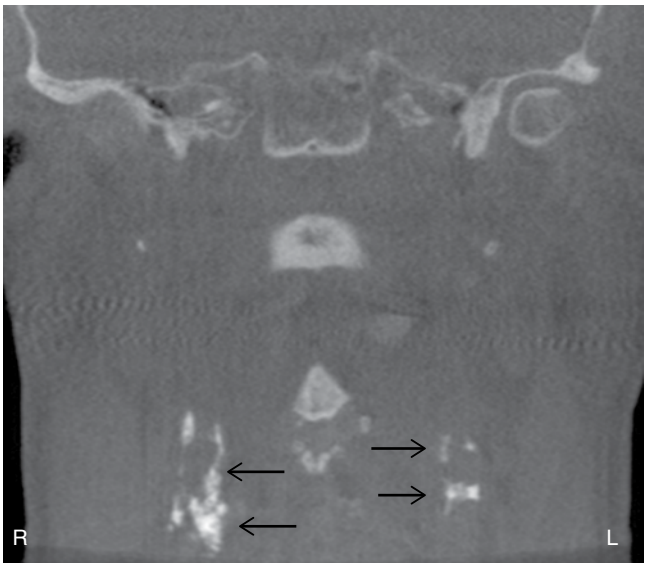

Figure 7.26. Coronal view showing bilateral carotid artery calcifications (black arrows).

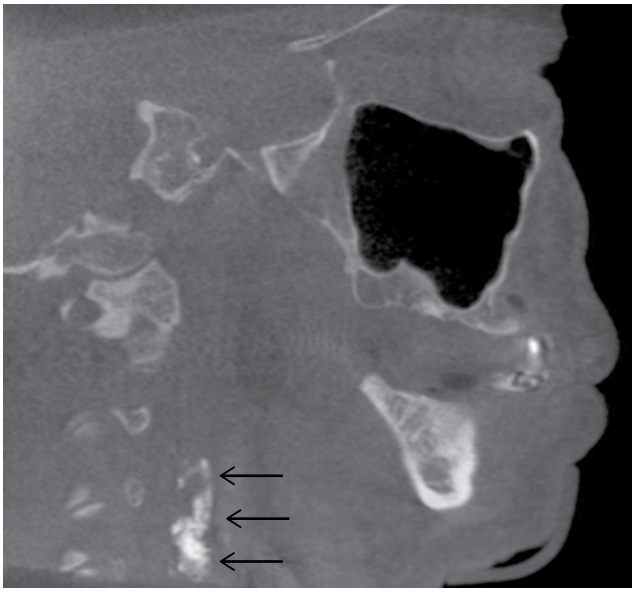

Figure 7.27. Sagittal view showing unilateral carotid artery calcifications (black arrows).

Differential Interpretation There is no differential interpretation due to the location of this finding.

Treatment/Recommendations The patient should be referred to his or her primary care physician. This ensures that the patient and primary care physician are aware of the full extent of any underlying atherosclerotic disease and/or other systemic disease contributing to the calcifications.

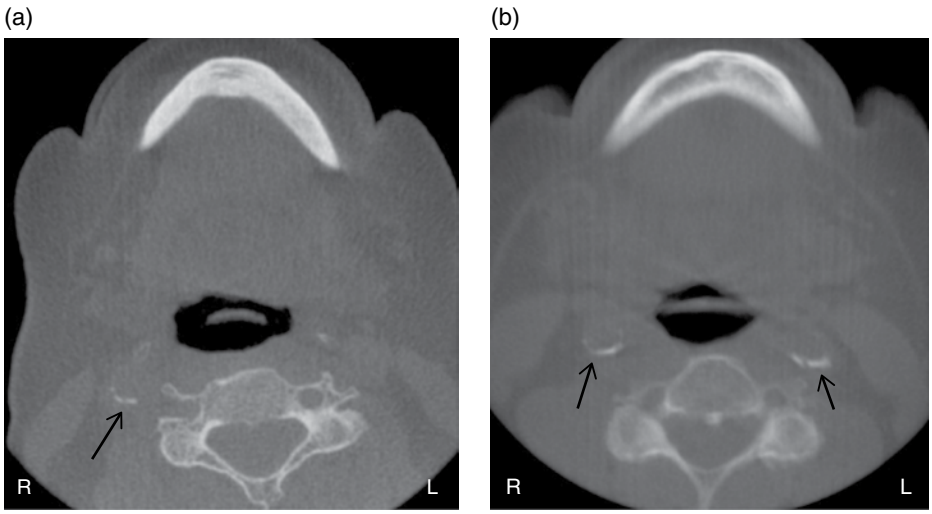

Figure 7.28. (a) Axial view showing unilateral carotid artery calcification (black arrow); (b) Axial view showing bilateral carotid artery calcification (black arrows).

References

Anatomy

Netter, F. (2004). *Atlas of Human Anatomy*, 3d ed. Icon Learning Systems, Teterboro, NJ.

Clefts

Keats, T., and Anderson, M. (2007). *Atlas of Normal Roentgen Variants That May Simulate Disease*, 8th ed. Mosby, Philadelphia, PA.

Popat, H., Drage, N., Durning, P. (2008). Mid-line clefts of the cervical vertebrae—an incidental finding arising from cone beam computed tomography of the dental patient. *British Dental Journal*, **204**, 303–6.

Smoker, W. R. K. (1994a). Craniovertebral junction: Normal anatomy, craniometry, and congenital anomalies. *RadioGraphics*, **14**, 255–77.

Os terminale

Bertozzi, J. C., Rojas, C. A., Martinez, C. R. (2009). Evaluation of the pediatric craniocervical junction on MDCT. *AJR*, **192**, 26–31.

Keats, T., and Anderson, M. (2007). *Atlas of Normal Roentgen Variants That May Simulate Disease*, 8th ed. Mosby, Philadelphia, PA.

Smoker, W. R. K. (1994). Craniovertebral junction: Normal anatomy, craniometry, and congenital anomalies. *RadioGraphics*, **14**, 255–77.

Viswanathan, A., Whitehead, W. E., Luerssen, T. G., et al. (2009). "Orthotopic" ossiculum terminale persistens and atlantoaxial instability in a child less than 12 years of age: A case report and review of the literature. *Cases Journal*, **2**, 8530–35.

Subdental Synchondrosis

Karwacki, G. M., and Schneider, J. F. (2012). Normal ossification patterns of atlas and axis: A CT study. *Am J Neuroradiol*, **33**, 1882–87.
Keats, T., and Anderson, M. (2007). *Atlas of Normal Roentgen Variants That May Simulate Disease*, 8th ed. Mosby, Philadelphia, PA.
Piatt, J. H., and Grissom, L. E. (2011). Developmental anatomy of the atlas and axis in childhood by computed tomography. *J Neurosurg Pediatrics*, **8**, 235–43.
Smoker, W. R. K. (1994). Craniovertebral junction: Normal anatomy, craniometry, and congenital anomalies. *RadioGraphics*, **14**, 255–77.

Congenital Block Vertebrae

De Graaff, R. (1982). Congenital block vertebrae C2-C3 in patients with cervical myelopathy. *Acta Neurochir*, **61** (1–3), 111–26.
Keats, T., and Anderson, M. (2007). *Atlas of Normal Roentgen Variants That May Simulate Disease*, 8th ed. Mosby, Philadelphia, PA.
Klimo, P., Rao, G., Brockmeyer, D. (2007). Congenital anomalies of the cervical spine. *Neurosurg Clin N Am*, **18**, 463–78.
Knoplich, J. (1992). Isolated vertebral blocks in the cervical spine. *Rev Paul Med*, **110** (1), 2–7.
Samartzis, B., Lubicky, J. P., Shen, F. H. (2008). "Bone block" and congenital spine deformity. *Ann Acad Med Singapore*, **37** (7), 624.

Degenerative Joint Disease

Leonardi, M., Simonetti, L., Agati, R. (2002). Neuroradiology of spine degenerative disease. *Best Practice & Research Clinical Rheumatology*, **16** (1), 59–87.
Luoma, K., Vehmas, T., Gruonblad, M., et al. (2009). Relationship of Modic type 1 change with disc degeneration: A prospective MRI study. *Skeletal Radiol*, **38**, 237–44.
Narayan, P., and Haid, R. W. (2001). Treatment of degenerative cervical disc disease. *Neurologic Treatment*, **19** (1), 217–29.
Rao, R. D., Currier, B. L., Albert, T. J., et al. (2007). Degenerative cervical spondylosis: Clinical syndromes, pathogenesis, and management. *J Bone Joint Surg Am*, **89**, 1360–78.

Carotid Artery Calcification

Pette, G. A., Norkin, F. J., Ganeles, J., et al. (2012). Incidental findings from a retrospective study of 318 cone beam computed tomography consultation reports. *Int J Oral Maxillofac Implants*, **27**, 595–603.

8 Temporomandibular Joints

Gayle Reardon

The Temporomandibular Joints

Imaging assessments of the temporomandibular joint graphically depict clinically suspected disorders of the jaw joints. It is radiographic examination and imaging that play an important role in the diagnosis and management of most temporomandibular joint (TMJ) disorders. Several techniques have been used for the examination of the TMJ, including conventional tomography, magnetic resonance imaging (MRI), arthrography, computed tomography (CT), and, recently, cone beam computed tomography (CBCT). CT and MRI allow for better appreciation of the soft tissues of the joints, which, in turn, allows a better understanding of anatomy and pathophysiology of internal derangements related to disc displacement.

Normal Anatomy and Function

The mandible and temporal bones comprise the osseous components of the temporomandibular joint. The head of the mandibular condyle comprises the inferior component of the joint and the temporal bone contributes the mandibular fossa (glenoid fossa) and articular tubercle, forming the superior osseous part of the joint (Figures 8.1–8.4). The articulating surfaces of the temporomandibular joints are covered by a thin layer of dense fibrous tissue, rather than the cartilaginous coverings found in most other joints of the body.

The temporomandibular joint disc is a biconcave (bow-tie shaped) fibrous structure located between the condylar head and the mandibular fossa of the temporal

Interpretation Basics of Cone Beam Computed Tomography, First Edition.
Edited by Shawneen M. Gonzalez.

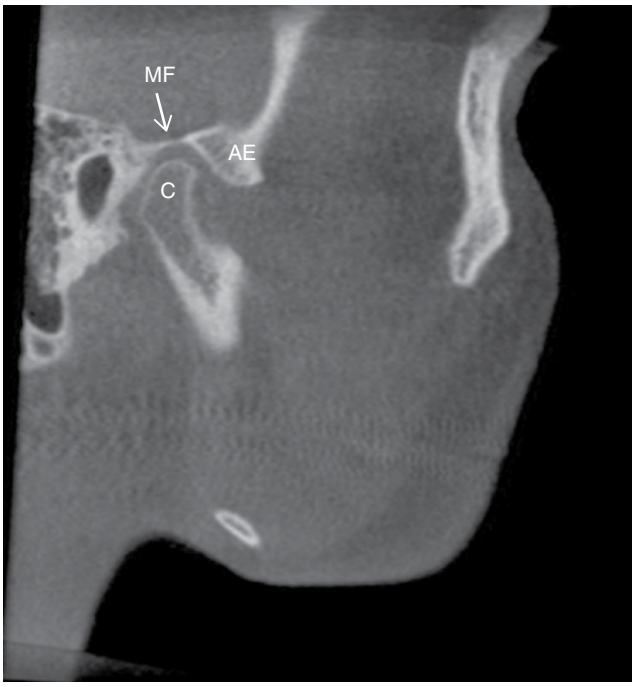

Figure 8.1. Sagittal slice showing the condyle (C), mandibular fossa (MF), and anterior articular eminence (AE).

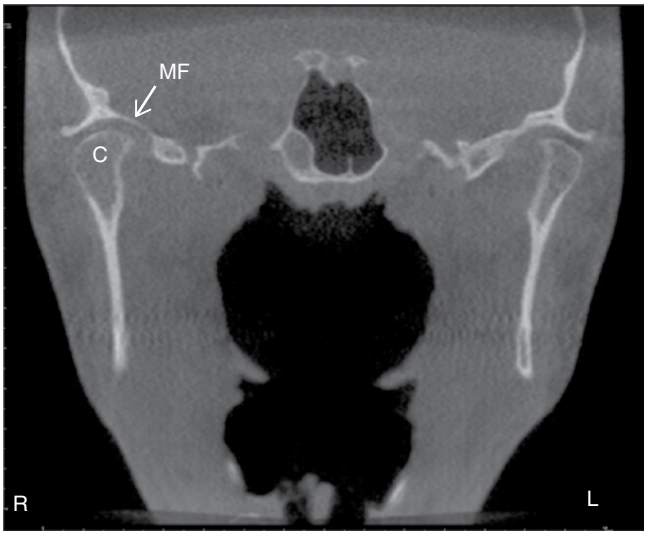

Figure 8.2. Coronal slice showing the condyle (C) and mandibular fossa (MF).

bone. The disc is round or oval in shape and has a thick periphery and thin dentral portion. Mediolaterally, the disc measures approximately 20 mm. In a normal joint, the posterior band is located over the condyle and the thinner central zone is located between the condyle and the posterior part of the articular tubercle. The anterior band is located under the articular tubercle. The entire joint is surrounded by a joint

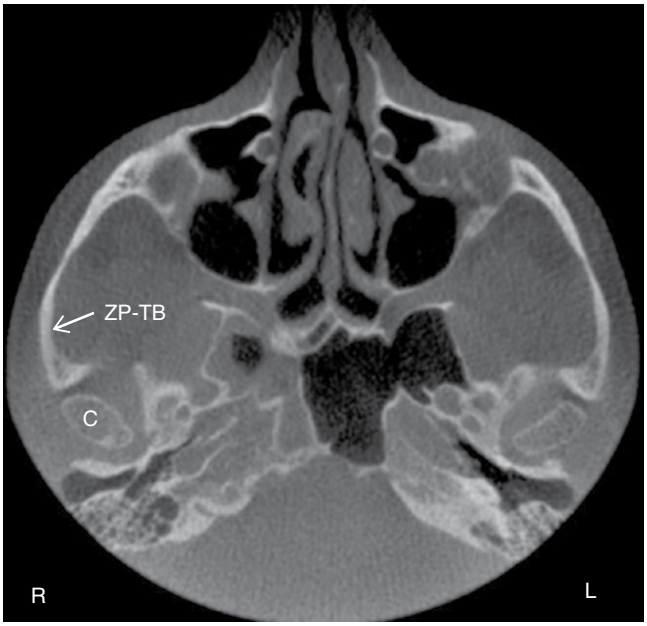

Figure 8.3. Axial slice showing the condyle (C) and zygomatic process of the temporal bone (ZP-TB).

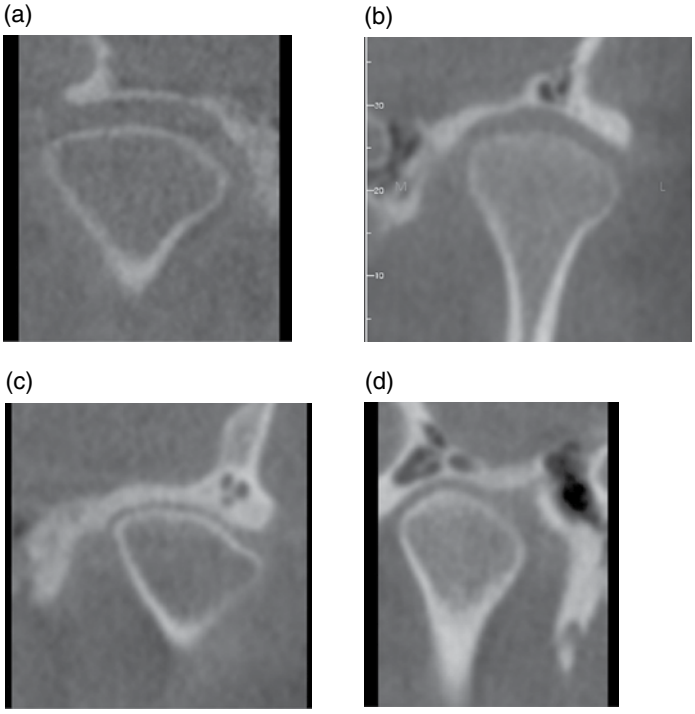

Figure 8.4. Coronal slices (a,b,c,d) showing various shapes of the condyle.

capsule emerging from the temporal bone and extending to attach to the neck of the condyle. Posteriorly, the disc is attached to the temporal bone and to the condyle by the posterior disc attachment. The posterior attachment is very important in internal derangements of the temporomandibular joint. The posterior attachment is also referred to as the bilaminar zone (from old histologic studies), or the retrodiscal tissue, and it consists of loose fibrous connective and elastic tissue components. Anteriorly, the disc attaches to the joint capsule and merges with the superior head of the lateral pterygoid muscle.

The craniomandibular articulation is complex because it involves two separate synovial joints, which function in unison within the same joint capsule. This allows for proportionally greater movement of the TMJ in relation to the actual physical size of the joint. The principal function of the disc is to permit relatively large movements within a small joint while maintaining stability. Rotation and translation occur in both the superior and inferior joint spaces, however, rotation is more evident in the inferior joint space while translation is predominant in the superior joint space. After the initial rotation, translation occurs in the superior and subsequently in the inferior joint space. During translation, the condyle and the disc translate together under the articular tubercle. All during mandibular movement, the thin central portion of the disc is located between the condylar head and the articular tubercle suggesting that the thicker periphery of the disc and the thick posterior and anterior bands act as functional guide for joint movement.

A fibrous capsule defines the anatomical and functional boundaries of the joint. Medially and laterally, the capsule is firm, which contributes to its stabilization during movement. The medial capsule is not as strong as the lateral capsule, which is reinforced by the temporomandibular ligament laterally. Anteriorly and posteriorly, the capsule is loose enough to allow for mandibular movement. The temporomandibular joint is supported by two accessory ligaments to protect the joint during wide excursive movements.

The first is the stylomandibular ligament, which runs from the tip of the styloid process to the angle and posterior border of the mandible. The second, the sphenomandibular ligament, runs from the greater wing of the sphenoid bone to the lingual of the mandibular ramus. The sphenomandibular ligament attaches separately from the medial capsule.

The capsule encloses the condyle and merges into the periosteum of the condylar neck. Laterally, the more firm attachment of the capsule extends below the condylar neck. It is shorter medially where it blends into the periosteum of the condylar neck below the medial pole of the condyle. The articular capsule completely surrounds the articular surfaces of the concave mandibular fossa (glenoid fossa) and the convex articular eminence, both formed by the squamous part of the temporal bone. Any condyle excursion beyond the anteriosuperior insertion of the capsule is classified as hypermobility.

The capsule consists of two layers, an outer fibrous layer and an inner layer of synovial tissue. The synovial layer produces synovial fluid with a function that serves three purposes: to reduce friction between articular surfaces by serving as a lubricant, to provide nutrition to the nonvascularized tissues of the articulating surfaces and the disc, and to remove debris from the joint spaces. There is only enough synovial fluid to outline the joint surfaces. If larger amounts of joint fluid are present, it is an indication of joint pathology.

The joint has an intracapsular disc that divides the synovial cavity into noncommunicating upper and lower compartments. The disc consists of dense collagenous tissue without innervations or vascularization. In the child and adolescent, the disc is composed of dense collagenous fibers; in the elderly person it is fibrocartilage. In the newborn, the entire disc is of equal thickness. This changes as the TMJ begins to function. With function, the disc adapts to the configurations of the opposing surfaces resulting in its final biconcave "bow tie" appearance. The posterior and anterior thick parts are called posterior and anterior bands. The undersurface of the disc and the superior aspect of the condylar head fit perfectly together during all jaw movements.

The disc attaches firmly to the condyle medially and laterally so is able to move only slightly in the mediolateral direction. Posteriorly, the disc is continuous with the posterior disc attachments (the retrodiscal pad), which consists of loose connective tissue with large elastic fibers and fat. It is highly vascular and well innervated in addition to being outlined by synovial membrane. The posterior attachments can easily become compressed and, because of its structure, it is unfit for articulation, which may occur when the disc is displaced. If the undersurface of the posterior discal attachment is damaged, the disc can translate to a position anterior to the condyle, resulting in an anterior disc displacement.

During jaw movement, the condyle rotates smoothly against the central underside of the disc. The disc and condyle move as an integrated complex in the healthy joint. It is magnetic resonance imaging (MRI) that enables the depiction of both soft and hard tissues of the joint and provides us with visualization of the relationship of the hard and soft tissues.

Developmental Abnormalities

Based on their etiology and time of appearance, developmental conditions can be classified as congenital malformations with associated growth disorders and as primary growth disorders. Hemifacial microsomia, condylar aplasia, condylar hypoplasia, or condylar hyperplasia are the most common craniofacial malformations. Facial asymmetry is the most prevalent clinical sign of developmental conditions in the TMJ region. CBCT and 3D CBCT provide diagnostic information about the size, shape, and accurate position of the mandibular condyle. They also provide information about morphology, inclination, displacement, or deviation of the lateral and medial surfaces of the mandibular rami and body.

Hemifacial Microsomia

Definition/Clinical Characteristics

Hemifacial microsomia is the second most common facial birth defect after cleft palate/lip occurring in approximately 1 in 5000 live births with variable frequencies reported. It occurs more frequently in males than females. It is the most frequent syndrome from first and second branchial arches. It may not be appreciable in infancy and is usually evident by the age of 4 years. Characteristic clinical findings include

facial asymmetry and ear anomalies. The right-side facial underdevelopment is more frequent than left-side underdevelopment. Skin tags between ear and corner of mouth occur. Seventh cranial nerve palsy is frequent. Other findings include dental malocclusion, hypodontia, and plagiocephaly in 10%. Bifacial microsomia has been reported.

Radiographic Description

It is seen on radiographs as an underdeveloped mandible without a mandibular condyle. A flat zygomatic arch without a mandibular fossa may be evident.

Condylar Aplasia

Condylar aplasia is the absence of one or both condyles.

Condylar Hypoplasia

Definition/Clinical Characteristics/Radiographic Description

Condylar hypoplasia is an undersized condyle with normal morphology. It may be congenital, developmental, or acquired. Some examples include: micrognathia, Treacher Collins syndrome, secondary effects of radiation, or the result of infection. It generally presents with an underdeveloped ramus and body of the mandible on the same side creating asymmetry of mandible. Degenerative joint disease (DJD) or osteoarthrosis is a long-term sequela (Figures 8.5 and 8.6).

Differential Interpretation

Juvenile rheumatoid arthritis presents with problems in other joints or the result of Rh factor incompatibility. Another differential includes severe DJD; however, this is found in an older-aged individual.

Treatment/Recommendations

Treatment options include orthognathic surgery, bone grafts, and orthodontic therapy.

Figure 8.5. Reconstructed pantomograph showing left condylar hypoplasia (white arrow).

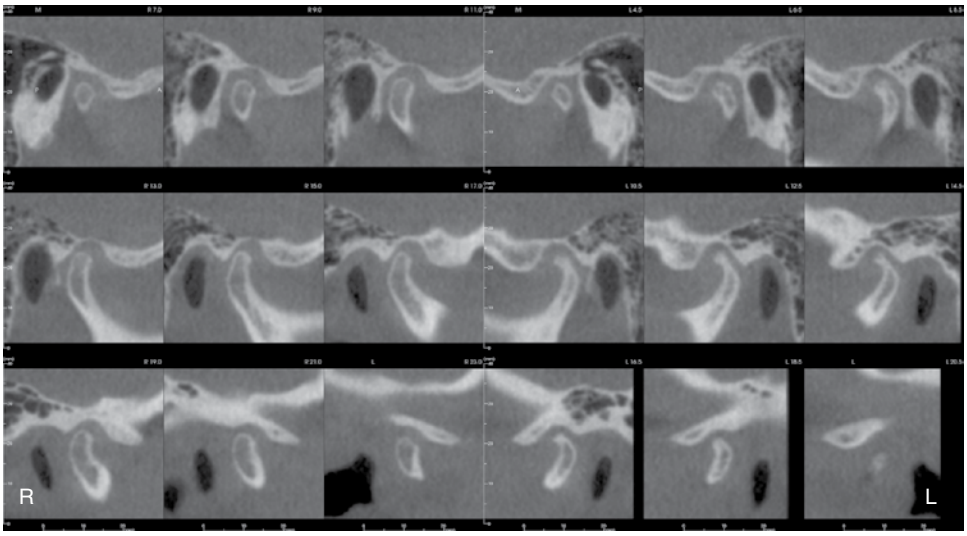

Figure 8.6. Cross-sectional slices of the right and left condyles. Right condyle shape and size within the range of normal. Left condyle is smaller than the range of normal.

Condylar Hyperplasia

Definition/Clinical Characteristics/Radiographic Description

Condylar hyperplasia is the enlargement and occasional deformity of the mandibular condyle. There is an increase in cortical thickness with maintenance of a normal trabecular pattern. This is most commonly seen in young males with a mean age of 20 years. It presents as hyperplasia of the ipsilateral mandible in the same side as the condylar hyperplasia and mandibular asymmetry. It is generally self-limiting and ends at approximately the same time as cessation of skeletal growth. (Figures 8.7 and 8.8).

Differential Interpretation

Differential interpretation includes osteochondroma, condylar osteoma, and large osteophyte or beaking of the mandibular condyle. Osteochondroma is irregular growth, which continues after the cessation of skeletal growth. Large osteophyte or beaking of the mandibular condyle are characteristic of osteoarthrosis and are found in older-aged individuals.

Treatment/Recommendations

Treatment is frequently orthodontics with orthognathic surgery.

Juvenile Arthrosis (Boering's Arthrosis)

Definition/Clinical Characteristics/Radiographic Description

Juvenile arthrosis presenting with condylar hypoplasia: Initially the condyle presents within the range of normal and becomes abnormal during growth. It presents with secondary degenerative changes and is typically seen in females. A "toadstool

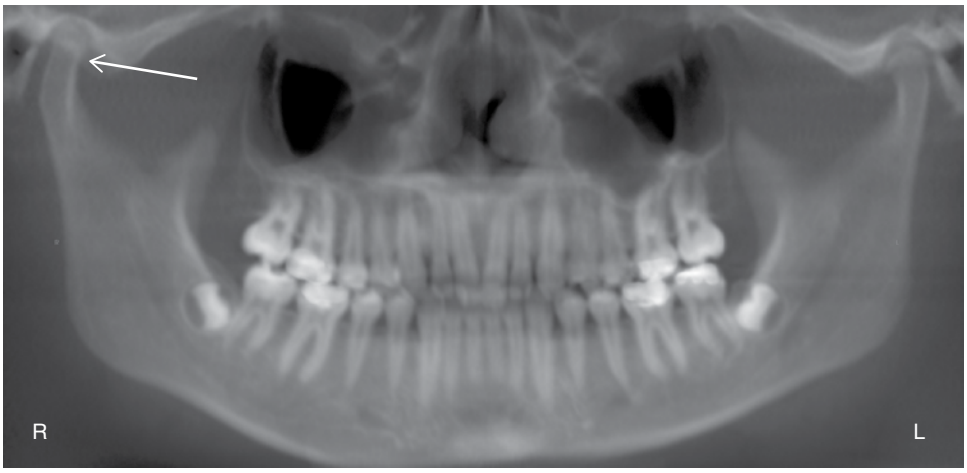

Figure 8.7. Reconstructed pantomograph showing right condylar hyperplasia (white arrow).

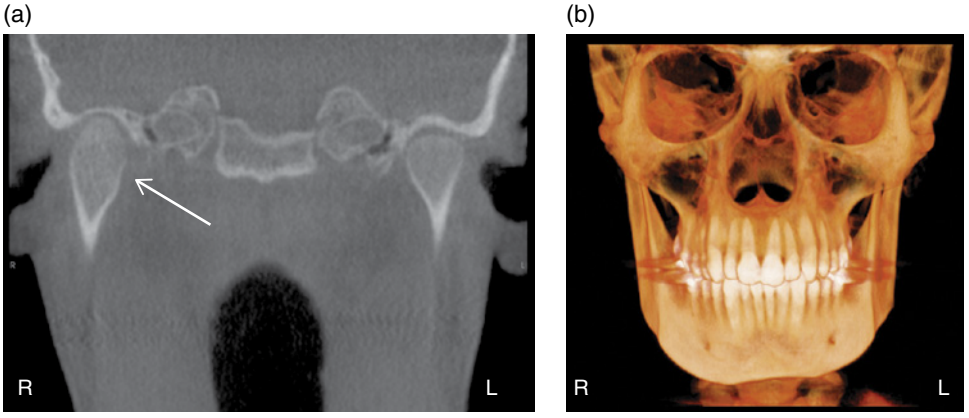

Figure 8.8. (a) Coronal slice showing right condylar hyperplasia (white arrow); (b) 3D reconstruction showing mandibular asymmetry.

appearance" with marked flattening and apparent elongation of the superior surface and posterior inclination of the mandibular condyle is frequently seen. The condylar neck is short or may be absent. There is flattening of the mandibular (glenoid) fossa and deepening of antegonial notch(s).

Differential Interpretation

Differential interpretation includes developmental condylar hypoplasia, rheumatoid arthritis, degenerative joint disease (DJD), and condylar degeneration after orthognathic or temporomandibular joint surgery.

Treatment/Recommendations

Orthognathic surgery and/or orthodontics.

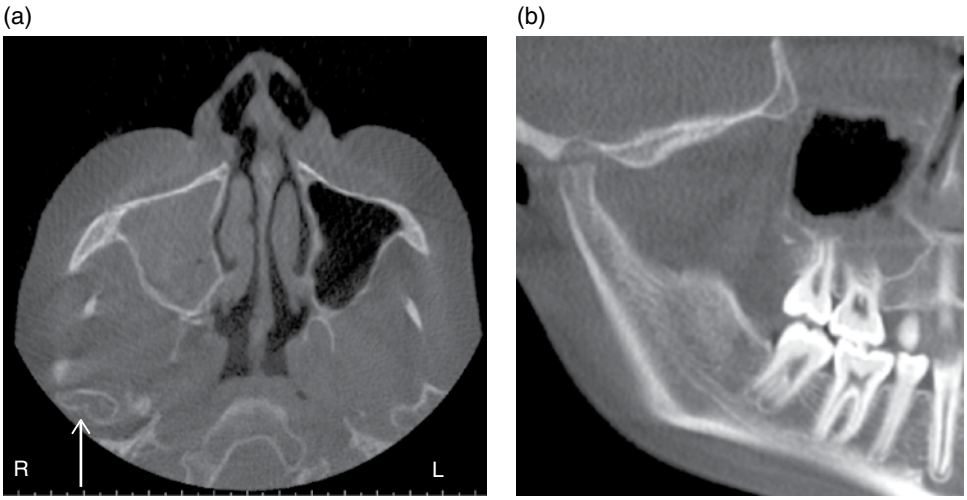

Figure 8.9. (a) Axial slice showing notching of the right condyle consistent with bifid condyle (white arrow); (b) Rotated sagittal slice showing notching on the superior aspect of the condyle.

Coronoid Hyperplasia

Definition/Clinical Characteristics/Radiographic Description

Coronoid hyperplasia may be developmental or acquired. It may be secondary to ankylosis. It is generally seen in males around the time of puberty and presents with a progressive inability to open their mouth. The coronoid process is considered hyperplastic if the tip of coronoid process extends at least one centimeter above the inferior rim of the zygomatic arch. It may cause remodeling of the zygomatic process of maxilla.

Differential Interpretation

Differential interpretation includes an osteochondroma or osteoma due to its irregular shape, which may develop secondary to other causes of trismus. Example: soft tissue causes or temporomandibular joint ankylosis.

Treatment/Recommendations

Surgical removal with postoperative physiotherapy.

Bifid Condyle

Definition/Clinical Characteristics/Radiographic Description

The condyle presents with a vertical depression, notch, or deep cleft in the condylar head. The location of the "notch" may be in the mediolateral or anteroposterior plane (Figures 8.9 and 8.10).

Differential Interpretation

A vertical fracture may appear like a bifid condyle and may also be an etiology for bifid condyle.

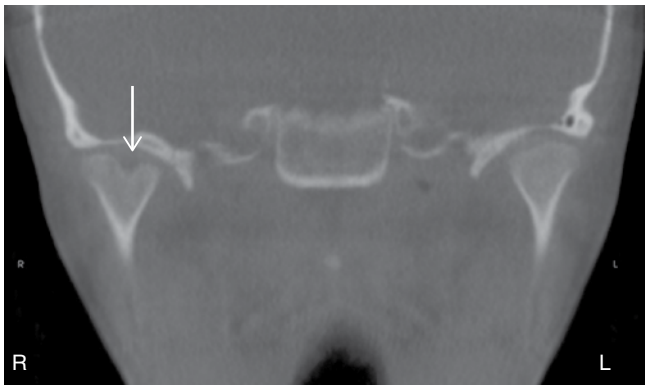

Figure 8.10. Coronal slice showing notching on superior aspect of right condyle consistent with bifid condyle (white arrow).

Treatment/Recommendations

Treatment is indicated only if the patient is symptomatic.

Soft Tissue Abnormalities

Internal Derangements

Internal derangement is a general orthopedic term implying a mechanical fault that interferes with the smooth action of a joint. Internal derangement is thus a functional diagnosis. For the temporomandibular joint, the most common internal derangement is disc displacement. This is most often the disc displaced anteriorly, anterolaterally, or anteromedially. When this occurs, the posterior band of the disc prolapses anteriorly rather than remaining in its normal position between the condylar head and mandibular fossa. This results in positioning of the condyle beneath the posterior disc attachment rather than under the disc causing the condyle to close on the posterior attachment (retrodiscal tissues) rather than upon the disc itself.

Medial or lateral displacements of the disc are also relatively common. Posterior disc displacement also occurs but rarely. When posterior disc displacement occurs, it is seen in conjunction with medial disc displacement. Pure lateral and medial disc displacements do occur but not as commonly as those in conjunction with anterior disc displacements.

Functionally, disc displacements occur with and without reduction. In disc displacement with reduction, the disc is anteriorly displaced in the closed-mouth position but reverts to a normal superior position during opening. In disc displacement without reduction, the disc lies anterior to the condyle during all mandibular movements and the normal condyle-disc relationship is not resumed.

Summary of internal derangement:

- There is an abnormality in position and morphology of the articular disc, which may interfere with normal function of the joint.
- Most often the displacement is to the anterior, however, the disc can also be displaced medially and laterally.

- Causes of disc displacement include parafunctional habits, jaw injuries, whiplash injury, or forced opening beyond the normal range of movement.
- A "reducing" disc resumes its normal position relative to the position of the condyle; a click is present.
- A "nonreducing" disc refers to a disc that remains displaced throughout the entire range of mandibular movement and may lead to a closed or open lock. The condyle and disc are never together in their "normal" and desired relationship.
- Internal derangements may be symptomatic or asymptomatic.

The disc may become deformed, thickened, fibrotic, or perforated.

Remodeling and Arthritis

Remodeling

Definition/Clinical Characteristics/Radiographic Description

Remodeling occurs due to adaptive response to excessive forces applied to the joint. Alterations in the shape of the condyle and articular eminence include flattening, cortical thickening, subchondral sclerosis or abnormal appearance (only if pain and/or dysfunction present or severe radiographic changes are seen). It may be unilateral and is not invariably a precursor to degenerative joint disease.

Differential Interpretation

Differential interpretation includes early degenerative joint disease with erosions, osteophytes, and loss of joint space.

Treatment/Recommendations

There is no treatment necessary. An occlusal splint may be considered.

Degenerative Joint Disease (DJD), Osteoarthritis

Definition/Clinical Characteristics

When the ability of the joint to adapt to excessive forces is exceeded, breakdown occurs. Etiology includes acute trauma, hypermobility of the joint, parafunction and/or internal disc derangement. This is not an inflammatory condition, so "osteoarthritis" is a misnomer. It is more commonly seen in females than males. Deterioration includes the loss of articular cartilage and bone erosion. Proliferation includes cortical thickening, osteophyte formation, sclerosis of the articular surface, and subchondral sclerosis.

Radiographic Description

Radiographically degenerative joint disease presents with flattening, subchondral sclerosis, loss of cortex/surface erosion, Ely cyst/subchondral cyst formation, osteophyte, which can form loose joint bodies known as joint mice. There is reduced joint space and long-term nonreducing disc displacement, which can lead to DJD. Anterior

open bite can occur if the condyle is resorbed and articular surface of temporal bone is also resorbed (Figures 8.11–8.14).

Differential Interpretation

Differential interpretation is broken into two categories: erosive and proliferative. Radiographic erosive differential includes rheumatoid arthritis with severe erosion. Radiographic proliferative differential includes osteochondroma and osteoma.

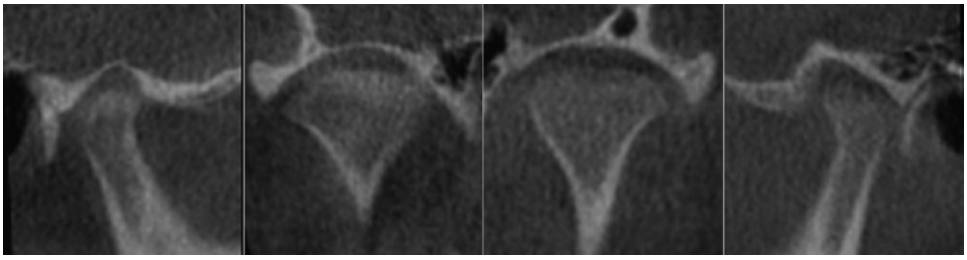

Figure 8.11. Sagittal and coronal slices showing normal condylar morphology.

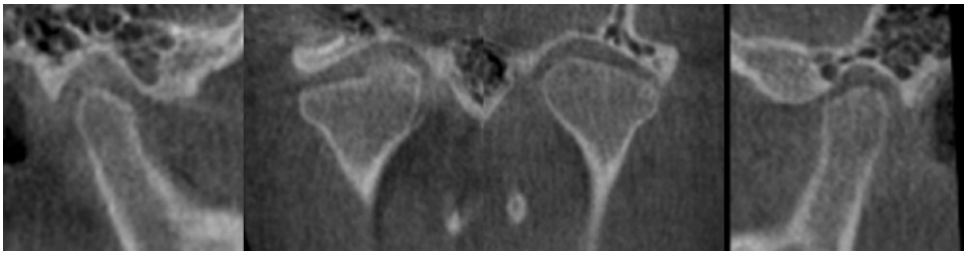

Figure 8.12. Sagittal and coronal slices showing moderate degenerative joint disease.

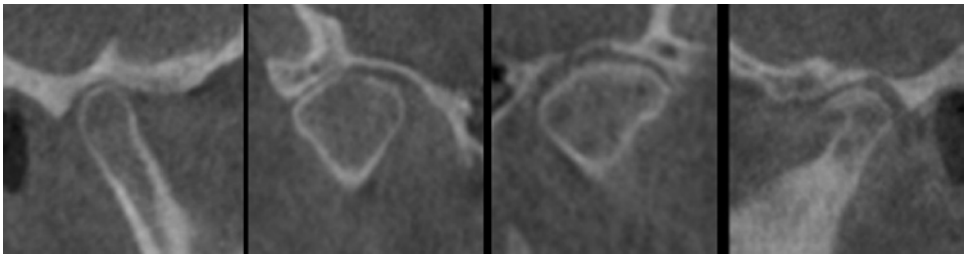

Figure 8.13. Sagittal and coronal slices showing moderate degenerative joint disease of the left condyle.

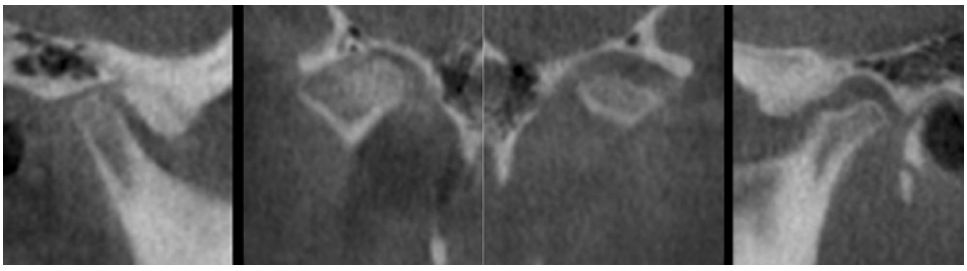

Figure 8.14. Sagittal and coronal slices showing moderate to severe degenerative joint disease.

Treatment/Recommendations

Treatment is a variety of things including splint therapy, anti-inflammatory drugs, and/or physiotherapy.

Osteoarthrosis (Degenerative Arthritis)

Definition/Clinical Characteristics

Osteoarthritis or degenerative arthritis is an age-related disorder that is more frequent in females than in males. The ratio of females to males with this degenerative condition is approximately 7:1. The progression and severity of osseous changes in the condylar head and mandibular fossa tend to increase with age. Patients with osteoarthritis affecting the TMJ usually complain of pain or tenderness in the joint and masticatory muscles, reduced range of motion or deviating jaw function, and crepitus during mandibular movements. CBCT is a valuable imaging modality for the diagnosis of degenerative changes in the osseous components of the TMJ.

Radiographic Description

The most common radiographic findings in early osteoarthritic changes include flattening of the condyle, irregular cortical outlines, cortical bone erosions and subchondral cyst formation, osteophyte formation, reduced joint space, and bony contact with mouth open. In moderate or severe osteoarthritis, osseous changes include extensive osteophyte formation, subcortical cyst formation, resorption of the condylar head or mandibular fossa, absence of joint space, or bony contact and sclerosis of both the condyle and mandibular fossa. Sclerosis is a less-frequent radiographic finding, but it develops secondarily in the more progressive forms of the disease and in older age groups (Figures 8.15–8.17).

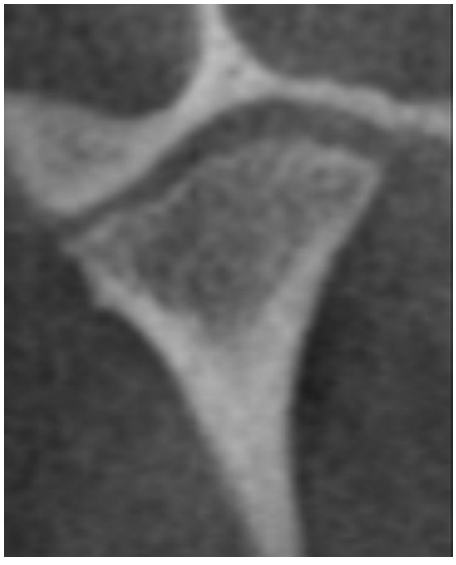

Figure 8.15. Coronal slice showing flattening of the condyle.

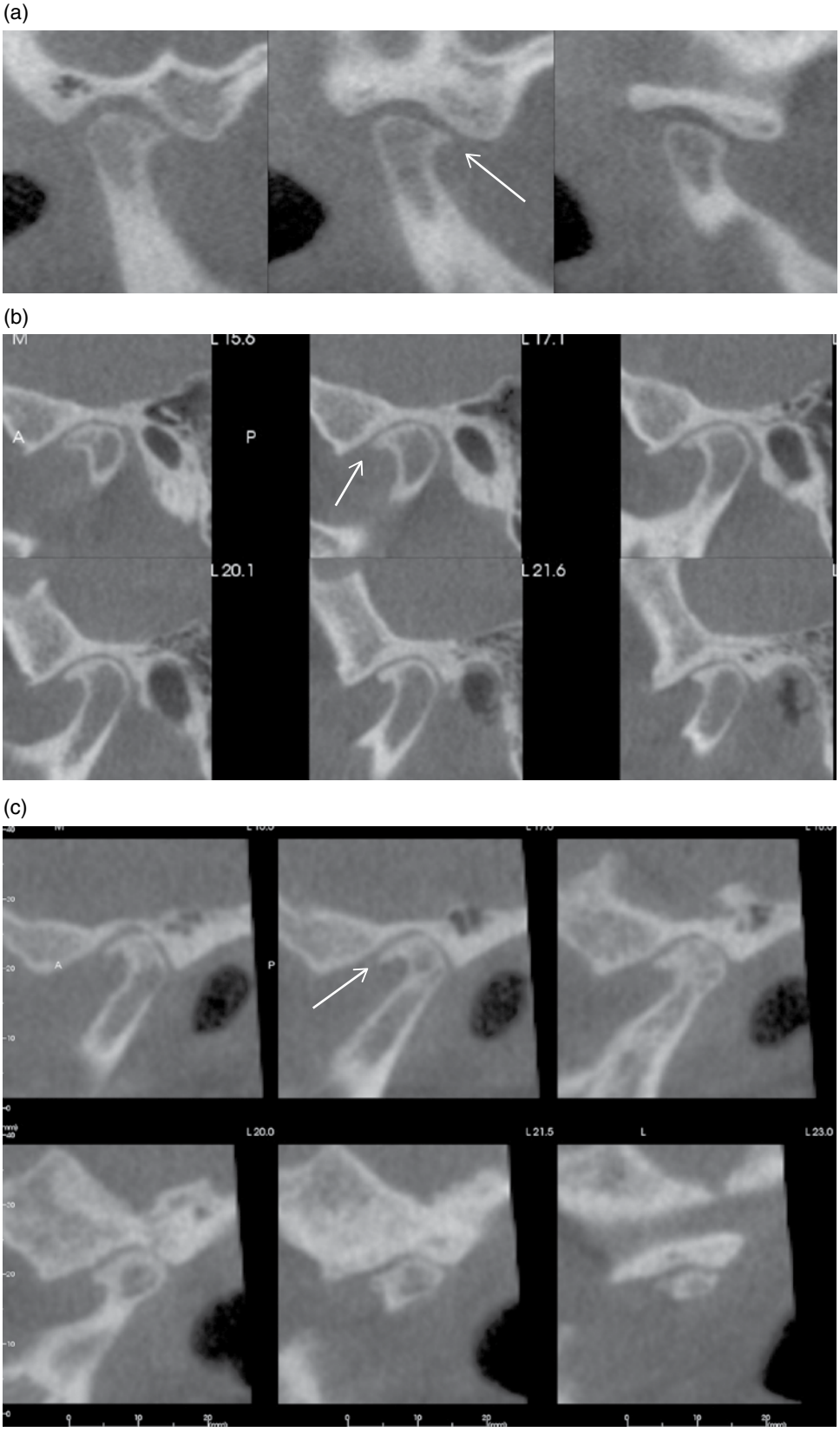

Figure 8.16. Cross-sectional slices (a,b,c) showing anterior osteophyte formation (white arrow).

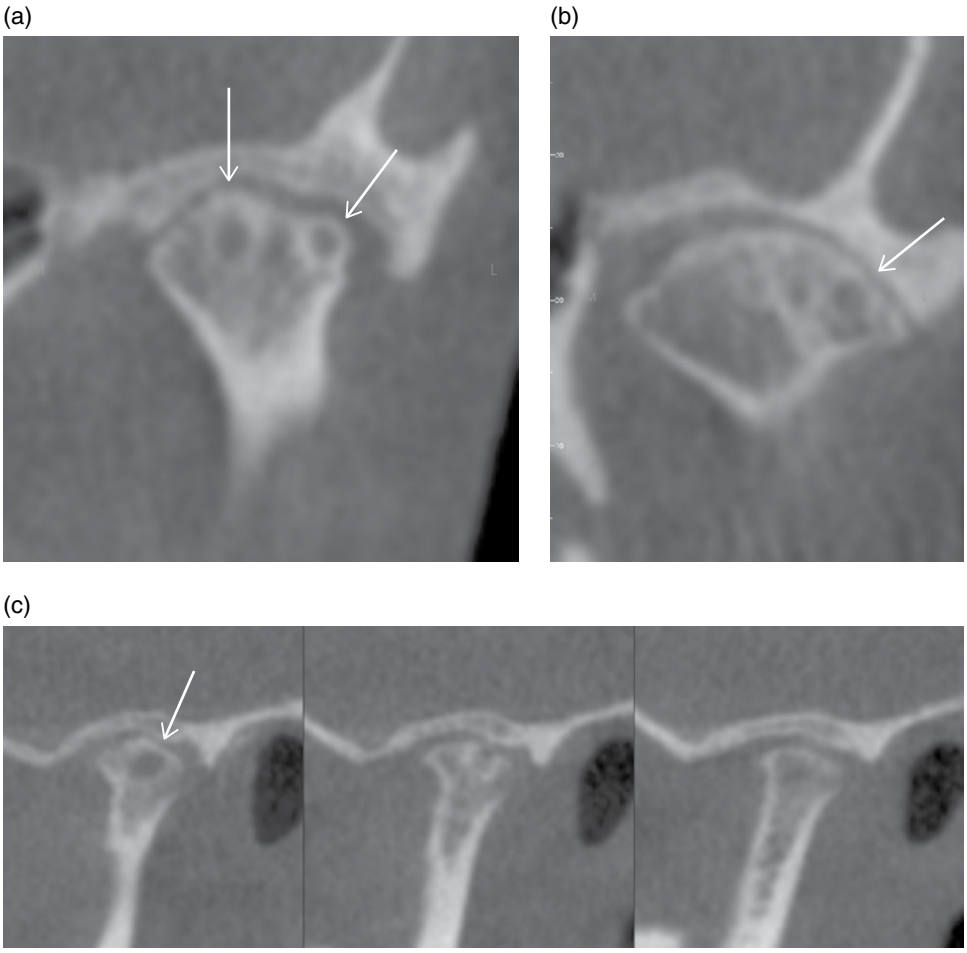

Figure 8.17. Coronal slices (a,b) showing subchondral cyst formation (white arrows); (c) Cross-sectional slices showing subchondral cyst formation (white arrows).

Rheumatoid Arthritis

Definition/Clinical Characteristics

Rheumatoid arthritis is the most common chronic inflammatory disease of unknown etiology and is classified as one of the collagen-vascular (autoimmune) diseases. It primarily affects the periarticularstructures, such as the synovial membrane capsule, tendon sheaths, and ligaments. Rheumatoid arthritis affects mostly women, with a female to male ratio of 3:1 and a peak onset in patients between 40 to 60 years of age. Patients with rheumatoid arthritis usually complain of bitemporal headache, dull pain worsening with function, and a limitation of condylar movement. An anterior open bite secondary to condylar changes can occur. The clinical examination may reveal pain on palpation, crepitus, and hypomobility. In the early stages, small peripheral joints of the hands and feet are affected first. Clinical and radiologic examinations reveal involvement of the TMJ in about 70% of patients with rheumatoid arthritis. It is also seen in the knees, hands and other joints. In late stages of the disease, ankylosis may develop.

Radiographic Description

The most common radiographic findings in the condylar head and mandibular fossa are flattening, erosions, resorption, and sclerosis. In many cases, the joint space may be reduced. In late stages of the disease, radiographic examination may reveal osteophyte formation on the condylar head, a sharp pointed condyle, and posterior ramus shortened in length causing premature posterior occlusion and anterior open bite. Radiographic findings in patients with rheumatoid arthritis are similarto those in patients with osteoarthritis. However, reduced joint space and osteophyte formation are more common in patients with osteoarthritis, whereas erosions and resorption of the condylar head are more frequently found in patients with rheumatoid arthritis (Figures 8.18 and 8.19).

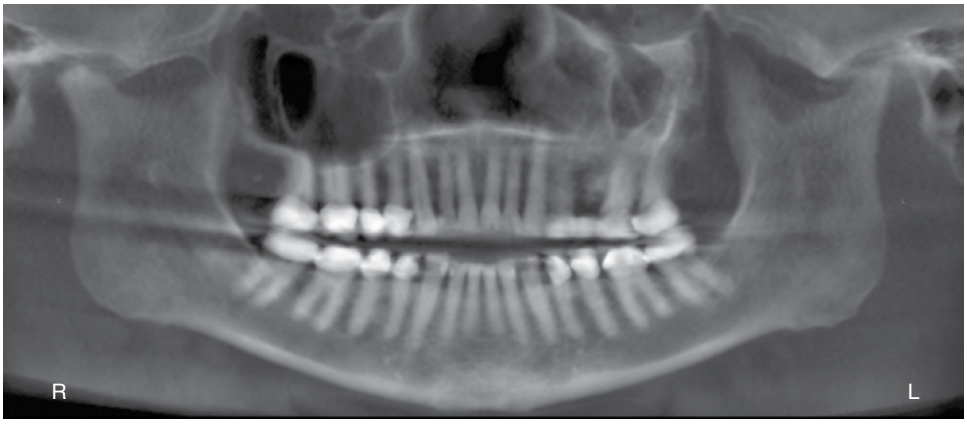

Figure 8.18. Reconstructed pantomograph of patient with rheumatoid arthritis. Note the severe flattening and loss of condylar height bilaterally.

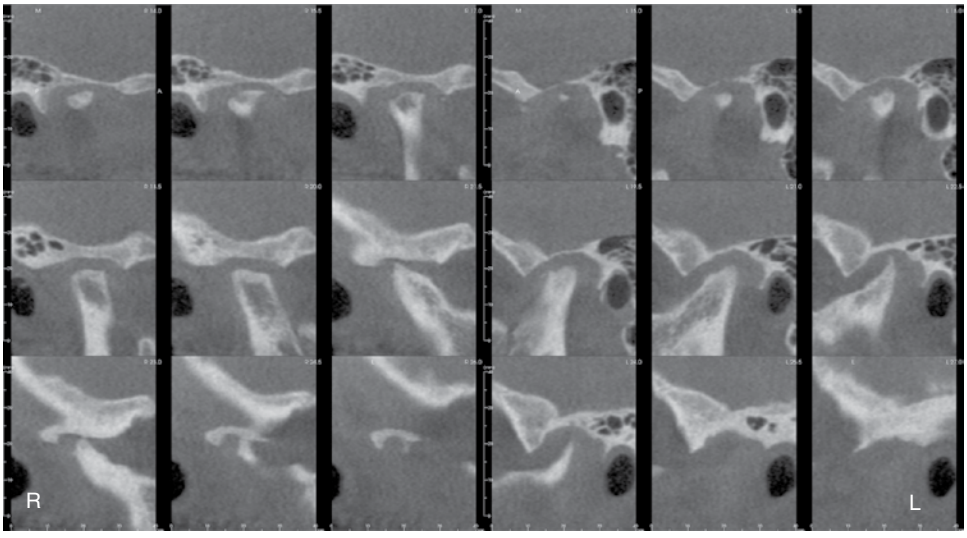

Figure 8.19. Cross-sectional slices showing severe bony destruction of the right and left condyles.

Differential Interpretation

Differential interpretation includes severe DJD and psoriatic arthritis. Psoriatic arthritis patients will have a history of skin lesions, osteopenia and severe erosions of articular eminence which are more characteristic of rheumatoid arthritis.

Treatment/Recommendations

Treatment options include analgesics, NSAIDS, corticosteroids, physiotherapy and/or joint replacement surgery.

Juvenile Arthritis (Juvenile Rheumatoid Arthritis/Juvenile Chronic Arthritis/Still's Disease)

Definition/Clinical Characteristics

Juvenile arthritis is a chronic inflammatory disease typically found in patients less than 16 years of age with a mean age 5 years of age. It presents with synovial hypertrophy; joint effusion; and swollen, painful joints. There is cartilage and bone destruction. Rheumatoid factor may be present. Involvement of the temporomandibular joint occurs in approximately 40% of all cases. It may be either unilateral or bilateral. Clinical characteristics include micrognathia, which is seen in young with less development of mandible, a "bird face," and anterior open bite.

Radiographic Description

Radiographic findings include osteopenia and impaired mandibular growth. Changes in the temporomandibular joints include erosions, "pencil-shaped" small condyle, flattening, fibrous ankylosis, secondary degenerative changes, abnormal disc shape, and deepening of the antegonial notch. The ramus may present with diminished height, dorsal bending, or obtuse angle of ramus relative to body of mandible (Figures 8.20 and 8.21).

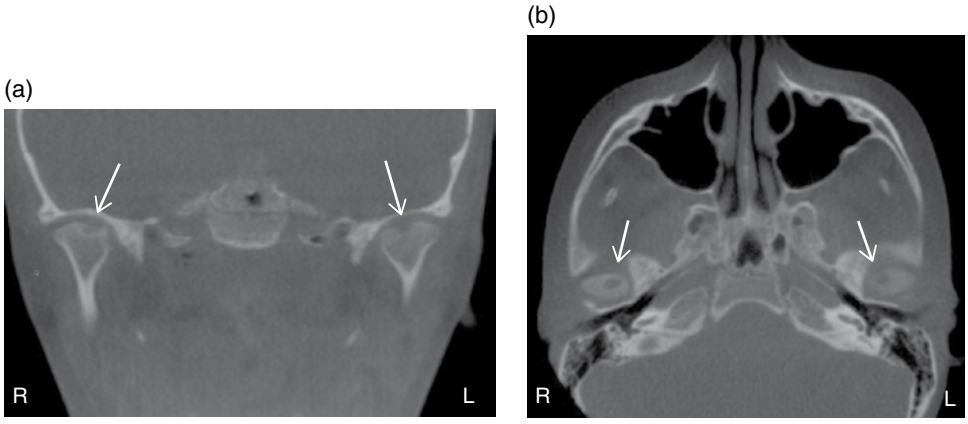

Figure 8.20. (a) Coronal and (b) axial slices showing erosions on the superior aspect of the right and left condyles in a patient with juvenile arthritis (white arrows).

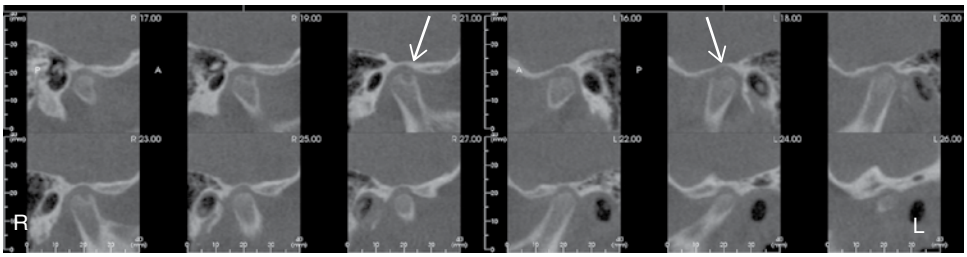

Figure 8.21. Cross-sectional slices showing erosions of the right and left condyles (white arrows).

Psoriatic Arthritis

Definition/Clinical Characteristics/Radiographic Description

Psoriatic arthritis has skin lesions present. The temporomandibular joints are associated in 7% of all cases. These patients are seronegative so no rheumatoid factor is present and it is indistinguishable from rheumatoid arthritis on radiographs. Occasionally, profound sclerotic changes are evident.

Septic Arthritis

Definition/Clinical Characteristics

Septic arthritis is a rare infection and inflammation of joint. The infection can spread from either the parotid, otic, mastoid, osteomyelitis from mandibular body/ramus, middle ear infection or hematogenous spread from distant nidus. It is more commonly seen in people with rheumatoid arthritis, diabetes, and/or immunosuppression. Children may present with septic arthritis after blunt trauma with hematoma formation, which is adequate for microorganism growth. It is typically unilateral with the mandible deviated to unaffected side due to joint effusion.

Radiographic Description

Radiographically the joint space may be widened with erosion and thinning of the cortex. Other radiographic findings include osteopenia, sequestra formation, periosteal reaction, and osseous ankylosis. Inhibited mandibular growth can take place if it occurs in a young person.

Differential Interpretation

Differential interpretation includes degenerative joint disease and rheumatoid arthritis. Diagnosis can be made via joint aspirate and is typically unilateral with clinical signs and symptoms of infection. Other inflammatory changes in adjacent areas seen include the mastoid air cells, mandibular ramus, and parotid. On MRI T2 weighted image joint effusion, abscess, and muscle enlargement may be seen. Scintigraphy with Technetium 99 shows increased bone metabolism and Gallium shows signs of infection.

Synovial Chondromatosis (Synovial Chondrometaplasia, Osteochondromatosis)

Definition/Clinical Characteristics

Synovial chondromatosis is a rare benign condition that mainly affects the superior joint space, although it can involve the inferior joint space when a perforated or a deformed disc is present. It is characterized by the formation of fragments of cartilage and loose bodies in the synovial membrane of the affected joint. Synovial chondromatosis is more frequent in females than males, with a predilection ratio of 4:1, respectively. Clinical symptoms of synovial chondromatosis are not pathognomic and usually include joint swelling, pain, intracapsular sounds (clicking, crepitus, or both), and a limitation of joint movement.

Radiographic Description

The most common CBCT findings in patients with TMJ synovial chondromatosis include the presence of multiple, loose, calcified nodules in the joint space, sclerosis of the mandibular fossa and the condylar head, irregularity of the osseous cortical surface, and often widening of the joint space. Usually the condyle exhibits osseous changes similar to those seen in osteoarthritis patients. Loose calcified nodules in CBCT images can appear as multiple articular radiopacities of varying sizes and shapes. In many cases, temporal bone sclerosis and extension of the lesion into the intracranial fossa, infratemporal fossa, or lateral pterygoid muscle are seen.

Differential Interpretation

Differential interpretation includes chondrocalcinosis, synovial chondromatosis, degenerative joint disease with joint mice, and chondro/osteosarcoma. Chondrocalcinosis presents with larger nodules and peripheral cortex than synovial chondromatosis. Synovial chondromatosis has larger loose bodies. Chondro/osteosarcoma present with severe bone destruction.

Treatment

Treatment includes removal of the loose bodies and removal of abnormal synovial tissue.

Chondrocalcinosis (Pseudogout, Calcium Pyrophosphate Dihydrate Deposition Disease)

Definition/Clinical Characteristics

Chondrocalcinosis is an acute or chronic synovitis with precipitation of calcium pyrophosphate dehydrate crystals in joint space. It is uncommon in the temporomandibular joint and usually involves other joints. It is more commonly unilateral and more common in males than females.

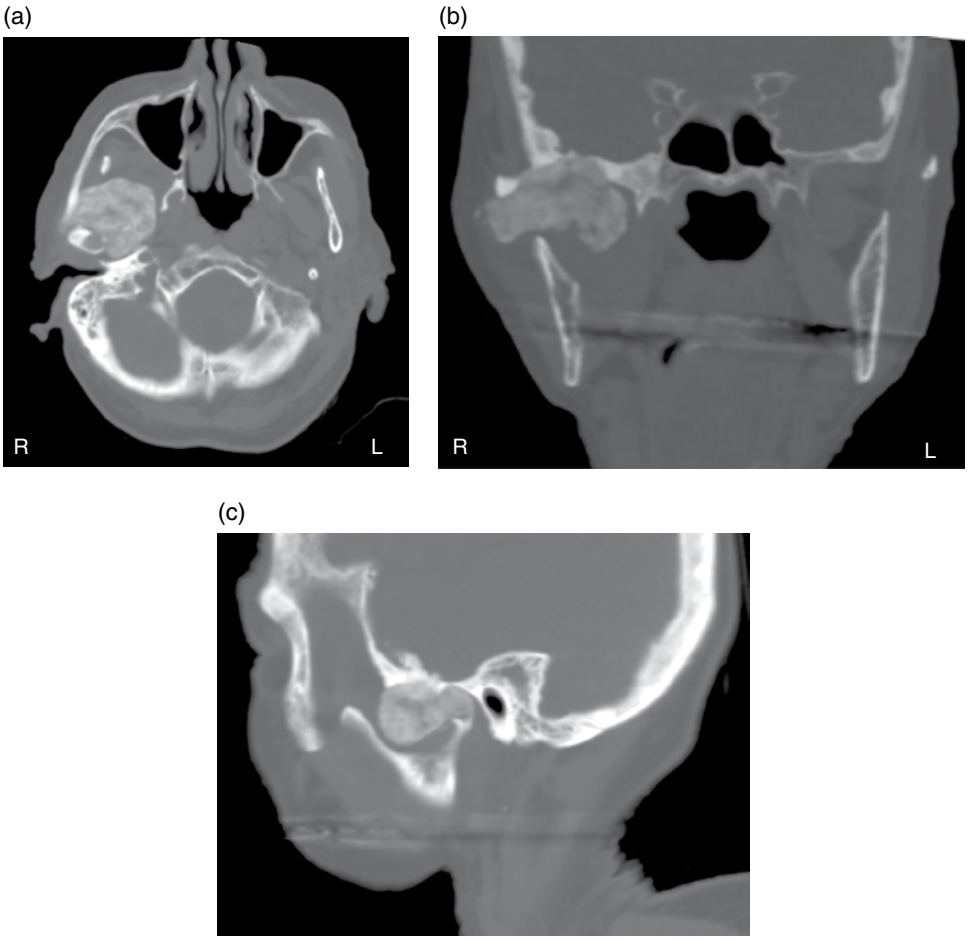

Figure 8.22. (a) Axial, (b) coronal, and (c) sagittal slices showing increased radiopacity of the right condyle in a patient with pseudogout.

Radiographic Description

It appears as fine radiopacities with even distribution in joint space as compared to synovial chondromatosis. Bone erosions with severe increase in condylar bone density and swelling and edema of muscles may be present (Figure 8.22).

Differential Interpretation

Differential interpretation includes synovial chondromatosis, degenerative joint disease with joint mice, and chondro/osteosarcoma.

Treatment

Treatment options include surgical removal of deposits, steroids, aspirin, NSAIDS, and colchicine.

Trauma

Effusion

Definition/Clinical Characteristics

Effusion is influx of fluid into a joint. It may be either trauma from hemorrhage or inflammation from exudate. Causes include internal derangement, traumatic injuries, arthritis, and rheumatic diseases. Clinical findings include swelling, pain, limited motion, hearing difficulties, and difficulty occluding posterior teeth because of fluid in the joint.

Radiographic Description

T2 weighted MRI shows internal derangement with normal joints and high signal (hyperintense signal).

Differential Interpretation

Septic arthritis with signs and symptoms of infection present in septic arthritis.

Treatment

Treatment options include anti-inflammatories and surgical drainage occasionally.

Dislocation

Definition/Clinical Characteristics

The condyle may present outside the mandibular fossa but inside the capsule. It occurs bilaterally and is most commonly displaced anteriorly. It may be associated with condylar fracture. Clinical findings include inability to close the mouth with pain and/or muscle spasms. It is possible to reduce the mandible by manipulation.

Radiographic Description

The condyles are located anterior and superior to the summit of articular eminence (clinical information is important, because it could be normal range of motion for that specific patient).

Differential Interpretation

Fracture dislocations.

Treatment

Treatment is typically manual manipulation and surgery for fractures.

Fracture

Definition/Clinical Characteristics

The consequences of traumatic injury to the condyle depend on its location. Condylar fractures may be intracapsular or extracapsular. Extracapsular fractures are (subsequently) classified into high, medium, or low with regard to their position. These fractures can be displaced, nondisplaced, or dislocated, and depending on the direction of the fracture, they can be horizontal, vertical, or sagittal. If the fracture is located in the condylar neck, the condylar head often becomes dislocated. CBCT is a useful diagnostic tool for the diagnosis of TMJ fracture.

Radiographic Description

A cortical outline irregularity can be (or is usually) depicted and, in case of a condylar neck fracture, the condylar head is usually dislocated in a forward-medial direction. The most common location is the condylar neck with dislocation of condylar head. Unilateral is more common and may be accompanied by parasymphyseal or body fracture on the opposite side. It can lead to growth inhibition in a young person. For those less than 10 years, there is a high remodeling potential and less deformity than older patients. For those less than 3 years, severe asymmetries are possible. Other radiographic findings include ankylosis, radiolucent or radiopaque lines, step defects, condylar head fracture with vertical or compressive patterns. Remodeling typically shows as flattening, degenerative joint disease. Hemarthrosis may present with blood in the joint.

Differential Interpretation

Differential interpretation includes developmental abnormalities. A Towne's view shows medial displacement of condyle.

Treatment

No treatment is necessary if adequate mandibular movement is present.

Neonatal Fractures

Forceps injury during delivery may lead to fracture of condyle(s). Clinically, this presents as severe mandibular hypoplasia, lack of development of the glenoid fossa and eminence with "partly opened pair of scissors" appearance due to overlapping of fracture fragments. Differential includes developmental hypoplasia. Treatment includes orthodontics and orthognathic surgery for mandibular asymmetry.

Ankylosis

Definition/Clinical Characteristics

True ankylosis is in the joint and may be either fibrous or bony. False ankylosis is unrelated to the joint and examples include: muscle spasm, myositis ossificans, or coronoid process hyperplasia. If it is unilateral, possible causes include trauma or

infection. Common causes for bilateral ankylosis include rheumatoid arthritis. If present during infancy, it is likely due to a birth injury caused by forceps.

Radiographic Description

Fibrous ankylosis presents as irregular erosions on articular surfaces with a narrowed joint space and jigsaw puzzle appearance. Bony ankylosis presents as small or large osseous bridges/large bony masses. Other radiographic findings include degenerative changes, coronoid hyperplasia, and deepening of antegonial notch because of the pull of muscles when opening the mouth.

Differential Interpretation

Differential interpretation includes condylar tumor. With a history of trauma, infection, or other joint diseases, should consider ankylosis.

Treatment

Treatment includes surgical removal of osseous bridge or bony mass.

Tumors

Benign Tumors

Definition/Clinical Characteristics

Osteochondroma or osteocartilaginous exostosis is the most common benign tumor of the TMJ and is most commonly seen in the second or third decade of life. It usually affects the condyle and is defined as an exophytic bone mass emanating from the cortex, which may cause limited mouth opening and jaw deviation to the contralateral side. Most frequently, patients with condylar osteochondroma develop facial asymmetry and/or malocclusion. In radiographic examinations, osteochondroma is depicted as a tapering radiopaque mass usually extending from the anteromedial aspect of the condyle along the tendon of the lateral pterygoid. CBCT findings show an enlarged condyle with irregular outline or an abnormal pedunculated mass attached to the condyle.

Benign neoplasms seen in the temporomandibular joints include: osteochondroma, osteoma, osteoblastoma, chondroblastoma, fibromyxoma, giant cell lesions, aneurysmal bone cysts, and Langerhans cell histiocytosis, which is considered benign in White and Pharoah (2004).

Radiographic Description

There is a range of radiographic findings including condylar enlargement, irregular in shape, altered trabecular pattern, radiolucency/radiopacity, or abnormal pedunculated mass.

Differential Interpretation

Unilateral condylar hyperplasia.

Treatment

Surgical excision.

Malignant Tumors

Malignant tumors of the TMJ are very rare lesions. The majority of reported cases in the literature include osteosarcomas, chondrosarcomas, and metastatic tumors. Osteosarcoma and chondrosarcoma are malignancies with a slight male predilection and are characterized by the formation of neoplastic bone or cartilage by the tumor cells. The most common clinical findings are pain, swelling in the preauricular region, and a reduced range of joint motion. Metastasis from a distant site may occur in the TMJ region, but the clinical signs and symptoms usually resemble those of common temporomandibular disorders and most often include unilateral facial swelling, a limitation of mandibular mobility, pain, and mandibular deviation. In patients who do not respond to treatment, the clinician should reconsider the initial diagnosis and include in the differential diagnosis the possibility of a malignant lesion. CBCT is very important in the diagnosis of malignancies. Malignant tumors are characterized by bone destruction with poorly defined borders and irregular margins, erosion of the cortical plates, and minimal expansion. Pathologic calcifications and condylar deformity may be detected. In case of suspected malignancy, CBCT examination should be followed up with other imaging modalities, such as MRI, CT, nuclear scan, or positron emission tomography.

Malignant neoplasms seen in the temporomandibular joints include: primary malignancy or metastasis, chondrosarcoma, osteosarcoma, synovial sarcoma, and fibrosarcoma. Parotid salivary gland malignancies, rhabdomyosarcoma, and regional carcinomas may extend into the TM joint. Metastatic lesions are most common from the breast, kidney, lung, colon, prostate, and/or thyroid. Bone destruction presents as ill-defined and irregular in shape. Chondrosarcoma presents as discrete soft-tissue calcifications with destruction.

Differential Interpretation

Differential interpretation includes severe degenerative joint disease but will have more peripheral bone destruction, osteophyte(s), and no soft-tissue swelling or mass. Sarcoma and other tumors have more central destruction of bone.

Treatment

Treatment includes wide surgical removal. For metastatic lesions, treatment options include palliative, radiation, and chemotherapy, if indicated.

References

Isberg, A. (2001). *Temporomandibular Joint Dysfunction, A Practitioner's Guide*, ISIS Medical Media.

Larheim, T. A., and Westesson, P. L. (2006). *Maxillofacial Imaging*. Springer, New York, NY.

Som, P. M., and Curtin, H. D. (2003). *Head and Neck Imaging, Volume One*. Mosby, St. Louis, MO, pp. 995–1050.

White, S., and Pharoah, M. (2004). *Oral Radiology, Principles and Interpretation*, Mosby, St. Louis, MO, Chapter 25.

9 Implants

Shawneen M. Gonzalez

Introduction

This chapter covers aspects regarding implant placement including accuracy of measurements, Hounsfield units, and mandibular nerve tracing. This chapter will not go into depth about stent construction or different software applications capable of this.

Imaging for Implant Purposes

American Academy of Oral and Maxillofacial Radiology (AAOMR) Recommendations

In 2000, the AAOMR recommended conventional CT to create cross-sectional slices for implants. Since this original statement, CBCT availability has increased. The AAOMR published a position statement on implants imaging specifically regarding CBCT use in June of 2012 with 11 primary recommendations.

Initial Examination

Recommendation 1

Panoramic radiography should be used as the imaging modality of choice in the initial evaluation of the dental implant patient.

Interpretation Basics of Cone Beam Computed Tomography, First Edition.
Edited by Shawneen M. Gonzalez.

Pantomographs or panoramic radiograph units show information about both the maxilla and mandible and associated structures that may create issues with implant placement such as the mandibular nerve and maxillary sinuses. Accuracy of measurements on pantomographs is not always reliable as there are many factors that may distort the final image. One of the most common factors is patient positioning. Measurements are able to be made only in an inferior-superior aspect and not facial-lingual width of the ridge.

Recommendation 2

Use intraoral periapical radiography to supplement the preliminary information from panoramic radiography.

Periapical radiographs have a high spatial resolution showing minute detail. Again, as with pantomographs, error in positioning of the image receptor can create distortion in the final image making accurate measurements not possible.

Recommendation 3

Do not use cross-sectional imaging, including CBCT, as an initial diagnostic imaging examination.

CBCT imaging should be recommended only after an initial evaluation; using CBCT as an initial diagnostic tool is in violation of recommendations from the AAOMR, ADA, and EADMFR (see Chapter 2).

Pre-operative Site-Specific Imaging

Recommendation 4

The radiographic examination of any potential implant site should include cross-sectional imaging orthogonal to the site of interest.

This recommendation is consistent with the AAOMR's stance in 2000. This allows for visualization of ridge morphology and bone quality in the area of the proposed implant(s) placement.

Recommendation 5

CBCT should be considered as the imaging modality of choice for pre-operative cross-sectional imaging of potential implant sites.

The use of CBCT is lower radiation dose compared to traditional CT.

Recommendation 6

CBCT should be considered when clinical conditions indicate a need for augmentation procedures or site development before placement of dental implants.

This includes areas of possible bone grafts including a possible maxillary sinus lift with graft placement.

Recommendation 7

CBCT imaging should be considered if bone reconstruction and augmentation procedures have been performed.

This is to evaluate bone graft uptake for adequate bone prior to implant placement.

Post-operative imaging

Recommendation 8

In the absence of clinical signs or symptoms, use intraoral periapical radiography for the postoperative assessment of implants. Panoramic radiographs may be indicated for more extensive implant therapy cases.

Radiographs are used to assess the bone-implant interface and whether the implant shows adequate osseointegration over time. CBCT images are not recommended due to streak artifacts created by the metal implant obscuring the implant-bone interface.

Recommendation 9

Use cross-sectional imaging immediately postoperatively only if the patient presents with implant mobility or altered sensation, especially if the fixture is in the posterior mandible.

The immediate CBCT use is to evaluate whether there has been nerve involvement especially in the posterior mandible.

Recommendation 10

Do not use CBCT imaging for periodic review of clinically asymptomatic implants.

The routine use of CBCT is not recommended and violates recommendations by the EADMFR (see Chapter 2).

Recommendation 11

Cross-sectional imaging should be considered if implant retrieval is anticipated.

CBCT imaging is recommended to aid the surgeon in removal with the least amount of trauma to the surrounding structures.

Linear Measurement Accuracy

The accuracy of linear and volumetric measurements with CBCT is very important prior to implant placement to ensure preventing damage to adjacent vital structures such as the mandibular nerve canal and/or maxillary sinuses. Linear measurements using dry skulls without soft tissue and with soft tissue were shown to have no statistical difference in measurements made on both the skulls and CBCT scan (Figure 9.1). Varying voxel size from 0.2 mm to 0.4 mm showed no statistical difference in linear measurements of width and height of dry skulls. This allows a practitioner to use a larger voxel size for implant placement creating a reduction in radiation exposure to the patient.

(a)

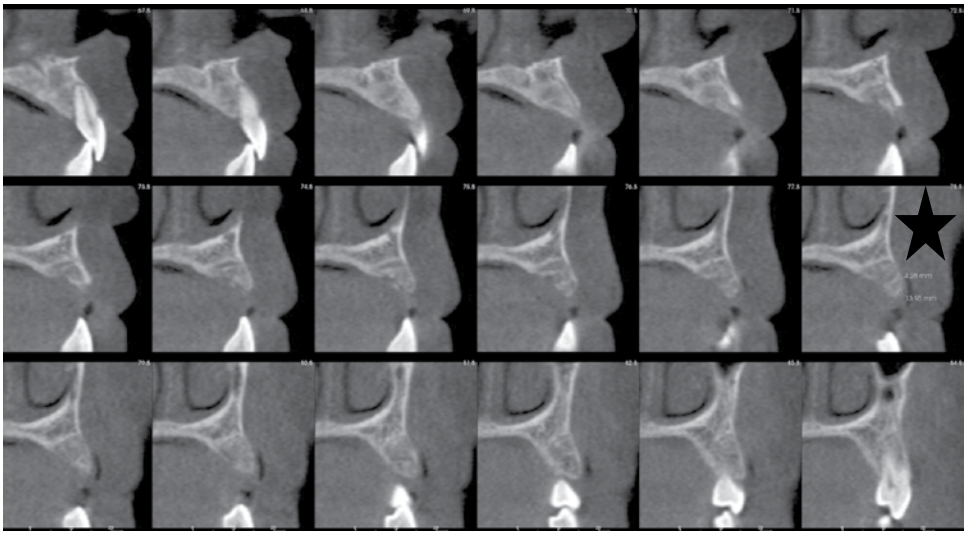

(b)

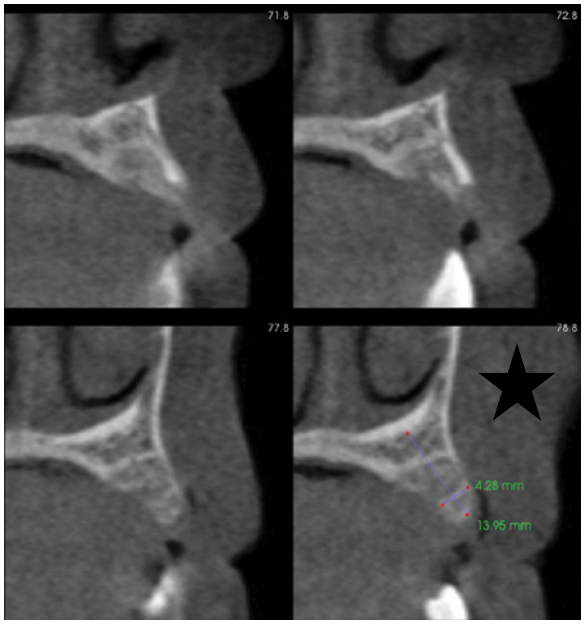

Figure 9.1. (a) Cross-sectional slices through anterior maxilla with 1.0 mm spacing between each slice and measurements (black star); (b) Close-up of cross-sectional slices with measurements (black star).

Grey Values and Hounsfield Units

A Hounsfield unit (HU) is "the numeric information contained in each pixel of a CT image. It is related to the composition and nature of the tissue imaged and is used to represent the density of tissue" (Medical Dictionary). Hounsfield units have a wide

Table 9.1. Hounsfield units for various tissues frequently captured on a CBCT scan.

Tissue	Hounsfield unit
Air	–1000
Fat	–100
Water	0
Bone	1000

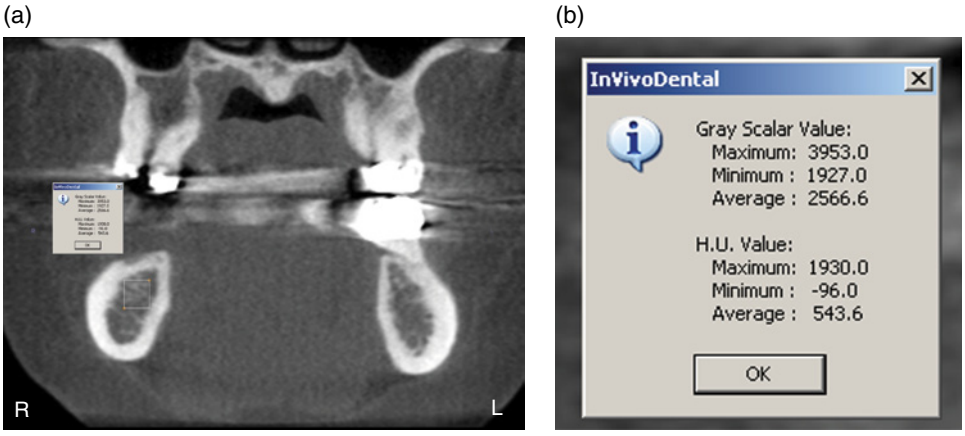

Figure 9.2. (a) Coronal view showing sample bone area of bone selected (white box) for Hounsfield unit calculation using InVivo software; (b) Close-up of grey levels and Hounsfield units for selected bone using InVivo software.

range from –1000 to +1000 (Table 9.1). Bone will present with a HU of +400 and increase as it becomes denser such as cortical bone. CBCT imaging is primarily a hard-tissue imaging modality, whereas traditional CT imaging is both hard-tissue and soft-tissue imaging modalities. Various grey levels are still seen on scans of various soft tissues. Hounsfield units used in CBCT imaging are actually grey values used with linear attenuation coefficients (Figure 9.2). Studies have shown strong correlation between grey levels and Hounsfield units. Accuracy of these Hounsfield units has varied showing differences due to patient positioning, patient size, and image artifacts. When used for implant placement, the Hounsfield units should be used as a general idea of bone density and not exact units.

Mandibular Canal

The location of the mandibular canal and anterior extension of the mandibular canal (sometimes referred to as mandibular incisive canal) are important when placing implants in the mandible. On pantomographs, the anterior extension of

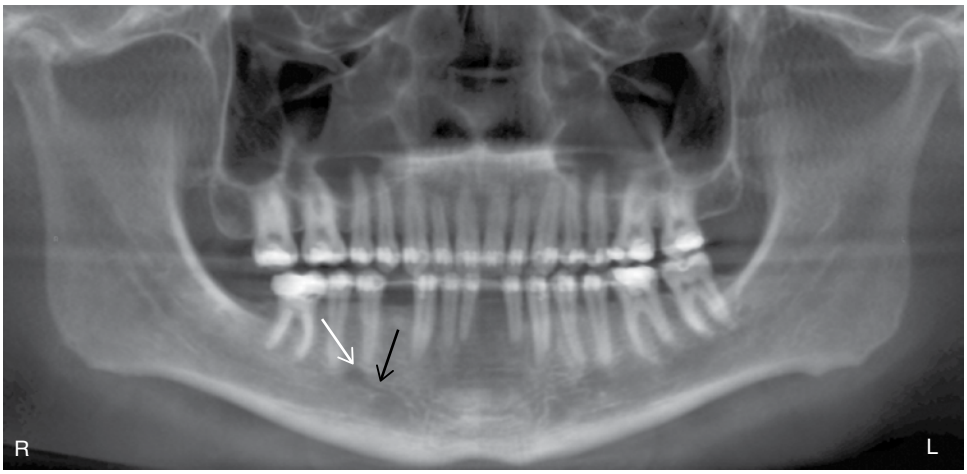

Figure 9.3. Reconstructed pantomograph from a CBCT scan showing the anterior extension of the mandibular canal (black arrow) inferiorly and anteriorly from the mental foramen (white arrow) as a thin radiolucent line.

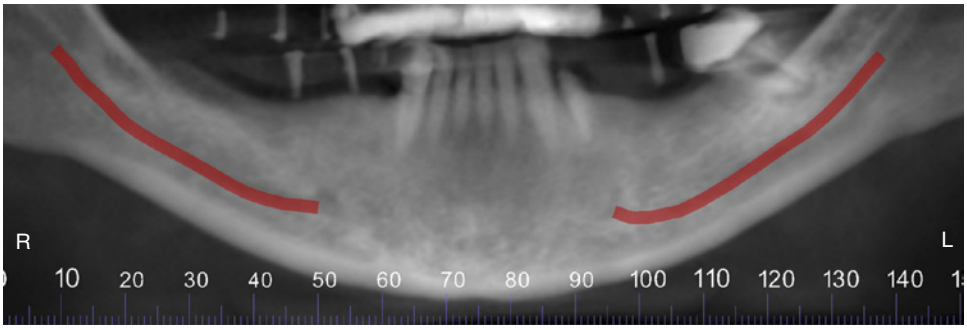

Figure 9.4. Reconstructed pantomograph from a CBCT scan showing right and left mandibular canal noted in red.

the mandibular canal is visible in up to approximately 51.7% of patients. On CBCT scans, the mandibular canal is clearly visible on approximately 53%–87.9% of all patients (Figures 9.3–9.5). When identifying the mandibular canal, cross-sectional slices, axial views, and sagittal views (Figure 9.6) are commonly used. Acquiring a CBCT does not guarantee that a difficult to view mandibular canal will be evident.

Virtual Implant Placement Software

There are several different software options regarding virtual implant placement. Due to the wide scope of different programs, this chapter will merely show examples of what those virtual implants look like in the CBCT software and cross-sectional views (Figure 9.7). For more information on specific software options, it is recommended to contact the company directly.

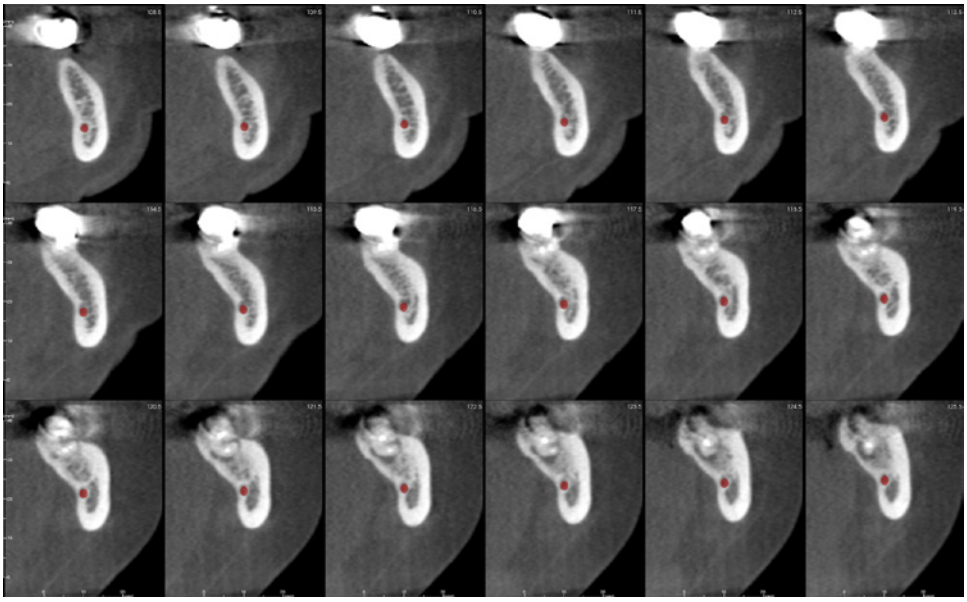

Figure 9.5. Cross-sectional views showing mandibular canal noted with red circles.

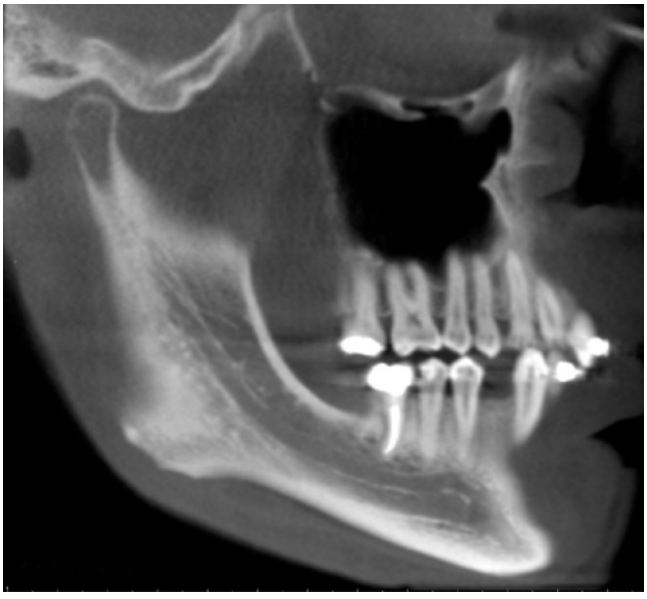

Figure 9.6. Rotated sagittal view showing mandibular canal as radiolucent band with thin radiopaque borders.

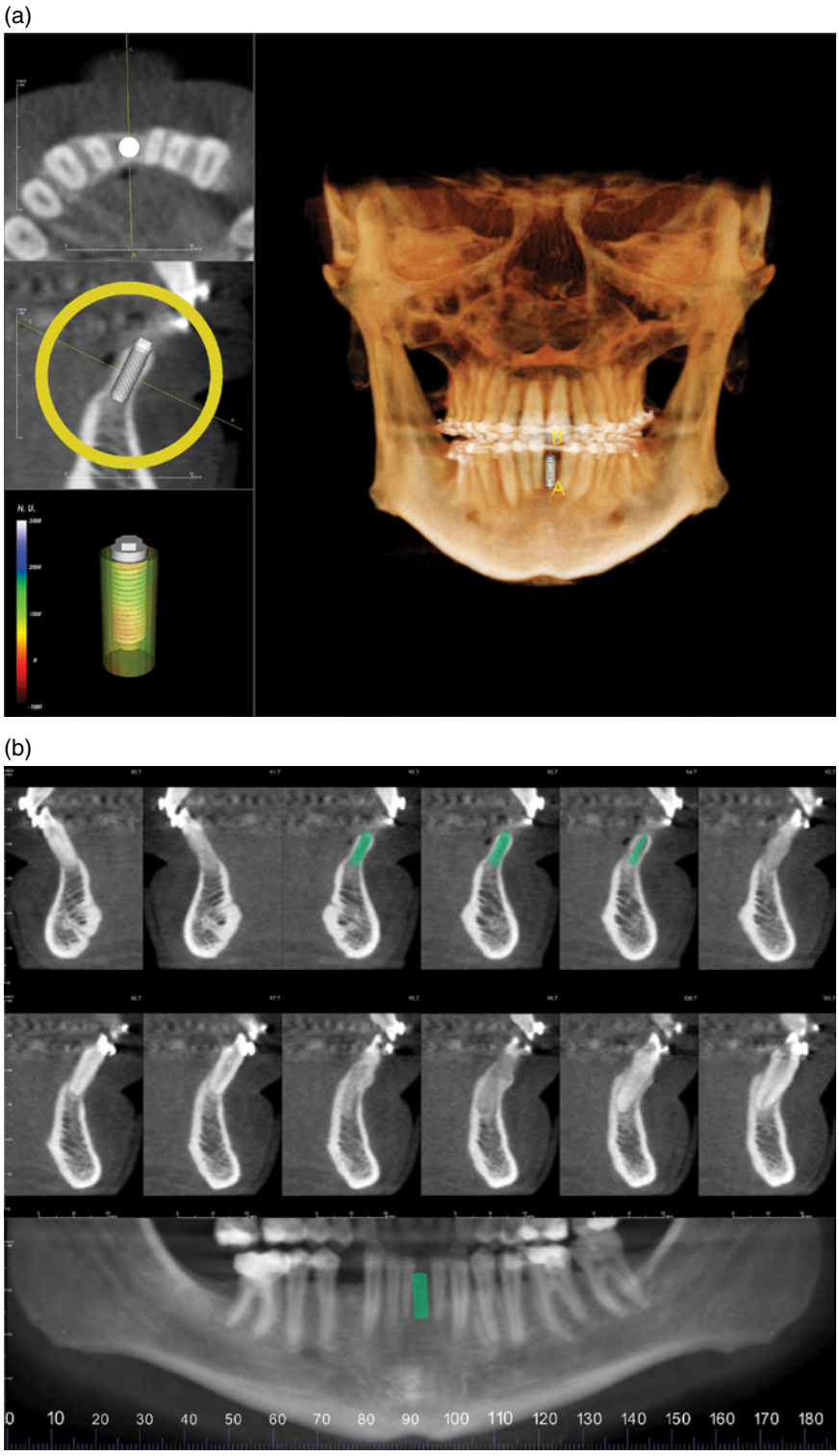

Figure 9.7. (a) Implant screen using InVivo software with corresponding axial (top left box) and single cross-sectional slice (middle left box) and Hounsfield units (bottom left box); (b) Cross-sectional slices with 1.0 mm spacing showing virtual implant (green) and surrounding bone.

References

Ganguly, R., Ruprecht, A., Vincent, S., et al. (2011). Accuracy of linear measurement in the Galileos cone beam computed tomography under simulated clinical conditions. *Dentomaxillofac Radiol*, **40** (5), 299–305.

Jalili, M. R., Esmaeelinejad, M., Bayat, M., et al. (2012). Appearance of anatomical structures of mandible on panoramic radiographs in Iranian population. *Acta Odontol Scand*, **70** (5), 384–89.

Klinge, B., Petersson, A., Maly, P. (1989). Location of the mandibular canal: comparison of macroscopic findings, conventional radiography, and computed tomography. *Int J Oral Maxillofac Implants*, **4**, 327–32.

Lofthag-Hansen, S., Grondahl, K., Ekestubbe, A. (2009). Cone-Beam CT for preoperative implant planning in the posterior mandible: Visibility of anatomic landmarks. *Clin Implant Dent Relat Res*, **11** (3), 246–55.

Mah, P., Reeves, T. E., McDavid, W. D. (2010). Deriving Hounsfield units using grey levels in cone beam computed tomography. *Dentomaxillofac Radiol*, **39** (6), 323–25.

Medical Dictionary. http://medical-dictionary.thefreedictionary.com/Hounsfield+unit.

Oliveira-Santos, C., Capelozza, A. L. A., Dezzoti, M. S. G., et al. Visibility of the mandibular canal on CBCT cross-sectional images. *J Appl Oral Sci*, **19** (3), 240–43.

Parsa, A., Ibrahim, N., Hassan, B., et al. (2012). Reliability of voxel gray values in cone beam computed tomography for preoperative implant planning assessment. *Int J Oral Maxillofac Implants*, **27**, 1438–42.

Ping, H. S., and Kandaiya, S. (2012). The influence of the patient size and geometry on cone beam-computed tomography Hounsfield unit. *J Med Phys*, **37** (3), 155–58.

Reeves, T. E., Mah, P., McDavid, W. D. (2012). Deriving Hounsfield units using grey levels in cone beam CT: A clinical application. *Dentomaxillofac Radiol*, **41** (6), 500–508.

Sheikhi, M., Ghorbanizadeh, S., Abdinian, M., et al. (2012). Accuracy of linear measurements of Galileos cone beam computed tomography in normal and different head positions. *Int J Dent*, **2012**, 214954.

Torres, M. G. G., Campos, P. S. F., Segundo, N. P. N., et al. (2012). Accuracy of linear measurements in cone beam computed tomography with different voxel sizes. *Implant Dent*, **21** (2), 150–55.

Tyndall, D. A., Price, J. P., Tetradis, S., et al. (2012). Position statement of the American Academy of Oral and Maxillofacial Radiology on selection criteria for the use of radiology in dental implantology with emphasis on cone beam computed tomography. *Oral Surg Oral Med Oral Pathol Oral Radiol*, **113** (6), 817–26.

Zoller, J. E., and Nuegebauer, J. (2008). *Cone-beam Volumetric Imaging in Dental, Oral and Maxillofacial Medicine*. Quintessence, Germany.

Appendix 1 Sample Reports

Shawneen M. Gonzalez

Introduction

This appendix includes sample reports of different areas captured on cone beam computed tomography (CBCT) scans. The three reports show example reports for CBCT scans made for various reasons. The general health report is an example of a report for a CBCT scan made with no obvious pathosis. The pathology report is an example of a report for a CBCT scan where there was obvious pathosis and the practitioner wanted more information about the nature and location of the disease process prior to determining the next treatment step. The implant report is an example of a report for a CBCT scan where the practitioner wanted to know quantity of bone for implant placement planning.

Interpretation Basics of Cone Beam Computed Tomography, First Edition.
Edited by Shawneen M. Gonzalez.

General Health Report

LEGACY 3D IMAGING

302 County Road
P.O. Box 3
Morrill, NE 69358
Phone: 308.225.4434

Patient: **Birth Date:** **Sex:**

Indication: Radiopacities – right and left mandible

Radiology Report

The patient was referred for a cone beam CT (i-CAT) on ----------. A cone beam CT dataset (8cm x 16cm, 20 seconds, 0.3 voxel, 120 kVp, and 18.45mAs) of the anterior half of the skull and cervical vertebrae was acquired and reconstructed. The resultant axial, coronal, sagittal, panoramic and orthoradial reconstructions were examined.

Teeth/Jaws:

1	2	3	4	5							12	13	14	15	16
		31	30	29		27				22			20	19	18

There is enostosis (dense bone island) in the area of the missing mandibular left third molar (#17).

There is a well-defined radiopaque entity apical to the mandibular left second premolar (#20) and first molar (#19). The radiopacity is that of cortical bone. The appearance is consistent with focal idiopathic osteosclerosis.

There is a well-defined, mixed radiolucent/radiopaque entity apical to the right mandibular molars (#30 & #31). The appearance is suggestive of cemento-ossifying fibroma; however cemento-osseous dysplasia cannot be ruled out.

Reconstructed pantomograph slice

There is no evidence of gross carious lesions. There may be smaller carious lesions, but this study is inadequate to evaluate for these. The generalized bone pattern is within the range of normal.

Maxillary Sinuses/Airway:
The visualized borders of the maxillary sinuses and mastoid air cells appear to be intact; there is no evidence of pathosis in these sinuses. The visualized airway appears patent.

Cranial Skull Base/Brain:
The cranial skull base appears to be within the range of normal. There are no gross abnormalities evident within the brain tissue.

Cervical Spine/Neck:
Portions of the first through fifth cervical vertebrae are depicted. There is a normal width of prevertebral soft tissue. There is asymmetrical joint space narrowing and osteophyte formation consistent with mild degenerative joint disease. There are multiple radiopaque entities in the right and left tonsillar region. The appearance is consistent with tonsiliths.

Interpretation

1. Probable cemento-ossifying fibroma – right mandible (#30 & #31)
2. Focal idiopathic osteosclerosis – left mandible (#20 & #19)
3. Enostosis - # 17

Shawneen Gonzalez DDS, MS
Oral & Maxillofacial Radiologist
Assistant Professor, UNMC College of Dentistry
smgonzalez@unmc.edu
402-472-1370

Pathology Report

LEGACY 3D IMAGING

302 County Road
P.O. Box 3
Morrill, NE 69358
Phone: 308.225.4434

Dr:

Patient: **Birth Date:** **Sex:**

Indication: Large radiolucent lesion – left posterior mandible. It appears to be associated with impacted # 17. Need to know relations of inferior alveolar nerve to # 17 and cyst and extent of bone remaining. Tooth # 18 is mobile. Patient has no numbness and occlusion is stable at this time. It is suggestive of dentigerous cyst or odontogenic keratocyst.

Radiology Report

The patient was referred for a cone beam CT (i-CAT) on ----------. A cone beam CT dataset (8cm x 16cm, 20 seconds, 0.3 voxel, 120 kVp, and 18.45mAs) of the anterior half of the skull and cervical vertebrae was acquired and reconstructed. The resultant axial, coronal, sagittal, panoramic and orthoradial reconstructions were examined.

Teeth/Jaws:

2	3	4	5	6	7	8	9	10	11	12	13	14	15	
31	30	29	28	27	26	25	24	23	22	21	20	19	18	
														17

There is a well-defined radiolucent entity with multiple radiopaque flecks within it extending from the impacted left mandibular third molar (#17) to the mesial of the first molar (#19). There is thinning and expansion of the facial and inferior cortical plates with a discontinuity of the lingual cortical plate. There is external resorption of the apices of the first molar (#19) and second molar (#18). The entity is directly adjacent to the mandibular canal which is being displaced inferiorly. The mandibular canal is on the lingual aspect of the impacted third molar (#17) and directly adjacent to it. The appearance is suggestive of a calcifying epithelial odontogenic tumor (CEOT). (Cross-sectional slices at end of report)

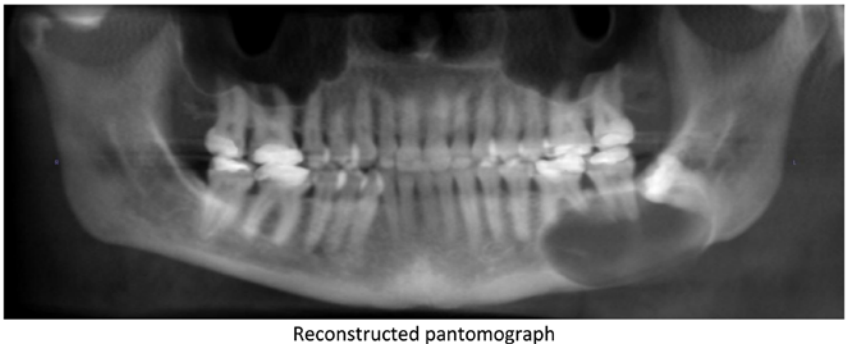

Reconstructed pantomograph

There is no evidence of gross carious lesions. There may be smaller carious lesions, but this study is inadequate to evaluate for these. There is no evidence of gross periodontal disease. The generalized bone pattern is within the range of normal. There is anterior osteophyte formation of the right condyle. The appearance is consistent with osteoarthrosis. The visualized left condyle appears within the range of normal.

Paranasal Sinuses/Nasal Cavity/Airway:
The visualized borders of the paranasal sinuses and mastoid air cells appear to be intact; there is no evidence of pathosis in these sinuses. The visualized nasal cavity is within the range of normal. The airway appears patent.

Cranial Skull Base/Brain:
The visualized cranial skull base appears to be within the range of normal. There are no gross abnormalities evident within the brain tissue.

Cervical Spine/Neck:
Portions of the first through third cervical vertebrae are depicted. There is a normal width of prevertebral soft tissue. There is asymmetrical joint space narrowing consistent with mild degenerative joint disease. There are multiple radiopaque entities in the left tonsillar region. The appearance is consistent with tonsiliths.

Interpretation

1. Probable calcifying epithelial odontogenic tumor (CEOT) – left mandible.

Shawneen Gonzalez DDS, MS
Oral & Maxillofacial Radiologist
Assistant Professor, UNMC College of Dentistry
smgonzalez@unmc.edu
402-472-1370

Cross-sectional slices

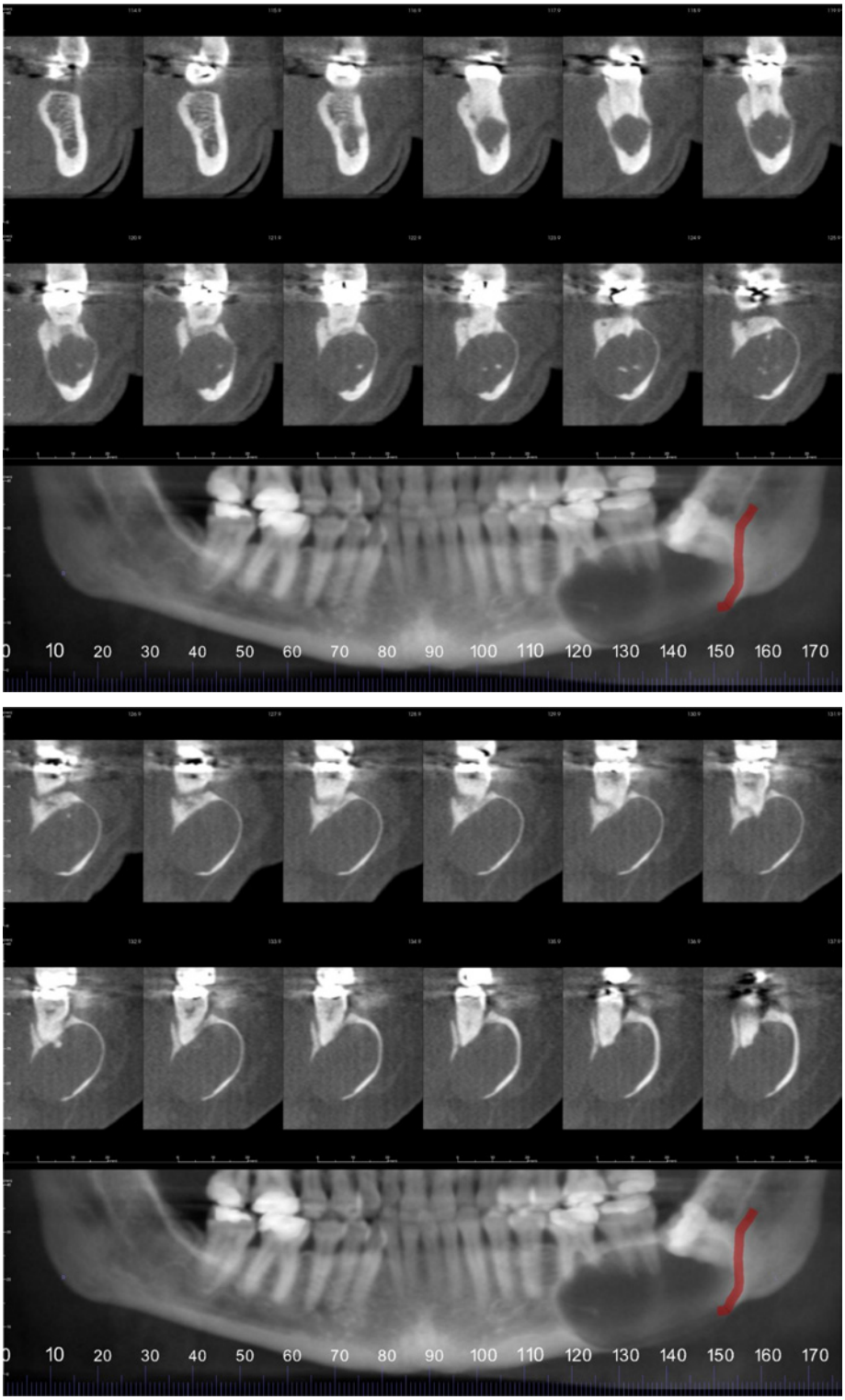

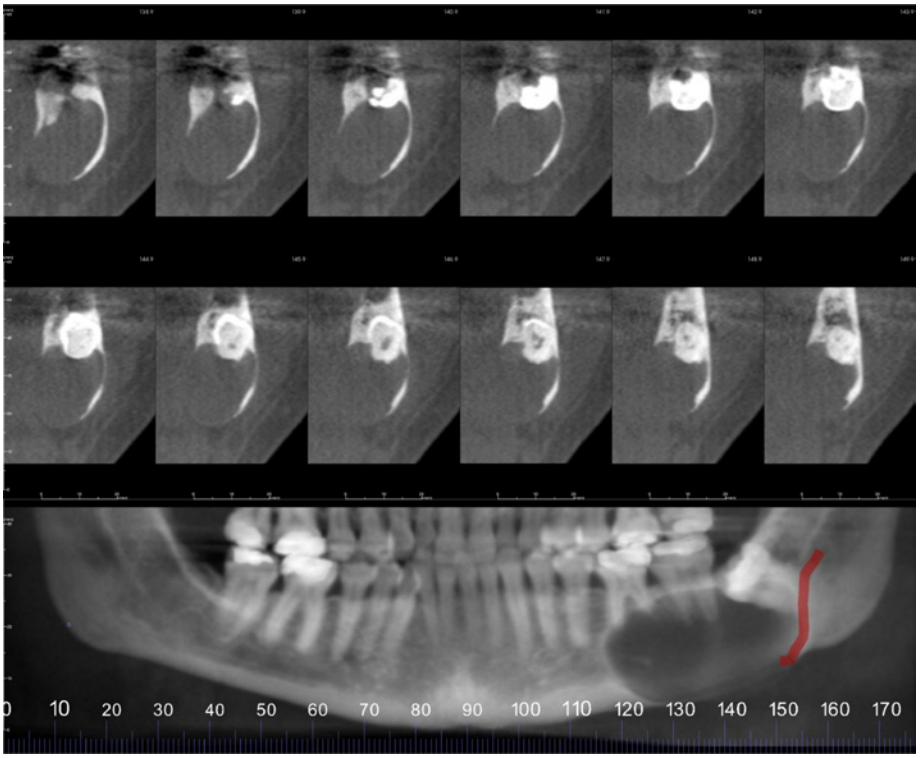
10 20 30 40 50 60 70 80 90 100 110 120 130 140 150 160 170

sg

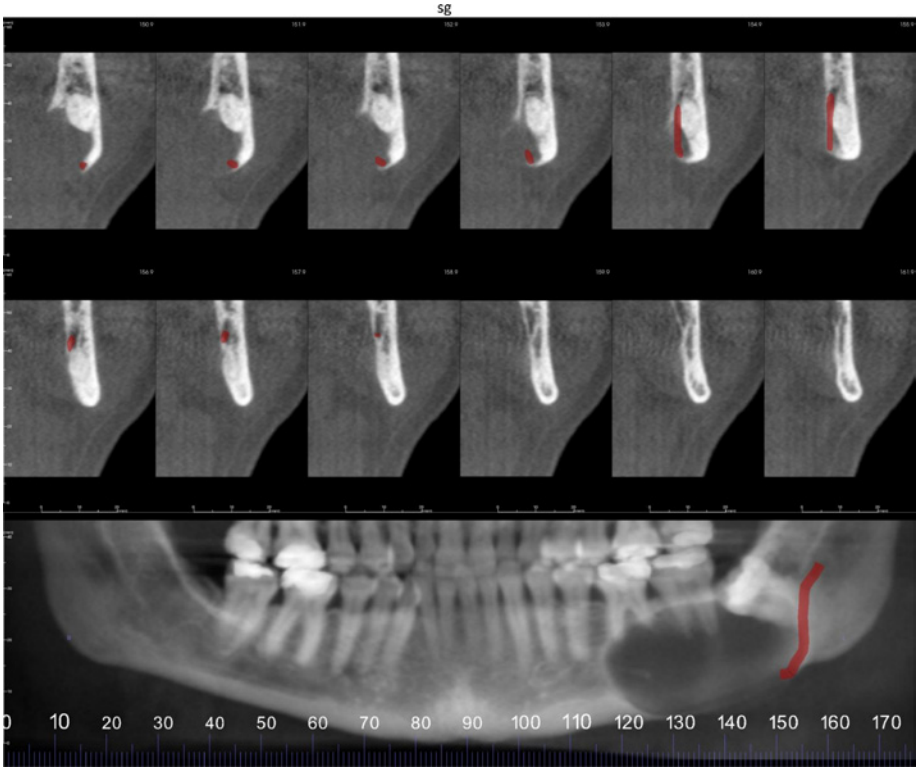
10 20 30 40 50 60 70 80 90 100 110 120 130 140 150 160 170

Implant Report

LEGACY 3D IMAGING

302 County Road
P.O. Box 3
Morrill, NE 69358
Phone: 308.225.4434

Dr:

Patient: **Birth Date:** **Sex:**

Indication: Implants

Radiology Report

The patient was referred for a cone beam CT on ----------. A cone beam CT dataset of the anterior half of the skull and cervical vertebrae was acquired and reconstructed. The resultant axial, coronal, sagittal, panoramic and orthoradial reconstructions were examined.

Teeth/Jaws:

2	3	4		6	7	8	9	10	11					15
31	30	29		27	26	25	24	23	22	21	20	19	18	

In the area of the missing maxillary left first premolar (#12), there is approximately 12.4 mm height of bone and 5.7 mm width of bone. In the area of the missing maxillary left second premolar (#13), there is approximately 6.9 mm height of bone and 5.8 mm width of bone. In the area of the missing maxillary left first molar (#14), there is approximately 4.3 mm height of bone and 9.7 mm width of bone. In the area of the maxillary left second molar (#15), there is approximately 8.9 mm height of bone and 8.0 mm width of bone.

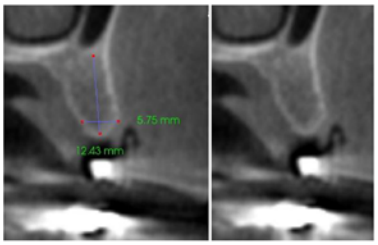

12 area

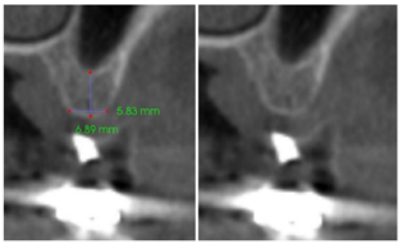

13 area

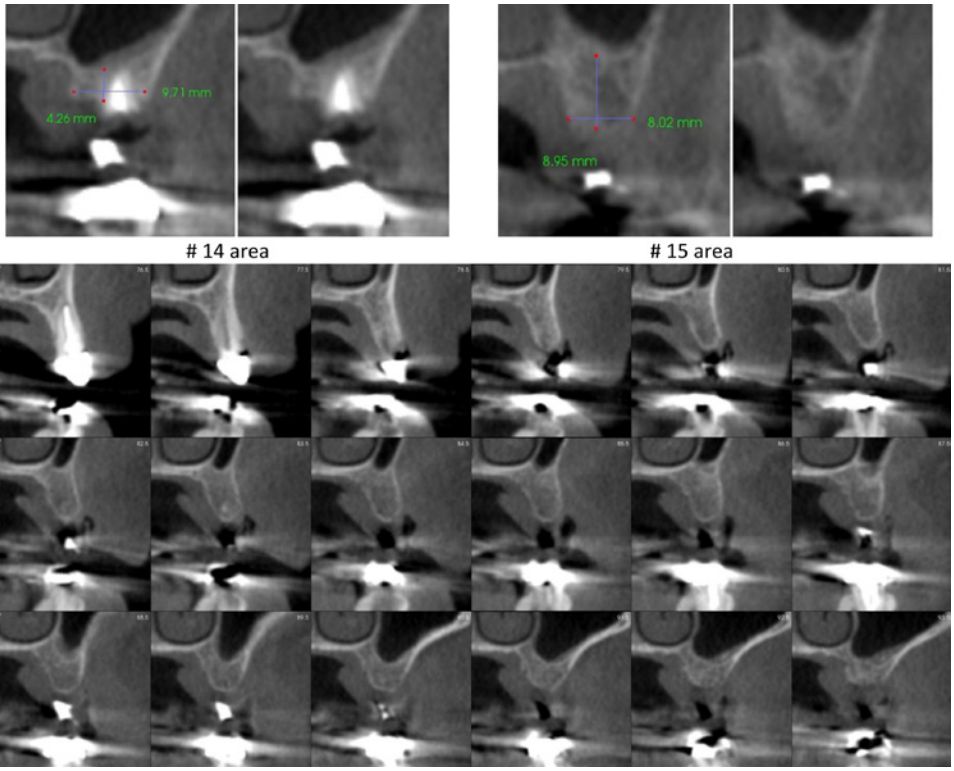
9.71 mm
4.26 mm
8.02 mm
8.95 mm
14 area
15 area

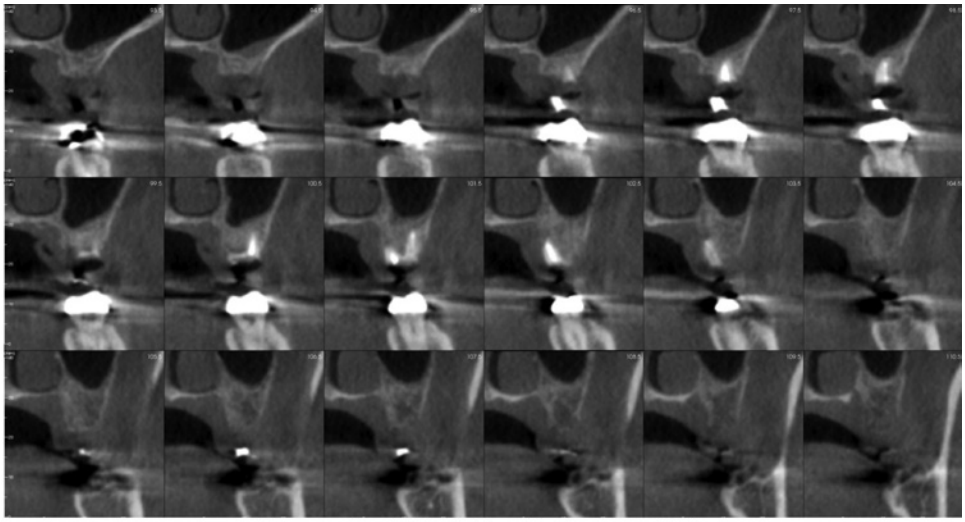

Cross-sectional slices left maxilla (1 mm spacing)

There are retained root fragments of the maxillary left second molar (#15) present.

There is rarefying osteitis (abscess, cyst and/or granuloma) associated with the maxillary right lateral incisor (#7). There is a widened periodontal ligament space associated with the maxillary right second molar (#2), left canine (#11), mandibular right first molar (#30) and second molar (#31).

There may be smaller carious lesions, but this study is inadequate to evaluate for these. There is no evidence of gross periodontal disease. The generalized bone pattern is within the range of normal. There is flattening with subchondral cyst formation of the right and left condyles. The appearance is consistent with osteoarthritis.

Paranasal Sinuses/Nasal Cavity/Airway:

The visualized borders of the paranasal sinuses and mastoid air cells appear to be intact. There is minimal soft tissue thickening of the maxillary sinuses. There is a radiopaque entity in the mucosal thickening on the floor of the left maxillary sinus. The appearance is consistent with inspissated mucous. This is an incidental finding. The bilateral osteomeatal units are patent. The nasal septum is deviated to the right. The airway appears patent.

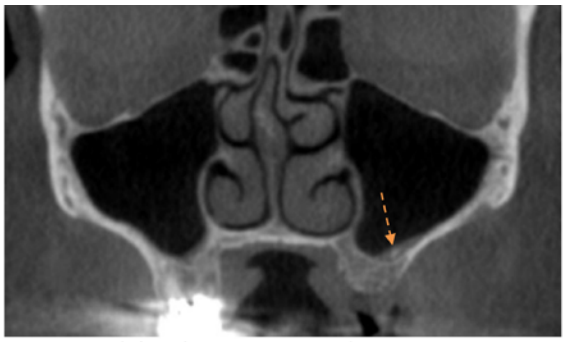

Coronal slice showing inspissated mucous – arrow

Cranial Skull Base/Orbit/Brain:
The cranial skull base appears to be within the range of normal. The bilateral orbital borders and globes appear to be within the range of normal. There is pineal gland calcification.

Cervical Spine/Neck:
Portions of the first through fourth cervical vertebrae are depicted. There is a normal width of prevertebral soft tissue. There is asymmetrical joint space narrowing. The soft tissues of the neck are within the range of normal.

Interpretation

1. Quantity of bone in edentulous left posterior maxilla noted above.
2. Retained root fragments - # 15.
3. Rarefying osteitis - # 7.
4. Widened periodontal ligament space - # 2, 11, 30, 31.
5. Osteoarthritis – right and left condyles.

Shawneen Gonzalez DDS, MS
Oral & Maxillofacial Radiologist
Assistant Professor, UNMC College of Dentistry
smgonzalez@unmc.edu
402-472-1370

Appendix 2 Resources

Introduction

This appendix contains recommended reading and websites you can visit to learn more about cone beam computed tomography.

Websites

American Academy of Oral and Maxillofacial Radiology: http://www.aaomr.org/

ConeBeam: http://www.conebeam.com/

EADMFR (SedentexCT): http://eadmfr.info/sedentexct

Marcilan (Maxillofacial Radiology Cone Beam CT Interactive Learning and Navigation): http://www.marcilan.com/

Recommended Reading—Articles

CDA. CBCT and legal issues (January 2010): http://www.cda.org/Portals/0/journal/journal_012010.pdf

Dr. Bicuspid. CBCT incidental findings (February 2013):

http://www.drbicuspid.com/index.aspx?sec=sup&sub=img&pag=dis&ItemID=312577&wf=37#.URAQ5d41g8o.twitter

Interpretation Basics of Cone Beam Computed Tomography, First Edition.
Edited by Shawneen M. Gonzalez.

JADA. CBCT incidental findings (February 2013 abstract): http://jada.ada.org/content/144/2/161.abstract

Recommended Reading—Books

Koenig, L. J. *Diagnostic Imaging: Oral and Maxillofacial*. Amirsys, 2011.

Larheim, T. A., and Westesson, P. L. *Maxillofacial Imaging*. Springer, 2008.

Miles, D. E. *Color Atlas of Cone Beam Volumetric Imaging for Dental Applications*. Quintessence, Germany, 2008.

Zoller, J. E. and Nuegebauer, J. *Cone-beam Volumetric Imaging in Dental, Oral and Maxillofacial Medicine*. Quintessence, Germany, 2008.

Index

Note: Italicized page locators indicate illustrations; tables are noted with *t*.

Interpretation Basics of Cone Beam Computed Tomography, First Edition.
Edited by Shawneen M. Gonzalez.